Embedding Nanofibres in Fabrics

Elizabeth Adelaide Wheeldon

Doctor of Philosophy

University of York

Chemistry

February 2018

Abstract

Low molecular weight gelators (LMWGs) form a network through non-covalent interactions to immobilise solvent and form a gel. Upon drying, the solvent evaporates, leaving behind nanofibres. The main aim of this project was to enhance the filtration properties of a non-woven fabric while minimising impact on the intrinsic air permeability and water vapour permeability. A range of supramolecular nanofibres were investigated, based on 1,3:2,4-dibenzylidene-D-sorbitol (DBS) and compared to *N,N',N"*-tris(2-ethylhexyl)-1,3,5-benzenetricarboxamide (BTA) as a benchmark, which has been previously used in the literature in a similar way.

Various self-assembled nanostructures have been successfully incorporated into a non-woven fabric including DBS, BTA, DBS-$CONHNH_2$, DBS-SCH_3, DBS-OCH_3 and small amounts of additives including a DBS dimer, poly(ethylene glycol) and poly(vinyl acetate). The nanoscale morphology was similar for all DBS derivatives. However, BTA gave rise to much larger nanofibres. Non-woven fabrics prepared with DBS, BTA, DBS-SCH_3 and a mixture of both DBS and BTA were scaled up and tested for air permeability (AP) and water vapour permeability (WVP). It was found that in most cases, there was a negative correlation between AP and concentration of gelator used to prepare the fabric, although WVP did not appear affected by the presence of nanofibres. The exception was DBS-SCH_3 which, at the loadings tested, did not appear to impact on AP. Fabrics prepared with a mixture of DBS and BTA produced a self-sorted network, with three different length-scaled fibres (DBS, BTA and fabric). All the modified fabrics gave AP and WVP results in the range of current protective textiles.

Fabrics prepared with DBS and BTA performed very similarly under filtration testing, both in forced conditions and in a more realistic setting. There was some evidence that the smaller DBS nanofibres were physically more robust. Substitution of BTA is thereby possible with a cheap, commercial product, DBS. Under realistic conditions, both gelators enhanced the filtration of a non-woven fabric against aerosols.

Table of Contents

List of Tables

List of Figures

List of Schemes

Acknowledgements

I would like to sincerely thank my academic supervisor, Professor David Smith, for all his invaluable support and guidance throughout my PhD studies. His vast expertise in gels and chemistry and particularly, his support and help while thesis writing was irreplaceable.

Thanks also go to my industrial supervisor, Dr Michael Dennis, whose provided expert knowledge of the current protection and testing techniques throughout my PhD and was incredibly helpful during my write up phase. I especially thank DSTL for sponsoring my PhD studies. Thanks also go to Dr Ningtao Mao, my second academic supervisor for sharing his vast knowledge of textiles.

I have learnt lots of new testing techniques, so thanks go to Peter Jones and Angie Hopkins from DSTL for their help with the realistic aerosol testing at SSAU, and Andrew Nicholls also from DSTL for his invaluable assistance with forced filtration aerosol testing at Porton Down. Thanks also to Jianguo Qu at Leeds University, who taught me how to run water vapour permeability and air permeability testing.

Thanks go to the support and technical staff in York who have helped and supported me with various techniques; Dr Andrew Leech (CD), Heather Fish (NMR), Dr Karl Heaton (MS), Ian Wright and Jon Barnard (SEM at York Jeol Nanocentre).

Thanks to all the past and present members of the Smith group, particularly Dr Stephen Bromfield and Dr Ana Campo Rodrigo for being awesome postdocs and attempting to expand my vocabulary (both in English and Spanish), Dr Nicole McLeod and Dr Daniel Cornwell for help with the synthesis, rheology and answering my never-ending questions, Dr Buthaina Albanyan, Dr Vânia Vieira and Kirsten Hawkins for keeping me giggling.

I am incredibly grateful for the support of my family, especially my Mum and Dad. Even though I often confused you when talking about my work, you were always willing to listen and encourage, often offering a new perspective on topics or trying to suggest new ideas. Thank you to my friends for checking I was surviving particularly while writing and for not giving up on inviting me to events, reminding me there was a life outside my PhD. Thanks to Skye for providing great cuddles, a hot water bottle while I was writing and always knowing when I needed a writing break.

I am especially grateful to Ben, thank you for sticking with me, especially through my write up phase. There really aren’t words to thank you for what you’ve done. I love you.

Declaration

I declare that this thesis is a presentation of original work and I am the sole author. This work has not previously been presented for an award at this, or any other, University. All sources are acknowledged as References.

Chapter 1 - Introduction

1.1 Industrial Problem and Application to Protective Clothing

Inexpensive, relatively easy to produce with the potential to create mass casualties using small quantities, chemical warfare agents (CWAs) are a serious threat. The Geneva Convention prohibits the development, production, stockpiling and use of chemical weapons, but in fact, the threat of chemical terrorism has the potential to exceed the impact of the use of most modern firearms.[1]

All chemicals have the potential to be biologically active, many are toxic but only some are known as poisons. Poisonous chemicals have been extracted from plants since the Middle Ages, and there are multiple examples of chemicals used as weapons during a campaign or battle, the Chinese used arsenical smokes as early as 1000 BC. Industrial expansion in the 19th century created the possibility of modern chemical warfare agents.[2] Chemical warfare agents are extremely toxic chemicals that can be dispersed as a gas, liquid or aerosol, or adsorbed to particles forming a powder.[2] CWAs can incapacitate humans with potential death.[3]

In Ypres, Belgium, 22nd April 1915, the Germans released chlorine gas onto the battlefield with the aim to harm enemy personnel; the beginning of modern chemical warfare. The unexpected success of this first attack encouraged the Germans to use chlorine further in the preceding months. Shortly after the first chlorine attack, the Allies created primitive emergency protective masks, significantly reducing the effects of chlorine, which prompted the Germans to escalate their attacks to the use of phosgene. The use of toxic chemicals during World War I caused over 100 000 deaths and 1.2 million casualties.[2] Also first used in WWI, “mustard gas” was dispersed as fine liquid droplets of sulfur mustard. This is a blistering agent, that was lethal in *ca.* 1% of cases but would incapacitate effectively and remain on the ground for weeks. Sulfur mustard has been used repeatedly throughout military history, with the most recent attack by the ISIS regime in recent years.[4]

The chemical structures of some of the CWAs used in WWI can be seen in Figure 1-1. Millions of civilians were killed by the Nazi regime using hydrogen cyanide gas during World War II. Other uses of chemical warfare agents are scattered throughout history, from that first attack in World War I through to 1990s, including the Vietnam war and the Iran-Iraq war.[2] In 1994, Sarin (a nerve agent) was released in Matsumoto by a Japanese cult and in 1995, 15 stations of the Tokyo Subway system were filled with diluted sarin gas. There were 12 fatalities and more than 5500 injuries.[5] Ineffective methods of delivery limited the number of deaths.[5]

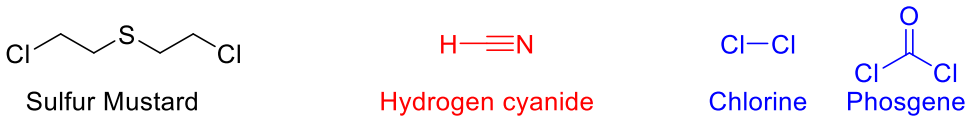

Figure 1-1.Examples of chemical warfare agents used during WWI: Sulfur Mustard (blistering agent), Hydrogen Cyanide (blood agent), Chlorine and Phosgene (choking agents).

1.1.1 Brief History of Protective Clothing

Protective clothing against CWAs in World War I entailed impermeable rubber clothing including boots, gloves and a mask. This prevented the CWA penetration, but also stopped the escape of perspiration vapour, making it extremely uncomfortable to wear for any length of time.[6] Impermeable protective suits were developed for German civil defence personnel, protecting against sulfur mustard and Sarin for five hours but required two people to help the wearer get into the suit.[7] Although offering effective protection, the limits of practical use led to the development of alternatives. Permeable clothing was designed to reduce the heat load on the wearer, binding a layer of activated carbon (either particulate or bound in polyurethane foam) between two layers of textiles. These more breathable fabrics permit the transportation of water vapour and the active carbon adsorbs CWAs. Breathable materials bring their own disadvantages including penetration of aerosols, contamination by fuels, oil, solvents, poisons and degradation of protective power over a few days.[6]

The Israelis developed a new approach to reduce heat stress based on selective water permeability of ‘impermeable’ clothing.[8] These researchers suggested the use of activated charcoal in films made with water permeable polymers, such as poly(vinyl alcohols) or cellophane. The reduced thickness and weight of the material reduced discomfort, and the continuous structure enhanced thermal conductivity and water permeability.[6] However, a continuous increase in body temperature was observed. The Chinese made a fine carbon-containing permeable gauze fabric. The high surface area of the gauze and the use of fine carbon fixed by a binder gave a resultant material surface area of 860 m^2 g^{-1}.[9] Another carbon-containing flannel was developed by the Chinese, one side of the flannel was treated with activated carbon and the other with oil repellent agents. The suit was mass produced and supplied to the Chinese army.[10] Since the 1960s, many countries have provided their army personnel with charcoal-containing, permeable protective suits. The Chinese also developed suits consisting of two layers; an outer polyvinyl alcohol-cotton blend for camouflage and waterproofing,

and an inner cotton flannel layer finished with one side of charcoal powder-adhesive and the other side oil repellent. This suit was light, protective and had a storage life of three years.[11] Spherical activated carbon adsorbers embedded in carbon protective textiles are known as Saratoga. These were originally developed in Germany, providing excellent chemical agent protection, launderability and reusability.[12] Fabric and fibrous forms of activated carbon are very expensive, whereas granular and powdered activated carbon are cheaper. The spheres used in the Saratoga carbon protective textiles offer a compromise between cost and performance.[6]

In 1988, the CWU/66P chemical protective clothing suit was developed for US aircrew. This suit consisted of a Saratoga laminated permeable woven fabric providing good protection, even after repeated washing, with reduced thermal burden, and durability for long-term use.[13] The benchmark of chemical protective suits became the Saratoga chemical protective overgarment of the U.S. Marine Corps, providing protection for more than 24 hours with a wear time of 45 days and still providing protection after at least six wash cycles.[6] Obsel and Stein from Czechoslovakia introduced polyester non-woven textiles as protective textiles, consisting of powdered activated carbon fixed with an acrylate binding agent. The random orientation of polyester fibres efficiently trapped toxic vapours and gases.[14] Over the years, many other developments have been made but generally most suits consist of multi-layer or laminated fabrics with activated carbon. In more recent times, protective suits have become an academic challenge. Ramkumar and co-workers reported the development of lightweight, non-woven protective clothing incorporating an activated carbon layer for chemical adsorbency.[15] Ramaseshan and co-workers from the National University of Singapore produced electrospun nanofibres to form a highly porous mesh and large surface area to volume ratio, demonstrating better protective performance with the potential to provide a sensing interface.[16] As a general strategy, nanofibres could also allow incorporation of other species such as metal nanoparticles. Metal nanoparticles (Ag, MgO, Ni, Ti etc) that have proven abilities in decomposing warfare agents, could also be embedded in nanofibres although this has not yet been achieved.[6] For example, three different polymer fibres were electrospun, followed by treatment with $AgNO_3$ and UV irradiation. These silver nanoparticle-containing nanofibres were highly active against microbes and the authors suggested could have potential as an air filter.[17-19]

Clothing typically covers the body with an air gap between the two. An external air flow such as wind or body movement, causes the movement of air around the body, whereas some will penetrate through the clothing and into the air gap, allowing

deposition onto the skin. The air permeability of a material and a given external air velocity dictates the amount of air which flows around the body and penetrates through the barrier, therefore the permeability of the clothing has a significant impact on the deposition of potentially harmful aerosols.[20] Current full barrier protection comes from impermeable hazardous material (HAZMAT) suits, whereas permeable adsorptive protective overgarments such as joint service light integrated suits technology (JSLIST) and battle dress overgarment (BDO) are based on functionalized activated carbon.[21] Modern impermeable suits tend to consist of nylon fabric coated with neoprene outside and butyl rubber inside, whereas permeable clothing tends to be three layers; oil and water repellent and fire retardant nylon, carbon coated non-woven and cotton.[2] Current chemical weapons protection in the field is offered by heavy clothing with low air permeability making it unsuitable for prolonged use. The aim of this study is to investigate a wearable solution with some level of aerosol protection.

1.2 Gels

Gels consist of a solid phase suspended in a liquid phase, and are used in daily life (for example toothpaste or contact lenses).[22, 23] Dorothy Jordan Lloyd defined a gel as “if it looks like a gel, it must be a gel”.[24] However, a gel is typically made up of at least two components, a liquid and a gelling substance.[25] The colloidal chemistry definition of a gel is a dispersion of molecules of a liquid within a solid in which the solid is the continuous phase and the liquid is the discontinuous phase. The liquid is entrapped within the gel network.[26-28] The gel is neither a solid nor a liquid, which lends itself to unique viscoelastic properties. There are multiple ways of forming a gel. The gels encountered in daily lives tend to be based on polymers.[29] These can either form through covalent bonding and cross-links between polymer chains, producing an entangled network, which tends to be thermally irreversible due to the strength in the covalent bonds, or form through non-covalent interactions holding the polymer chains together.[30]

1.3 Low Molecular Weight Gelators

Low molecular weight gelators (LMWGs) are small molecules that self-assemble into a solid-like nanoscale network within the liquid phase, via non-covalent interactions, e.g. hydrogen bonding, van der Waals forces, π-π stacking, dipole-dipole, solvent effects, charge transfer or coordinate bonds.[30-36] Molecules self-assemble into fibrils, which can bundle together to give larger fibres, and then tangle to form a sample-spanning

network, see Figure 1-2. This entangled network can immobilise the flow of bulk solvent using capillary forces and some specific solvent-gelator interactions.[25, 37, 38] Often, <1 wt/v% of gelator is required to form a gel. The weak nature of non-covalent interactions means that supramolecular gels tend to exhibit thermal reversibility.[30]

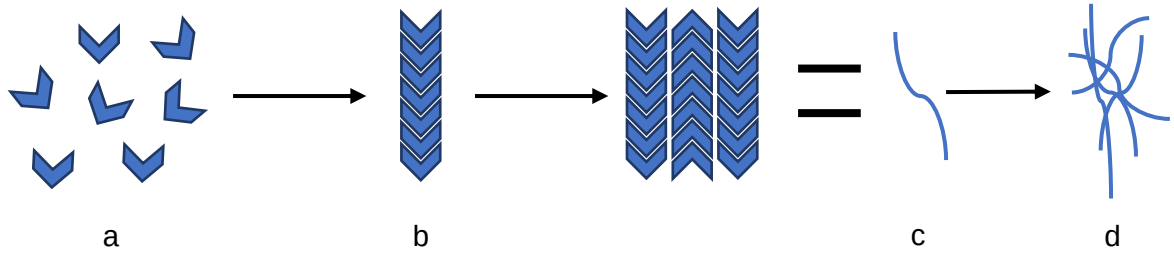

Figure 1-2 Self-assembly of a gelator from individual molecules (a) to fibrils (b) which bundle into fibres (c) which entangle to form gel network (d).

1.3.1 Gel Formation

Typically, solvent is added to a small quantity of gelator which is then heated to dissolve the gelator, although other stimuli can also be used.[23, 25] As the solution cools, the non-covalent interactions between gelator molecules drive the self-assembly into fibrils with one-dimensional order.[38, 39] These fibrils can then interact with one another to form fibres and potentially form fibre bundles which can, in turn, result in a variety of morphologies, including tapes, ribbons, fibres, sheets, vesicles or micelles.[22, 27] Interactions between fibres determines the final structure. A continuous gel network requires 'cross-link' type interactions between fibres from either entanglement and/or branching of fibres.[39] Ultimately a three-dimensional sample spanning gel network is formed (Figure 1-2).[25]

1.3.2 Gelation or Crystallisation

Gelation is closely linked to crystallisation, in fact, some might state they are competing processes.[40-42] Informally, gelation is sometimes referred to as crystallisation gone wrong.[40] Heating to dissolve gelator molecules as described in Section 1.3.1, has three potential outcomes; random aggregation giving a precipitate, ordered aggregation giving crystals or aggregation resulting in a gel (Figure 1-3).[23, 38, 39]

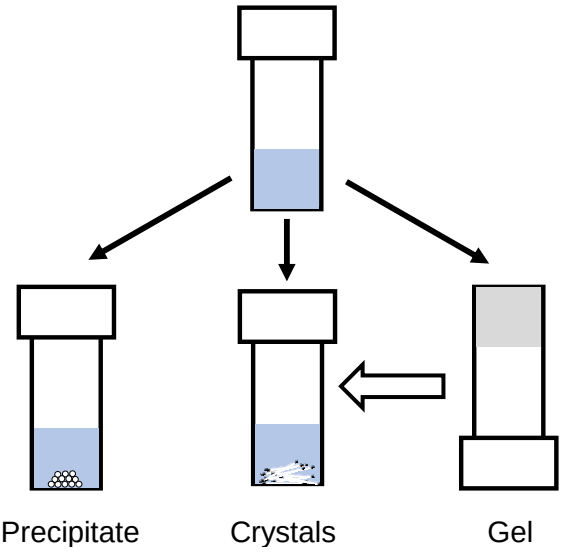

Figure 1-3. Three possible outcomes from the aggregation of dissolved molecules at a given concentration. Over time gels can degrade to form crystals.

Crystallisation can also occur after gel formation, ultimately leading to the collapse of the gel.[32] Gels are generally kinetically trapped, rather than being the most thermodynamically stable aggregate.[32, 40] Over time, the gel fibres can, therefore, dissociate and reorganise into crystals.[43-45] The lifetime stability of a gel is thus important. Various studies including the work of Wang, have tried to correlate crystal molecular packing to packing in a gel network, finding some similarities but generally finding that crystals and gels have different packing arrangements.[45-47] Changing the molecular structure of the gelator can direct the formation of either gels or crystals, although this is unpredictable.[41, 42, 44]

Identifying whether a molecule will form a gel or crystallise is still very difficult, most gelators are discovered serendipitously.[48] However, there are some general guidelines for the ability of a molecule to form a gel.[28, 48, 49] The molecule must be able to form non-covalent interactions, ideally in one-dimension (three-dimensions could encourage crystal formation). There also needs to be a balance of solubility in the solvent. The material must not be too soluble, or it will remain in solution, but not be too insoluble to encourage precipitation or crystallisation.[22, 31]

Modification of a known gelator is somewhat more common than designing a new gelator from scratch.[50, 51] The structure of the self-assembling molecule can influence the macroscopic properties of the material, so by introducing different functional groups to the molecule, it is possible to change the functionality of the resulting gel. As such,

organic synthesis can be considered to 'program in' functionality to the nanoscale network and effectively tune the properties of the gel.[35, 52, 53]

1.3.3 Response to Stimuli

As a result of the non-covalent interactions underpinning them, supramolecular gels are often responsive.[52] They can respond to different factors including physical stimuli such as light,[54, 55] heat-cool cycles or sonication,[56] or chemical stimuli such as a change in pH,[47, 57-59] cations, anions,[33, 60] redox reagents[61] and enzymes[62] to either form or break the gel network. Gels can be responsive to more than one stimuli, making them multi-responsive.[63] Many supramolecular gels are thermoreversible.[57] All gels have a thermal property defined as T_{gel}, the temperature of the gel-sol transition. At the T_{gel} value, the entropic gain outweighs the enthalpic cost of disassembly and the gel converts into a sol.[27, 64]

1.3.4 Importance of Solvent Choice

Generally, the gelator accounts for <1 wt/v% of the gel, the majority being solvent.[23, 25, 32, 65] The solvent is, therefore, of vital importance and can play a critical role in controlling gel properties. Some LMWGs are known to gel multiple solvents including organic solvents,[22, 51] aqueous media,[25] ionic liquids,[66, 67] liquid crystals[68-70] or even electrolytes for conductive and battery applications.[71-75] Most gelators can only form gels in a particular type of solvent due to gelator-solvent interactions. Solvents have been reported to have an impact on the morphology of gels.[48, 65, 76-79] As one example, an organogelator based on L-glutamic acid demonstrated significant changes in morphology in different polarity solvents (Figure 1-4). Even on treatment of the xerogel (dried gel) with solvent vapours, the morphology changed from nanofibres to either nanotubes with open mouths (DMF) or chiral twists (chloroform).[78]

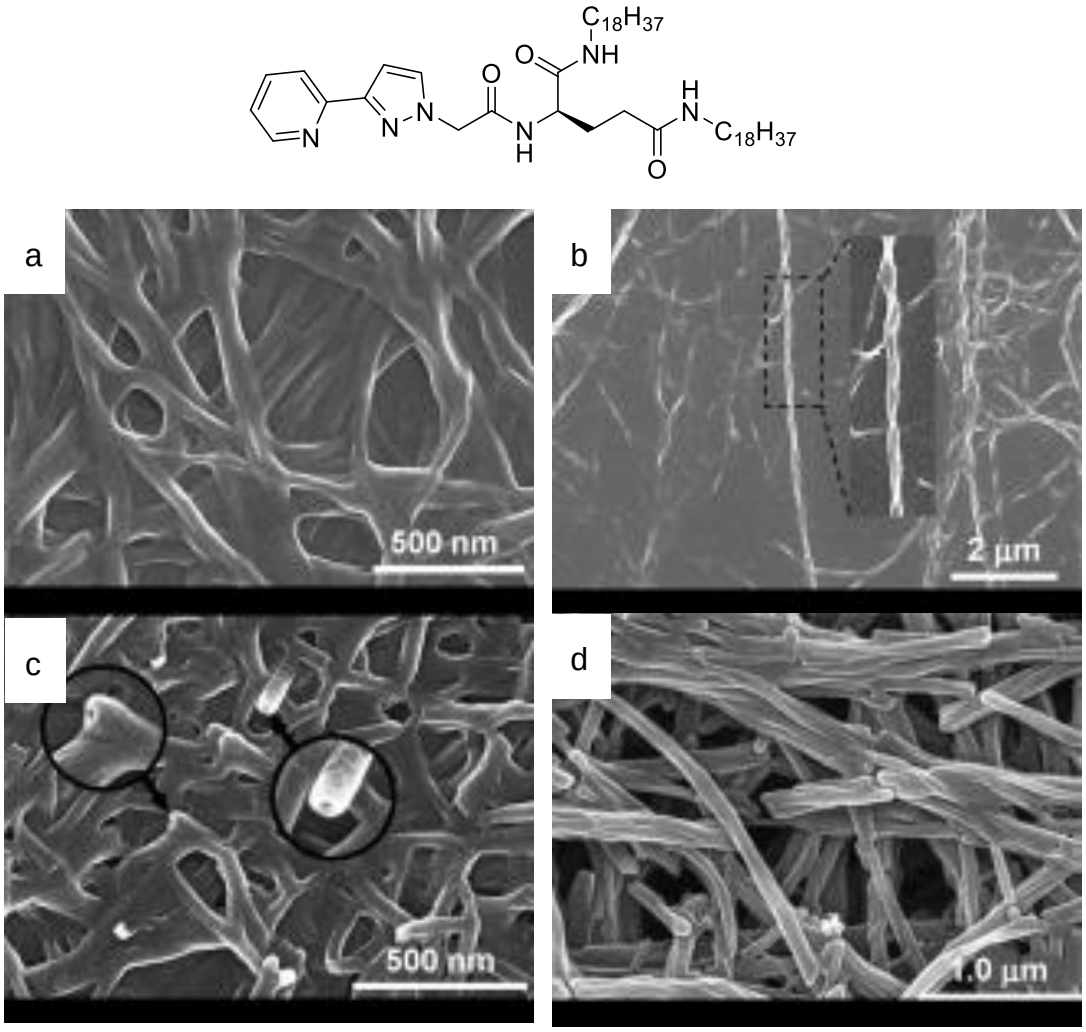

Figure 1-4. SEM images of gels of *N,N'*-bisocta-decyl-2-(3-(pyridin-2-yl)-1H-pyrazol-1-yl)-L-glutamic amide (abbreviated as PPLG) that were formed in (a) toluene, (b) $CHCl_3$, (c) DMF and (d) MeOH showing different morphologies reproduced and adapted with kind permission from John Wiley & Sons.[78]

Numerous attempts have been made to correlate gelation with different solvent parameters,[80] e.g. Kamlet-Taft parameters,[81] Hildebrand solubility parameters[82, 83] and Hansen solubility parameters.[65, 77, 82, 84-91] Studies have even tried to compare and combine the use of these diverse parameters to gain additional understanding of solvent properties with respect to gelation.[83, 86, 92-94] Traditionally in polymer science, the Hildebrand solubility parameter is used, which describes cohesive energy between solvent molecules determining the probability of a solute dissolving in another solvent. Although this is effective for predicting the behaviour of non-polar species in non-polar solvents, it is less effective when concerned with specific polarity or hydrogen bonding. Hansen solubility parameters (HSPs) overcome the limits of the Hildebrand solubility

parameter by quantifying the energy contributions into different terms. HSPs split solvent interactions into; δ_d, δ_p and δ_h representing dispersion forces, polarity and hydrogen bonding interactions, respectively. Dispersion interactions include atomic forces such as van der Waals forces.[77, 95]

The first application of HSPs to gelation behaviour was by Raynal and Bouteiller.[82] They found that the solvents gelled by a single gelator, all had similar HSPs.[82] HSPs are now the most commonly used method to predict the response of a gelator in a specific solvent.[65, 77, 82, 84-91]

1.4 Material Behaviour of Gels

1.4.1 Minimum Gelation Concentrations

Each gelator has a minimum concentration at which it forms a gel referred to as the critical gelation concentration (CGC) or minimum gelation concentration (MGC). This value varies according to the solvent and gelator. The polymorph of the solid form of the gelator can also impact on its ability to form gels.[96]

Below the MGC, it is possible that nanofibres exist but are not sufficient to form a network, or alternatively that no nanofibres exist. This will depend on the cooperativity of the assembly process.[97, 98]

1.4.2 Rheology

One of the most common approaches to measure macroscopic materials behaviour is rheology. Derived from the Greek *rhéos* meaning stream or anything that flows, rheology is the study of flow and deformation of materials. Rheometers apply a shear stress to a material and measures the resultant deformation. All materials respond differently depending on the timescale of measurement.[99] Most solids flow over a long time period. Window glass, for example is a very viscous fluid with a shear viscosity of 10^{12} Pa s whereas water can act as a solid during very short time periods. This means that almost all materials are viscoelastic, at least to some extent.[100]

Deformation is the relative displacement, the distance moved by the material when a force is applied. Modes of deformation can include volume changes, extensional strain and shear strain. Gels are usually considered as incompressible materials, thereby simplifying analysis by analysing shear strain deformation only.[101] This deformation can be divided into two individual components; flow and elasticity. Flow represents an irreversible deformation, so the material will never return to its original form even once

the stress is removed. Flow properties are defined by viscosity (or resistance to flow), which is measured by applying a shear stress to a fluid. Elasticity represents a reversible deformation, so the material can recover its original form after the stress is removed. The elasticity is studied by applying a stress and measuring the deformation or strain. Viscoelastic materials, such as gels, show both elastic and viscous characteristics when oscillatory stress is applied.[102] They can be soft and deformable like a liquid but they can also hold their shape like a solid.

Equation 1-1 and Equation 1-2 define strain and stress, respectively.

Equation 1-1

$$Strain\,\gamma = \frac{change\ in\ dimension}{original\ dimension} = \frac{\Delta x}{x}$$

Equation 1-2

$$Stress = \frac{Force}{Area} = \frac{F}{A}$$

Applying an oscillating stress to an ideal solid will generate an elastic response, producing perfectly in-phase stress and strain, i.e. a phase difference of 0°.[103] Applying an oscillating stress to an ideal liquid will generate a viscous response, producing perfectly out-of-phase stress and strain, i.e. a phase difference of 90°. In reality, most materials are viscoelastic so lag somewhere between these ideals of 0° and 90°, an example of which can be seen in Figure 1-5.[100] A rheometer can measure this “phase angle” and usually reports it as tan δ (Equation 1-3). This is a measure of the viscous/elastic ratio for the given frequency. [100,102] Phase angle shows the relative importance of the liquid-like viscosity and solid-like elastic components.

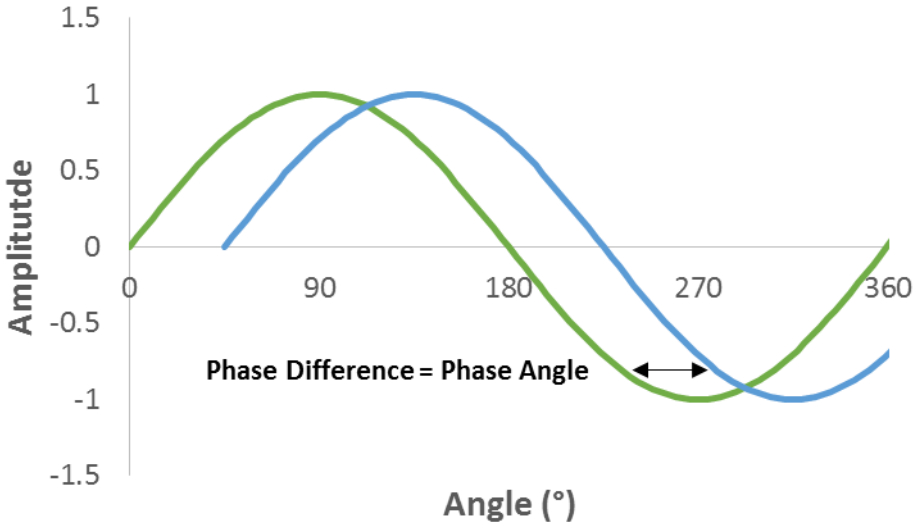

Figure 1-5. Sinusoidal curves representing stress and strain with the black arrow showing the phase angle.

Equation 1-3[104]

$$Tan\ \delta = \frac{G"}{G'}$$

The complex shear modulus G* (Equation 1-4), a common output of rheological experiments, consists of an elastic component and a viscous component, measuring the energy stored and dissipated, respectively.[100] G' (Equation 1-5) is the storage modulus, representing the elastic/solid component of the response, the elasticity associated with the energy stored during elastic deformation.[41, 102, 105] G" (Equation 1-6) is the loss modulus, representing the viscous/liquid component of the response, the ability to flow under stress (to dissipate/absorb the energy).[41, 102] G" characterises the damping property, so it is expected that increased G" represents increased toughness.[106]

Equation 1-4

$$G^* = (G'^2 + G"^2)^{\frac{1}{2}}$$

Equation 1-5

$$G' = G^* \cos\delta$$

Equation 1-6

$$G" = G^* \sin\delta$$

For viscoelastic materials, G'>G". Characteristic gel behaviours include G'>>G" (usually G'>10G") with both being independent of frequency.[41, 103, 107, 108] G'<10G" is defined as a "weak gel" in the literature,[107] though little consideration will be given in this work to whether a gel is defined as strong or weak. It has been argued that strong gels can rupture and fail, whereas weak gels are more likely to flow and therefore recover.[100] Some gels are recoverable due to the lack of permanent crosslinks allowing the system to flow but not rupture.[107] This allows control of the mechanical properties of a gel through molecular architecture.[109] Mechanical properties of a low molecular weight gel largely depend on the fibre density of the network and the number of cross-links between the fibres.[101]

Rheometers with a parallel plate geometry apply a back and forth oscillatory stress producing plots of G' and G" against stress, time or temperature to allow calculation of different parameters including yield stress, thermal stability or recovery time after destruction.[41, 102] Serrated surfaces can be used on the rheometer plates to avoid slippage.[104]

To obtain data about the material properties of a gel, firstly an oscillatory strain amplitude sweep is carried out at a fixed frequency to establish the linear viscoelastic region (LVR, i.e. G' and G" are independent of frequency). G' exhibits a pronounced plateau normally over at least the second time scale and a G' which is greater than G" in the plateau region (Figure 1-6).[110] The end of the LVR region has been defined in this work as a deviation of >10% from the original G' value.

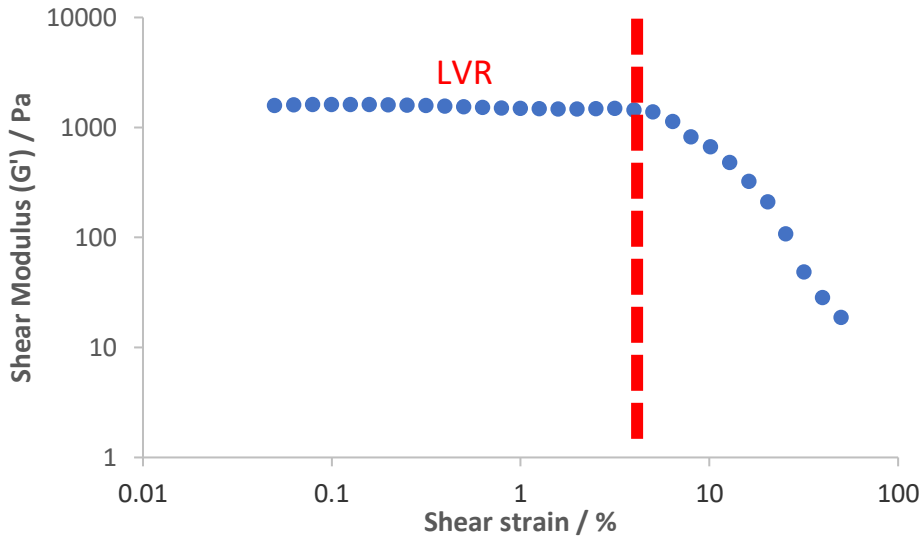

Figure 1-6. Amplitude sweep at a fixed frequency to establish LVR. LVR can be seen here below about 5% shear strain.

Once the LVR has been identified, a complex shear strain within this region is chosen to carry out the next measurements (usually about 0.5%). Then an oscillatory frequency sweep is performed to allow measurement of G' and G". Large amplitude oscillations can break the gel.[109] At this point G' shows a sharp collapse corresponding to the loss of fibre interconnectivity.[104]

A crossover point on the frequency sweep, where G' = G", is the point at which the material loses its viscoelasticity and behaves as a viscous material (gel to solution transition).[102] This is how T_{gel} is usually measured using variable temperature control on a rheometer, i.e. the temperature at which the crossover occurs is defined as the T_{gel}.

1.5 1,3:2,4-Dibenzylidene-D-sorbitol (DBS) and its derivatives

1,3:2,4-Dibenzylidene-D-sorbitol (DBS) is used industrially as a bulk chemical and therefore has commercial relevance.[51, 111-123] DBS is a well-known low molecular weight gelator, originally discovered in 1891 by Meunier.[124] It is a white crystalline substance synthesised by the condensation of D-sorbitol and two equivalents of benzaldehyde, a process catalysed by the use of an acid. DBS has a butterfly-like shape, with the sugar backbone forming the 'body' and the aromatic rings the 'wings' Figure 1-7.

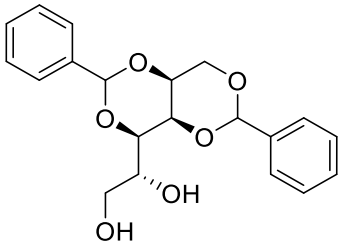

Figure 1-7. 1,3:2,4-Dibenzylidene-D-sorbitol (DBS).

In 1926, Thomas and Sibi formed organogels using DBS in a number of different solvents without a formal definition of the chemical structure. The Second World War resulted in many low molecular weight gelators finding additional applications such as engine greases and napalm. It was this interest that led to studies to explore the reactivity and establish the chemical structure of DBS.[125, 126]

DBS was originally reported by Meunier as a mixture of two isomeric diacetals, with different physical properties.[124] He reported that they had different melting points, a unique solubility in boiling water and one formed a gel while the other did not. Wolfe and co-workers discovered that DBS actually exists as a single species in 1942, both the mono- and tri-substituted derivates can be present as by-products (Figure 1-8).

They also proposed that DBS had the acetal functionalisation in the 1,2,3 and 4 positions.[127]

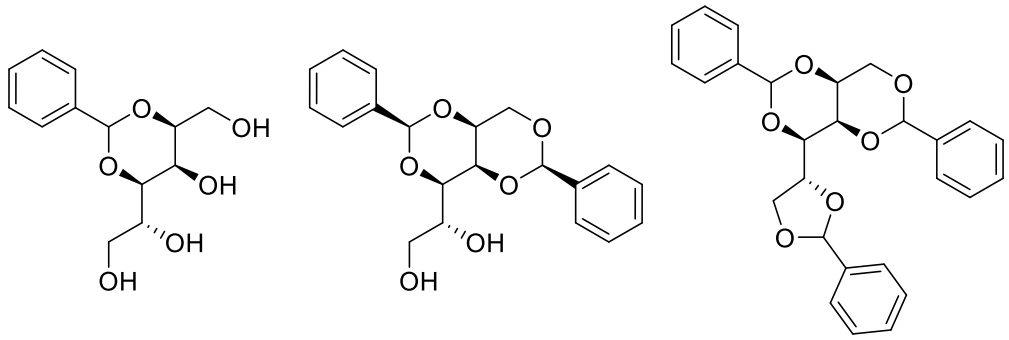

Figure 1-8. Structure of 2,4-monobenzylidene-D-sorbitol (MBS) (left), 1,3:2,4-dibenzylidene-D-sorbitol (DBS) (middle) and 1,3:2,4:5,6-tribenzylidene-D-sorbitol (TBS) (left).

Angyal and Lawler determined the connectivity of DBS as 1,3:2,4 through experimental hydrolysis to yield the previously reported 2,4-monobenzylidene-D-sorbitol.[128] In more recent work, it was found that 2,4-monobenzylidene-D-sorbitol forms via the rearrangement of 2,3-monobenzylidene-D-sorbitol (a less thermodynamically stable intermediate due to the five-membered ring).[129]

The synthesis of DBS proceeds with thermodynamic control, so it is safe to assume that bulky aromatic groups are equatorial on the acetal carbon atoms which form new chiral centres. The full structure was thus described in the 1970's by Brecknell as 1,3(*R*):2,4(*S*)-dibenzylidene-D-sorbitol.[130]

1.5.1 Synthesis

Murai *et al.* recommended using a mixture of solvents during DBS synthesis, selecting cyclohexane and methanol.[116] The hydrophilic solvent (methanol) aids dissolution of the starting materials, whereas the hydrophobic solvent (cyclohexane) supports precipitation of the product. The synthesis is a condensation reaction, and Song *et al.* were the first to use a Dean-Stark trap to remove water during the reaction.[131] Once crude DBS is produced, it is possible to remove the impurities (tri- and mono-substituted DBS) by washing with boiling water followed by boiling dichloromethane, respectively.[57]

1.5.2 Self-Assembly

Molecular mechanics analysis of a single DBS molecule confirmed an energy minimized structure with equatorial aromatic rings (Figure 1-9).[132] More recently,

Alperstein and Knani also determined the configuration of a single molecule, in agreement with those of Wilder[132], with phenyl rings in almost equatorial positions, but they also showed an intramolecular hydrogen bond between the 5-OH and 6-OH groups.[133]

Figure 1-9. Energy minimised structure of DBS reproduced from ref 132 with permission from John Wiley & sons.

The butterfly-like structure of DBS gives it its ability to self-assemble in a wide range of organic solvents.[86] DBS self-assembles via intermolecular hydrogen bonding (of the 5-OH/6-OH) and π-π stacking, although there is current debate over which is the predominant driving force for the self-assembly (Figure 1-10). Some argue that π-π stacking is the dominant contributor,[134] for others both π-π stacking and hydrogen bonds are considered crucial.[132] Various studies have investigated solvent polarity and DBS gelation.[135] As discussed in Section 1.3.4 DBS has often been studied as a gelator with HSPs due to its ability to gelate such a wide range of organic solvents,[77, 86, 87] although other sugar-based gelators have also been considered.[90] It has been argued that different interactions can dominate in different solvents. In low polarity solvents, intra- and intermolecular hydrogen bonding is favoured, whereas, in high polarity solvents, hydrogen bonding between DBS and the solvent becomes favoured, meaning any assembly has a greater solvophobic component.[135] It is thought that the 6-OH group is more important than the 5-OH group in the self-assembly of DBS, as it has been reported that gelation occurs when 5-OH is blocked by selective protection, but not when the 6-OH is blocked,[136] unless the moiety modification of the 6-OH involves a hydrogen bond donor.[137] On further analysis, Yamasaki *et al.* proposed that the 5-OH can intramolecularly hydrogen bond to an acetal oxygen or intermolecularly hydrogen bond with the solvent limiting gelation. The 6-OH is intermolecularly hydrogen bonded to an acetal oxygen, favouring self-assembly. This analysis led to a proposed self-assembly model of DBS, dominated by hydrogen bonding.[136]

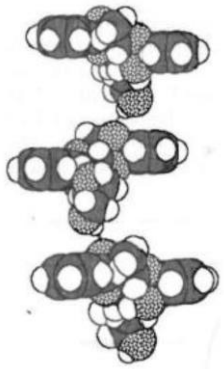

Figure 1-10. Qualitative model proposed by Yamasaki, dominated by hydrogen bonding adapted from Ref 136 with permission from The Chemical Society of Japan.

There is clearly a contribution from both hydrogen bonds and π-π stacking of DBS molecules depending on the solvent used. In non-polar solvents, intermolecular hydrogen bonding predominantly underpins self-assembly. For example, modelling DBS as a gelator for poly(propylene), Alperstein and Knani found the dominant intermolecular interaction was 6-OH/6-OH, with contributions from the corresponding 5-OH/6-OH and 5-OH/5-OH.[133] This agrees with the previous work from Yamasaki[136] and Wilder,[132] cementing the importance of the 6-OH group and the importance of solvent in the intermolecular interactions. No significant π-π interactions were observed but this is likely due to the apolar environment of poly(propylene). In more polar solvents, the solvent competes with these hydrogen bonding interactions, making them less significant, and the interactions of phenyl rings become more important, either through π-π stacking or solvophobic interactions. The ground state dimerization of DBS molecules was investigated in relatively polar alcoholic solvents by Watase *et al.*[134] In this work, it was suggested that the 1,3-phenyl ring and the 2,4-phenyl ring both overlapped with that of another molecule, meaning the self-assembly of DBS was facilitated by solvophobic effects and/or π-π stacking, although other calculations have suggested that the DBS molecules do not necessarily stack neatly on top of one another.[132] DBS seems to adapt to its environment, making it useful in a very wide range of industrial applications (see Section 1.8).

1.6 Derivatives of DBS

Modification of the aromatic groups tends to be via choice of benzaldehyde during DBS acetal formation.[138-143] Modification of the free alcohol groups (5-OH and 6-OH) can be achieved either before or after acetal formation. Feng and co-workers reported

numerous new DBS derivatives from modification of the aromatic groups in good yields (Figure 1-11).[144] Chen *et al.* also worked with methyl substituted DBS, showing organogel formation in propylene carbonate.[145] Other work also based on methyl substituted DBS and dichloro- substituted DBS demonstrated organogelation in a range of solvents, particularly alcohols.[131, 146] Dichloro- substituted DBS demonstrated different chiral nanostructures dependent on the solvent used. In non-polar solvents, rope-like left-helical fibres formed compared to smooth, non-helical fibres in polar solvents. Stan *et al.* demonstrated that the nitro derivative could be hydrogenated to amines, which could then be alkylated giving three additional derivatives.[147]

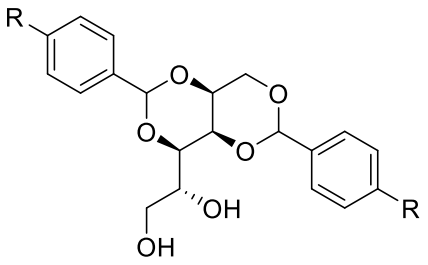

R = H, CH_3, OCH_3, CN, F, Cl, NO_2

Figure 1-11. DBS derivative modified on aromatic groups by Feng *et al.*[144]

The Smith group has reported the synthesis of novel DBS derivatives with ester, carboxylic acid and acyl hydrazide groups on the aromatic rings.[50, 57] The latter two compounds are formed from the conversion of DBS-ester by either saponification or hydrazination, respectively. Both of these latter gelators function in water – unlike DBS itself (Figure 1-12).[50] The nanofibres formed from these modified DBS derivatives have been shown to interact with additives and remove them from solutions.[50, 148]

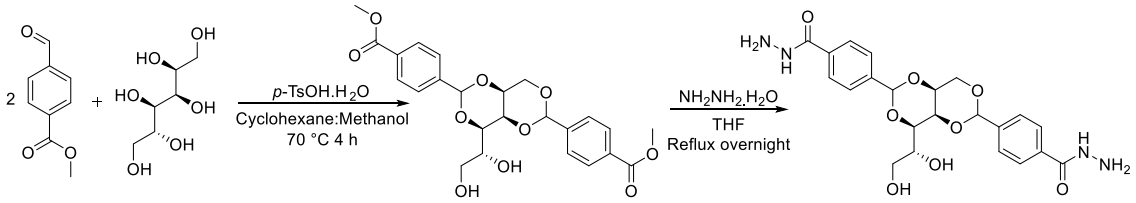

Figure 1-12. Synthetic scheme to form DBS-CONHNH$_2$ from Smith *et al.*[50]

The free hydroxyl groups were modified by Feng *et al.* who used acid chlorides to esterify the free hydroxyl groups into mono- or bis-esters.[144] Malle and Luukas also patented esterification of the more nucleophilic primary alcohol group, or both primary and secondary alcohols, attaching a variety of alkyl chain lengths.[149] They also

reported both diesters with different chain lengths, and a bola-amphiphile of DBS, using a diacid chloride to join two molecules of DBS.

1.7 Introduction of the BTA gelator

N,N',N"-Tris(2-ethylhexyl)-1,3,5-benzenetricarboxamide is one of many benzenetricarboxamide derivatives. For the purposes of this, BTA is used to represent any 1,3,5-benzenetricarboxamide derivative (Figure 1-13).

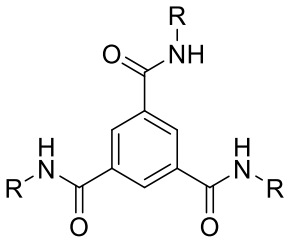

Figure 1-13. Generic BTA structure.

The first 1,3,5-benzenetricarboxamides (BTAs) were synthesised in 1915 by Curtius, who used benzene 1,3,5-tricarboxylic acid to reach the triacyl triazide from the triester.[150] More modern synthetic methods start with 1,3,5-benzenetricarboxylic acid chloride and react it with a range of amines under basic conditions to form a large variety of BTA derivatives.[151]

BTA compounds are usually C_3 symmetric, often referred to as discotic. These disc-like molecules often self-assemble into columnar aggregates.[152-154] BTA exists in monomeric form at high temperatures but self-assembles on cooling, in a cooperative fashion, to yield one-dimensional helical columnar stacks (Figure 1-14).

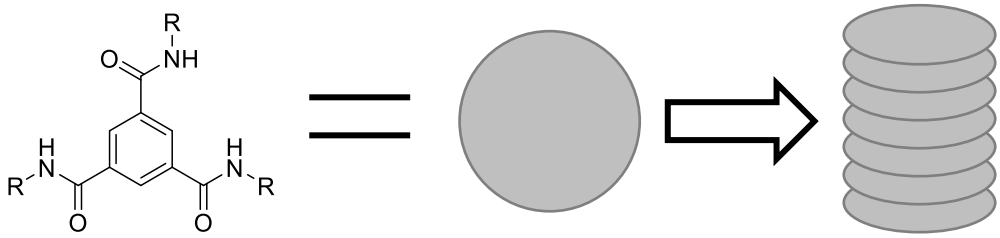

Figure 1-14. Schematic of BTA derivative self-assembly.

1.7.1 Self-Assembly of BTA Derivatives

BTAs have generated much interest because of their supramolecular aggregation. The general consensus is that they organise via three fold hydrogen bonding into helical

columnar stacks,[97, 98, 152-157] with large aspect ratios.[97, 158] Density functional theory was used to show BTA derivatives tend to forms one-dimensional aggregates from hydrogen bonding.[97] These hydrogen bonds were confirmed by IR spectroscopy.[152] A detailed study of the self-assembly of BTA derivatives using UV-vis and circular dichroism spectroscopy indicated a cooperative mechanism,[98] while CD confirmed the helical nature of the aggregates[159] resulting in a strong amplification of chirality. The introduction of a single chiral molecule can organise many achiral ones – a so-called "sergeants and soldiers" mechanism.[98, 153, 159-161]

Depending on the precise derivative, BTA can form supramolecular fibres through π-π stacking of the central aromatic scaffold in addition to hydrogen bonds between the amides. Aromatic amides tend to prefer co-planarity of both the benzene ring and the carbonyl group for reasons of conjugation, meaning that BTA monomers are planar and have zero dipole moments. However, the BTA structure requires a partial tilt (Figure 1-15) to satisfy the intermolecular hydrogen bonding demands,[154] thereby generating a dipole moment. As these generated dipoles of molecules orient in the same direction, the magnitude of the total column dipole moment can, in principle, increase with number of molecules in the column.[152]

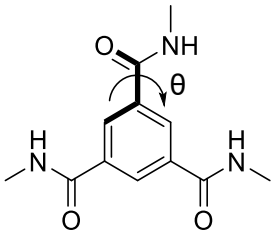

Figure 1-15. Partial tilt of amide out of plane ≈ 12 ° of BTA 1 from ref 154.

There is a disagreement in the literature about exactly how these macrodipoles are generated and the size associated with them. Traditionally all three intermolecular hydrogen bonds were thought to be orientated in the same direction.[152, 155, 162] Molecular dynamic simulations on a dimer of BTA showed two amide NH groups and one carbonyl oxygen oriented along the same direction as shown in Figure 1-16.[163] Each intermolecular hydrogen bond possesses a dipole moment between the carbonyl oxygen of one molecule and the amide hydrogen of another. Classical electrostatic interactions between these dipoles dictate the most energetically favoured configuration would have all dipoles antiparallel. However, three hydrogen bonds between a pair of molecules cannot all be antiparallel, so instead one hydrogen bond dipole flips. There are more conformations for two antiparallel interactions, meaning the

aggregate is stabilized on entropic grounds in addition to energetic grounds (depending on the substituent), making a two donor, one acceptor configuration thermodynamically more stable than a three donor arrangement (4 to 8 J mol^{-1}).[163]

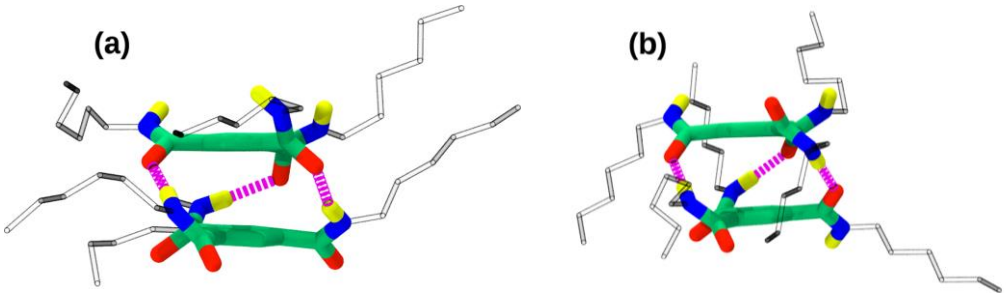

Figure 1-16. Two configurations of dimer of BTA derivative 2 (a) 3 donor, (b) 2 donor, 1 acceptor reprinted with permission from Ref 163. Copyright 2014 American Chemical Society.

However, both configurations will generate macrodipoles[155, 160, 161, 164-166] At low concentration macrodipole-macrodipole interactions are comparatively weak due to the distance between columnar stacks.[167] As higher concentrations are reached, the distances between columnar stacks become smaller, meaning the macrodipole-macrodipole interactions become more significant,[153] these macrodipoles can cancel each other out.

The details of self-assembly depend on the connectivity of the amide moiety (Figure 1-17). Both structures form columnar stacks with a preferred helicity, in the absence of any chiral centres, an equimolar mixture of left and right-handed forms. Both structures have been shown to be stabilised by 3-fold hydrogen bonding in the same way although C=O centred structures form stronger hydrogen bonds than N-centred structures due to the higher energetic penalty for rotation around Ph-NH compared to Ph-CO.[166, 167] Solid-state NMR and Car-Parrinello molecular dynamics show N-centred structures form asymmetric helices which lead to weaker aggregates,[168] and amplification of chirality is less pronounced (Figure 1-18).[154]

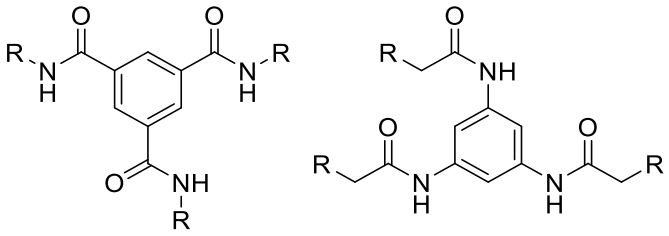

Figure 1-17. C=O centred BTA structure and N centred BTA structure.

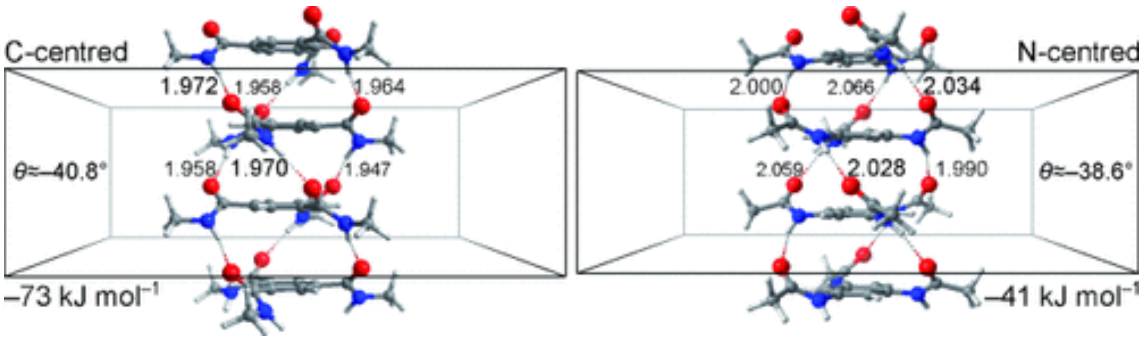

Figure 1-18. Self-assembly of BTA derivatives 3 into columnar aggregates reprinted from Ref 154 with permission from John Wiley & sons.

Other subtle changes in the chemical structure can also influence columnar order. Removal of the aromaticity from the core results in larger dipoles.[167] This is probably due to the decrease in restricted rotation around the bonds associated with the cyclic backbone and potential energy penalty for conjugation with the aromatic ring. Changing the aromaticity of the core did not affect self-assembly (Figure 1-19).[165]

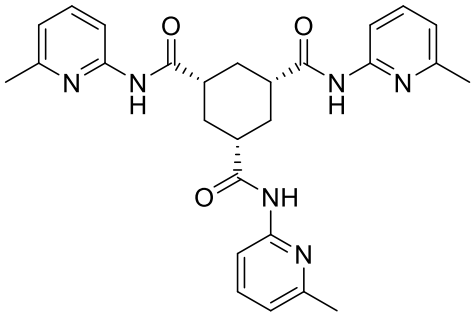

Figure 1-19. An example of a cyclohexane triamide derivative 4 which demonstrated three fold hydrogen bonding from ref 165.

Self-assembly of BTAs also depends on the composition of the peripheral groups. Subtle changes in the side groups can influence both the morphology and behaviour of the materials formed. Bushey described a substituted core with groups other than hydrogen on the 2,4,6 positions. These structures formed the same hydrogen bonding interactions as the unsubstituted system.[169] Introduction of chiral, non-racemic, soluble alkyl side chains gives one-dimensional aggregates with a preferred helical sense.[98, 159] Chirality has even been introduced using isotope substitution. The first example of isotope substitution to induce supramolecular chirality was achieved by Cantekin *et al.* Specifically deuterium substitution was used to introduce chirality, resulting in small energy differences between different diastereomers which are amplified on self-assembly.[157]

A solid-state study of bulky side groups on a BTA core, showed that self-assembly was driven by the packing of side groups (π-π stacking) not intermolecular hydrogen bonding as usual. However, this is due to the balance between the intermolecular interactions, meaning this consideration is only relevant for very sterically-demanding side chains such as in Figure 1-20.[170]

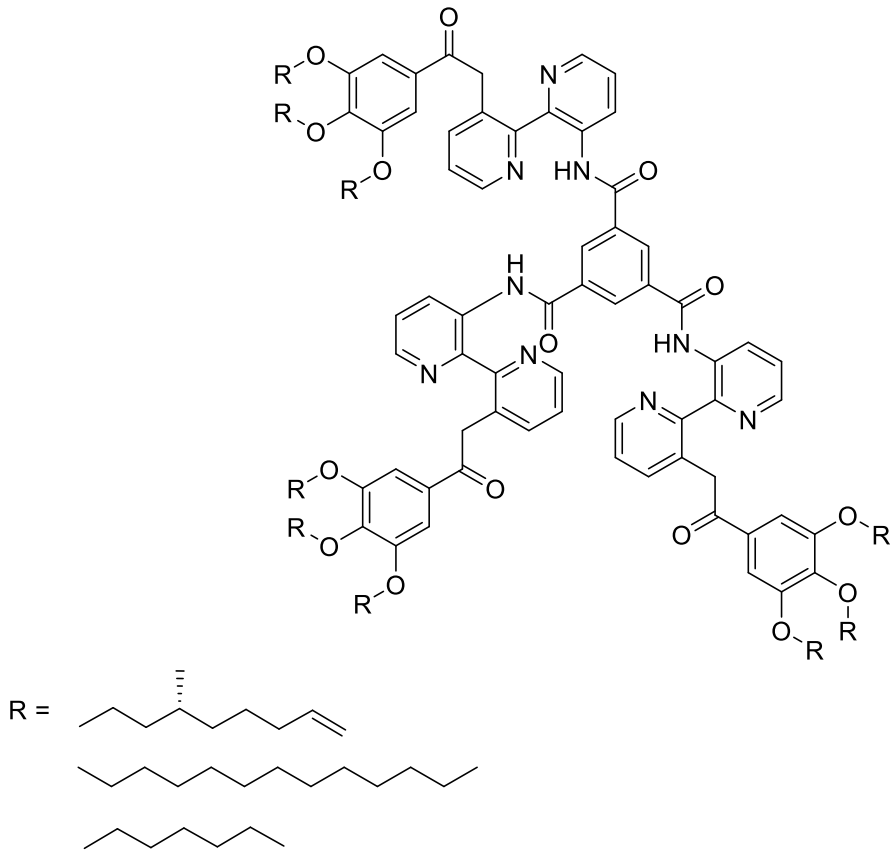

Figure 1-20. Example of sterically demanding side chains with side group packing dominating the self-assembly, BTA derivatives 5,6 and 7, from ref 170.

The different substituents can also lead to different materials behaviour on a bulk scale. C=O centred structures show liquid crystal behaviour with simple linear chains as substituents. Aggregation can be further stabilized by branched side chains rather than linear chains.[152] N-centred structures only show liquid crystallinity with chiral substituents.[151, 154]

Molecular structure can also influence the properties of BTA derivatives. A study comparing three derivatives (Figure 1-21) showed differences in nanofibre diameter of up to an order of magnitude (0.21 μm for BTA 10 *vs.* 2 μm for BTA 8). Through nanomechanical bending experiments, the rigidity of nanofibres formed from different derivatives, showed up to three orders of magnitude difference. The Young's modulus

clearly showed the different size effects,[156] and the numerical values achieved were comparable to electrospun poly(amide) fibres.[171] Through tuning the molecular structure, the macroscopic properties (including toughness) could also be tuned.[156]

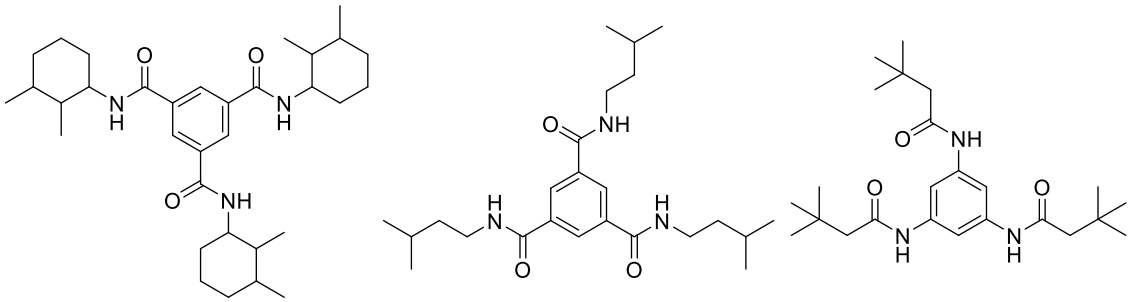

Figure 1-21. BTA derivatives investigated for mechanical properties, BTA 8, 9 and 10.

Two component BTA based gelator systems have also been reported. The combination of a N centred and a C=O centred BTA gave more stable packing than a single component and resulted in a different morphology, which was tuneable by the ratio of components.[172]

1.8 Applications of LMWGs

The tuneability and ability of gels to responsd to stimuli has allowed them to be used in a range of applications[35] including lubrication,[173-175] nucleation and clarification of polymers,[176] the food industry,[177-179] ink products,[180] 3D printing,[181] wood stain,[182] fluid detergents,[183] controlled fragrance release,[184] improved stability in black crayons[185] and personal care products[149, 186-188] with potential future applications in catalysis,[189-193] tissue engineering/regeneration,[194-205] sensing,[60, 206] and even art conservation[207, 208] among many others.

One of the oldest applications of supramolecular gels is as a lubricant, in fact, early gel-type greases were used in the Middle East on chariot axles from the 17th century BC. Lithium grease based on the lithium salt of 12-hydroxystearic acid (Figure 1-22) overcame significant problems with previously used greases based on animal fat, particularly improving thermal stability and water solubility.[209, 210] Lithium grease was marketed as a multipurpose grease, underpinning modern grease technology. Later a series of bis-urea gelators was patented for use as lubricants.[173-175]

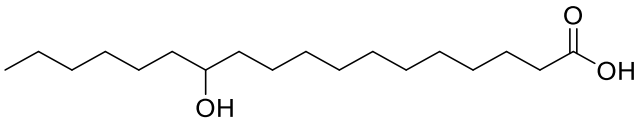

Figure 1-22. Chemical structure of 12-hydroxystearic acid.

World War II created an interest in mineral oil gelation, leading to one of the earliest multicomponent gels. In 1942, Napalm was developed at Harvard University,[211] a powder which is mixed with fuel to form a flammable gel. The formulation was not published until the end of World War II, but original Napalm was a mixture of aluminium salts of naphthenic and palmitic acids,[212, 213] leading to the name, **na**phthenic and **palm**itic acids, Figure 1-23.[214] Naphthenic acid is an unspecific mixture of several cycloaliphatic carboxylic acids with a range of backbone lengths. Napalm was used extensively by the U.S. as an incendiary agent in flamethrowers and bombs. A slow burn rate at a high temperature, and with good adhesion to surfaces to increase its effectiveness. Napalm causes severe burns (second and third-degree burns) against personnel and generates large amounts of carbon monoxide as it deoxygenates available air, as it burns through incomplete combustion. Modern napalm replaced the LWMG with poly(styrene) and benzene to gel the fuel.

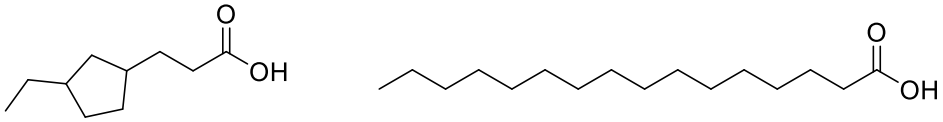

Example of a naphthenic acid Palmitic acid

Figure 1-23. Napalm is based on a mixture of aluminium salts of naphthenic and palmitic acids.

Small molecule hydrogels have been used in pre-clinical regenerative medicine research to restore biological and mechanical function to tissue.[35] Self-assembling peptides have been used to repair severed optical tracts of hamsters. Application of hydrogel promote regeneration and knit brain tissue together, allowing restoration of vision.[196] Alakpa and co-workers observed stem cell differentiation and growth on supramolecular scaffolds, based on peptide hydrogels with tuneable physical properties.[202]

The nucleation and clarification of thermoplastic polymers is a current significant use of LMWGs.[176] The gelator is dissolved in a polymer monomer, and as the system cools, the gel network self-assembles and the nanofibres formed help nucleate the

polymer.[215] This results in improved mechanical properties, shorter processing times and reduces the haze of the resulting material (improving the clarity).[216] DBS and it's derivatives are widely used as nucleating and clarifying agents,[51, 217-219] for example, <0.7 wt% DBS in poly(olefins) gave rise to increased transparency, with resistance to shrinkage of moulded plastics.[220] This structure was further modified on the periphery aromatic rings, to improve the properties of the materials formed.[114, 221] Fluorinated DBS demonstrated excellent resistance to shrinkage and heat deterioration, with improved clarity and without loss of mechanical or chemical properties, and was patented as a clarifier for poly(olefins) for injection mould plastics such as syringes.[222] These derivatives also increased the temperature of polymer crystallisation, allowing the moulds to be opened more rapidly after injection, leading to cost saving by reducing processing times. DBS and its derivatives are used for packaging for cosmetics, transparent doors and electric component parts,[114, 220] but were not suitable for poly(propylene) food packaging due to the transfer of odour and taste to the food. To overcome these issues, the aromatic rings were substituted with alkyl groups, reducing leaching.[223] Millad®3988 is dimethyl substituted DBS (with methyl groups in the para and one of the meta positions on both aromatic rings) and is marketed by Milliken with extensive industrial use. Millad®8000 has been further optimised by modification of the sorbitol backbone in addition to the para position of the aromatic rings (Figure 1-24).[224] DBS has also shown improved crystallisation rates with other polymers such as poly(lactic acid)[225] and ultrahigh molecular weight poly(ethylene).[226]

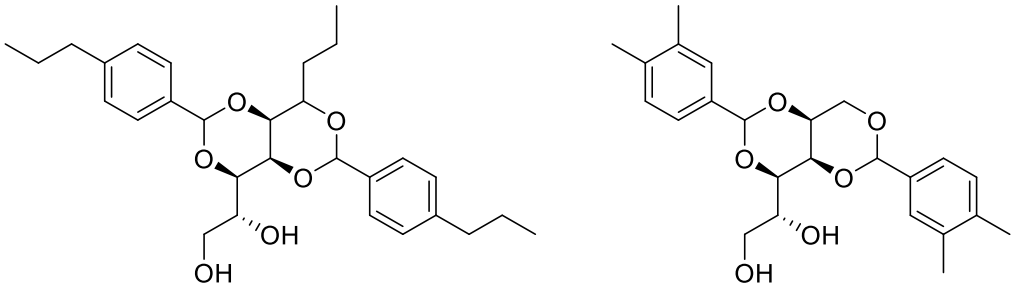

Figure 1-24. Structure of Millad®8000 and Millad®3988, DBS based gelator.

As potential nucleating and clarifying agents for isotactic poly(propylene), there is an important comparison between BTA-type materials and DBS-type materials. Sorbitol derivatives (DBS based), at low concentrations (0.1-0.3 wt%), increase the peak crystallisation temperatures of isotactic poly(propylene), reducing the necessary production cycle. These derivatives also reduced the turbidity of the produced polymer by 65%. However, these derivatives can come with issues such as sublimation, blooming and thermal decomposition. Similarly to DBS, BTA derivatives have been

shown to nucleate and clarify polymers.[158, 217, 219] BTAs with bulky, aliphatic side chains are effective clarifying and nucleating agents for isotactic poly(propylene).[158] Using very low weight percentages (0.02 wt/v%), BTA derivatives can tune the turbidity of isotactic poly(propylene) to highly transparent with almost no haze. They can also induce the mechanically distinct isotactic poly(propylene) β polymorph which helps provide toughness. The α polymorph can increase strength and stiffness.[217] Therefore, by tuning the BTA derivative and the amount used, the balance between the two polymorphs can be controlled. For example, BTA 12 induces a fourfold increase of the β polymorph compared to BTA 11 (Figure 1-25).[217]

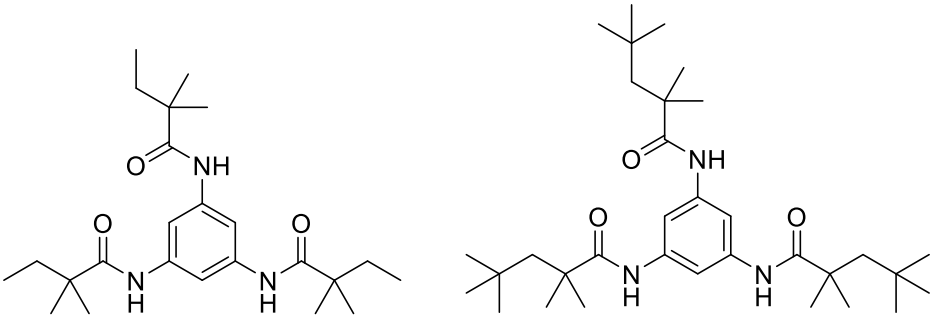

Figure 1-25. BTA derivatives 11 and 12 for inducing different polymorphs in isotactic poly(propylene) from ref 217.

The combination of polymers with LMWGs has been demonstrated to improve composite performance.[59] Nanoporous membranes have been templated by LWMG nanofibres, by polymerisation of methacrylate,[227, 228] methyl(methacrylate)[229] and poly(lactic acid),[230] followed by subsequent washing out of LMWG nanofibres. A general schematic of templating can be seen in Figure 1-26. Moffat and Smith enhanced the modulus of poly(styrene) using self-assembled nanofibres, by an order of magnitude, with potential for toughened coatings.[231, 232] Tseng and Lai also demonstrated DBS-templated polymerisation of styrene in the presence of a chemical cross-linker.[233] This poly(styrene) showed a specific surface area much greater than the untemplated counterpart.[234] DBS and its derivatives[235] have also been used to direct the orientation of polymer crystallisation in the case of poly(propylene),[236] poly-(ε-caprolactone)[237] and even in electrospun poly-(ε-caprolactone).[238] Just as polymers can be templated, other structures can be templated using this method too. Shinkai *et al.* used cholesterol-based gelator nanofibres as a template to prepare hollow fibrillar silica,[239] before demonstrating that chirality could be transferred into the sili*ca.*[240, 241]

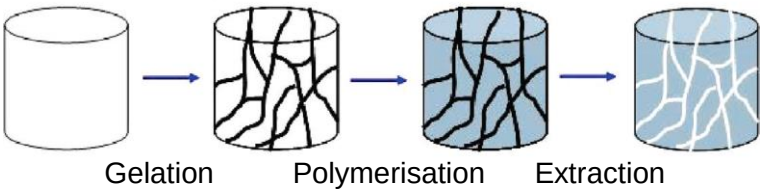

Figure 1-26. Example schematic of templating with LMWG and polymer; homogeneous solution of gelator and monomer formed then LMWG network is formed (through external stimuli such as cooling), polymerisation occurs then LMWG network is extracted (e.g. washing, heating etc…) adapted with permission from Ref 234. Copyright 2009 American Chemical Society.

Nakano and co-workers modified the surface roughness of glass using a supramolecular polymer. A perfluoroalkyl gelator was applied to the surface of the glass, leaving a thin film xerogel as the solvent evaporated. The packing of the gelator fibres on the dried glass surface, led to an increase in surface roughness and hence hydrophobicity, as demonstrated by water contact angles >150°.[242]

LMWGs have been used in personal care products. Some deodorant gel sticks are based on LMWGs. DBS has been used as a gelator of glycols and alcohols with acidic aluminium antiperspirant salts, producing clear antiperspirant sticks,[243] originally patented by Roehl for RightGuard, with a long history of formulation optimisation.[186, 187] Other companies have patented other gelators such as 12-hydroxystearic acid and its derivatives for this use, even investigating two component gel systems.[244] Further optimisation of deodorant sticks is ongoing. L'Oréal patented DBS esters for lipstick production, demonstrating significant advantages compared to wax-based lipsticks.[149] A range of organogelators have been used in water and oil emulsions as oil-soluble thickeners for a range of personal care products including sunscreen, foundation and other creams.[188]

The world's first glue stick, 'Pritt Stick' was launched in 1969 as a small and portable way to accurately apply adhesive (similar to lipstick), and was based on long chain aliphatic acid salts. In aqueous solvents, these formed gel-like solids to support the polymer adhesive.[245] The polymer adhesive used was changed to improve the formulation.[246] DBS has also been reported as a gelation agent for glue stick formulation, with improved performance and stability in hot-humid climates.[247] Incorporation of different solvents further improved the safety of DBS-derived glue sticks.[248]

Dental composites made with methacrylate polymers can have incomplete photopolymerisation of the monomers, leading to oral health issues. These composites can also suffer from shrinkage. LWMGs including DBS have been investigated as additives to dental polymers and showed improvements in terms of preventing shrinkage.[249, 250] A range of organogelators based on oxalyl amides and amino acid sugars, have been patented for the modification of dental composites.[251] The range of gelators named in this patent is rather large, suggesting careful formulation and tuning of rheological properties could result in numerous dental applications, including corrective dentistry and prostheses such as crown, dentures, veneers and artificial teeth.

LWMGs have shown potential in the clean-up of oil spillages due to their inherent ability to gel oil selectively.[252] In 1976, Saito and co-workers patented a glutamic acid based gelator in benzene, which took only 20 minutes to selectively gel oil in the presence of seawater.[253] The gel formed could be easily separated from the seawater by simple filtration. DBS and derivates were also patented for this application by Kobayashi and co-workers in 1985. Sprayed onto kerosene in sea water, a DBS-containing solution gelled the fuel, the resultant gel could be lifted off the seawater and allowed fuel recovery.[254] A range of LMWGs have since been reported as selectively gelling hydrocarbons and a variety of fuels from their biphasic mixtures with water.[255, 256]

Work by Ragahavan and co-workers demonstrated the potential of supramolecular gelators (DBS) to limit crude oil loss to the environment in the event of underwater pipeline damage. Toluene was used as a model of crude oil, with DMSO as a co-solvent to fully solubilise the gel rendering the gelator inactive and allowing the solution to flow through the model underwater pipeline. If the system encountered a leak, the DMSO partitioned in the surrounding water, dropping the polarity of the effective gelator solvent and inducing gelation. The gel forms selectively at the pipeline damage, minimising further loss of oil (Figure 1-27).[257]

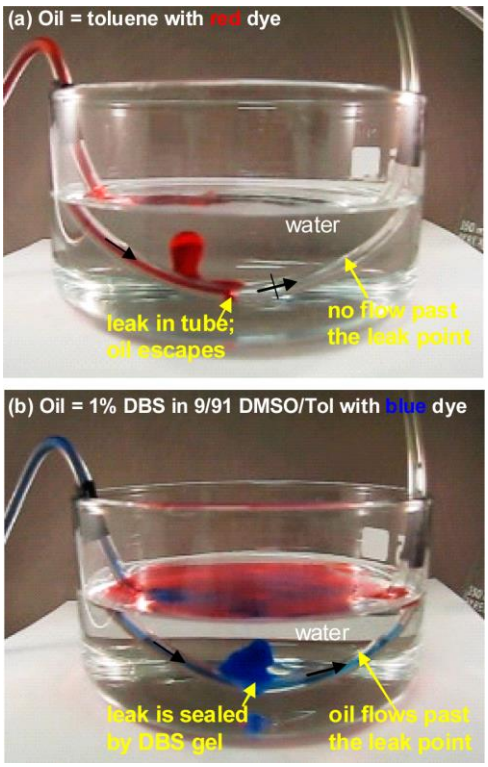

Figure 1-27. Demonstrating self-repair of an oil leak from a tube submerged in water with gelator present adapted with permission from Ref 257. Copyright 2015 American Chemical Society.

Supramolecular nanofibres have potential as environmental remediation agents. Their large surface area lends itself to adsorb large quantities of contaminants.[258] For example, a phenylalanine-based hydrogel was dried with divalent metals, creating a dried metallated xerogel which demonstrated dye uptake.[259] In another nice example, Hayes and co-workers used aromatic urea-based gelators to achieve much higher dye uptake levels,[260, 261] although in the initial work gels were formed in the presence of dye but later used the addition of a preformed gel to a solution containing dyes. The Smith group demonstrated that DBS-$CONHNH_2$ could demonstrate high levels of dye removal from water.[50] Further work demonstrated selectively removing precious metals from a solution containing other common metals. Nanofibres nucleated the reduction of precious metals (Au, Ag, Pd and Pt) into nanoparticles due to their reduction potentials. The gold embedded gel was then strengthened by agarose and used as a modified electrode surface.[148] Many authors also report the reusability of gels when used for water purification, where the contaminants can be extracted and the gel recycled.[50, 262]

LMWGs have also been investigated for drug delivery, pioneered by Leroux and co-workers, who use L-alanine and tyrosine-based organogelators for a variety of drug

delivery systems.[263-265] These include controlled release over two to three weeks of leuprolide, a drug used in prostate cancer hormone treatment.[266] A hydrogel formed from pyrene-functionalised Vancomycin exhibited improved antibiotic activity. Although drug release was not achieved, this could be used in wound dressings due to the mechanism of Vancomycin activity.[267] A wide range of drug molecules have been modified into gelators and used for drug release or pharmaceutical activity.[62, 268] Organogels based on fatty acid esters have incorporated drugs such as tramadol for external application, giving high skin permeability and drug release, thus allowing efficient transdermal absorption of pharmaceutical composites.[269] Ibuprofen has demonstrated sustained release from 12-hydroxystearic acid organogels,[270] while other drugs are rapidly released.[271] Ibuprofen and naproxen have been encapsulated and demonstrated pH-mediated drug release from DBS-$CONHNH_2$ hydrogels (Figure 1-28).[272] The gels were prepared with both pharmaceutical and gelator present and naproxen was fully released at pH >5.5. Chivers *et al.* recently combined this work with a photo-initiated polymer gel resulting in a hybrid gel with directional pH release.[273] The tunability of a two component approach was further demonstrated by Barthélémy and co-workers who reported an injectable hydrogel for controlled release of a model protein in an animal model.[274] The encapsulation of a pharmaceutical within a gel can have additional benefits. Pseudoephedrine is a highly effective over the counter decongestant which can be used in the synthesis of methamphetamine. By encapsulation inside an LWMG, it can still be used for its decongestant properties with controlled release but makes extraction of pure pseudoephedrine time consuming and tedious. If used as a gel in the synthesis of methamphetamine, the gel would break down and contaminate the product, thereby allowing the continued use of pseudoephedrine as an over the counter medication.[275] BTA derivatives are stable under aqueous conditions, but through the introduction of water-labile groups, microcapsules can be prepared that hydrolyse over time or under specific conditions, can release into the environment.[276] This allowed the production of BTA based micro-capsules for drug delivery with an ‘all or nothing’ cargo release through a predictable pH-dependent degradation with non-toxic byproducts.

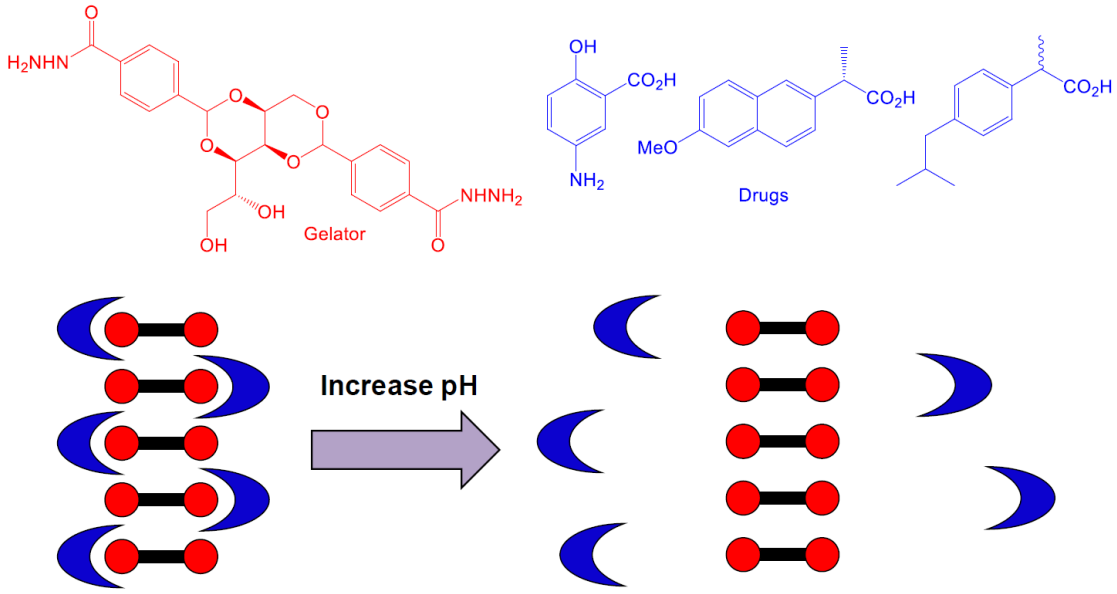

Figure 1-28. Hydrogel formed with DBS-CONHNH$_2$ showed pH-dependent release of mesalazine, naproxen and ibuprofen, reproduced from Ref 272 with permission from The Royal Society of Chemistry.

LMWGs have also been investigated in the presence of CWAs and their mimics. Lee and co-workers demonstrated a urea functionalised LMWG which led to a gel-sol transition on exposure to liquid nerve agent simulant (diethylchlorophosphate - DCP).[277] Gale and co-workers attempted the first gel-phase remediation of CWAs. Cyclohexylidiamide based gelators could gel nerve agent simulant (dimethyl methylphosphonate - DMMP) effectively immobilising it.[278] A more reactive nerve agent (DCP) could not be gelled but did result in a gel-sol phase transition with accompanying colour change. These same organogels made with DMSO and 4-nitrobenzaldoxime (used for CWA decontamination) could be used to absorb, encapsulate and decontaminate relative volumes of both simulants (DCP and DMMP) *in situ*.[279] If large volumes of DCP were present, the organogel collapsed to release local, high concentrations of the reactive decontaminant. Gale and co-workers developed a simple LMWG which could detect soman and chemical weapon simulants, DCP and DMMP (Figure 1-29) causing a gel-sol transition.[280] To create a practical detection mechanism, they embedded a copper coil in the gel; as the gel broke down, the coil dropped, completing a circuit with electrical contacts to result in illumination of a 'warning' light (Figure 1-29).

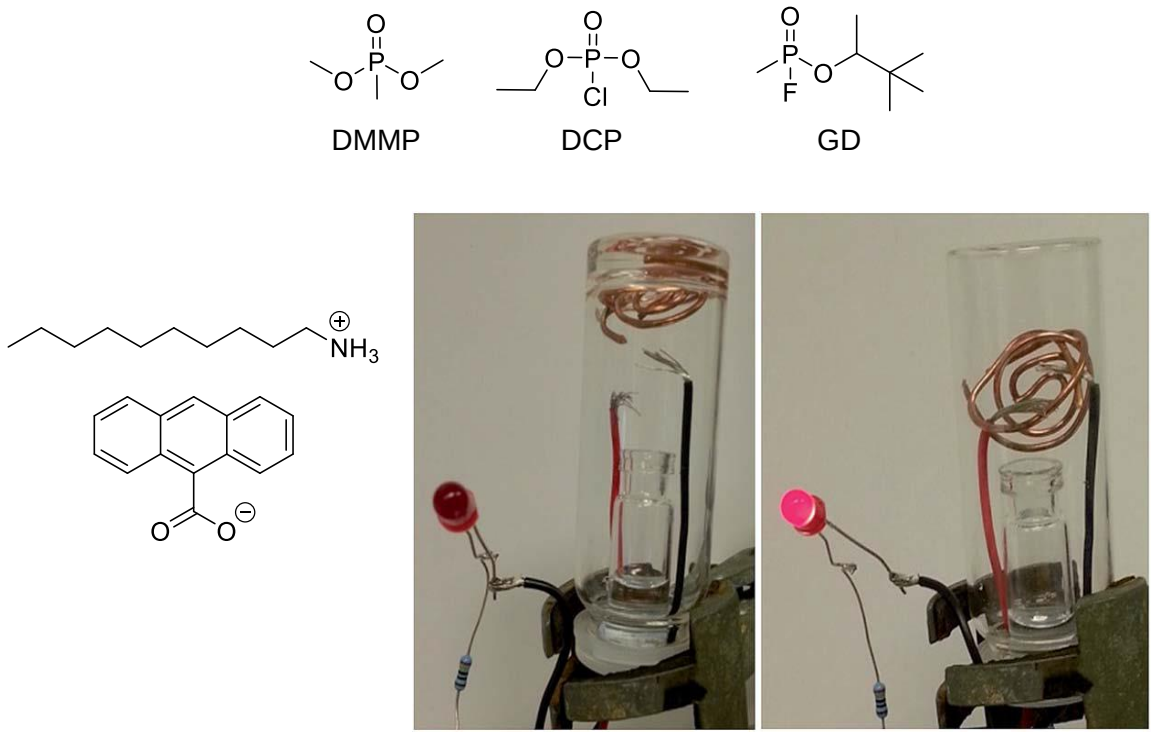

Figure 1-29. Chemical structures of CWA simulants; dimethyl methylphosphonate (DMMP) and diethylchlorophosphate (DCP) with chemical warfare agent soman (GD) followed by gelator used to create gel, left image: Copper coil suspended in organogel above sample vapour; right: organogel dissolved resulting in release of copper coil completion of electrical circuit and illuminated 'warning' LED reproduced from Ref 280 with permission from The Royal Society of Chemistry.

1.9 Two component gels

As described by Buerkle and Rowan, there are multiple ways to form a gel with two components: (i) two components both required for gelation, (ii) two components which form gels individually, or (iii) a gelator and an additive.[32, 281, 282] Examples of additives are found in the literature,[283] as these can both help and hinder gelation,[284, 285] but will be discussed in more detail in Section 1.10.1.

For systems where both components have potential to gelate, there are four scenarios as shown in Figure 1-30 and proposed by Adams, Raeburn, Buerkle and Rowan.[32, 281, 282] The gelators can: (a) coassemble in an alternating way or (b) coassemble in a random way, (c) self-sort into individual fibres or (d) disrupt the gelation so no gel forms. Cooperative, orthogonal and disruptive mixtures are all seen using different mixtures of gelators.[286] The structure of the gelators plays a vital role in the outcome.

Different structure motifs encourage self-sorting, while similar structures encourage co-assembly.[281]

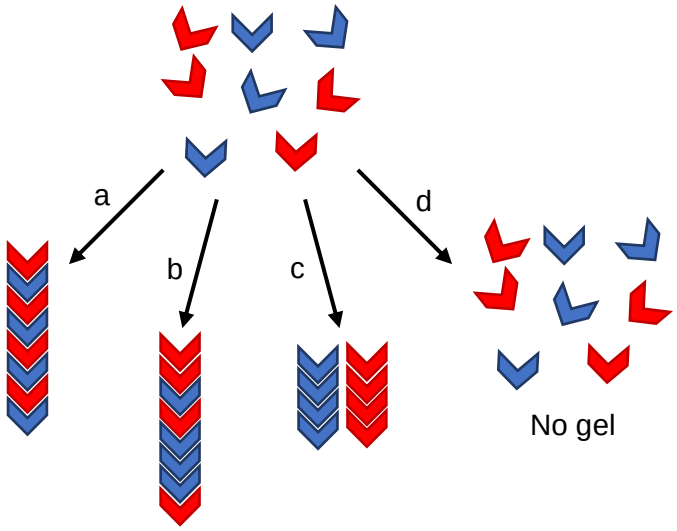

Figure 1-30. Schematic of options for two gelator component system: (a) ordered coassembly, (b) random coassembly, (c) self-sorting and (d) gelation disruption.

Sugiyasu and co-workers created a temperature driven self-sorting network, generating bulk heterojunctions with potential use in optoelectronic devices.[287] They found that the absorption spectra and circular dichroism were purely additive, with direct overlap of the individual components in the mixture. Smith and Smith also demonstrated a self-sorting two component system based on a protected sorbitol derivative and cholesterol-based gelator, which was characterised by NMR spectroscopy, and DSC and SEM image analyses to show two independent networks.[288] The independent self-sorting networks were detectable at molecular, nano-, meso- and macro length scales. DSC analysis showed independent thermal characteristics, associated with each individual gelator, both present in the mixture. SEM was inconclusive due to similar length scales of the fibres created. Moffat and Smith showed two different fibre diameters, illustrating true self-sorting via SEM.[289] Their results also demonstrated that one network can dominate specific properties of the mixed system, in this case thermomechanical. Draper and co-workers also demonstrated self-sorting of two different fibre diameters (although closer in size than the previous Smith work), with absorption spectra that were direct additions of the individual components.[290]

In 2016, Onogi and co-workers demonstrated *in situ* real-time imaging of self-sorted supramolecular nanofibres consisting of a peptide gelator and an amphiphilic phosphate.[291] Similar fibre morphologies were indistinguishable by TEM. However,

different fluorescent probes added to the nanofibres allowed visualisation of self-sorted fibres through confocal laser scanning microscopy.

Adams and co-workers used a range of two component LMWG systems to demonstrate different co-assemblies on sequential protonation of the two gelators with different pKa values to prepare gels with different material properties.[286] They also produced another two component LMWG system using the same principle. On UV irradiation after assembly, the trans isomer of one gelator could be converted to the cis isomer, disassembling one of the networks. The G' of the gel network decreased as the second network disassembled in the presence of the first.[292] Cornwell *et al.* produced a multicomponent gel based on two DBS derivatives, which were pH-triggered at two different pH values, leading to multidomain formation. The first gelator was protonated and assembled, then the second gelator was assembled by UV irradiation of a photo-activated acid generator. The use of a mask allowed one network to be written into another as the pH was only lowered in the unmasked region.[293]

The properties of two component systems can be tailored by tuning the ratio of components.[32, 294] In some cases, non-linear effects are observed, with one gelator directing the assembly through a 'sergeants and soldiers' effect.[294] The absolute modulus of a gel (found by rheology) can be the average of the two combined systems or higher than expected (order of magnitude higher than either individual gelator), suggesting coassemblies with synergistic effects. This work also demonstrated cooperative, disruptive and orthogonal assemblies from different mixtures, resulting in different gel properties.[286]

1.10 Branching

Increasing fibre branching can change the behaviour of nanofibre materials and may yield smart nano-fabrics with enhanced behaviour. Both physical and chemical approaches to achieve branching will be considered here.

1.10.1 Physical modification (additive)

One approach to modify the morphology of self-assembled fibres and introduce branching is the addition of a soluble polymer.

Liu *et al.* in 2002, provided the first evidence that branching can be induced by additives. In two papers, the authors used L-DHL (lanosta-8,24-dien-3β-ol:24,25-dihydrolanosterol = 56:44) in di-isooctylphthalate to demonstrate the concept. At 10 wt% using a heat-cool method, under SEM coupled with a CO_2 super-critical fluid-

extraction technique, the gelator formed only non-branched needle-like fibres, with the temporary contact with each other forming an opaque, viscous paste. However, on adding 0.004/0.006 wt% ethylene/vinyl acetate copolymer (EVACP) the microstructure changed and interconnecting nanofibres were formed, creating a solid-like gel. The rheological properties changed as a function of concentration of additive. The authors introduced the concept of “crystallographic mismatch”, where the additive strongly adsorbs on the growing tip of the fibre, therefore hindering the sequential perfectly symmetric alignment of L-DHL needed to grow fibres in an axial manner, so instead the fibres can also grow through a two-dimensional mechanism (Figure 1-31). The authors proposed that EVACP affects the kinetics of fibre formation rather than bridging existing fibres.[295,296]

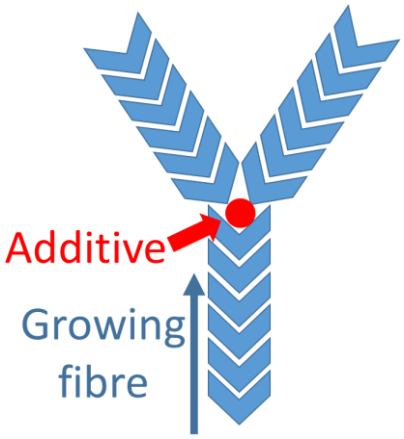

Figure 1-31. Schematic of physical additive branching.

The authors also managed to achieve branching without using an additive with a different gelator, GP-1 which they also identified as occurring via a “crystallographic mismatching” growth mechanism (Figure 1-32).[297] Branching occurred spontaneously during self-organization of the network at room temperature in an initial nucleation – growth – branching – growth – branching process. In their later work, they continued to influence gel properties, forming spherulites in propylene glycol and mixed fibre/spherulites in benzylbenzoate. Upon addition of poly(methyl methacrylate comethacrylic acid) (PMMMS) and EVACP, fibre nucleation slowed and the amount of branching increased. However, EVACP actually inhibited fibre formation in propylene glycol and only spherulites were formed.[298,299]

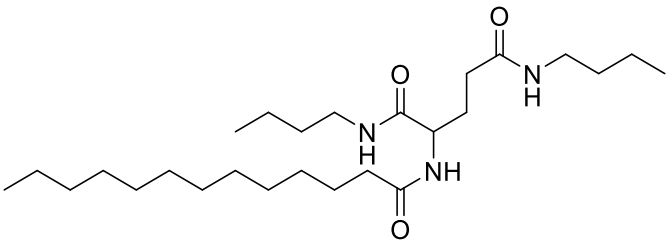

Figure 1-32. Chemical structure of GP-1 gelator from ref 297.

Cui *et al.* demonstrated stabilisation of a gel on addition of poly(2-hydroxyethyl methacrylate, which helped prevent collapse into needle-like crystals.[46] The authors suggested this was due to the branching effect originally suggested by Liu *et al.*[296] Rogers and co-workers investigated non-isothermal cooling effects on fibre length using 12-hydroxystearic acid, also attributed to a crystallographic mismatch mechanism.[300]

Chakraborty and co-workers found that incorporating chitosan into a folic acid gel increased the density of branches and improved mechanical properties.[283] Three different polymers were added to benzenedicarboxylic acid derived gelators, increasing gel strength for two of the polymers investigated.[301] The Adams group added dextran to naphthalene-dipeptide hydrogelators (in a pH-dependent system) and demonstrated that on changing the molecular weight or wt% of the dextran, the viscosity of the system and therefore the gelation time changed, leading to a reduction in mechanical strength. They argued that the increased viscosity slowed the diffusion of the LMWG and therefore slowed self-assembly and limited lateral interactions.[302] This is quite a different observation to those reported previously particularly by Liu. Later work by the Adams group investigated the rheology of gels with various dextrans and polymers. Again, they found that additives decreased mechanical strength as the interconnectivity of the spherulites decreased. The work suggests that the polymer identity can have a substantial effect on the rheology of the gel, with some polymers having indirect effects (viscosity changes) and others have direct interactions with the gel fibres.[303] There is an ongoing debate in the literature as to whether the mechanism is indeed a physical mismatch (therefore branching) mechanism or whether the results are due to increased solvent viscosity. Nonetheless, in the literature, it has been shown that a very small amount of polymer additive can have a significant impact on the properties of a gel.

1.10.2 Chemical modification (dimer)

Chemical modification for branching would require adapting the chemical structure to try and encourage branching. This would be an innovative step and there is no

literature precedent. Hayes and co-workers have successfully linked two gelators by an alkyl group and demonstrated correlations of chain length with mechanical properties and minimum gelation concentration.[304] Encouraging branching using this method will be discussed further in Section 1.13.

1.11 Fabrics

Fabrics are created with a hierarchical structure similar to an LMWG. The smallest units are called fibres (analogous to fibrils), characterised by being much longer than they are thick. These fibres are interlaced to form threads (synonymous with gel fibres). Threads are twisted to form yarns (larger DBS fibres) and yarns then make up the fabric (equivalent to a full gel network).[305] However, it is important to note that all of these objects are several orders of magnitude larger than nanofibres. There are many different types of fabrics including wovens, knits and non-wovens. Their names describe the manufacturing process used to create the fabric. Fabrics are used for many different applications including clothing and bedding, but also for less common applications such as protection or filtration.

Typical wovens consist of a warp (longitudinal threads, along the length of fabric) and a weft (perpendicular directional threads or transverse threads), which are then woven together. Knits consist of loops of yarn, called stitches. Knits contain wales (vertical threads) and courses (horizontal threads). The type of yarn/fibres, stitch type and needle size can all be tuned to achieve a specific property such as heat retention. Similar to weaving, a knit is a two-dimensional fabric, but in a knit, the yarn follows a meandering path rather than the straight parallel yarns seen in weaving. Each yarn forms loops above and below its mean path allowing it to be stretched in different directions, giving knitted fabrics more elasticity than woven fabrics, which means knitted fabrics are more easily deformed. Non-woven fabrics are simply sheets of fibres (often polymers) physically or chemically connected, with voids and openings. These random fibre webs are weak. There are different mechanisms of strengthening, including adhesive bonding, mechanical interlocking by needling, fluid jet entanglement and thermal or stitch bonding.[305] A schematic of the different basic fabric types is seen in Figure 1-33.

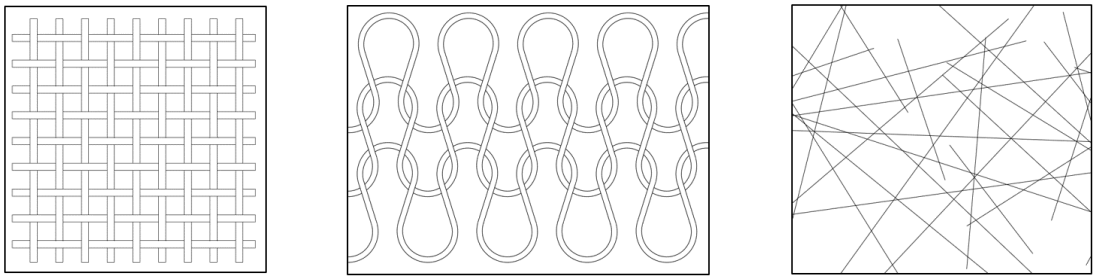

Woven Knit Non-woven

Figure 1-33. Schematic of different fabrics; woven, non-woven and knit.

The fibres used to make a fabric can be natural or synthetic. Synthetic fibres tend to absorb less water and have better mechanical properties than natural fibres. The nature of the fibre also determines fabric properties such as lifetime, coating compatibility, water absorption, adhesion etc.

Cotton is the most widely used fabric in the world. It has its excellent properties, being comfortable, easy to dye, stable and high-water absorption. It is made almost entirely of cellulose (90-96 wt%), which is a natural product (Figure 1-34).[306, 307]

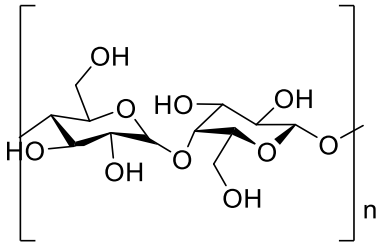

Figure 1-34. Structure of cellulose.

Cotton is one of the main textiles which has been modified, for example changing the hydrophobicity, increasing the reactivity towards dyes, and developing self-cleaning, anti-stain or conducting fabrics to reduce build-up of static charge.

1.12 Fabric Modification

Fabrics have been modified or altered for millennia; for example, the ancient Egyptians used herbs and spices as antibacterial agents to preserve their wraps for mummies.[308] Fabrics can be modified in a variety of ways; the structure of the fibre which makes up the fabric can be replaced completely and redesigned for a specific purpose (such as in Kevlar©), the surface groups can be altered through chemical reactions, or the surface can be altered by coating with another substance.[305]

1.12.1 Methods of Chemically Modifying Fabrics

This discussion will only consider chemical modifications which do not alter the molecular structures of fibres, so the design of fabrics such as Nomex© and Kevlar© or physically changing parameters for electrospinning[309] will be excluded from this discussion.

Chemical modification tends to take place through finishes or “built-in” methods. Finishing methods include coating or laminating, whereas built-in methods include modification of the fibres, threads or yarns by addition of surface groups.[310] Modification can also be achieved before the fibres are made, with an encapsulated phase change material (PCM) being added to a polymer solution before extrusion, thereby resulting in PCM within the fibres.[311]

Built-in methods include anything that alters the surface groups but can alter the structure of the whole fabric. These methods include plasma treatment, grafting, the use of crosslinkers and electrostatic and covalently bound species. Coatings change specifically the surface properties.[312] Good bonding is required between the fabric and a finish or coating for durability.[313] It can be difficult to accurately classify fabric modifications. For example, the chemical grafting of cyclodextrins to cotton and wool fabrics, through poly(carboxylic acids) as linkers,[314] changes only the top layer of the textile so could be classed as a coating, but as it uses crosslinkers and covalent bonds it could also be classed as ‘built-in’.

The three main fabric modification methods covered in the rest of this introduction are dipping, plasma treatments and layer-by-layer deposition.

In dipping, the fabric is submerged in a solution then removed and allowed to dry.[315-318] In pad-drying, the excess solution is squeezed out between rollers (Figure 1-35).[307, 308, 314, 319-324] The setting of these rollers dictates the percentage “pick-up”. The fabric is then dried (and if necessary, cured). More complicated dipping methods also exist, such as direct roll coating, where a roller is partially submerged in the coating solution, indirectly transferring the solution onto the fabric as it passes through the rollers. However, these are not as commonly used in the literature so are not discussed further here.

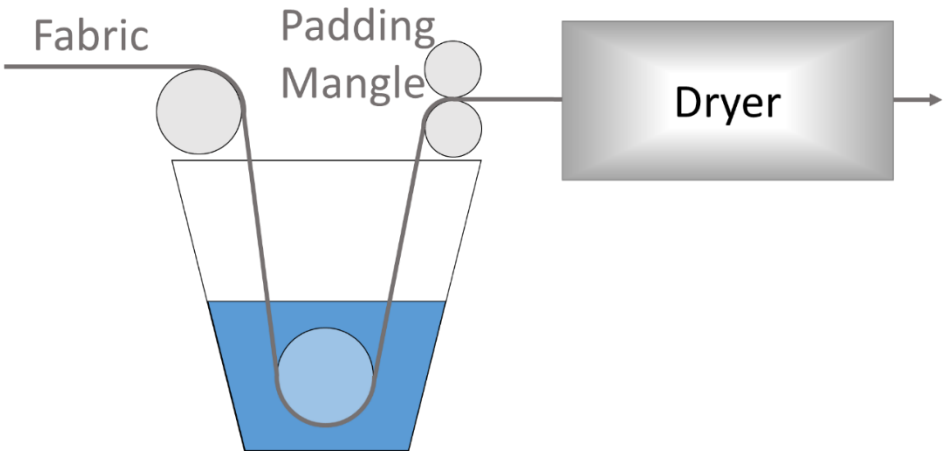

Figure 1-35. Schematic of padding mechanism.

Plasma treatment bombards the surface of the fabric with a partially ionized gas, modifying the surface. This can be done under elevated pressure or atmospheric pressure with a variety of different gases, giving a range of modifications. Low or atmosphere pressure tends to be used for textile modification. Plasma treatment can modify the surface to give enhanced wettability, or hydrophobicity, improved dyeing and printing compatibilities, and can be used as a pre-treatment for additional steps, such as increasing adhesion between fabric and a coating or similar.[313, 325-327]

Layer-by-layer deposition was first published by Decher in 1997.[328] It involves soaking in alternating polyanion and polycation solutions with washes in-between. This allows controlled layer deposition with electrostatic adhesion, hence the name “layer-by-layer”. It is a simple, inexpensive technique which normally forms stable films in air.[329]

1.12.2 Antibacterial Textiles

Textiles in close proximity to the human body are commonly known to provide a suitable environment for microorganism growth. As the public awareness of hygiene increases, there is an apparent need for anti-microbial modification of fabrics. Many anti-microbial agents cannot be used in this situation, due to their toxicity towards humans. A well-known sample antibacterial agent is silver.

Silver has been known as an antimicrobial agent since ancient times, and can be traced back to the Ancient Greeks and the Roman Empire. Silver was widely used in hospitals before the introduction of antibiotics, which replaced it.[330] More recently, it has come back into favour and, according to the Consumer Products Inventory, from *The Project on Emerging Nanotechnologies*, over 1600 products claim to include some form of engineered nanoparticle, of which over 25% contain silver.[331] Silver nanoparticles

have been included in clothing, such as shoes or socks, and there is evidence that they limit the growth of odour-causing bacteria.[332] Work by Dubas *et al.* showed that silver nanoparticles, deposited using layer-by-layer deposition on silk or nylon, exhibited an 80% reduction in bacterial growth.[333]

There has been much research into silver nanoparticles in textiles, for instance investigating binder additives, stability, durability, and silver application methods to maximise the textile's antimicrobial properties.[332-338] For example, Zhang *et al.* used hyperbranched polymers to bind silver nanoparticles to a cotton fabric, which showed a 99% bacterial reduction of both gram positive and gram negative bacteria and maintained its properties even after 20 domestic washes.[339] Without a binder, the textiles lost 40% of their bacterial reduction after 20 domestic washes.[340]

A 2008 paper from Benn *et al.* tested six brands of socks advertised to contain silver nanoparticles. Five of the six brands contained detectable levels of silver ranging from 2 to 1360 µg-Ag/g-sock, confirmed by scanning electron microscopy (SEM). The socks leached silver on washing with water.[341] This work was followed by a similar study on the washing of silver nanotextiles, which actually washed the textiles.[342]

Jiang *et al.* plated a polyester-cotton blend fabric with silver, which then showed enhanced antibacterial activity.[323] Gorensek also managed to simultaneously apply nanosilver and dyes to cotton by modifying the exhaust dyeing procedure and achieved increased antibacterial activity.[343]

In summary, although there are questions about the use of nanoparticle silver in textiles, especially associated with silver ion toxicity,[344-346] it is clear that nanoparticles can enhance fabric properties.

Chitin, poly(1,4)-2-acetamido-2-deoxy-β-D-glucose, is the second most abundant natural polymer. Chitosan is the deacetylated form with a structure similar to cellulose (Figure 1-36).[308, 322] Chitosan has been used in a variety of textile modifications from polymeric core-shell particle[319] to cotton modifications[306,308] and demonstrates enhanced antibacterial activity.

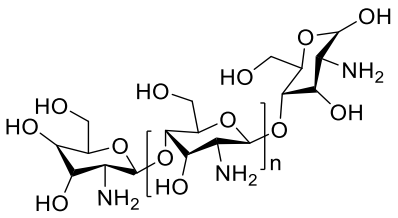

Figure 1-36. Structure of Chitosan.

Lee and Cho used chitosan and fluoropolymers to treat cotton and wood pulp/polyester spunlaced non-wovens for increased antimicrobial activity and blood repellency for use on hospital gowns. Cotton could provide reusable gowns, whereas the non-woven would provide a single-use garment. Chitosan increased the antimicrobial activity of both fabrics. Once fluoropolymers were applied as repellents, the antimicrobial activity was reduced, but nonetheless, it remained higher than untreated fabrics. These fabrics were relatively durable to washing and treatment did not significantly change air permeability.[322] This example demonstrates a multi-polymer modification of two fabrics and how different polymers can be applied during different parts of the process for different outcomes.

Chitosan has also been used to modify poly(propylene) non-woven fabrics, showing increased antimicrobial activity, but stiffening the fabric, decreasing the air permeability and tensile strength. The effectiveness of antimicrobial activity was dependent on the strain of bacteria.[321] Huh *et al.* showed that plasma pre-treatment produced peroxides on the surface of the fabric, allowed better covalent coupling to chitosan, which showed increased antimicrobial activity and wettability.[325]

1.12.3 Reactivity to Dyes

Dyeing cotton generates a lot of polluted wastewater and is quite energy intensive. Cotton only has a moderate affinity for dyes and will build up negative charge in water, repelling anionic dyes.[317] This repellency is overcome in industry by lengthening the dyeing times and using a high concentration of dye. The increased concentrations require multiple washes to remove the unfixed dye, leading to large amounts of waste.[347] With cotton being commonly used, this has therefore been a key area of research.

Cotton can be modified with cationic sites to attract the anionic dyes. The hydroxyl groups of cellulose can be modified, e.g. via reaction with epoxy-propyl-trimethyl-ammonium chloride[347], or 3-chloro-2-hydroxypropylmethylammonium chloride,[307] or the introduction of amino groups via ether linkages.[348-351] The introduction of amines into the cellulose structure make it analogous to wool. Fang *et al.* appended acrylamide through a Michael addition followed by a Hoffmann degradation to introduce aminoethyl groups (Scheme 1-1). Surface modification was confirmed by IR spectroscopy.[317] This helped dye utilization but wash fastness and rub fastness were the same as the untreated fabric.

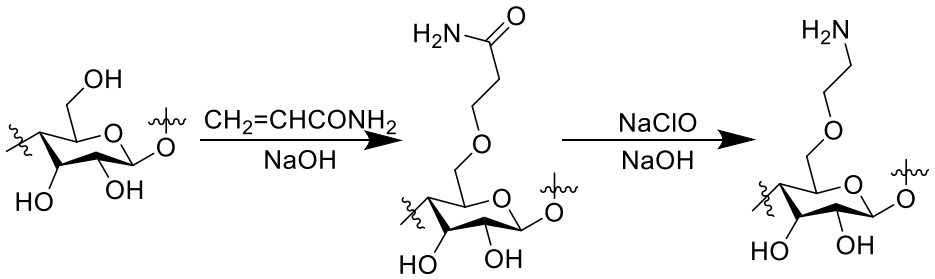

Scheme 1-1. Modification reaction from ref 317.

1.12.4 Modifying the Hydrophobicity of a Fabric

The hydrophobicity of a fabric is often modified. Hydrophobicity is the ability to repel water. Most fabrics are modified to increase hydrophobicity simply by increasing surface roughness.[352, 353] It is also very common to use fluorinated systems as a water repellent. One of the most famous fluorinated systems is poly(tetrafluoroethane) (PTFE), sold under the brand name Teflon© (Figure 1-37).

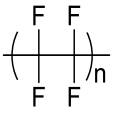

Figure 1-37. Chemical structure of poly(tetrafluoroethane) (PTFE).

PTFE was accidentally discovered in 1938 by Plunkett,[354] and commercialised in 1946. It is a high molecular weight thermoplastic polymer that is chemically inert to most substances, insoluble in almost everything, has a hydrophobic and oleophobic surface and is non-stick. The hydrophobic surface comes from the electronegativity of the surface fluorines which can induce a dipole. Their chemical inertness comes from the C-F bond strength. PTFE has the 3rd lowest friction coefficient in the world making it non-stick. PTFE is applied as Gore-tex©, a common household name for waterproof clothing, providing waterproofing while maintaining breathability. Gore-tex is an expanded version of PTFE, in which the PTFE is stretched to create a highly porous material containing 70% air.[355, 356] Modern Gore-tex fabrics are multilayers containing nylon (for strength and durability) laminated with a PTFE sheet. Any liquid water is stopped by the PTFE layer, however, any water vapour on the inside of the garment can permeate. This diffusion of water vapour is driven by the partial pressure.[356] Before Gore-tex, truly waterproof fabrics were not breathable (e.g. oilskins, poly(urethane) coated fabrics, or poly(vinyl chloride) films). Other fabrics such as silicone or fluorocarbon treated fabrics are only marginally water resistant but are more breathable. Additional work has investigated coating substrates with polymeric

fluorocarbons rather than lamination, but these do not seem to be able to achieve the same level of protection.[357]

An attractive, environmentally friendlier alternative to waterproofing is to use a silica coating. This converts cotton, which is naturally hydrophilic, into a superhydrophobic material. SEM visualised the change in surface geometry, with the hydrophobic surface having a much greater surface roughness than the original cotton.[358] Zhu *et al.* created a highly hydrophobic surface on cotton and polyester using modified silica solutions applied via a pad-dry-cure method. Epoxy groups were used to covalently bond the cotton and modified silica via the cellulosic hydroxyl on the cotton. These covalent linkages led to a significant increase in durability to washing.[352]

Titanium dioxide has also been used to modify fabric hydrophobicity. Zhang *et al.* used titanium dioxide and poly(benzoxazine) to modify polyester non-woven fabrics through a dip coating and thermal curing process. This fabric could purify wastewater containing a soluble dye (useful for the disposal of the contaminated wastewater from cotton dyeing) offering a promising polluted water treatment. The fabric also demonstrated self-cleaning performance and removed oil and particle contamination.[318] Ding *et al.* used layer-by-layer deposition of titanium dioxide nanoparticles and poly(acrylic acid) on cellulose fibres to increase surface area and hydrophobicity.[329]

Flexible low molecular weight poly(dimethylsiloxane) (PDMS, Figure 1-38) has been covalently attached to a smooth surface through platinum catalysed hydrosilylation. This fabric had controllable dewetting and also gave a superoleophobic surface.[359, 360]

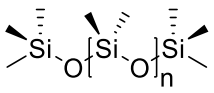

Figure 1-38. Chemical structure of poly(dimethylsiloxane).

Other techniques have also been used, such as aerosol-assisted chemical vapour deposition to coat surfaces and increase hydrophobicity.[353] Deng *et al.* created a superamphiphobic coating which was both superhydrophobic and superoleophobic (i.e. repels both water and oil) by deposition of carbon from soot, which is then coated with silica via chemical vapour deposition. They suggested this may have applications in goggles and outdoor applications.[312]

1.12.5 Smart Textiles

Fabrics have generated much recent interest due to advances in portable devices, wearable technology and responsive textiles. So-called “smart fabrics” are sometimes

also referred to as smart materials in the literature; they change their properties (configurational or physical) in response to a change (physical or chemical) such as temperature, pressure or force. Smart textiles can be categorized into many groups. For example, Zhang[361] and Van Langenhove categorised smart textiles into passive smart, active smart and very smart. They class passive as a textile which can only sense stimuli, active can sense and react and very smart can sense, react and adapt.

Stimuli-responsive polymers are one way to make smart textiles. The use of thermally responsive poly(*N*-isopropylacrylamide) (PNIPAM) has been very common. The polymers change their properties in response to external stimuli such as moisture[362], light[363], solvent[364], pH change[365], electricity[366] or magnetic field[367].[310] For example Kulkarni *et al.* used a surfactant-free dispersion copolymerisation of poly(*N*-isopropylacrylamide) and chitosan with a crosslinker to produce a stimulus responsive fabric. The water uptake of the fabric depended on pH and temperature.[324, 368] Work by Hu, Liu and Liu gave a tuneable water content in response to temperature and pH on a non-woven substrate with a polymer grafted to the surface. They suggest this work has applications in smart wound dressings and skin care.[369] Polymers can be incorporated through the construction of a non-woven melt blown fabric from the polymers themselves or incorporated later using polymer solution baths or spraying. Tourette *et al.* activated cotton using poly(*N*-isopropylacrylamide) and chitosan with a non-thermal plasma treatment in air to create a thermo-responsive hydrogel with a volume phase transition.[327]

Phase change materials (PCMs) store or release latent energy by undergoing a phase transition. For example, melting from a solid to a liquid. Incorporation of PCMs into a textile, by coating or encapsulation, allows them to store or release latent energy. NASA incorporated phase change materials into space suits to minimise the drastic temperature changes. The PCM within the fabric can melt, absorbing heat, keeping the astronaut cool, or *vice versa*. These phase change materials can be encapsulated in microcapsules, which can be added to a polymeric solution before fibre extrusion, thereby effectively loading the phase change material into the fibres. Other methods of applying phase change materials include; coating using polymer binders, surfactants, dispersants or antifoam agents and thickeners and lamination by incorporated in thin polymer films (e.g. poly(urethane) foam). These phase change textiles also have applications in sportswear, bedding to medicinal applications and footwear.[311]

Another common fabric modification is the use of titanium dioxide nanoparticles. These have the advantage of being UV active, technically making them a smart material, so

can be used as sun protection or for self-cleaning or stain repellency. They also have increased antibacterial activity.

Meilert *et al.* used poly(carboxylic acids) as spacers for attaching titanium dioxide nanoparticles to cotton through ester bond formation.[370] One carboxylic acid formed an ester with the free hydroxyl groups on the cellulose fibres, then a second carboxylic acid bound the titanium dioxide. This binds the titanium dioxide to the cotton, producing a self-cleaning textile. Without the spacer, none of the textiles bind efficiently to titanium dioxide. Self-cleaning properties come from the decomposition of the stains (e.g. wine, coffee, make-up and perspiration) under light irradiation, to release carbon dioxide and water (with SO_x and NO_x if present). Yuranova also used titanium dioxide on a cotton surface to produce self-cleaning fabrics, using silica as a binder.[371]

Another common approach to attach nanoparticles is through plasma treatments. Plasma pre-treatment introduces negatively charged groups to the surface of the textiles, increasing hydrophilicity and allowing titanium dioxide to attach electrostatically.[326]

1.12.6 Nanofibres for Protective Clothing

Over the past few decades, nanofibres have grown in popularity for use in single-use protective garments, being inexpensive, lightweight and offering effective protection.[372, 373] This is due to their small fibre size and therefore large relative surface area. The majority of nanofibres that have been used for protective applications are electrospun. Electrospinning processes have been patented for the production of filter media.[374, 375] Modified electrospun nanofibres have also been demonstrated for synthetic antiseptic wound dressings.[376] The origin of electrospun nanofibres came from Petryanov-Sokolov's work on fine fibre production in electrostatic fields, which was used to produce a filter protecting from radioactive aerosol release.[377, 378]

Electrospinning uses an electrical field to "draw" fine fibres from a polymer solution (or melt). When a sufficiently high voltage (10-50 kV) is applied to the tip of a capillary, electrostatic repulsions overcome the surface tension and fine jets of the solution are ejected and drawn to a grounded or oppositely charged collector. These jets tend to splay en-route, then as the solvent evaporates (or the melt cools), fibres form on the collector, as an interconnected anisotropic non-woven nanofibrous mat/fabric (Figure 1-39).[379, 380] The anisotropy of the non-woven fabric makes it difficult to predict permeability, as it will vary from region to region, although Mao and Russell created a model to try and estimate the permeability.[381] The processing conditions of

electrospinning such as solution viscosity and electric field strength, modify the fibre diameters formed.[309]

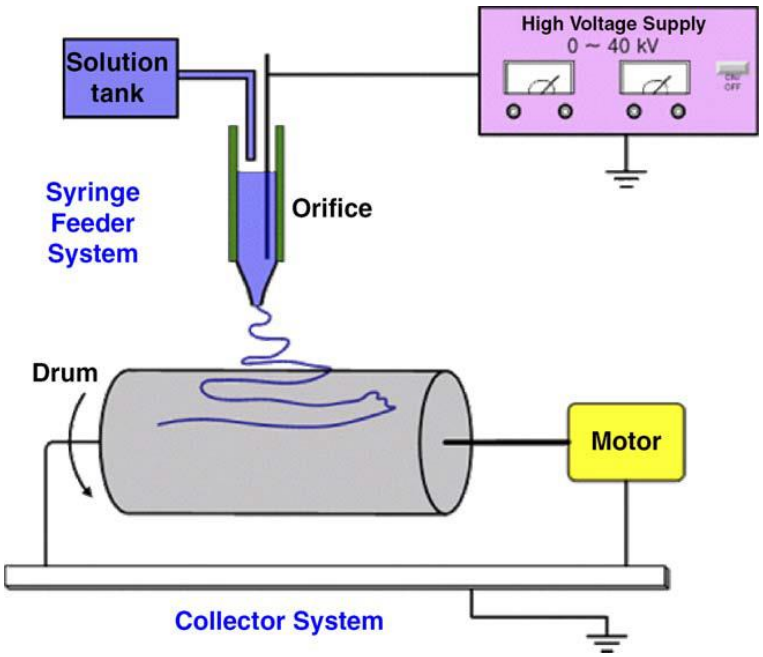

Figure 1-39. Schematic diagram of electrospinning process for nylon-6 nanofibres reproduced from Ref 382 with permission from Elsevier.

More recently, nanofibres of different types have been specifically investigated for non-disposable protective textile materials. A good filter should have a high filtration efficiency and a low pressure drop using fine fibres. For this application, air permeability and water vapour permeability are also both important to help maintain thermal comfort. A review of 36 different protective textiles in use (18 woven fabrics and 14 non-woven fabrics), identified the need for high barrier performance whilst maintaining thermal comfort. Most protective materials have an air permeability of between 0 and 100 $cm^3\ cm^{-2}\ s^{-1}$ and a water vapour permeability of around 480 $g\ m^{-2}\ day^{-1}$.[372] Non-woven fabrics, made from electrospun polymer nanofibres, have a small pore size making them suitable candidates for filtration, membranes and possibly protective clothing.[15, 20, 380, 382-392]

It is also important to consider the mechanism of nanofibre-based filtration (Figure 1-40). Classic theories based on orderly packed coarse fibres are inadequate in accounting for the influences of random fibre distribution and slip flow.[393] The use of small fibres normally results in high filter efficiencies due to the increased surface area to weight ratio. However, if the diameter of the fibre is comparable to the mean free path of air molecules (66 nm under normal conditions), “slip” occurs at the surface of

the fibre as the gas velocity is non-zero.[393] This reduces the drag force on the air flow (hence has the potential to reduce the effect of nanofibre on pressure drop).

The most obvious mechanism for removing particles by filtration is sieving, where the particles are larger than the gaps they are attempting to travel through, and therefore get trapped on the surface. This is particularly important for high density fibres. In reality, sieving may be the least important mechanism for filtering small aerosol particles because sieves tend to clog quickly, resulting in an increased pressure drop and shorter filter lifetimes.[394] Multiple mechanisms are responsible for aerosol particle removal (Figure 1-40).[309, 395] Interception is where a particle travels too close to the fibre (within a particle radius) and is therefore deposited on the fibre. Diffusion involves a collision between the particle and the fibre due to random Brownian motion (particularly important for particles <0.1 μm). Inertial impact results from larger particles having too much momentum to follow the curved path of the gas around the fibre, resulting in collision and deposition. Electrostatic deposition is generally important for charged fibres or particles, or those which can have dipoles, so will not be considered further here.[395] Both the size of the fibre and the particle influence which mechanisms are most important.[394] Using a fibrous material, aerosols are captured through the depth of the porous structure. The air flows through the interconnected voids formed by the nanofibres, with opportunities to deposit aerosol particles onto each fibre.[395]

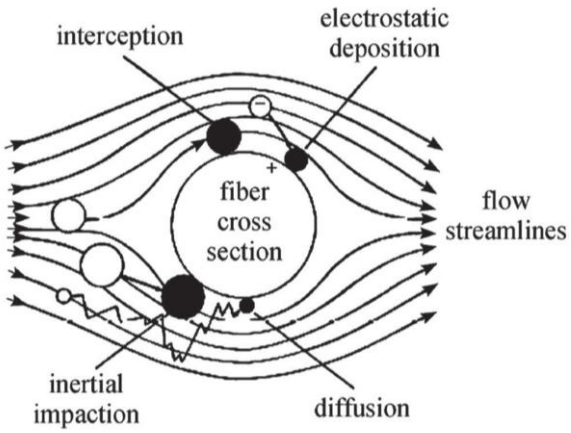

Figure 1-40. Primary filtration mechanisms reproduced from Ref 395 with permission from Elsevier.

Electrospun polymer nanofibres (such as a non-woven fabric), can provide enhanced protection against aerosol[20, 380, 385, 396-398] and liquids[399] as the fibre spacings can be smaller than aerosol particles.[394] Some examples of this enhancement include a thin film of poly(urethane) fibres deposited on top of an electrospun non-woven fabric,

offered increased barrier protection against a range of liquids. As fibre density increased, air permeability of the fabric decreased but there was no significant change in water vapour permeability.[400] In another example, a fine layer of electrospun nylon-6,6 poly-benzimidazole,-acrylonitrile and -urethane demonstrated good aerosol protection (correlating to add on mass) without significant change to water vapour permeability.[385] These results were supported by enhanced aerosol filtration of NaCl particles from electrospun nanofibrous mats of poly(amide-6) deposited onto a non-woven viscose substrate, while air permeability negatively correlated with nanofibre coating.[401] Similar results have been seen with poly(nylon-6,6) and other polymer based nanofibres, where a thin layer of nanofibre coating can show significant filtration.[392, 398, 401-406] Nylon-4,6 nanofibres have been shown to have superior aerosol protection comparative to all published electrospun nanofibres.[407]

Functionalised polymer nanofibre membranes have also been shown to hydrolyse chemical warfare simulants with increased reactivity and adsorption over activated charcoal.[21, 408] The process of electrospinning also allows direct application of electrospun webs to a fabric, eliminating costly manufacturing steps such as laminating and curing.[20, 385] It is possible that electrospun nanofibres could be applied to existing equipment as a coating, rather than having to remake new equipment, as demonstrated by the direct application of electrospun nanofibres to poly(urethane) foam containing activated carbon, which is a current component of protective clothing, eliminating all aerosol particle penetration.[20]

The main limitation of electrospinning is fibre diameter and throughput; fibre diameters of 10 nm have been reported but have very low throughputs, it is much more common to use diameters in the region of 100 nm to 1 µm.[378, 385].[378, 379] The smaller the nanofibre, the better the filtration performance.[390, 398, 402, 405, 409]

Another way to form nanofibres is through the formation of supramolecular gel networks. Supramolecular gels can be formed *in situ* and can form smaller nanofibres than electrospun polymers: one widely used industrial supramolecular gelator 1,3:2,4-dibenzylidene-D-sorbitol (DBS) forms nanofibres of *ca.* 10 nm. The poor robustness of non-covalent materials can limit their use, but robust non-covalent materials have been created through strong hydrophobic interactions, producing functional materials such as filtration membranes which rival covalent systems.[410] Supramolecular nanofibres may, therefore, bring the same advantages as electrospun nanofibres, such as high surface area, lightweight network good interconnectivity of pores and the potential to incorporate active chemistry. The non-covalent interactions which form the

supramolecular gel also lend themselves to recyclability and reusability; a recyclable supramolecular membrane has been demonstrated for size-selective separation of inorganic and biological nanoparticles.[410] Supramolecular gels have also been shown to interact with chemical warfare agent simulants,[411, 412] and have shown promise in filtration applications.

1.12.7 Fabric Modification with Supramolecular Nanofibres

Gelator nanofibres can be obtained by drying gels. These would be difficult to directly apply to fabric. It would also be possible to apply the system as a gel, attempting to spread it or potentially spray it, but this would present practical difficulties in ensuring homogenous coverage.

A better option is to apply a gelator in solution. As the solvent evaporates, the concentration of the gelator will increase and self-assembly will occur, depositing gelator nanofibres onto the fabric. This would allow for much easier processing and could also mean that the volatility of different solvents could control the morphology of the gelator networks formed. The fabric may also affect nanofibre deposition, for example, fabric yarn spacing. Hydrophobicity and wicking of the fabric could all influence how the gelator-containing solution spreads across the fabric. Textile finishes could have similar effects. Solvent would be crucial in trying to balance these factors.

Gels have been used to form layers on non-woven substrates. Gelation of a fluorinated bis-amide in the presence of a non-woven substrate led to a gel impregnated surface. As the solvent evaporated (organic or supercritical CO_2), it left behind assembled gelator fibres, producing a composite surface with a high surface area, roughness, water and oil repellency (Figure 1-41).[413]

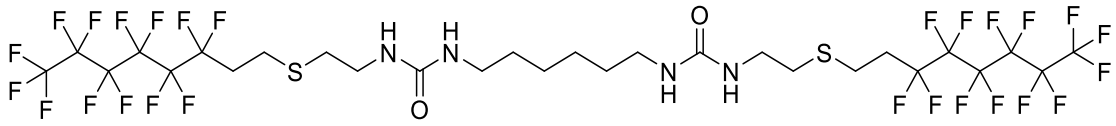

Figure 1-41. Example of a fluorinated bis-amide gelator used in ref [413].

Krishnan *et al.* produced a semiconducting fabric to reduce the build-up of static charge, for applications including operating theatres. They polymerized diyne-functionalised 4,6-*O*-benzylidene-β-D-galactopyranoside gelator via photoirradiation. The organogel can adhere to cotton fabrics through hydrogen bonding. They also tried to modify polyester, and nylon using the same procedure but found that the organogel had poor adhesion.[414]

Self-assembled nanofibres have recently been investigated to modify fabric filtration, potentially enabling a 'bottom-up' approach from simply dipping a fabric in a bath of solution containing dissolved gelator.

Misslitz *et al.* used 1,3,5-benzenetriamide based motifs (see Figure 1-42) to self-assemble into columnar stacks driven by hydrogen bond formation using a non-woven scaffold support. The nanofibre morphology observed was dependent not only on the structure of the compound, but also the solvent used, the concentration and the processing conditions.[415] They were the first to use a "bottom-up" approach, assembling the nanofibres inside the scaffold from individual molecules. They achieved this by dipping a non-woven fabric into gelator solution at elevated temperature. The solution penetrates the fabric and upon drying, the solvent evaporated and the molecules self-assembled into nanofibres within the scaffold, significantly increasing the surface area. The SEM image in Figure 1-43, shows a dried concentration of 7.0 wt% (from 1.0 wt% immersed solution), indicating the formation of nanofibres in individual voids on a non-woven material. The thicker fibres are non-woven microfibres and the thinner fibres are the self-assembled nanofibres. The concentration strongly influenced the fraction of filled openings in the fabric.[415] The nanofibres formed were *ca.* 500 nm in diameter,[415] and with a high surface area to volume ratio, promising for filtration.[397]

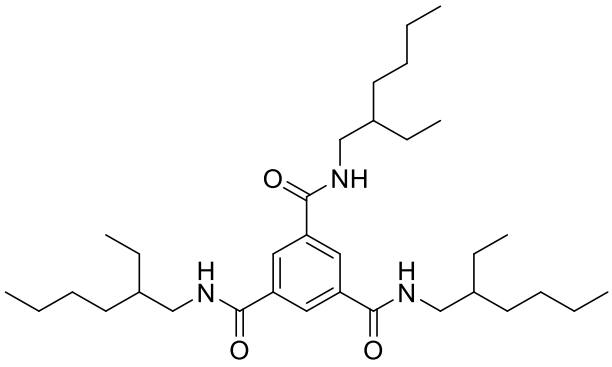

Figure 1-42. *N,N',N''*-tris(2-ethylhexyl)-1,3,5-benzenetricarboxamide (BTA based compound) from ref [415].

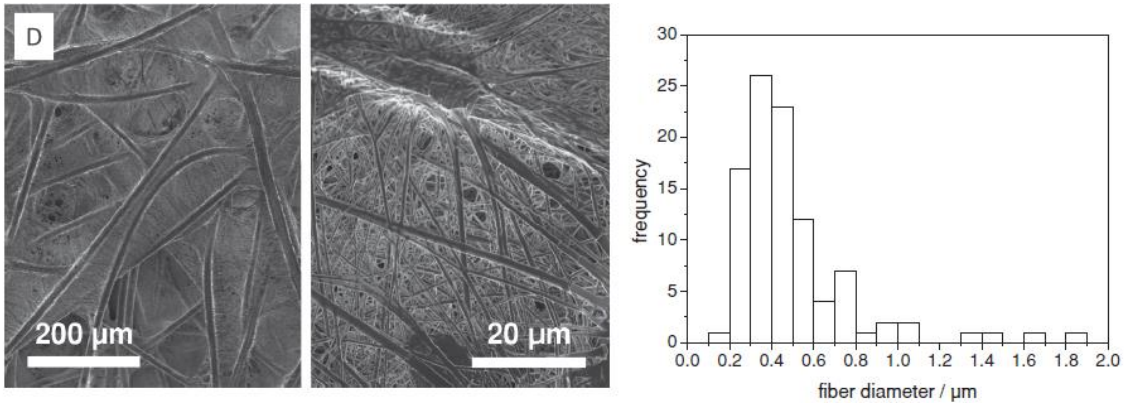

Figure 1-43. SEM images and fibre distribution for 7.0 wt% BTA derivative (Figure 1-42) reproduced from Ref 415 with permission from John Wiley & sons.

The nanofibre composites significantly increased the filtration of a range of particle sizes at a range of (low) concentrations. They found that the composites could remain intact for at least 24 h against an air flow of 3 m s^{-1}. Even using a relatively low final concentration of molecules (2.8 wt% through to 7.0 wt% dried from <1.0 wt% solutions), filtration efficiency increased across the entire range of particle sizes tested (0.2 to 1.0 µm) (Figure 1-44).[415]

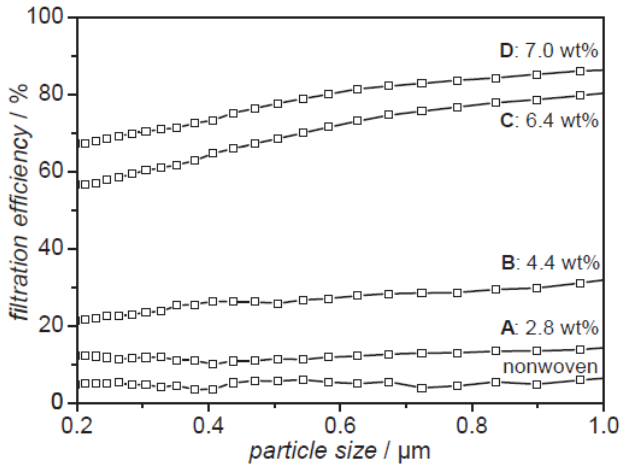

Figure 1-44. Average filtration efficiencies of composites with different content of nanofibres in non-woven support reproduced from Ref 415 with permission from John Wiley & sons.

Schmidt *et al.* published a deeper understanding in 2016, offering further advances into processing conditions and resulting properties based on different BTA derivatives (Figure 1-45).[416] They demonstrated that changes in the molecular structure and solvent influenced the diameter, distribution, homogeneity and pore size distribution, all of which correlated to filtration performance.

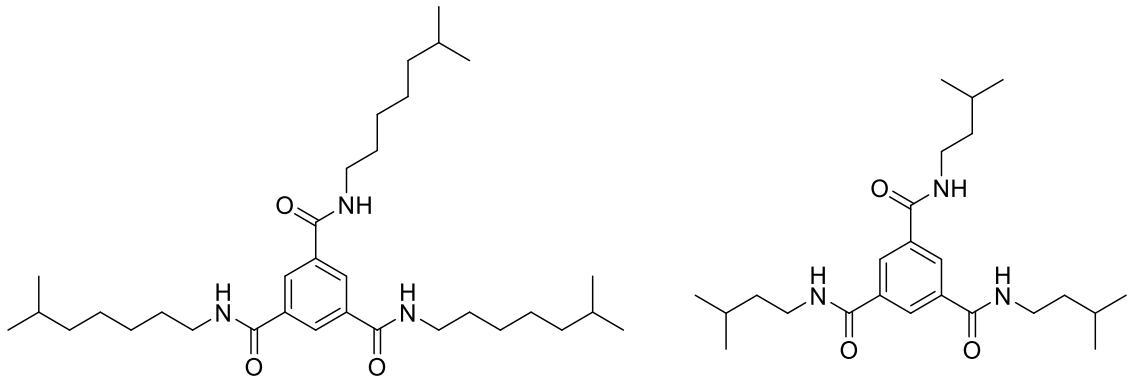

Figure 1-45. BTA structures used in more recent work on self-assembled nanofibres in a non-woven for air filtration.

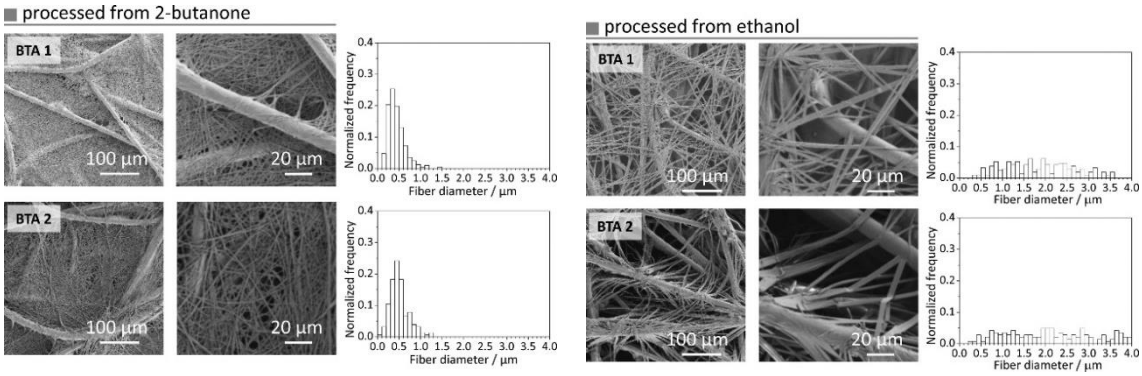

Figure 1-46. SEM images of both BTA structures and fibre diameters from 2-butanone and ethanol reprinted with permission from Ref 417. Copyright 2016 American Chemical Society.

The supramolecular fibres assembled from ethanol were much thicker than those from 2-butanone (2000 nm *vs.* 500 nm, Figure 1-46). BTA 1 (with the longer alkyl chain) had smaller and more uniform pore sizes. In terms of filtration efficiency, this derivative also outperformed its shorter counterpart. Improved efficiency was seen over the originally reported BTA structure, achieving 95% efficiency across the particle sizes tested compared to the *ca.* 80% seen in the initial work (Figure 1-47).

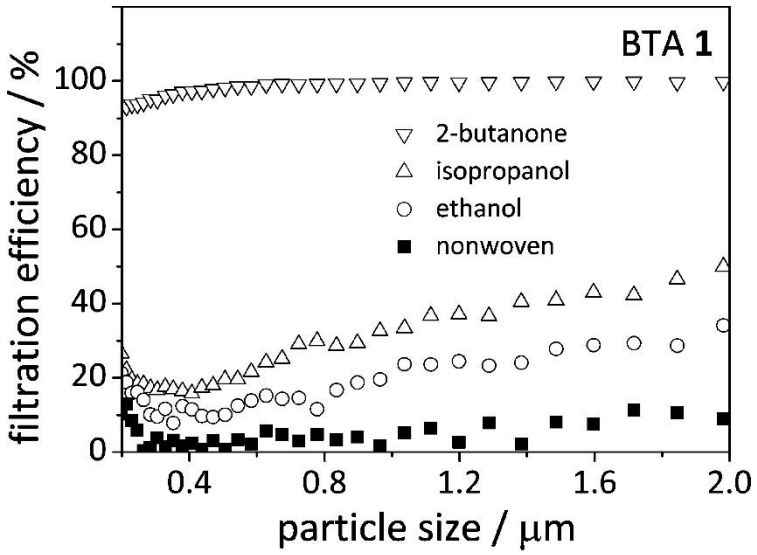

Figure 1-47. Filtration efficiency of BTA 1 reprinted with permission from Ref 417. Copyright 2016 American Chemical Society.

This most recent work, published during this thesis work, demonstrates the potential for filtration with 1,3,5-benzenetrisamides.

1.13 Aims

The main aim of this project was to develop self-assembling nanostructures, which could be incorporated into a single layer fabric via self-assembly methods to achieve enhanced repellency of organic fluids and aerosols with minimal change to the intrinsic properties of the fabric. Ideally, these would be based on low-cost, industrially viable DBS gelators, although alternative gelators were considered, and initially the BTA work was to be replicated. Furthermore, DBS can readily be modified (Figure 1-48). It was proposed to test different fabric modification methods including different solvents, concentrations and drying regimes in order to optimise fabric modification.

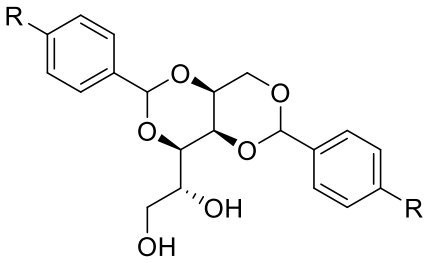

R = H	DBS (DBS)
CO_2Me	DBS-CO_2Me (DBS-ester)
$CONHNH_2$	DBS-$CONHNH_2$ (DBS-hydrazide)

Figure 1-48. Structure of target molecules.

The degree of branching and surface modification were also to be investigated, by tailoring the synthesis of the molecules, with the aim of achieving improved repellency to organic fluids and aerosols and to improve enhanced performance. For example, using a percentage of dimeric structure (a bolaamphilphile see Figure 1-49) could introduce an intrinsic branching point[27] as demonstrated by Hayes and co-workers with bis amide-aromatic urea supergelators.[304] Each DBS molecule could be involved in the self-assembly of a different fibril, with the "spacer" between the two molecules joining two fibrils together, (Figure 1-50), related to the concept of crosslinking in traditional polymer science.

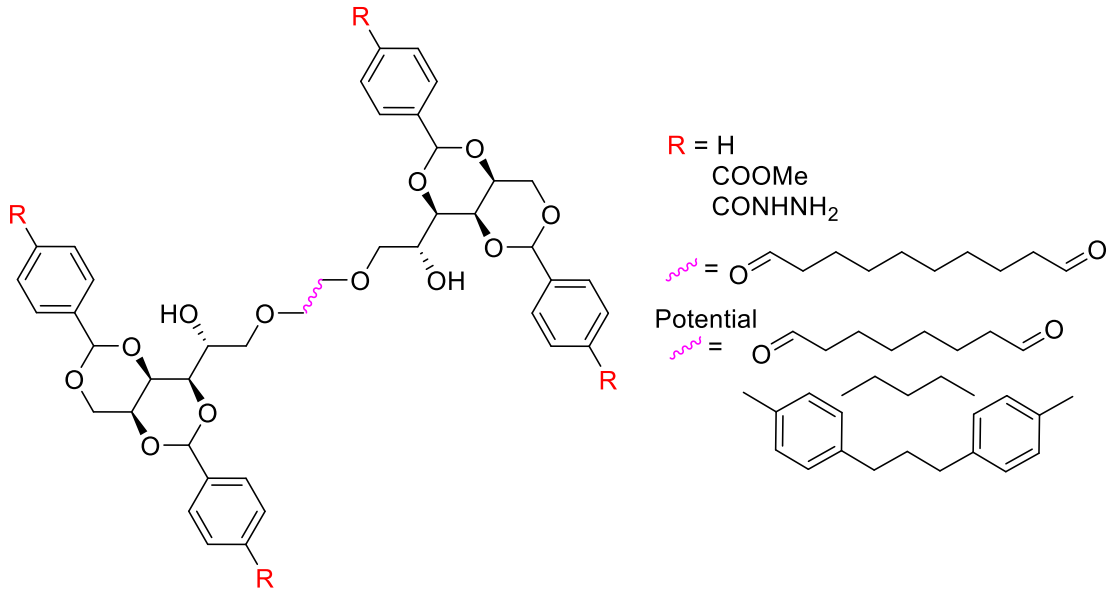

Figure 1-49. Potential dimer structure.

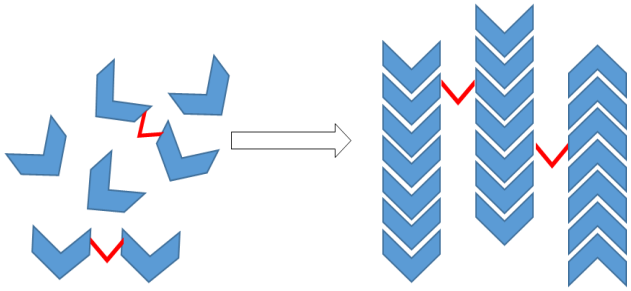

Figure 1-50. Schematic of chemical branching.

Alternatively, polymer additives could be introduced in an attempt to introduce physical crystallographic mismatch branching and generate highly branched samples spanning networks within the fabric.

In addition to using DBS and BTA as fabric modification agents, it was also possible to use a mixture of gelators to determine whether synergistic effects can be observed.

It was proposed to test the modified fabrics under a range of conditions including adverse environments, to explore their stability and potential use. Key tests such as air permeability and water vapour transmission can investigate changes to the intrinsic properties of the fabric. Particle filtration can identify enhanced fabrics. This testing was proposed to be achieved collaboratively by spending time in the laboratory of Dr Ningtao Mao (University of Leeds) and at Porton Down and Silsoe Application Spray Unit as part of DSTL.

Chapter 2 - 1,3:2,4-Dibenzylidene-D-sorbitol (DBS)

2.1 Introduction to the Industrial use of 1,3:2,4-Dibenzylidene-D-sorbitol (DBS)

DBS is used industrially as a bulk chemical and therefore has commercial relevance.[51, 111-123] DBS has featured in a large number of patents and has found real-world applications in a wide range of industries including personal care products (e.g. deodorant sticks and lipsticks) and polymer processing for both thermoplastic or plastic materials (nucleation and clarification).[217-219]

DBS possesses an ability to gel a wide range of solvents, allowing it to be commonly used in the formulation of personal care products to gel desired ingredients within the cosmetics industry. DBS use is widespread to produce desired thickness, strength and consistency in products. DBS has been used as a gelator of glycols and alcohols with acidic aluminium antiperspirant salts, producing clear antiperspirant sticks,[243] originally patented by Roehl.[186, 187]

Supramolecular nanofibre webs in non-woven scaffolds have been shown to have potential as filter media and for air filtration applications.[413, 415, 417] Although many examples of gelators are known, DBS is already produced on the bulk scale, it is cheap and available. Its gelation ability across a wide range of solvents, giving it a wide range of applications, also gives a plethora of potential nanofibre formulation methods. There are a wide range of accessible derivatives, which are also easy to synthesise, to provide additional scope and potential. DBS, therefore, makes a great candidate for trials in secondary network generation within a non-woven fabric support.

2.2 Synthesis of 1,3:2,4-Dibenzylidene-D-sorbitol (DBS)

DBS was synthesised using literature methods,[111, 418] which were subsequently modified by the Smith group.[57] This synthetic route involves a one-step condensation reaction between benzaldehyde and D-sorbitol in a 2:1 ratio with a (trace amount of) acid catalyst (Scheme 2-1).

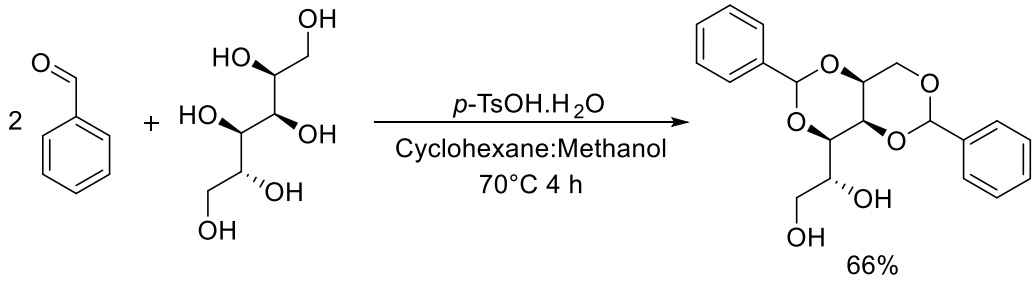

Scheme 2-1. Synthetic scheme of DBS.

D-Sorbitol was added to a mixture of cyclohexane and methanol. Dean-Stark apparatus was attached to the reaction flask, and the mixture was stirred at ~300 rpm using an overhead mixer at 50 °C for 20 minutes, under a steady flow of nitrogen gas. An azeotropic mix forms between the solvent system and the water from the reaction, helping to remove water while cyclohexane aids precipitation of the product. In a separate flask, *p*-toluene sulfonic acid monohydrate and benzaldehyde were stirred in methanol at room temperature for 20 minutes before being added dropwise to the D-sorbitol mixture. After the addition, the reaction temperature was increased to 70 °C and it was stirred for 4 hours. The mixture was allowed to cool, before being washed with cold ethanol to remove unreacted starting material and catalyst. The by-products of this reaction are shown in Figure 2-1.

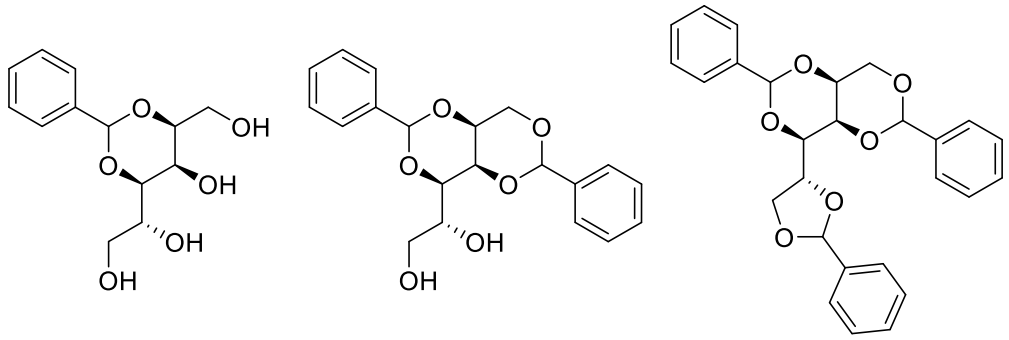

Figure 2-1. Monobenzylidene-D-sorbitol (MBS), Dibenzylidene-D-sorbitol (DBS) and Tribenzylidene-D-sorbitol (TBS).

The different solubilities of the by-products allowed for simple purification by washing. The mono-substituted derivative was removed by washing with hot water and tri-substituted derivative was removed by washing with hot dichloromethane. The product was crushed to give a white powder and obtained in a 66% yield. The product was characterised by ^{1}H NMR, ^{13}C NMR, MS and IR spectroscopies. Mass spectrometry showed mass ions with values of 381.1308 $[M+Na]^+$ (100%) which correlated to the molecular ion and sodium, and 359.1482 $[M+H]^+$ (25%) but no mass ions were present for mono- or tri-substituted products. Also, the ^{1}H NMR spectrum did not show multiple environments as would be expected if by-products were present.

In the following work, both synthesised DBS and commercial DBS will be used. DBS was sourced from a commercial supplier, NJC Europe, sold as “Geniset D”. Work has been done with both types of DBS, which type has been used for each experiment is highlighted, as there are some differences between the two DBS products. The commercial DBS tends to have lower minimum gelation concentrations than

synthesised DBS. It was proposed that commercial DBS will have a different purification method, as it would not be practical to wash DBS on a commercial scale. It is possible that this change in purification has influenced the polymorph of DBS formed, which in turn could change the solubilities of DBS, as polymorphs of other gelators have been shown in the literature to impact their ability to form gels.[96]

2.3 Minimum Gelation Concentration of Commercial DBS

The minimum gelation concentration (MGC) is the lowest amount of gelator needed to self-assemble into a gel. Below this concentration, upon dissolution and cooling, the solution does not form a sample-spanning gel. Below the MGC it is possible that nanofibres exist but are not sufficient to form a network, or that nanofibres do not exist. This will depend on the cooperativity of the assembly process.[97, 98] However, on drying, the concentration will in any case increase, and it can be argued that nanofibres will, in either eventuality, ultimately form. The MGC varies according to solvent and gelator selection. The MGCs of commercial DBS were investigated in thirteen different solvents, covering a range of solvent properties; from polar to non-polar and protic to aprotic. Eight of these thirteen solvents formed gels with DBS as expected, based on the great versatility of this gelator. MGCs are given in Table 2-1.

Table 2-1.Minimum gelation concentrations for commercial DBS.

Solvent	MGC (wt/v%)	Classification
Diethyl ether	Insoluble	Non-polar, aprotic
Cyclohexane	Insoluble	Non-polar, aprotic
Water	Insoluble	Polar, protic
Toluene	0.025	Non-polar, aprotic
1:1 Water:Methanol	0.1	Polar, protic
Chloroform	0.2	Non-polar, aprotic
Methanol	0.4	Polar, protic
Ethyl acetate	0.4	Borderline polar, aprotic
2-Butanone	0.6	Polar, aprotic
Acetone	0.6	Polar, aprotic
Acetonitrile	0.7	Polar, aprotic
THF	1.2	Borderline polar, aprotic
DMF	Solution	Polar, aprotic
DMSO	Solution	Polar, aprotic

In highly apolar solvents (e.g. cyclohexane) or polar solvents (e.g. water) DBS was insoluble. In very polar aprotic solvents (e.g. DMF/DMSO) the gelator simply dissolved and would not form gels. As the polarity decreases (from THF to toluene) then in general terms the MGC decreased. In other words, DBS assembles better in less polar, less hydrogen bonding solvents. However, there are exceptions to this behaviour such as the low MGC in methanol. A more quantifiable way of exploring solvents is to use solubility parameters.

2.4 Correlating Solvent Parameters and Minimum Gelation Concentrations of Commercial DBS

The contribution of individual solvent molecules, as well as their bulk properties, are incredibly important in the self-assembly of gelators.[80] Numerous attempts have been made to correlate gelation with different solvent parameters,[80] e.g. Kamlet-Taft parameters,[81] Hildebrand solubility parameters[82, 83] and Hansen solubility parameters.[65, 77, 82, 84-91] Hansen solubility parameters (HSPs) quantify the energy contributions from 3 weak interactions; δ_d, δ_p and δ_h representing dispersion forces, polarity and hydrogen bonding interactions, respectively. Dispersion interactions include atomic forces such as van der Waals forces of attraction.[77, 95]

HSPs are now the most commonly used method to predict the response of a gelator in a specific solvent.[65, 77, 82, 84-91] DBS has been studied as a gelator due to its ability to gelate such a wide range of organic solvents,[77, 86, 87] although other sugar-based gelators have also been considered.[90] Commonly, gelators and solvents tend to be classified into three different groups, those which are solutions, form gels or the gelator remains insoluble. By using the solubility parameters (in particular, plotting in three-dimensional Hansen space) of solvents and gelator outcomes, three spheres can be generated. Each sphere describes a different behaviour, and depending on the data analysis, all three spheres can have the same central point, or different. Generally, the consensus appears to be that with enough data, one can predict the gelation behaviour of a specific gelator in an unknown solvent (at a given concentration) by determining which shell the solvent parameters fit, but that these correlations cannot be extended beyond the original gelator on which they are founded. In studies reported by Rogers, the HSPs of DBS were defined as the central coordinates of the calculated solvent spheres describing gel behaviour (insoluble, gel or solution). These researchers concluded that the distance between the HSP of a solvent and the optimal gelation HSPs determine whether that particular solvent will form a gel.[85, 88] If the δ_h value of the

solvent was less than the coordinating value for the centre of the sphere, opaque gels formed. If the δ_h of the solvent was greater than that of the centre of the sphere, clear gels formed.[86] This supported other studies also conducted by Rogers on 12-hydroxystearic acid which found a similar result, the δ_h of the solvent and the centre of the sphere, defining the properties relating to the gelator, was responsible for the translucency of the gel formed.[85] This work was later picked up by Diehn working under Raghavan, who rationalised that the distance in Hansen space from the centre of the sphere of gelation to the solvent (R_0), quantifies the incompatibility between the two.[87] Gelation requires a moderate incompatibility, a balance between solubility and insolubility.[25] Too soluble and a solution forms, but too insoluble and the gelator remains undissolved, which correlates to the spheres generated.

$$R_0 = \sqrt{4(\delta_d^j - \delta_d^0)^2 + (\delta_p^j - \delta_p^0)^2 + (\delta_h^j - \delta_h^0)^2}$$

R_0 describes the distance from the gelator to the solvent in three-dimensional Hansen space where δ^j are the solvent parameters of the solvent and δ^0 are the parameters of the gelator.[82, 87]

Diehn also correlated the rheological properties and found that as R_0 increases, G' also increases, but the time required to gel decreases. It makes sense that stiffer gels (increased G') would results from an increase in incompatibility (increase R_0).

Collaborative work between Raghavan and Weiss has shown that once the behaviour of a gelator is established, one can predict the behaviour of gelator in a new solvent.[84, 88, 89]

It was interesting to plot the solvents used above against their Hansen solubility parameters. In particular, it was important to see if a quantitative parameter, such as MGC can be understood in this way, as most studies of solvent effects simply correlate gel/no gel at a fixed concentration with HSPs. The MGC of DBS in various solvents and the corresponding solvent Hansen solubility parameters can be found in Table 2-2.

Table 2-2. Minimum gelation concentrations for commercial DBS including Hansen solubility parameters for each solvent.

Solvent	MGC (wt/v%)	HSP		
		δP	**δH**	**δD**
Diethyl ether	Insoluble	2.9	5.1	14.5
Cyclohexane	Insoluble	0	0.2	16.8
Water	Insoluble	16	42.3	15.5
Toluene	0.025	1.4	2	18
1:1 Water:Methanol	0.1	13	16.8	16.25
Chloroform	0.2	3.1	5.7	17.8
Methanol	0.4	5.3	7.2	15.8
Ethyl acetate	0.4	12.3	22.3	15.1
2-Butanone	0.6	9	5.1	16
Acetone	0.6	10.4	7	15.5
Acetonitrile	0.7	18	6.1	15.3
THF	1.2	5.7	8	16.8
DMF	Solution	13.7	11.3	17.4
DMSO	Solution	16.4	10.2	18.4

As can be seen from Figure 2-2, as expected from previous work,[86, 87] the most solvating solvents cluster in the centre of the plotted Hansen space (DMF and DMSO). These solvents are best matched to the gelator and solvate it effectively, limiting the self-assembly. The most insoluble solvents tend to lie on the extreme edges. Here the solvent is poorly matched to the gelator, which therefore will not dissolve to enable assembly in the first place. Excluding methanol, water and the mixture, most of the gels lie between $5 \leq \delta_h \leq 10$, in between the two extremes of too soluble and too insoluble.

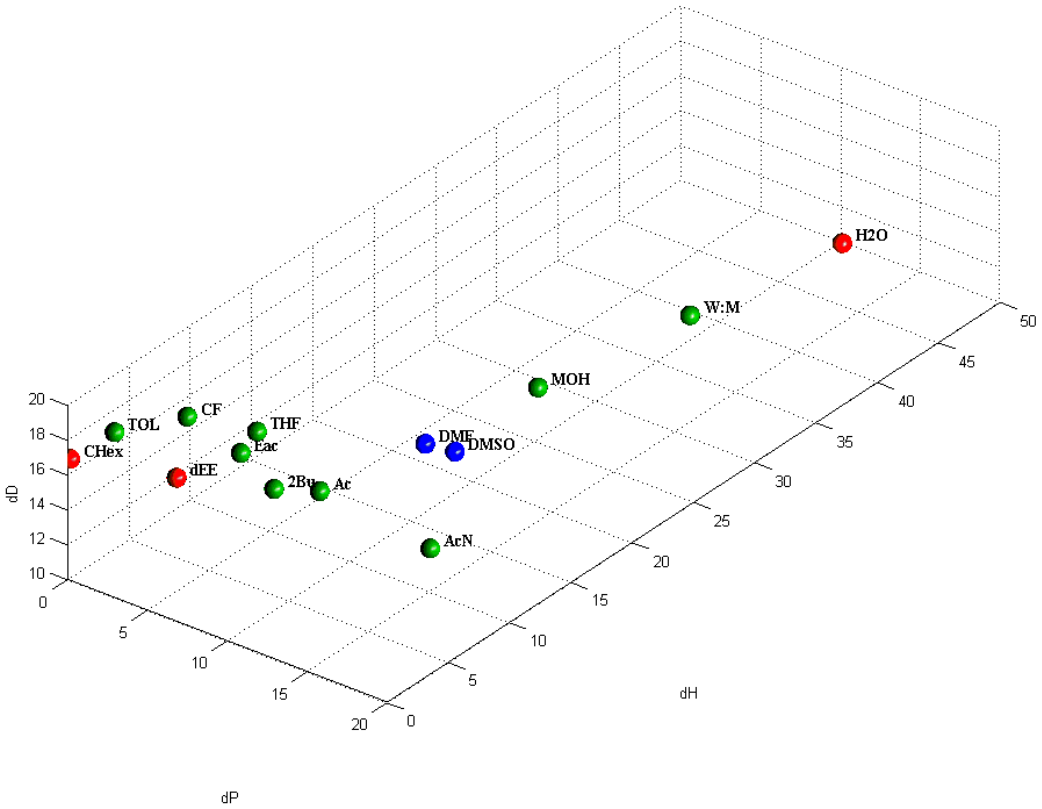

Figure 2-2. 3D plot for MGC of DBS using Hansen solubility parameters for the solvents for which MGC were measured; blue = solution, green = gel and red = insoluble.

Using software provided by Raghavan, concentric spheres of solubility were plotted as can be seen in Figure 2-3. These all had the origin coordinates of δ_p 15.1, δ_h 10.8, δ_d 17.9. These were similar to the centres from the original Diehn study which had the origin coordinates of δ_p 13.6, δ_h 6.4, δ_d 17.8 for DBS at 1 wt/v%.[87,90] Basically, three shells form from the same origin; the smallest sphere contains the solvents which form solutions with DBS, the next shell contains the solvents which form a gel and the outermost shell contains solvents in which DBS is insoluble. Our investigation supports the previously presented work and can be matched to this model.

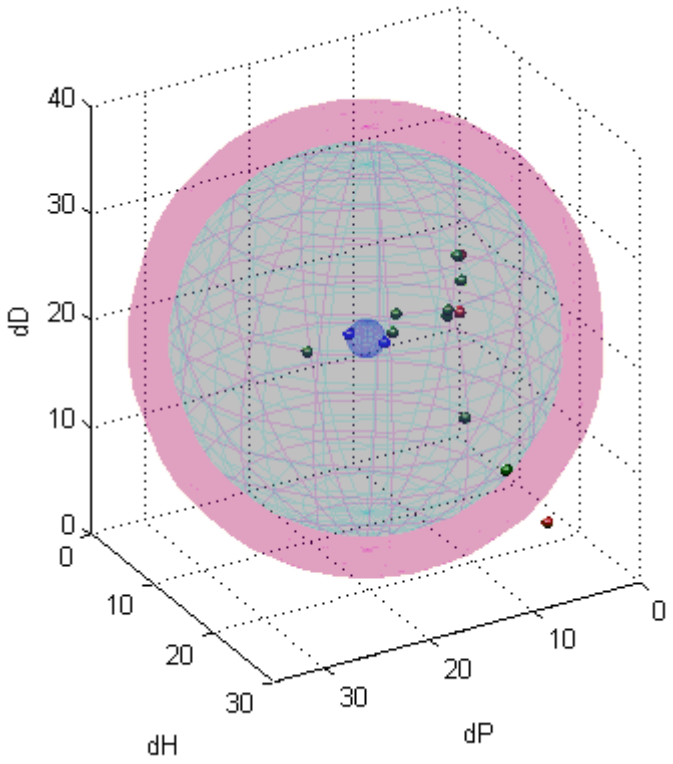

Figure 2-3. 3D plot for MGC of DBS using Hansen solubility parameters for the solvents for which MGC were measured, with spheres for gelation behaviour plotted; blue = solution, green = gel and red = insoluble.

To analyse this plot in more detail, the distance from the centre to each solvent was calculated and plotted against the corresponding MGC. The distance was calculated as the difference between each point and the coordinates of the origin of the shells. Unlike the previous study by Diehn, 2 δ_d was not required to generate reliable results. The distance, R_0, was defined by the following equation.

$$R_0 = \sqrt{(\delta_d^j - \delta_d^0)^2 + (\delta_p^j - \delta_p^0)^2 + (\delta_h^j - \delta_h^0)^2}$$

As can be seen from Figure 2-4, there is generally an inverse correlation between the centre of the concentric solubility spheres from the HSP plot and MGC with a gradient of -11.6, although the R^2 value was on 0.8 implying that this trend line represents a correlation, but could describe the data more accurately. The two outliers have been excluded from this trend line, demonstrated on the graph by orange borders. The less soluble the gelator in a particular solvent, the less gelator was required to form a gel network so the lower the MGC. Therefore the solubility of the gelator defines the MGC. Previous work has investigated if a gel forms but as far as is known, this is the first time that MGC has been correlated with HSPs.

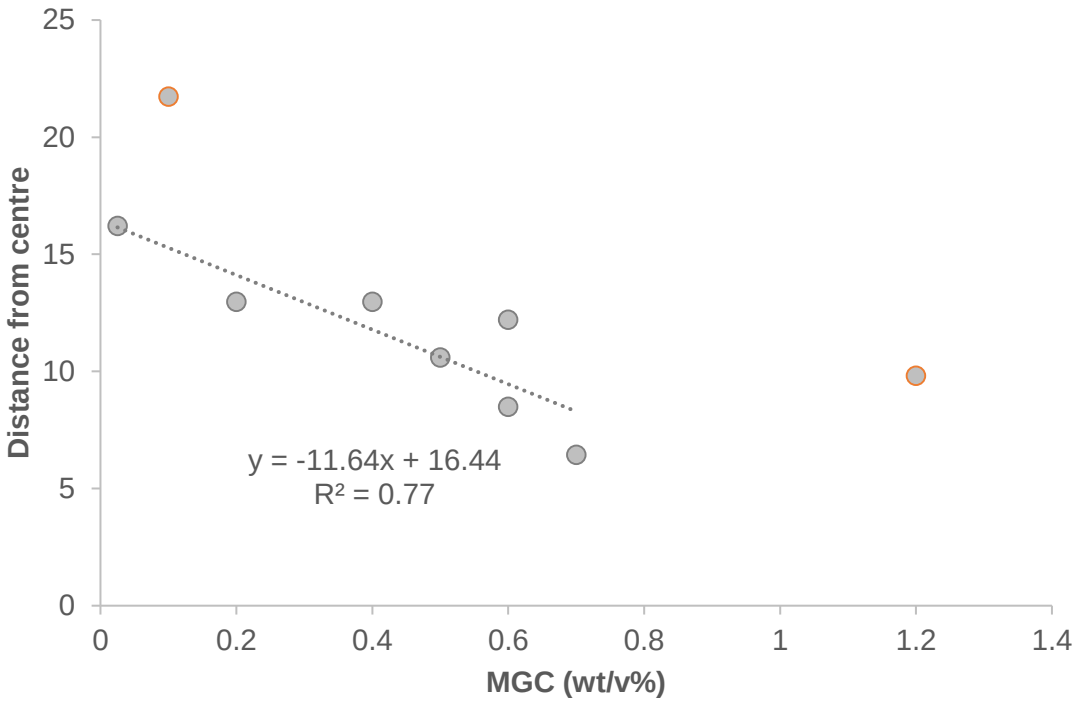

Figure 2-4. Graph of distance from centre concentric spheres on HSP plot *vs.* MGC for all solvents which formed a gel with DBS.

After finding this correlation between MGC and R_0, it was thought that it would be interesting to try to correlate the thermal stability of commercial DBS to MGC and concentration of gelator.

2.5 Thermal Stability of Commercial DBS

LMWGs are formed through application of an external stimulus, which might be physical or chemical.[25, 29] These gels are therefore responsive to varying stimuli, enabling many potential applications.[30, 35, 50, 51, 148, 258] The use of a heat-cool cycle is the most common way to form a gel, heating a small amount of solid gelator in a solvent until the gelator fully dissolves forming a clear homogeneous solution. This solution is then allowed to cool, allowing interactions to form between gelator molecules leading to aggregation and eventually a gel network forms. Applying high temperatures disassembles the gel into its solution state. The temperature at which a gel becomes a solution is known as the T_{gel}. The formation of a gel is normally enthalpically driven, meaning an increase in temperature shifts the equilibrium to the solution phase (increasing the entropy from having gelator molecules free in solution rather than organised aggregates).

The thermal stability of each gel was measured by finding the temperature at which a gel disassembles to its solution state, the T_{gel} of each sample. This was measured using a reproducible tube inversion test. The samples were heated at 0.5 °C min^{-1}, after each temperature increase increment, the sample vial was inverted. The temperature at which the gel could no longer hold its own weight upon inversion of the vial was recorded as the T_{gel} value. Predominantly, methanol and 2-butanone were selected as chosen solvents to correlate the importance of concentration on T_{gel}. As seen in Figure 2-5, as the concentration increased, T_{gel} increased, as would be expected due to the extension of the gel network.

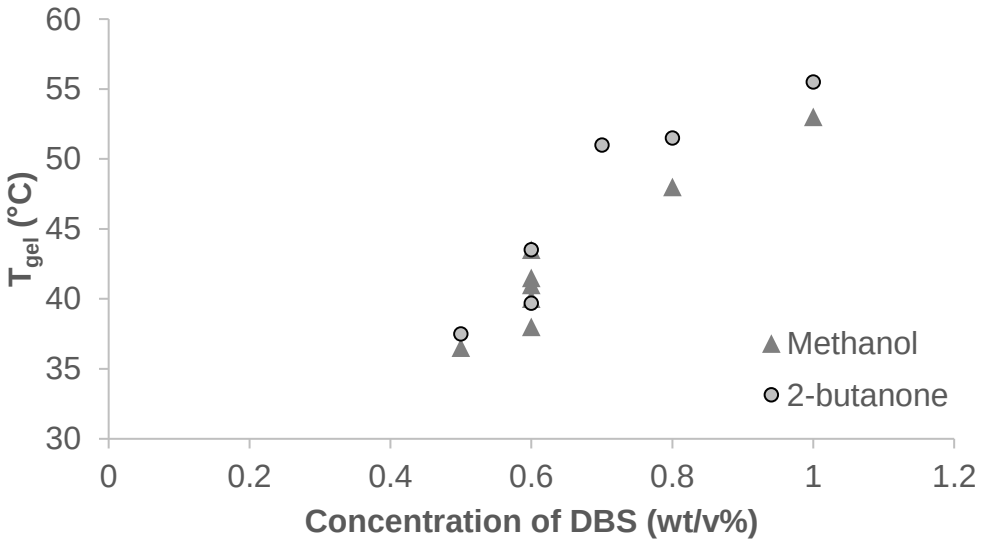

Figure 2-5. Thermal stability of DBS in methanol and 2-butanone.

All of the T_{gel} values shown in Figure 2-5 are above 35 °C. This is excellent in terms of application as it means that the nanofibres should be able to withstand the external temperatures imposed on them in realistic situations, without disassembling. These results also show that the 2-butanone gels are slightly more thermally stable than those produced in methanol at the same concentrations. These results prompted further investigation into the properties of the gel networks formed.

2.6 Rheology of Commercial DBS gels

The flow properties and the way in which gels respond under stress can provide insight into the composite materials properties. These properties are found through rheology, the science of deformation and flow, measuring a gel's response to an applied stress. Rheology is typically measured in two ways; viscosity (measuring flow) and oscillation (measuring deformation).[419] The storage modulus (G') quantifies the solid-like

characteristic of the system and the loss modulus (G") its liquid-like behaviour. For a gel, G'>>G" and independent of frequency. If G'>G", the material is solid-like and elastic, however, if G">G', the material is liquid-like and viscous. The rheological properties of a gel can provide information on the macroscopic properties of the gel network and give an indication of how it may respond within the fabric.

Rheological measurements were performed on commercial DBS gels on a Kinexus Pro+ stress-controlled rheometer. Samples were prepared by weighing out a known amount of gelator into a glass vial, then adding 1 mL of solvent. The samples were heated to under the boiling point of the solvent until all the gelator had dissolved forming a clear homogeneous solution. The samples were left overnight at room temperature to form gels. Due to the gelation kinetics, the samples had to be transferred onto the rheometer using a spatula. This leads to inconsistencies in the sample due to the shear force applied while moving the gel. DBS gels are fragile and their structure is strongly affected by shear to the point that loading disturbs the gel structure.[420] However, the gels took an impractical amount of time to form on the plate, so moving them once formed was preferable. The linear viscoelastic region (LVR) was determined from an amplitude sweep at 298 K, demonstrating the region where the strain does not disrupt the internal structure of the gel. A value from the LVR was then used during frequency testing to ensure the internal structure of the gel was not broken down, typically around 0.1% shear strain. An example of a typical amplitude sweep can be seen in Figure 2-6.

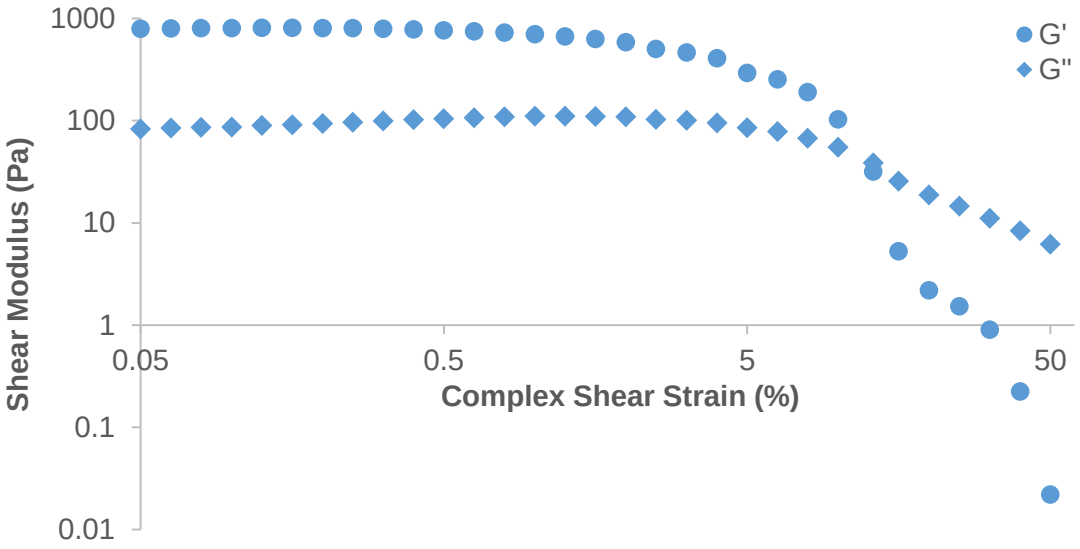

Figure 2-6. Typical rheological amplitude sweep to find the LVR region (0.6 wt/v% DBS in methanol).

Frequency sweeps of the same samples were performed at 293 K to determine the behaviour of the gelator networks. Both the storage modulus (G') and loss modulus (G") were determined for each sample and the response to increasing frequency recorded. These values were recorded as the value for which the gel was stable over a range of frequencies. The value of G' from the example in Figure 2-7 is *ca.* 5000 Pa.

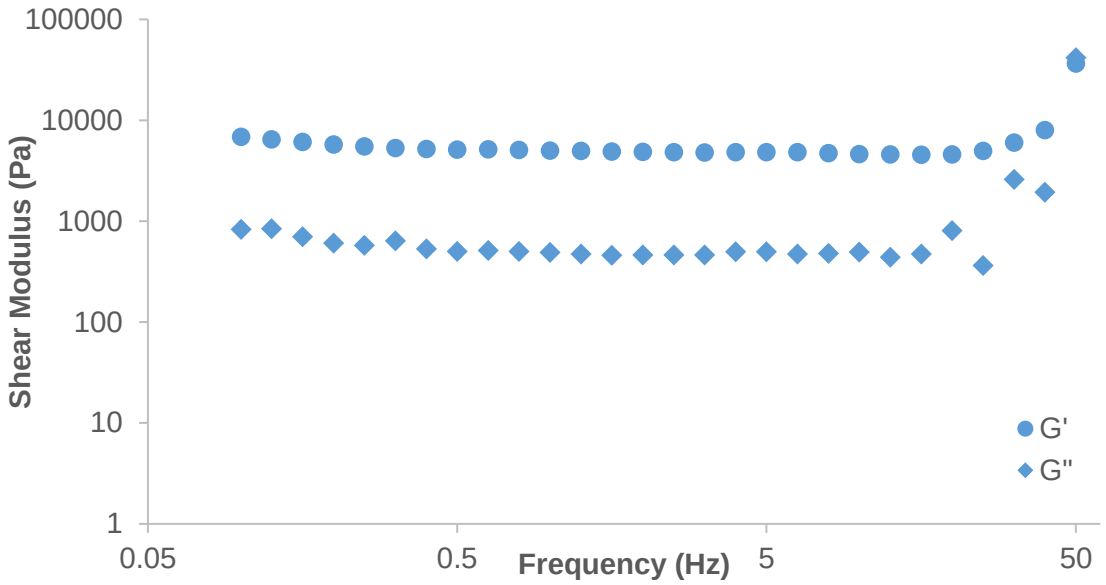

Figure 2-7. Typical rheological frequency sweep (0.6 wt/v% DBS in methanol).

2-Butanone produced gels with higher G' values than methanol (Figure 2-8) suggesting that these gels are stiffer, potentially as a result of stronger interactions between gelator molecules in this solvent. These results also support the T_{gel} values, 2-butanone generally formed gels with a higher thermal stability than methanol at the same concentration. Generally, the results also show a positive correlation with concentration. The higher the concentration of gelator, the stiffer the gel network formed (increased G'). These results are in agreement with those found by Santos and co-workers, who found that greater values of G' were observed for gels with a higher concentration of DBS.[420] Their work also found that solvent polarity and its ability to form hydrogen bonding may have significant effects on gel rheology. Santos and co-workers found that ethanol exhibited the lowest elasticity and stiffness of all the tested samples,[420] supporting the results with methanol that demonstrated the lowest stiffness in this comparison. The relationship between gel strength and stiffness with the nature of the solvent is not well-defined, with many factors which might be relevant like solvent polarity, molecular weight and potentially most importantly, its ability to form hydrogen bonds. The study of fibril morphology of DBS gels by Yamasaki demonstrated that in high polarity solvents, the hydrogen bonding between DBS and the solvent become

more predominant. This results in hydrogen bonds between DBS molecules becoming weaker, tending to produce weaker gels.[135] 2-Butanone is an aprotic solvent whereas methanol is a protic solvent. One could expect some interaction between the carbonyl group of 2-butanone and the 5-OH/6-OH of DBS. The protic solvent, methanol, contains hydrogen atoms which can form strong hydrogen bonds and can exchange rapidly with the DBS molecules forming the fibrils, resulting in weaker interactions between DBS molecules, and hence in weaker DBS gels as demonstrated by the results below in Figure 2-8.

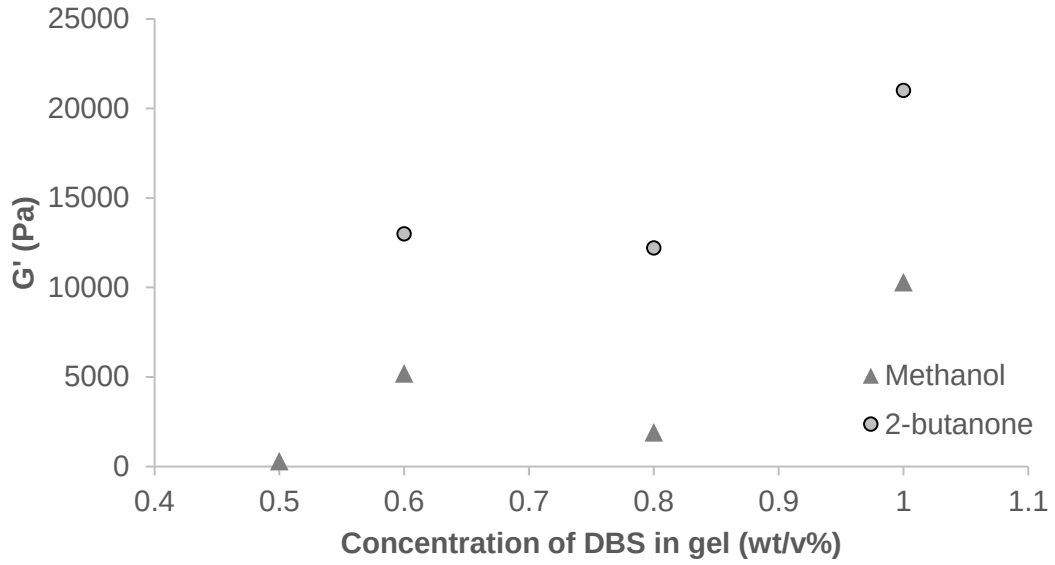

Figure 2-8. G' values for range of DBS concentrations in methanol and 2-butanone.

Rheology therefore shows that 2-butanone gives stiffer gels than methanol, which implies increased DBS intermolecular interactions, which could give more compact DBS fibrils resulting in a more robust nanofibre morphology. There was also a positive correlation between concentration and G'. This led to the morphological investigation of these gel networks using scanning electron microscopy (SEM).

2.7 Introduction to Reading SEM Images

When considering the SEM images presented in this thesis, the fabric fibres and DBS nanofibres are at two very different length scales. The fabric fibres can be seen at the 8 µm scale and the DBS gel nanofibres can be seen at the 15 nm scale. An SEM image is shown in Figure 2-9 to aid identification of different types of fibres in the following images. The nanofibres become more evident in the higher magnificent insert. The

term ‘aggregate’ is used to describe any morphology where multiple nanofibres bundle together, as the nanoscale network is shown to be indistinguishable.

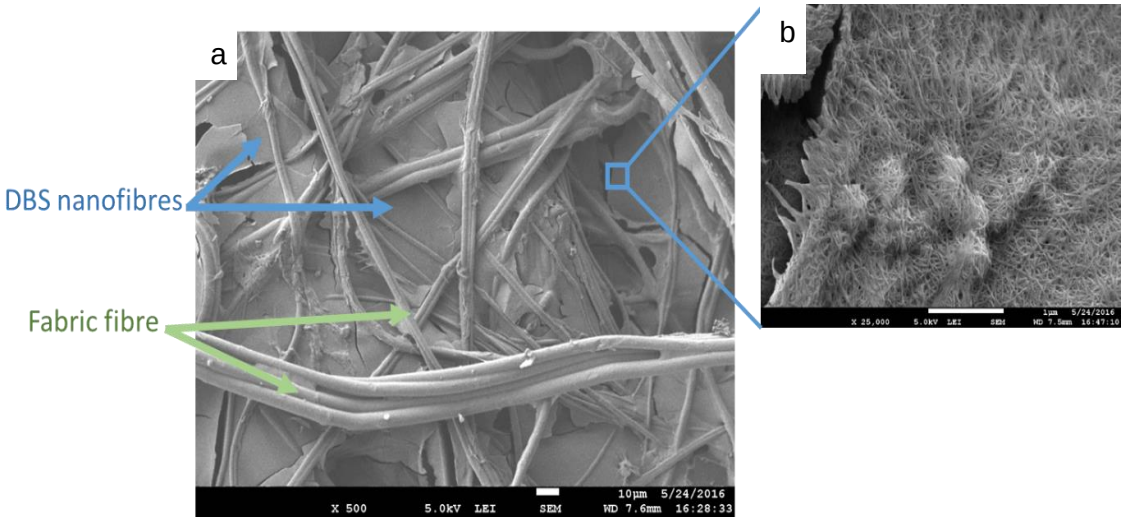

Figure 2-9. SEM images (a) demonstrating distinction of nanofibres and fabric at x 500 magnification, scale bar of 500 µm; (b) enhanced magnification image showing DBS nanofibres at x 15 000 magnification, scale bar of 1 µm.

It is also important to appreciate the in-sample variation, remembering that SEM images only show a snapshot of the sample. Each sample is imaged in at least three different areas and the images shown are representative of the sample as a whole. Where there were significant deviations across the sample, multiple SEM images have been incorporated to demonstrate this.

2.8 Solvent Investigation with Synthesised DBS on SEM Stubs

It is known that changing solvent polarity can affect the interactions responsible for self-assembly. As described earlier, various studies have struggled with solvent polarity and DBS gelation.[87,136,51] This importance of solvent polarity has also been demonstrated in the correlation of solvent parameters and MGC as seen in Section 2.4. Initially, synthesised DBS was dried directly onto SEM stubs, in the absence of fabric, from different solvent systems at a fixed concentration to investigate any potential differences in morphology, including DCM (apolar aprotic), DMF (polar aprotic) and a 1:1 water:methanol mixture (polar protic). This allowed characterisation of the basic nanofibre assembly before introducing the fabric. SEM images taken at x5 000 and x75 000 magnification for DCM, DMF and 1:1 water:methanol can be found in Figure 2-10. For other solvents used (methanol, toluene and chloroform), the images can be found in the appendix. Each sample was prepared in the same way and left to dry overnight

in a fume cupboard, the individual drying rates will depend on the volatility of the solvent. Different evaporation rates could influence the morphology formed. A fixed concentration of 0.5 wt/v% was selected to allow comparison of solvents which don't necessarily form a gel but should still produce nanofibres when dried down.

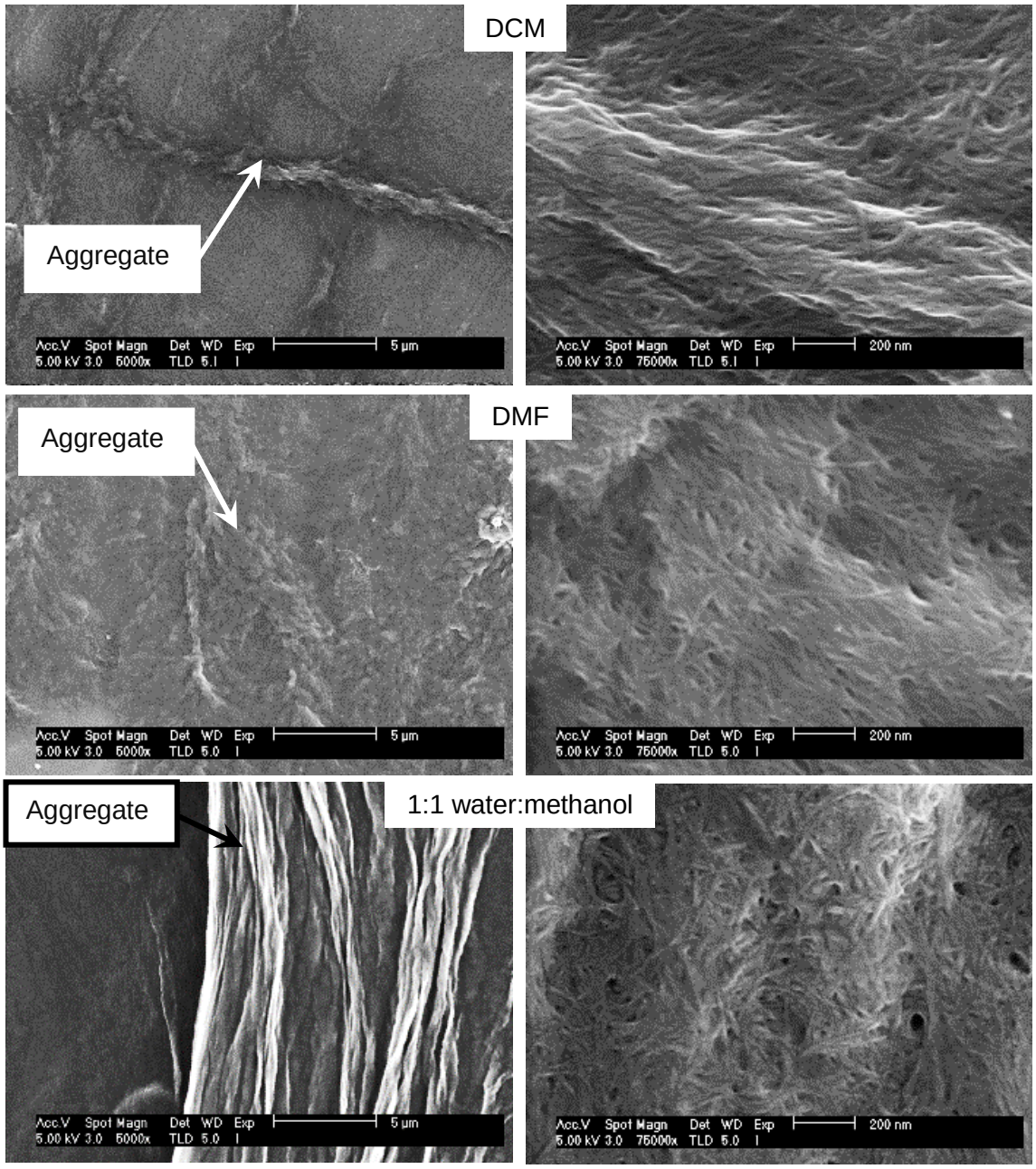

Figure 2-10. SEM images of 0.5 wt/v% DBS in DCM, DMF and 1:1 water:methanol on SEM stubs, scale bars at 5 µm and 200 nm.

It is evident that the nanoscale network (at x75 000 magnification, scale bar of 200 nm) appeared similar regardless of the solvent used, showing nanofibres with diameters in the region of 15 nm. The nanoscale networks appeared similar throughout, there didn't

appear to be any large changes in the “pore” size or fibre diameter or even the packing when the solvent was changed, so it was reasoned that the solvent from which the DBS nanofibres were dried cannot be a crucial factor for DBS nanofibre formation. This possibly results from the evaporation of solvent under atmospheric conditions, so the DBS nanofibres can rearrange as the solvent evaporates, leading to some thermodynamically favourable state, meaning the same nanofibre network is produced regardless of solvent. It is also interesting to note that nanofibre formation occurred even when dried from a non-gelling solvent such as DMF. So it would appear that there is no prerequisite to using a gelating solvent. As such, “greener” more industrially friendly solvents, like water, could therefore be investigated.

At lower magnification (x 5000, scale bar 5 μm), there were some slight differences in the networks formed. However, it was difficult to isolate differences between the networks because, even at this scale, the networks formed are non-uniform. When the images were produced, the rest of the sample was scanned to try and ensure that a representative sample had been imaged. It appears that different solvents produced differential amounts of stacking. Aggregation here refers to any microscale morphology of nanofibres. For example, out of the solvents shown here, DMF formed the flattest network, with the least significant stacking of nanofibres, followed by DCM. The mixture of 1:1 water:methanol appeared to show a higher degree of “stacking”, varying the height of the sample quite significantly in places. It would seem sensible that as the solubility of DBS is less in the more polar solvents, greater fibril-fibril aggregation appears to take place perhaps suggesting a greater degree of phase separation during drying as the system loses its solubility. As such, interpretation of the microscale network would suggest that matching the polarity of the solvent to that of the gelator may play a role in obtaining a better dispersed overall network of nanofibres.

Attempts were made to correlate the fibre diameters with the solvent used, but this turned out to be difficult. The Diameter J plug-in for Image J could not accurately segment the images due to the small fibre sizes and the density of fibres. It is good for samples which have been cryo dried, which have less dense nanofibres. When the fibre diameters were measured manually, it was found that the errors in the measurements were basically the size of the fibres themselves and therefore any trends were lost within errors. Visually, the fibre diameters looked consistent across all solvents, around 10-20 nm. This is supported in the literature by some work by Liu *et al.* who found that DBS fibril diameters remained almost constant at low concentrations.[77]

After looking at the different solvent systems and finding relatively few differences between the networks, the concentration within those solvent systems was changed to identify the significance of concentration on network formation.

2.8.1 Changing Concentration in Different Solvents

Chloroform

Chloroform and 1:1 water:methanol were investigated as examples of less polar and more polar solvents, respectively. Chloroform was investigated at a range of concentrations (0.1 wt/v% to 0.5 wt/v%). At a low 0.1 wt/v%, DBS in chloroform appeared to form two different morphologies. Figure 2-11 (a) shows broader “lumpier” fibres whereas (b) shows thinner straighter fibres. Both images show the second morphology to be in the minority.

Magnified images of both morphologies are visible in Figure 2-11. The two morphologies have significantly different fibre diameters: broader “lumpier” fibres consist of tiny 15 nm nanofibre diameters, whereas thinner straighter fibres are much larger, in the region of 50 nm.

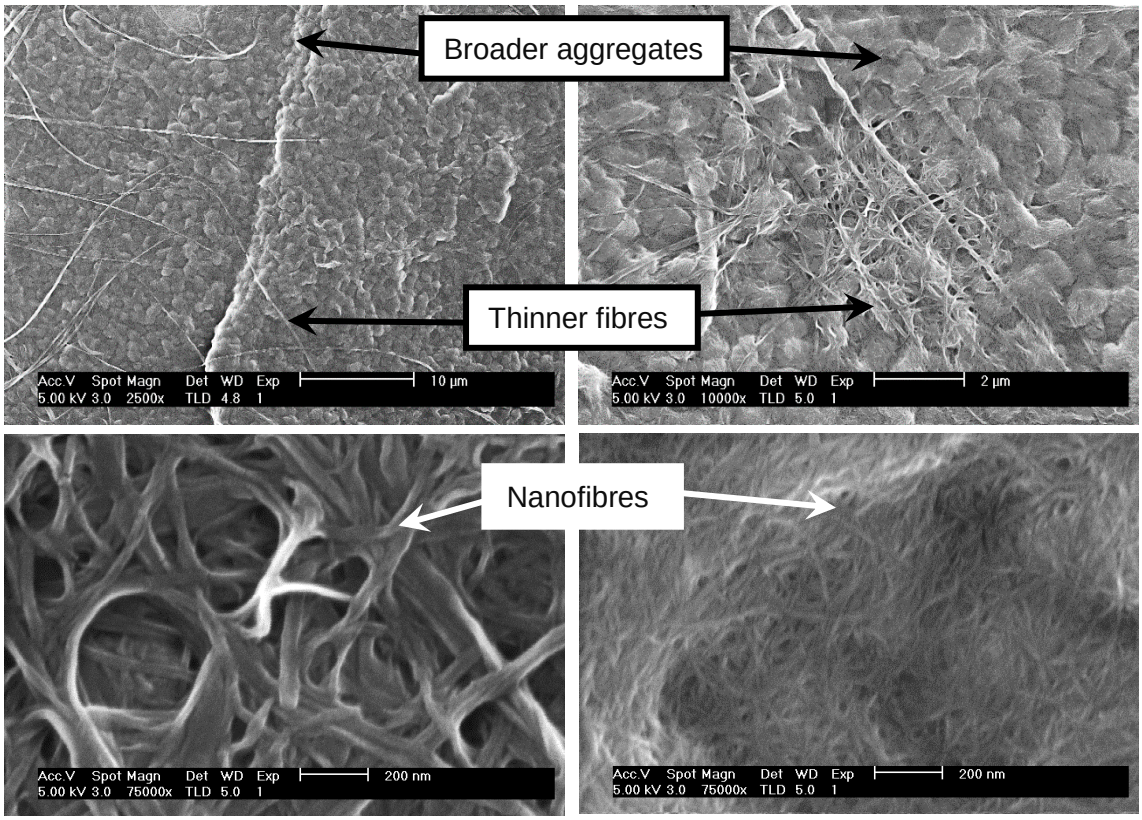

Figure 2-11. 0.1 wt/v% DBS in chloroform on SEM stubs showing two morphologies with scale bars of 10 µm, 2 µm, 200 nm and 200 nm.

As the concentration was increased to 0.3 wt/v% DBS, fewer of the thin straight fibres (from Figure 2-12) were seen. There appeared to be more of the broader fibre aggregates present.

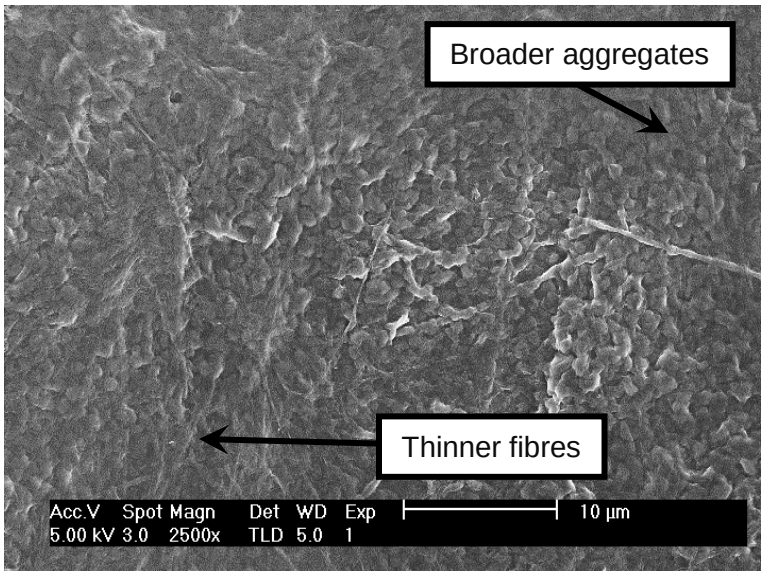

Figure 2-12. 0.3 wt/v% DBS in chloroform on SEM stubs, scale bar of 10 µm.

As the concentration was further increased to 0.5 wt/v% DBS in chloroform, both morphologies could be seen again. The thin fibres at 0.5 wt/v% seemed very similar to those at 0.1 wt/v%.

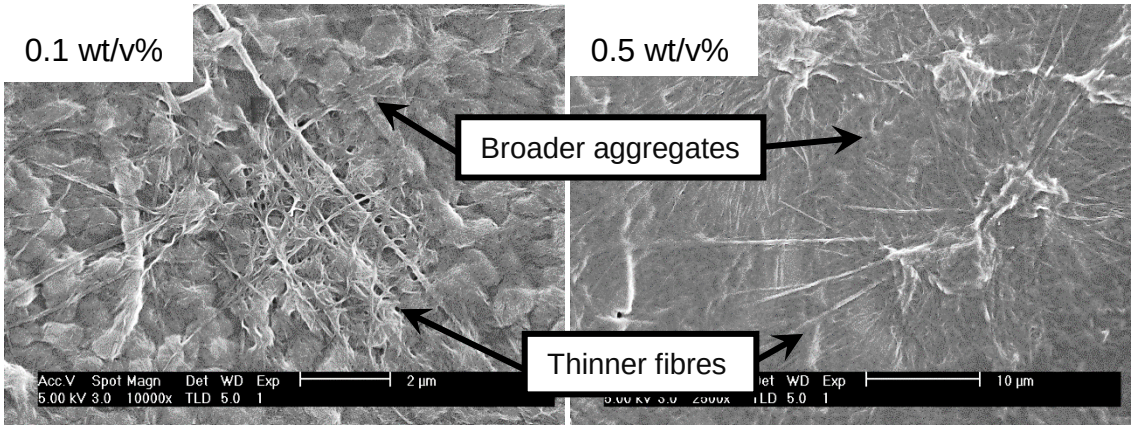

Figure 2-13. Comparative images of thin fibres in 0.1 wt/v% and 0.5 wt/v% DBS in chloroform on SEM stubs, scale bars of 2 µm and 10 µm.

1:1 water:methanol

The three samples in 1:1 water:methanol solvent mixture all looked very similar, especially at the nanoscale as seen in Figure 2-14. Even with the relatively poor resolution, it was easy to identify roughly the same sort of structures with what appear to be very similar, if not identical, fibre diameters.

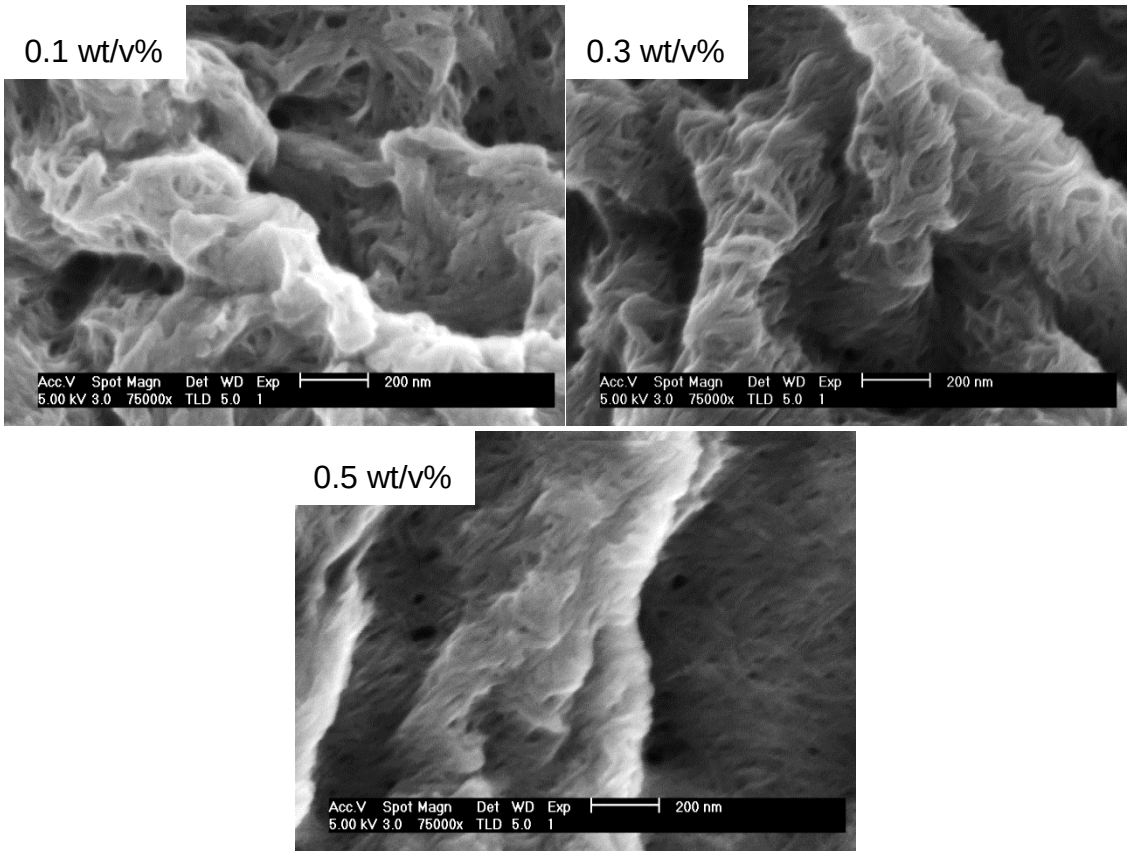

Figure 2-14. Nanoscale network of varying concentrations of DBS in 1:1 water:methanol on SEM stubs, scale bars of 200 nm.

The microscale networks were also very similar as can be seen from Figure 2-15. Again, the same sort of network can be seen, an effective “matting” across the surface of the sample.

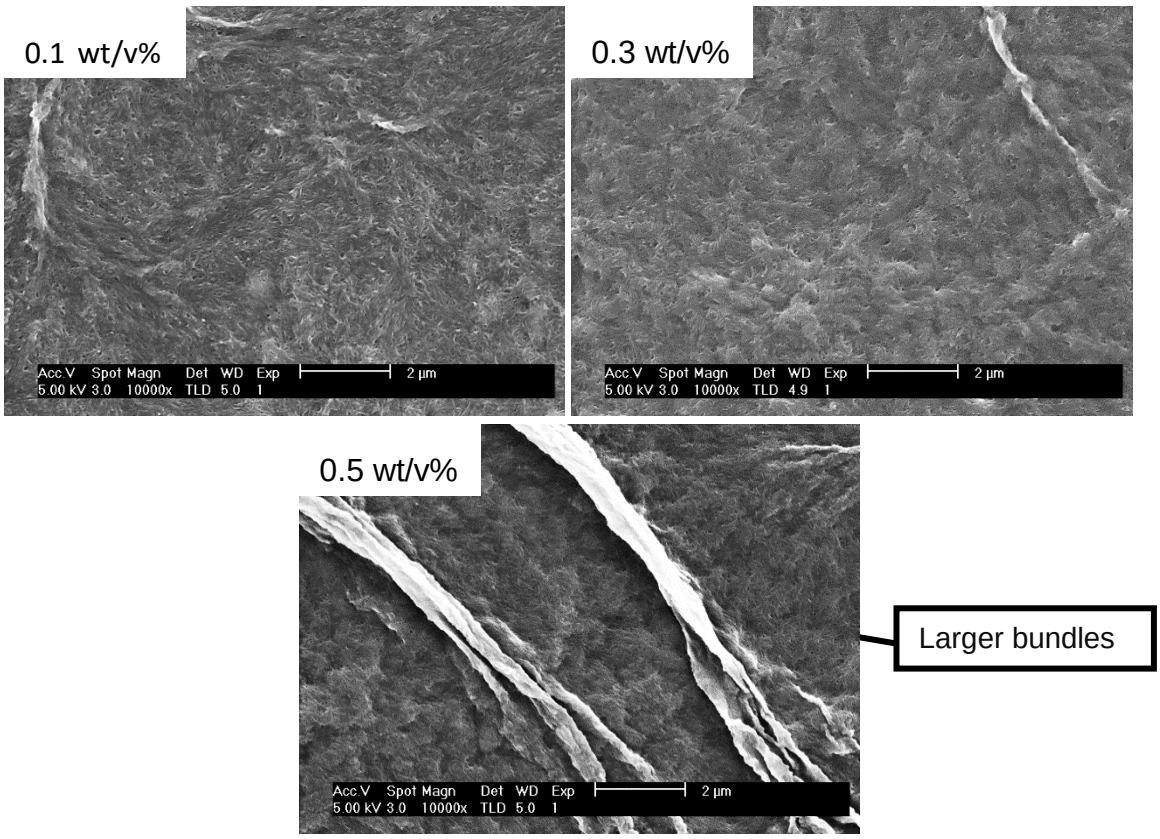

Figure 2-15. Comparison of microscale network of varying concentrations in 1:1 water:methanol on SEM stubs, scale bars of 2 µm.

At 0.5 wt/v% some larger bundles of aggregates were observed as described for other solvents in the previous section (2.8), but generally, all three concentrations gave similar images. The network looked slightly more solvated (wider diameter of fibres which look swollen) than in chloroform, which could be due to the differences in volatility of chloroform and water, meaning the water is harder to remove so the sample is less well dried. It appears that 1:1 water:methanol was an appropriate solvent for network formation, and was relatively independent of concentration with some bundling of fibres at 0.5 wt/v%. These larger bundles of fibres could be interesting for the application.

2.8.2 Vacuum

Two samples of 0.5 wt/v% DBS, one in methanol and one in 1:1 water:methanol, were dried under ambient conditions and under vacuum to investigate differences in network formation caused by forced, quick solvent removal.

In methanol, there appeared to be clear differences between drying under vacuum or at ambient pressure. In Figure 2-16, comparison of the low magnification images

suggested larger aggregated areas in the vacuumed sample compared to the non-vacuumed sample. These aggregated areas also looked different, more like “bushes” (i.e. with branches, dendrites) rather than ‘well dried’ objects seen in the ambient-dried sample. This would suggest faster drying can give rise to aggregates with larger surface areas as solvent is expelled more rapidly.

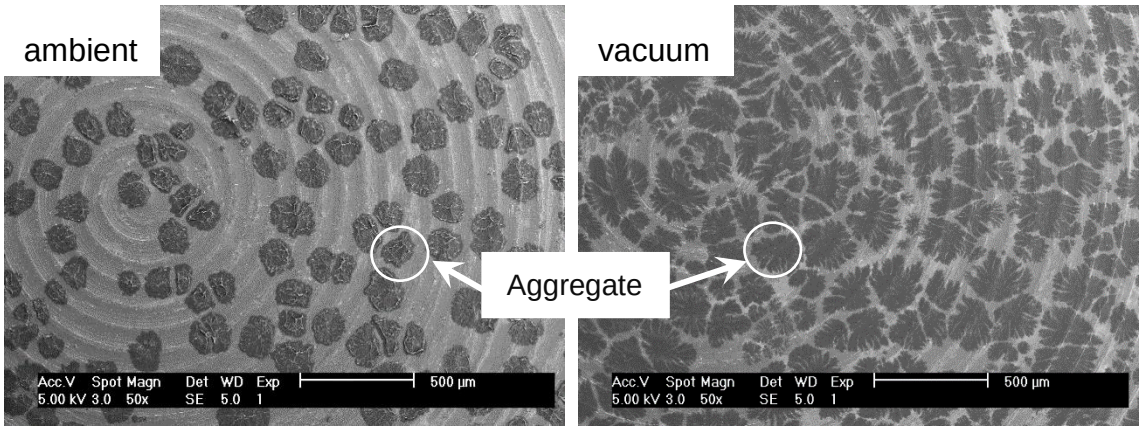

Figure 2-16. 0.5 wt/v% DBS in methanol under ambient conditions and under vacuum on SEM stubs, scale bars of 500 µm.

At high magnification, the nanoscale networks appeared very similar (as seen in Figure 2-17) suggesting that at the nanoscale the fibres formed are very similar. As such, the differences between images in Figure 2-16 were assigned to bulk sample drying effects rather than self-assembly differences.

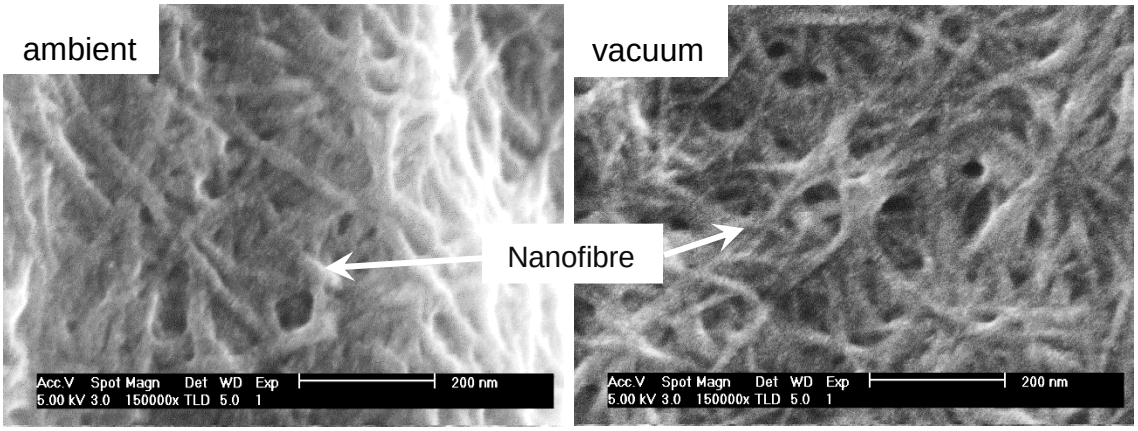

Figure 2-17. 0.5 wt/v% DBS in methanol under ambient conditions and under vacuum at high magnification on SEM stubs, scale bars of 200 nm.

More detailed comparison of the fibre sizes showed that the fibres dried under vacuum appeared narrower than the fibres dried in ambient conditions (approximately 15 nm *vs.* 25 nm). This is within the margin of errors for measuring the fibre size but it also

could be a result of rapid desolvation of the fibres, effectively deswelling them, making them thinner.

2.9 Proof of concept – Putting Synthesised DBS onto Fabrics

Having characterised the ability of synthesised DBS to form nanofibre networks on drying from relatively dilute conditions, it was important to demonstrate that this could occur in a fabric substrate.

As a proof of concept experiment, two fabric samples were prepared. The nylon-modified acrylic fabric is a wicking fabric, and was a military uniform textile. If the DBS nanofibres could assemble within this woven fabric, it would simply mean one additional step in the production process, rather than having to incorporate an entirely new textile into the current process in producing uniforms. This material is also liquid wicking so should be able to absorb solvent readily.

The two samples of fabric were roughly the same dimensions (*ca.* 10 mm x 10 mm) and weighed before the experiment. One fabric sample was soaked in methanol (2 mL), and the other soaked in a methanol solution containing 1.5 wt/v% DBS. This high concentration was used to ensure an abundance of gelator present, ensuring that any nanofibres were visible. The fabrics were then removed from the solvent-filled dish and left to dry under ambient conditions on an aluminium block. After approximately 10 minutes, the fabric soaked in just methanol had returned to roughly its original weight, whereas the fabric soaked in DBS gained *ca*. 3 mg, presumably due to the deposition of DBS nanofibres. Fabric masses can change with humidity and temperature so fabric weights can vary, however, the masses generally correlated with the expected trends. Visually from the SEM images in Figure 2-18, it was clear to see which fabric had been soaked in the DBS-containing solution, due to the appearance of white fibres on the surface of the fabric almost like a spiders web. In the sample soaked in only methanol, some of the dye leached out and turned the methanol green. 1.5 wt/v% is a concentration which is known to form a gel in methanol. This appeared to produce too much self-assembled material, overloading the fabric. As this was a proof of concept, the aim was to overload the fabric to visualise any nanofibres. The nanofibres had coated the surface fabric fibres rather than penetrating the fabric to form a network across the woven pores in the fabric fibre. There were also no nanofibres present in the gaps between the weave and the weft.

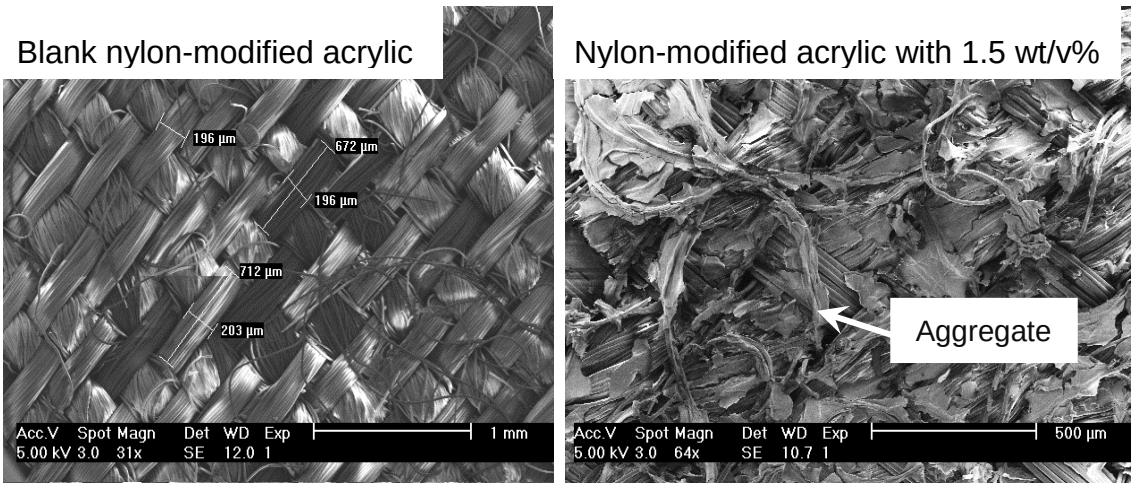

Figure 2-18. SEM images of nylon-modified acrylic fabrics treated without and with 1.5 wt/v% DBS in methanol, scale bars of 1 mm and 500 µm.

Figure 2-19 showed two SEM images of fabric samples at higher magnifications, one with no DBS and one treated with 1.5 wt/v% DBS. This made it possible to see the fibres appear to have attached to the fabric fibres within the fabric. The latter appear "hairier" than the blank fabric, implying that DBS has formed nanofibres on the fabric fibres. At a lower concentration, with better penetration, the nanofibres could possibly be encouraged to grow around the fabric fibres within the fabric.

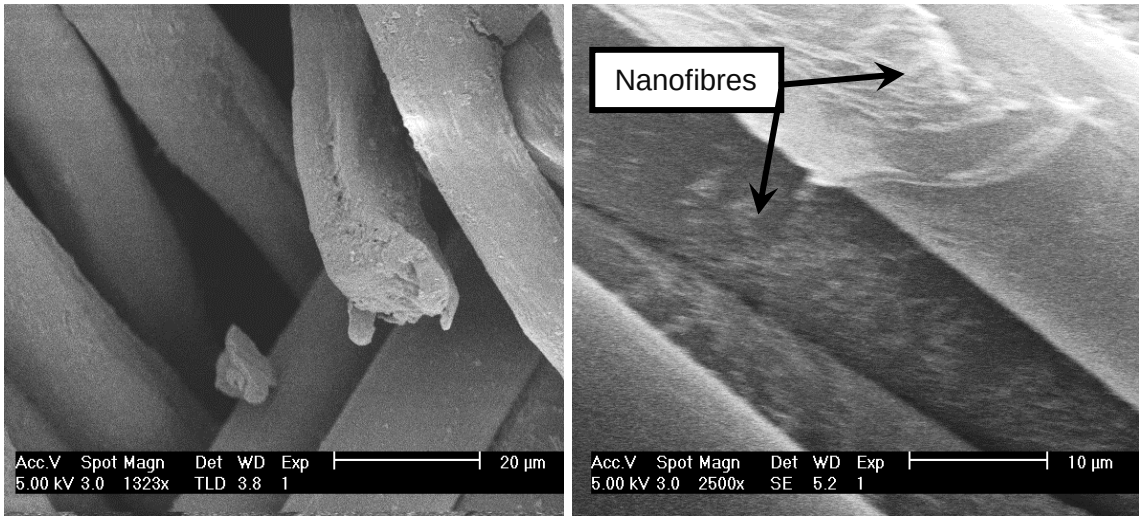

Figure 2-19. SEM images of nylon-modified acrylic fabric with no DBS, scale bar of 20 µm and fabric treated with 1.5 wt/v% DBS, scale bar of 10 µm.

After this proof of concept, it was clear that multiple variables could have an impact on the material produced. The solvent, concentration of gelator and fabric would all need to be individually investigated to produce an optimised system. Lower concentrations would be expected to spread across the fabrics, with emphasis given to the gaps

between the fabric fibre to determine whether nanofibres can assemble across the weave. Different solvents could also be considered, as more volatile solvents should evaporate quickly, which have the potential to leave larger fibres on the surface. By using a less volatile solvent, fibre formation could be slower, giving the molecules more time to penetrate the fabric. Using a tightly woven fabric, such as in the nylon-modified acrylic above, it is more likely to generate a robust material, so the nanofibres are less likely to change the intrinsic properties of the fabric. However, the lack of nanofibres on the crossing junctions for the weave and weft would suggest a tightly woven fabric could leave these junction points exposed to aerosol penetration. Using a much looser weave, with thinner, rounder fibres could also provide more gaps to fill with nanofibres. However, a looser weave might also make it more difficult to “bridge” all the gaps. It could also be that less uniformly structured fabrics need investigating.

2.10 Selection of Blank fabrics

After the initial, preliminary experiment on nylon-modified acrylic fabric, a fabric search was conducted for a looser weave fabric, with thinner, rounder fibres to provide a greater surface area with more gaps to fill with “nanofibres”. There were two carbon fabrics that looked, visually, to be suitable with a bit of flexibility in the fabric and plenty of holes or gaps for the nanofibres to fill. These carbon fabrics were also chosen as it was thought that the nanofibres could potentially be embedded within the activated carbon layer. Furthermore, the carbon in the fabric should improve the resolution of SEM analyses.

As can be seen in Figure 2-20, even at low magnification SEM images, the two carbon-based fabrics were very different. The sprayed carbon fabric had a lot of space between the areas of sprayed carbon and almost no regular structure to it. However, the carbon cloth laminated with knit had a regular structure with a looser weave than the nylon modified acrylic, but not so loose that the nanofibres would not be able to form a supplementary network between the fabric fibres. The carbon cloth was therefore carried forward into the next phase of testing.

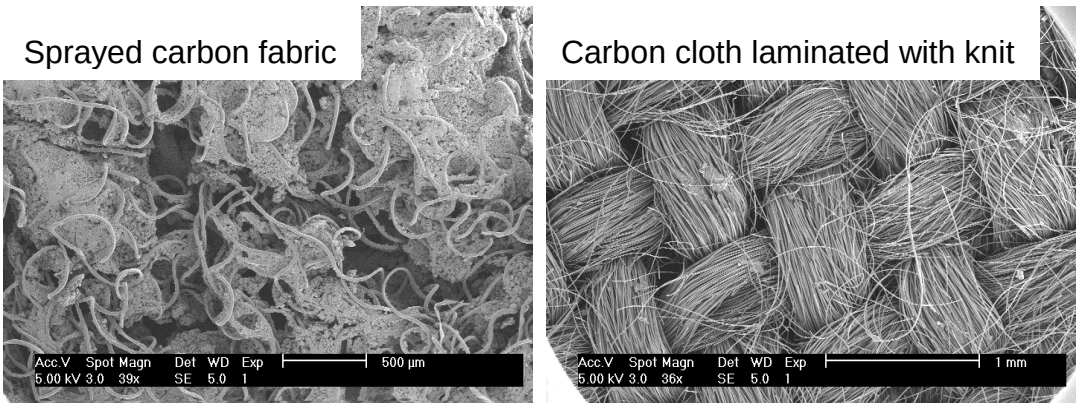

Figure 2-20. Low magnification SEM images to compare carbon fabrics, scale bar of 500 µm and 1 mm.

2.11 Dipping *vs.* Dropping of Synthesised DBS on Carbon Cloth

Two different approaches for loading self-assembled nanofibres into the fabric were then investigated: dipping and dropping. “Dipping” consisted of submerging the fabric in a bath of hot DBS solution (heated to dissolve the gelator). The fabric was left to soak for *ca.* 5 minutes, then removed and left on aluminium foil to dry. “Dropping” consisted of pipetting an aliquot (of *ca.* 0.15 mL initially) of hot solution onto the fabric, in an aluminium weighing boat which was then left to dry. Both methods of applying solutions were tested to see if there was an appreciable difference between them in terms of the modified fabrics formed. Three concentrations were investigated; 0.1 wt/v%, 1.0 wt/v% and 3.0 wt/v% synthesised DBS in methanol. The MGC of synthesised DBS in methanol is 1.0 wt/v%. Methanol was used as solvent to ensure comparability with the fundamental studies and to allow rapid evaporation, although for industrial application a less volatile solvent would likely be required.

Figure 2-21 shows SEM images of these three concentrations of synthesised DBS with samples prepared through both application methods to allow direct comparison. Generally, as the concentrations of gelator is increased, more nanofibres can been seen on the fabric in Figure 2-21. Overall, there is very little difference between the dipped and dropped samples, suggesting that the method of application may not be a crucial factor in the morphology of nanofibres formed. At 3.0 wt/v%, all of the fabric fibres were clearly coated but there was limited interlocking between the fabric fibres by the nanofibres. The aggregates followed the structure of the fabric fibre rather than filling in the gaps between them. This system would have potential to capture some particles. Some parts of the fabric might be expected to filter out particles, other parts (where there are no nanofibres) would probably not. However, with multiple layers of

fabric fibres, there would be potential for nanofibres to be present at a deeper layer, further into the fabric. As long as the fabric fibres overlapped throughout the depth of the fabric, some particles could be captured. The increased nanofibre deposition also seemed to physically stiffen the material. The material was still flexible but had more macroscopic rigidity as the concentration of applied DBS was increased.

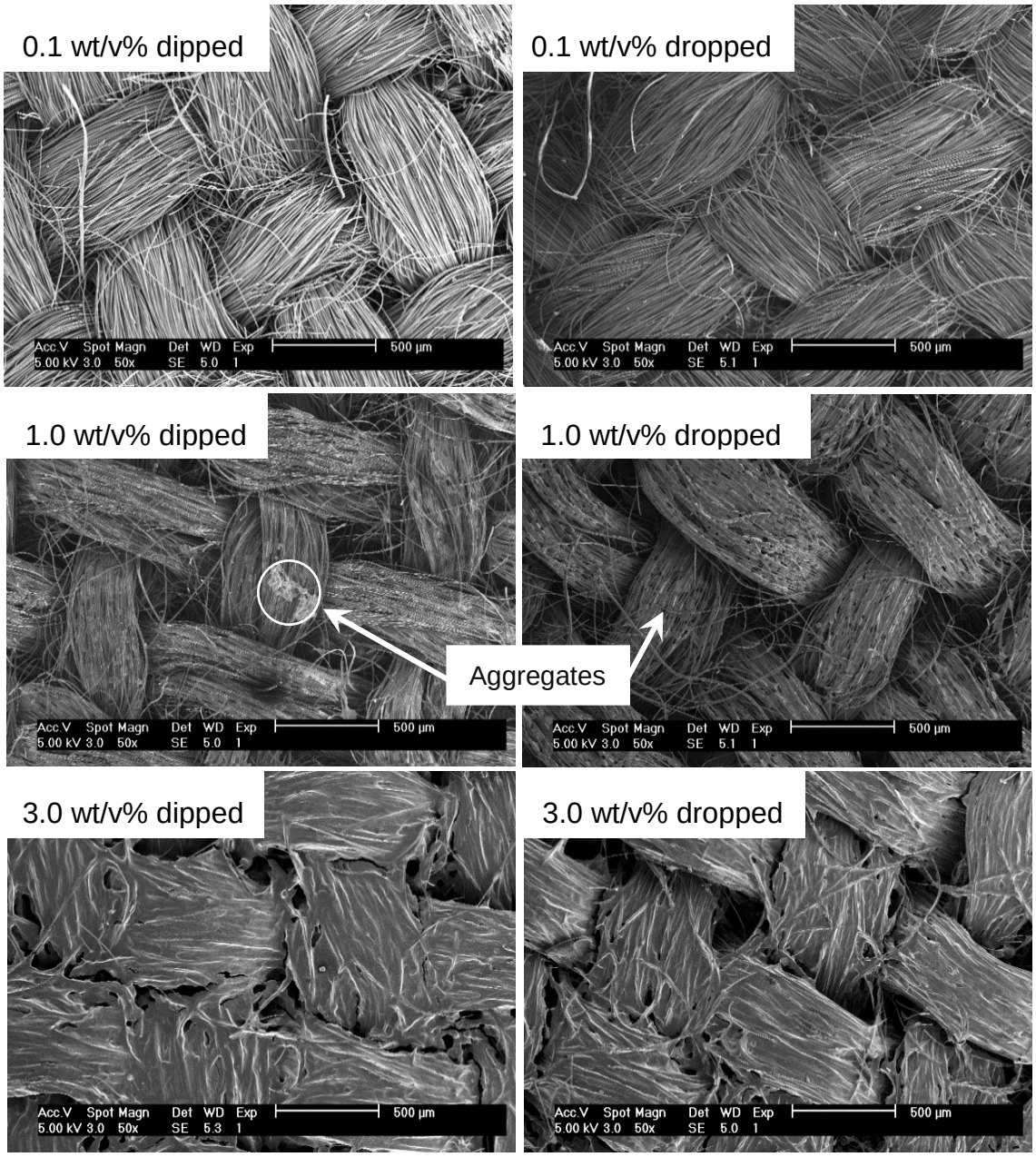

Figure 2-21. SEM images of carbon cloth treated with 0.1 wt/v%, 1.0 wt/v% and 3.0 wt/v% DBS in methanol dipped and dropped, scale bars of 500 µm.

Between the two 1.0 wt/v% samples, there were some small identifiable differences. The dipped sample didn't appear to have many aggregates between the fabric fibres,

certainly, they were less common than for the dropped sample. Also, no nanofibres were seen coating the surface of the individual fabric fibres. Instead, this dipped sample appeared to show one particularly large aggregate on the surface of the fabric. The dropped sample appeared to have “glue” between the individual fabric fibres. It was difficult to isolate the surface of these interconnecting aggregates but they looked like the fibrillar bundles seen in the DBS networks without the fabric present (see Figure 2-22). These aggregates also appeared to “blend” into the fabric fibre fibres. A few individual nanofibres were seen coating the fabric fibre fibres but generally most seemed to be forming these “glue” type aggregates. These differences were not seen with the other concentrations tested.

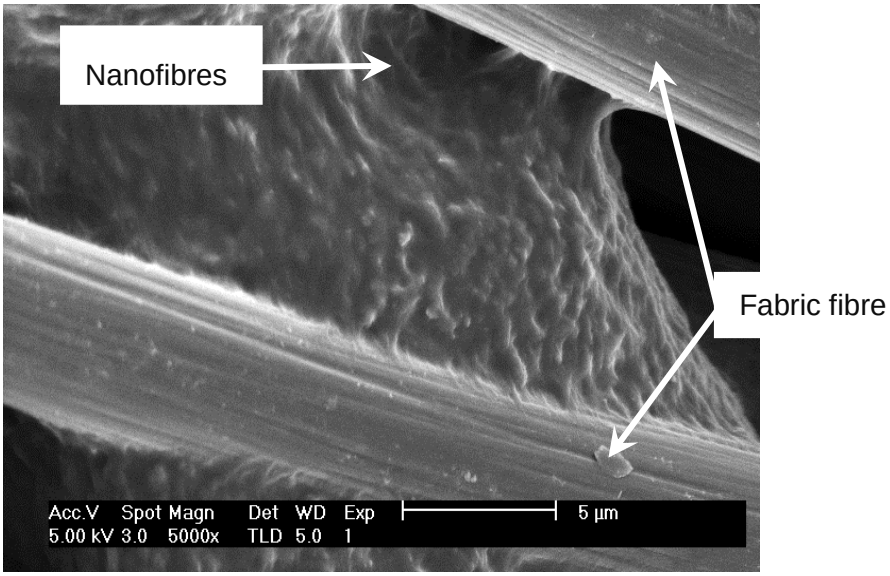

Figure 2-22. SEM images of carbon cloth laminated with knit treated with 1.0 wt/v% DBS in methanol, dropped, at higher magnification, scale bar of 5 µm.

Other concentrations in the range 1.0 – 3.0 wt/v% DBS in methanol were also investigated. When studying the mass deposited onto the fabric using each method, there was a general increase in the percentage mass change with increased concentration for each method of application. Figure 2-23 shows that generally, the two methods gave comparable results. The inaccuracy in pipetting could easily explain differences between dipped and dropped samples; within error the differences are negligible, it was clear that aliquot size was very important as explained further in section 2.11.1.

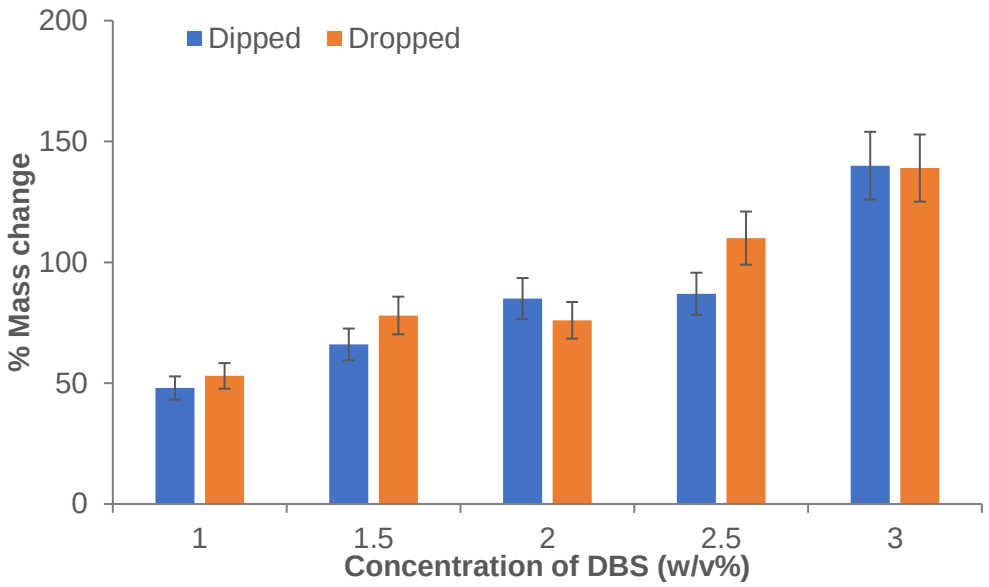

Figure 2-23. Percentage mass increase in fabrics at various concentrations using both application methods.

In general, the samples that were prepared by dipping seem to give more aggregated species, whereas the samples which were prepared by dropping an aliquot on top seemed to give a smoother, more uniform surface. This was demonstrated by two sample images in Figure 2-24 showing the structure of 2.0 wt/v% dipped and dropped on carbon cloth laminated knit. Aggregates were clearly seen on the dipped sample, whereas the dropped sample appeared to have a much smoother surface. This suggested aggregation is more controlled and slower in the dropped system; the slower aggregation forming fibres rather than clumpy aggregates. This suggests that drying effects may well be different in each of the samples, perhaps depending on the penetration of solvent into the fabric, and that drying effects/rates may affect self-assembly. Gelation is always a balance between solubility and crystallisation and it would appear that when samples are dipped and dried there is a greater tendency towards crystallinity. The difference between dipped and dropped could be due to a difference in the cooling. It could be that the submerged samples cool more quickly once removed from the solution bath, with a crystallisation type mechanism, i.e. the faster it cools, the more rapidly the aggregates form and therefore form rough aggregates form rather than smooth networks.

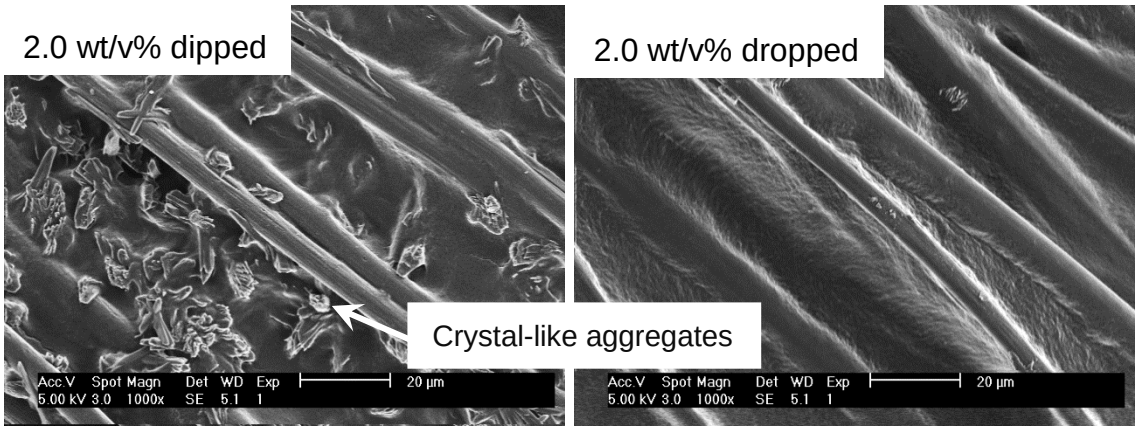

Figure 2-24. SEM images of carbon cloth prepared with 2.0 wt/v% DBS in methanol dipped *vs.* dropped, scale bars of 20 µm.

However, what appeared to be crystal-like aggregates were also found in the dropped sample prepared with 2.5 wt/v% DBS in methanol on carbon cloth laminated with knit in specific areas of the sample (Figure 2-25).

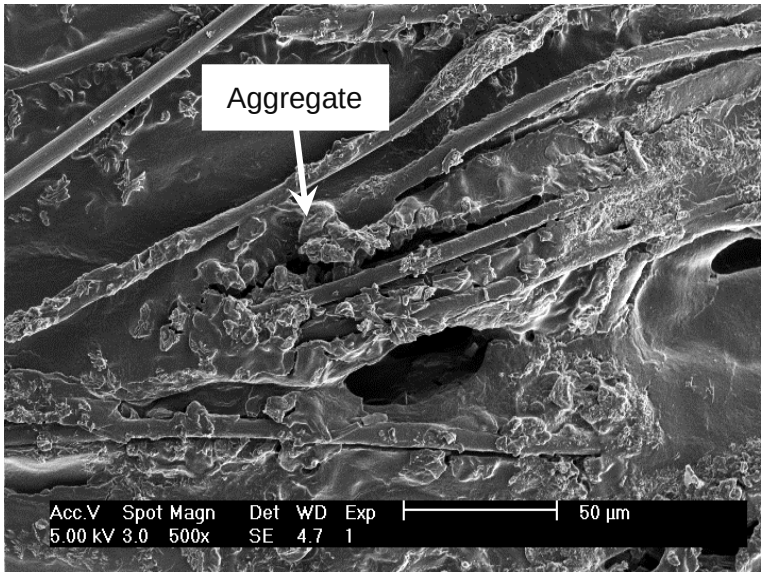

Figure 2-25. SEM image of carbon cloth treated with 2.5 wt/v% DBS in methanol laminated with knit dropped, scale bar of 50 µm.

This again emphasises the importance of viewing the whole of the sample and taking images from multiple locations across the sample. However, nonetheless, at lower concentrations, it appeared that these aggregates were less present when the sample was dropped onto the fabric and dried.

Nanofibres could be seen coating the fabric fibre at almost all concentrations (1.0 wt/v% to 3.0 wt/v%). As the concentration of the solution was increased, the “glue”

surrounding the individual fabric fibres appeared to get thicker. It is therefore clear that the fabric fibres appeared to nucleate and support the formation of the assemblies. This was somewhat problematic as it would be preferable for the fibrillar assemblies to span more effectively between the fabric fibres. This suggests that solvent clings to the fabric fibres during drying and hence self-assembled nanostructures are preferentially deposited there.

It was also considered useful to reduce the size of the aliquots dropped onto the fabric, as it might have been that the dropped samples were exposed to far more of the solution, and therefore more DBS, than could penetrate the dipped samples during their soaking period. By exposing the dropped samples to less liquid, it would clearly identify whether this was a crucial control variable.

2.11.1 Varying Aliquot Size of Dropping with Synthesised DBS

A range of aliquots were investigated, 2, 10, 25, 50, 75 and 100 μL were all pipetted onto individual fabric samples of approximately the same size (10 x 10 mm) and then dried by leaving under ambient conditions to let the solvent evaporate. The fabric weights before and after were recorded and then SEM images were taken.

The fabric samples were weighed before the application of the solutions and after drying (usually overnight). As expected, there was a proportional relationship between the weight increase and the aliquot size. The percentage weight increase was also considered as it was thought that this would account for any differences in surface area from the slightly different fabric sample sizes, assuming that the fabric is a constant density. Non-woven fabrics are known for their lack of uniformity and variable density, plus there will be variations in the dryness of the samples, but in both cases, a reasonable correlation with aliquot size was observed. The percentage mass increase for a fabric dipped into 1.0 wt/v% DBS was 48% (Figure 2-23). By inputting this into the line of best fit for the ‘dropped’ samples in Figure 2-26 for percentage mass increase, an aliquot of 47 μL should give the same mass increase using the dropping method. This provides an important point of reference between preparation methods and suggests how much sample can ‘naturally’ be taken up if a fabric is dipped.

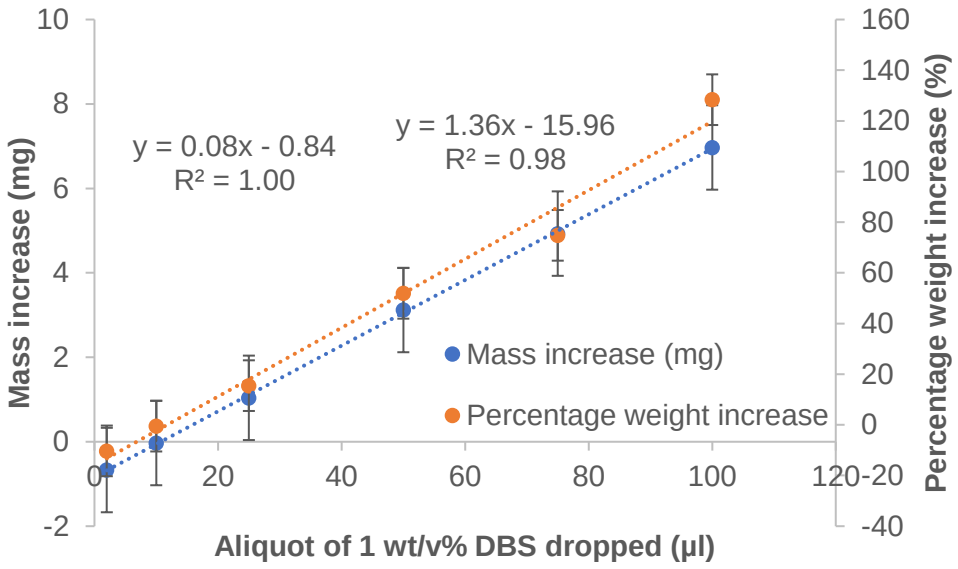

Figure 2-26. Graph of weight increase by aliquot size.

With aliquots between 2 and 25 µL, no nanofibres could be identified on the fabric fibres by electron microscopy, but the mass increase was proportional to the aliquot used, so there must be some additional material present on the fabric. It could be buried within the fabric sample, or within the fabric fibres and therefore not visible on the surface. On application of the liquid, the fabrics appeared to "wet". There was very little difference between the images as can be seen in Figure 2-27. Higher magnification SEM images have been used for 2 and 25 µL aliquots to demonstrate that any differences are negligible.

Increasing the size of the aliquot to 50 µL, saw the appearance of the previously observed deposition of nanofibre aggregates onto the fabric fibres. As the aliquot size was further increased, the amount of aggregation increased until 100 µL where the fabric appeared to be saturated, with every fabric fibre appearing to be covered by DBS nanofibres, which were beginning to form a fabric spanning thin layer of surface coverage.

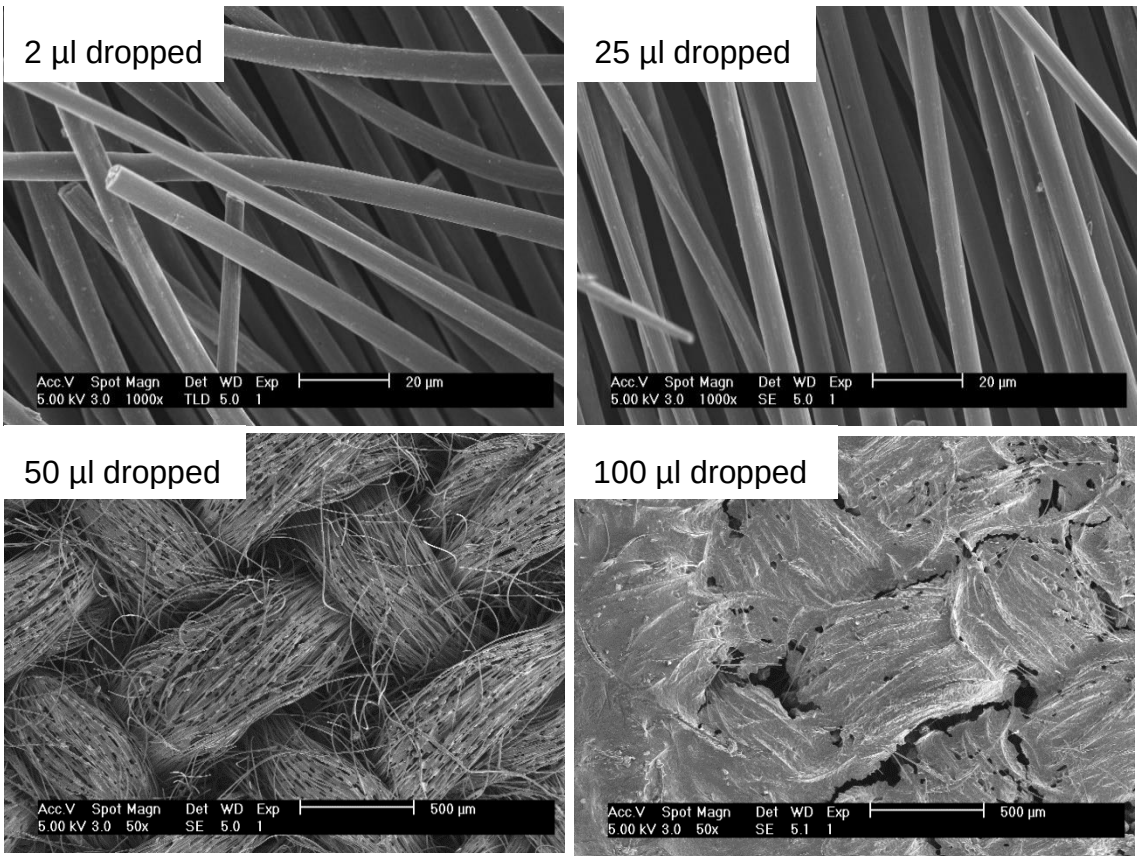

Figure 2-27. SEM images of carbon cloth treated with 2, 25, 50 and 100 µl of 1.0 wt/v% DBS in methanol, dropped, scale bars of 20 µm and 500 µm, respectively.

As expected, the more gelator-containing solution was dropped onto the fabric, the greater the deposition of nanofibres, both visually and by mass increase. The application method, although relatively effective, can obviously have large ramifications on the fabric, so in the interests of consistency and ease of industrial scale-up, dipping fabrics in a bath of gelator-containing solution is used exclusively from here on in.

2.12 Penetration of DBS Nanofibres via Cross-section of Carbon Cloth Fabric

Using SEM analysis, it can be difficult to establish if the solution was able to penetrate the fabric structure and therefore generate nanofibres (and aggregates) throughout the fabric, creating a multilayer filter. The alternative is that the aggregates are only found on the surface of the fabric. By cutting a previously used sample in half and imaging the sample perpendicularly (i.e. into the cut), it was hoped that nanofibres would be seen throughout the structure (implying that the solution was penetrating the sample).

Pleasingly, there were clearly DBS nanofibre aggregates throughout the sample, not just on the fabric fibres at the surface, but within the fabric as well (see Figure 2-28 b for a deeper image of the sample). This implied that the solution did penetrate the fabric and that nanofibres formed there. The images collected from this sample supported the hypothesis that the images of the top surface do reflect the overall sample. This proof of concept experiment demonstrated the potential of DBS assemblies to modify the network structure of a fabric.

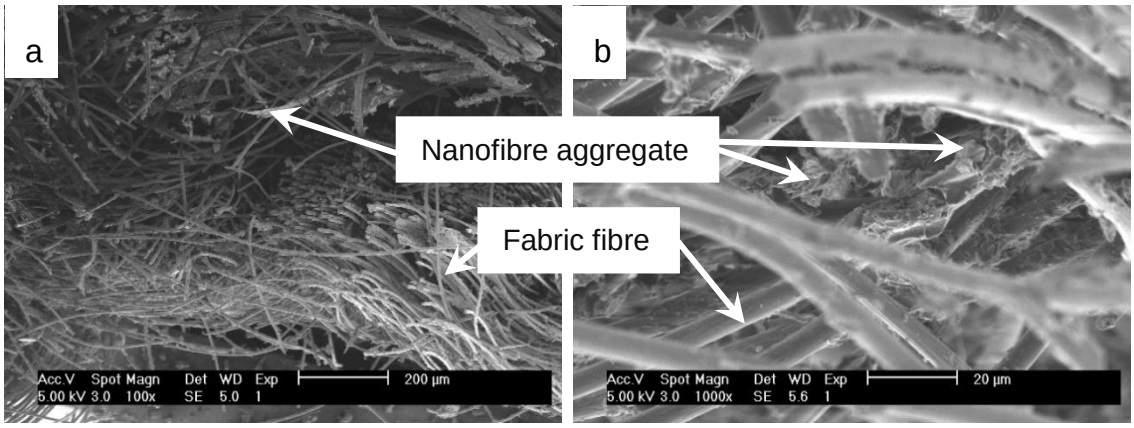

Figure 2-28. Cross-sectional SEM images of carbon cloth treated with 1.0 wt/v% DBS in methanol, 75 µl dropped, scale bars 200 µm and 20 µm.

2.13 Fabric Reselection

It was clear that the carbon cloth was an effective candidate for this kind of treatment. However, at this point, DSTL could no longer source this fabric and asked for a replacement to be found. It is of course, important, that an ideal fabric modification technology should have general applicability between different classes of fabric, and a range of fabrics previously supplied by DSTL were therefore considered including a polyester knit, cotton drill, nylon-modified acrylic, L560217, Helsa™ 3041 and two different types of non-woven fabric.

The ideal fabric would have a loose enough weave that the DBS nanofibres would have space to form, but not so much that there was too much empty space to fill. Ideally, the fabric fibre would be a smooth surface so that any nanofibres were easy to identify.

The polyester knit and cotton drill sourced from DSTL both appeared to have tiny aggregates on the surface of the fabric fibres, as can be seen from Figure 2-29, and a woven structure, so were not suitable.

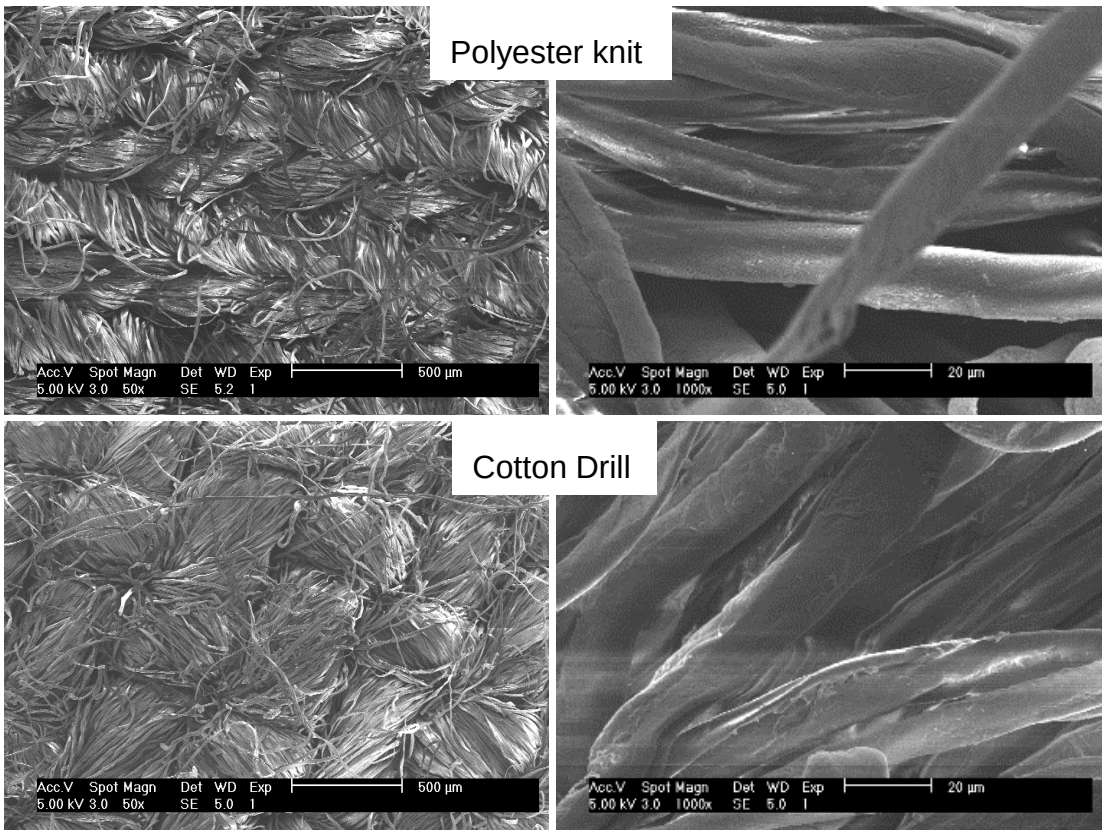

Figure 2-29. SEM images of non-carbon based fabrics with loose weave, polyester knit and cotton drill, at low and high magnification, scale bars 500 µm and 20 µm.

The nylon modified acrylic with a wicking agent finish and the L560217 looked too tightly woven (Figure 2-30) to provide a good substrate for nanofibre formation, there wouldn't be much space between the fabric fibres for the nanofibres to assemble. Helsa™ 3041 had a liquid repellent coating and aggregates could already be seen on the surface of the fabric fibre (probably linked to the liquid repellency). Helsa™ 3041 with the liquid repellent coating was initially tested to see if the solution would penetrate the fabric, or if the water repellency would stop the penetration and therefore inhibit nanofibre assembly. This knowledge could be useful in the future, particularly thinking for scale-up to industrial application, military fabrics are usually waterproofed and it is useful to know whether nanofibre fabric loading should be performed before waterproofing or whether it is possible to achieve it on a waterproofed fabric. Overall, the non-woven fabrics appeared the most promising due to their random orientation of loose fibres.

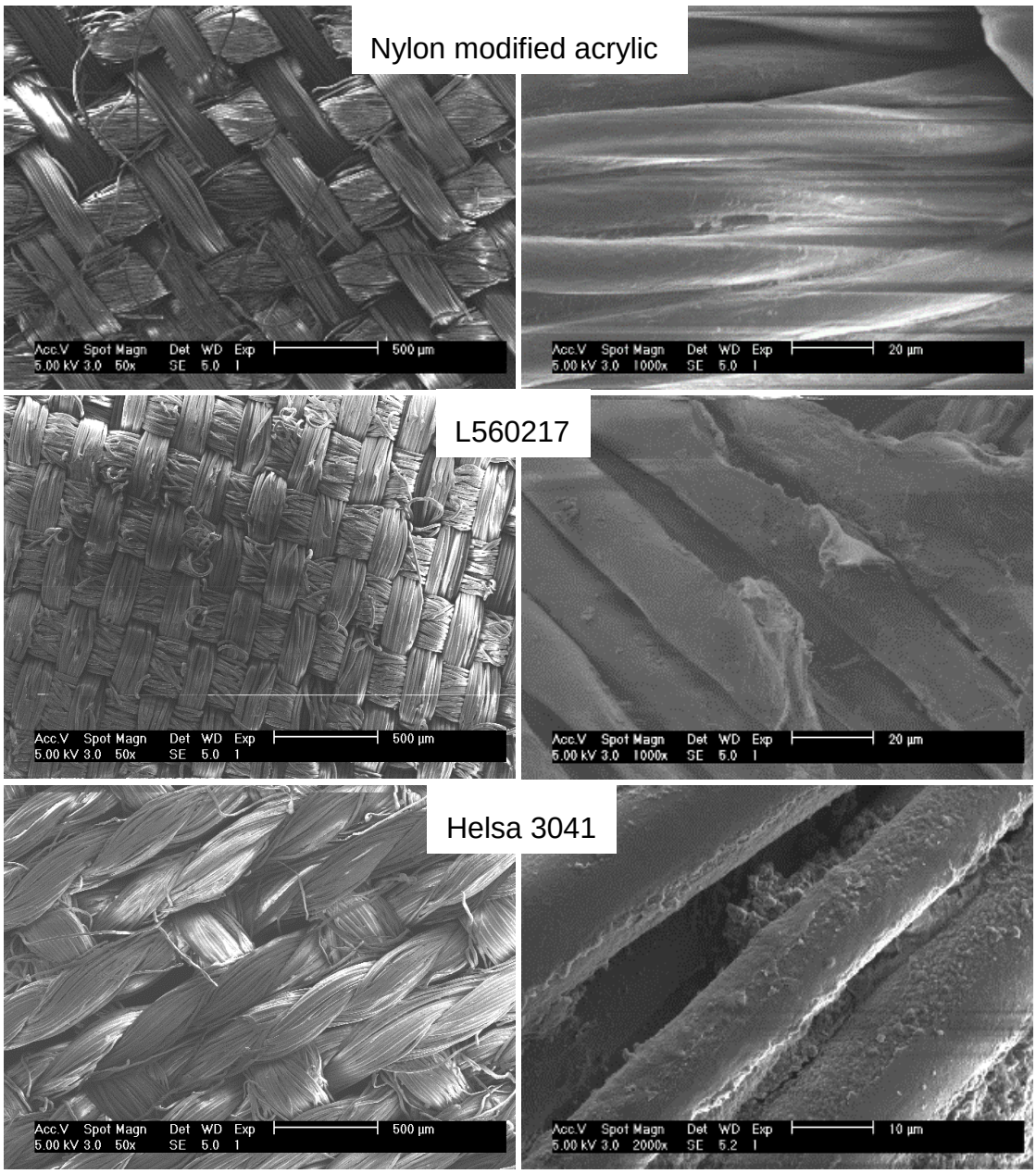

Figure 2-30. SEM images of non-carbon woven fabrics, nylon modified acrylic, L560217 and Helsa™ 3041, at low and high magnification, scale bars at 500 µm and 20 µm (Helsa™ 3041 10 µm).

Of the two non-wovens shown in the SEM images in Figure 2-31, the meltblown appeared to have relatively large “spot-welds” holding the different layers together (MSM: meltblown-spunbound-meltblown trilayer non-woven), while the spun appeared to have a more uniform structure. Therefore, the non-woven spun fabric was tested in the next stages of the project.

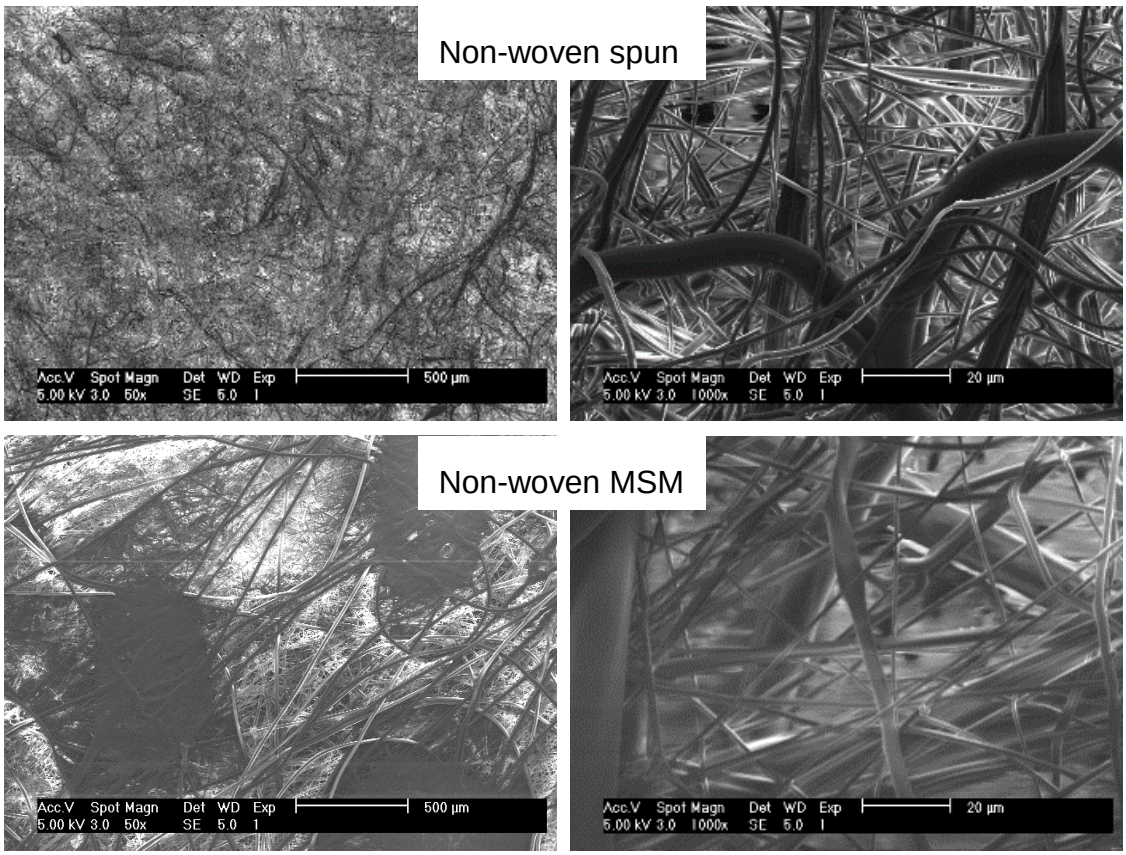

Figure 2-31. SEM images of non-woven non-carbon based fabrics, non-woven spun and MSM (meltblown-spunbond-meltblown trilayer), at low and high magnification, scale bars 500 µm and 20 µm.

2.14 Liquid Repellent Fabric Investigation

As described in section 2.13 on fabric selection, Helsa™ 3041 with a liquid repellent coating was investigated to determine whether nanofibre finishes could be applied after the liquid repellent has been introduced. A dipped fabric sample using 1.0 wt/v% synthesised DBS (at MGC) in methanol was prepared and compared with an unmodified sample. Methanol was selected as a solvent to potentially enhance the compatibility with fabric. The fabric visually did appear to wet and the solvent spread across the fabric but it did not appear to soak in as effectively as with other fabrics tested in this study.

The two fabric samples appeared indistinguishable in Figure 2-32. Even at higher magnification, the two fabrics were very similar. This would imply that the liquid repellent coating prevented the solvent penetrating the fabric. This, therefore, suggests

that in any ultimate application, it would be preferable to achieve nano-modification prior to fabric waterproofing.

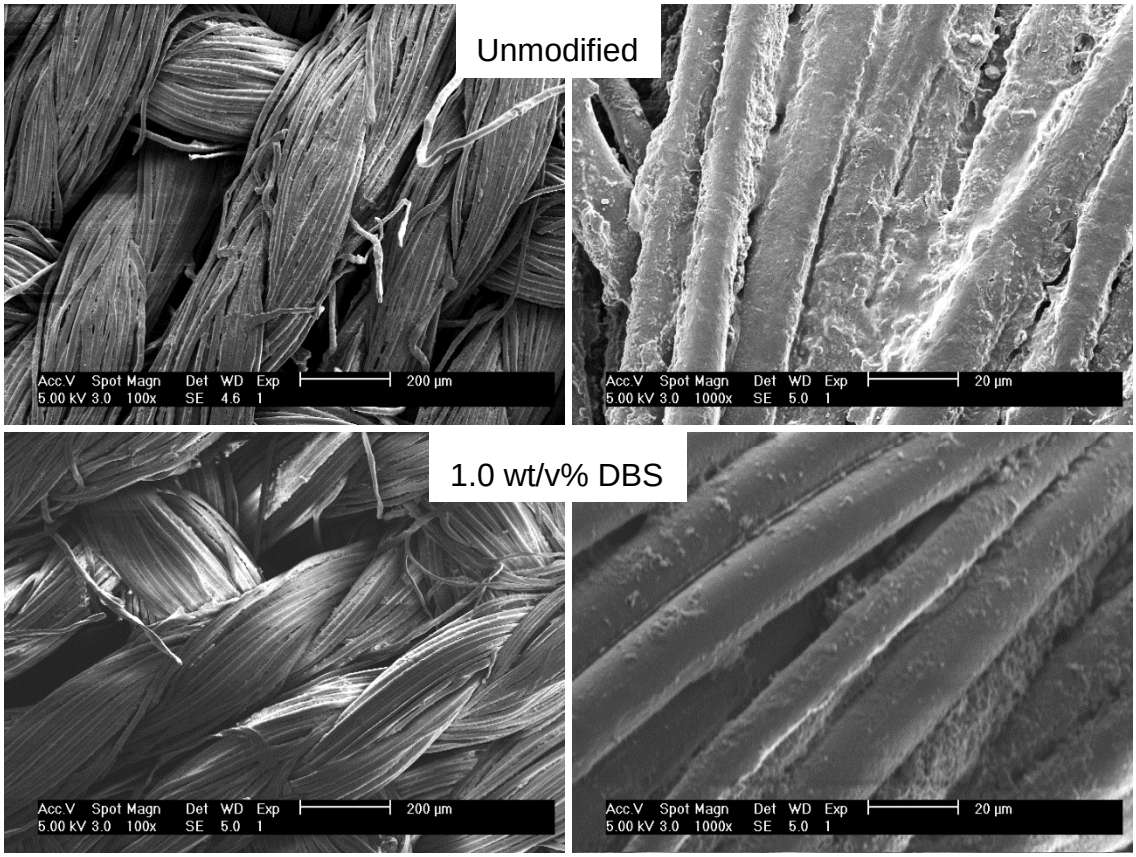

Figure 2-32. SEM images of Helsa™ 3041 water repellent at low and high magnification, scale bars of 200 µm and 20 µm.

2.15 Reproduction of Dipping and Dropping in Non-woven Fabric

Section 2.11 discussed observed differences between fabric samples prepared with different methods of solvent application. With the change of fabric to the non-woven spun from section 2.13, it was important to ensure that the previously completed work was still relevant. The non-woven fabric was investigated for the difference between dripping and dropping at 1.0 wt/v% and 5.0 wt/v% synthesised DBS in methanol, repeating some of the work seen in section 2.11. These concentrations were used as they are above the MGC of synthesised DBS (1.0 wt/v%).

Compared to the blank sample in Figure 2-31, both images (dipped and dropped) in Figure 2-33 appeared to show some DBS aggregates present in the non-woven, even at 1 wt/v% of DBS. From Figure 2-33, it is obvious that the dipped sample at 1 wt/v% has significantly more coverage and therefore fewer gaps than the dropped sample.

The dropped sample shows very little coverage at this concentration. It could be that the solution is not dispersing as well across the surface on this fabric when deposited on top, whereas, for the dipped sample, the solution has time to soak into all the gaps in the fabric. It could also be a drying effect if the two methods of application affect the way in which solvent is dried from the fabric. The 5 wt/v% DBS samples show quite a similar level of coverage, regardless of application method. Quantification was attempted, but due to the irregular orientation of non-woven fabric fibres, it was difficult to compare the two samples directly. Visually the dropped samples generally had more nanofibre aggregates than the dipped. The increased concentration leads to an expected increase in deposition of nanofibres (i.e. 5 wt/v% DBS has more coverage than 1 wt/v% for both application methods). The nanoscale network appeared the same throughout all these samples (x 75 000 magnification).

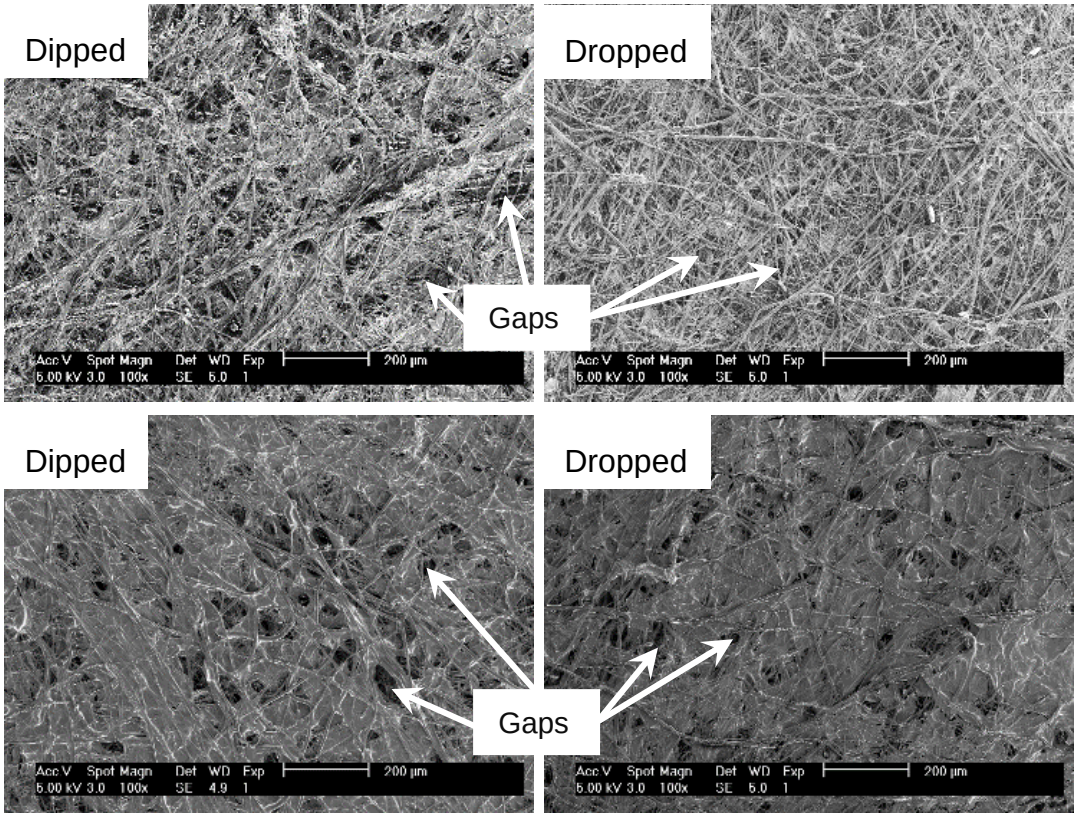

Figure 2-33. SEM images of non-woven fabrics treated with 1 and 5 wt/v% DBS in methanol dropped *vs.* dipped, scale bars 200 µm.

Taking a closer look at the 1 wt/v% sample, it is easier to see the differences between the two samples. Arrows point to filled gaps in both samples in Figure 2-34. The gaps which are empty of nanofibres show the fabric fibres through the gaps, whereas the gaps which are filled with nanofibres don't show the fabric fibres underneath, instead

show a sheet of nanofibres. The dipped sample shows more empty gaps (i.e. not filled with nanofibres) than the dropped sample which show more filled gaps.

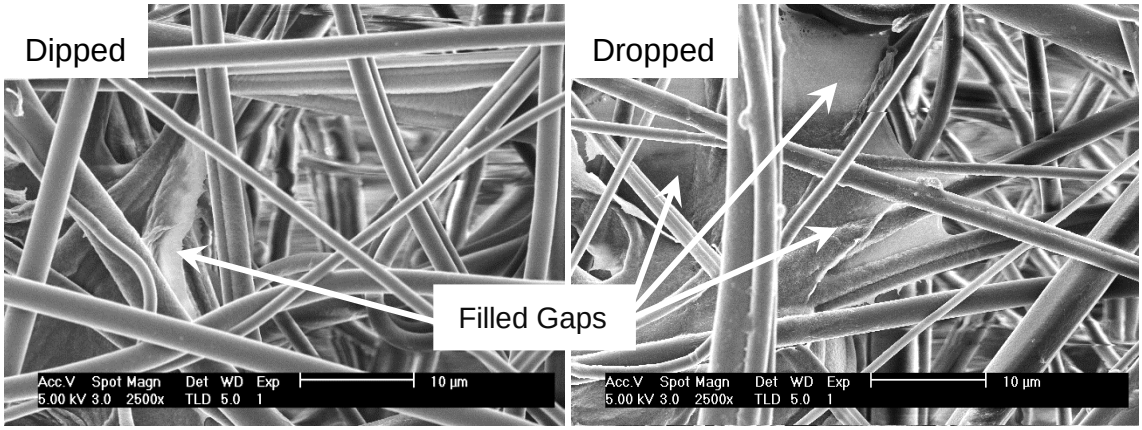

Figure 2-34. SEM images of non-woven fabric treated with 1 wt/v% DBS in methanol dropped *vs.* dipped, scale bars 10 µm.

Overall, the method of application still appears to have some influence on the formation of aggregates, but industrially the dipping process is easier to scale-up, and a decision was made to continue with this approach.

2.16 Connection Between Fabric Properties and Solvent System with Synthesised DBS

Ideally, the nanofibres should spread out, to achieve a less close-packed coverage of the fabric pores, but without blocking the surface entirely. To achieve this, the nanofibres would be less 'sticky', so they tended to aggregate less and instead, spread out throughout the fabric, spanning the pores providing more even coverage. Synthetic fabrics tend to lack affinity for water (neither hydrophilic nor hydrophobic), so by tuning the solvent system, a more distributed network may be achieved. Other solvents were then studied in an attempt to modify the solvent-fabric interface. A very hydrophilic cotton fabric was also provided, in order to compare different solvent systems in this fabric compared to the more hydrophobic non-woven.

The two different fabrics were investigated over a range of concentrations in both 1:1 water:methanol and methanol. The non-woven poly(propylene) 25 gsm fabric tested will be referred to as NW. 'Cotton' is a hydrophilic untreated woven cotton fabric, which has hydroxyl groups present on the surface of the fabric from the cellulose. By changing the solvent system to incorporate some water, the cotton fabric may encourage greater dispersion of the solution across and within the fabric. The samples were made up from solutions of varying concentrations. Blank fabrics were investigated

alongside those modified with 0.5 wt/v%, 0.75 wt/v% and 1 wt/v% synthesised DBS in 1:1 water:methanol and 1 wt/v% synthesised DBS in methanol.

As expected the non-woven fabrics show a random orientation of fabric fibres, while the cotton fabric shows an ordered woven structure. As can be seen from Figure 2-35, there are very few aggregates on these two different fabric types when prepared with methanol. The non-woven shows some small clumps of aggregated DBS, looking like “flakes” on the fabric fibres. In the cotton fabric, a few aggregates can just about be seen between fabric fibres, looking almost like “glue”. In contrast to the samples from methanol shown in Figure 2-35, it is easy to see DBS nanofibre aggregates in 1:1 water:methanol. The non-woven showed aggregates over most of the surface of the fabric, whereas the cotton fabric showed patchier aggregates sporadically over the surface. The hydrophilicity of the cotton fabric does not appear to be impacting on the aggregation of DBS nanofibres. The aggregates look relatively ‘clumpy’.

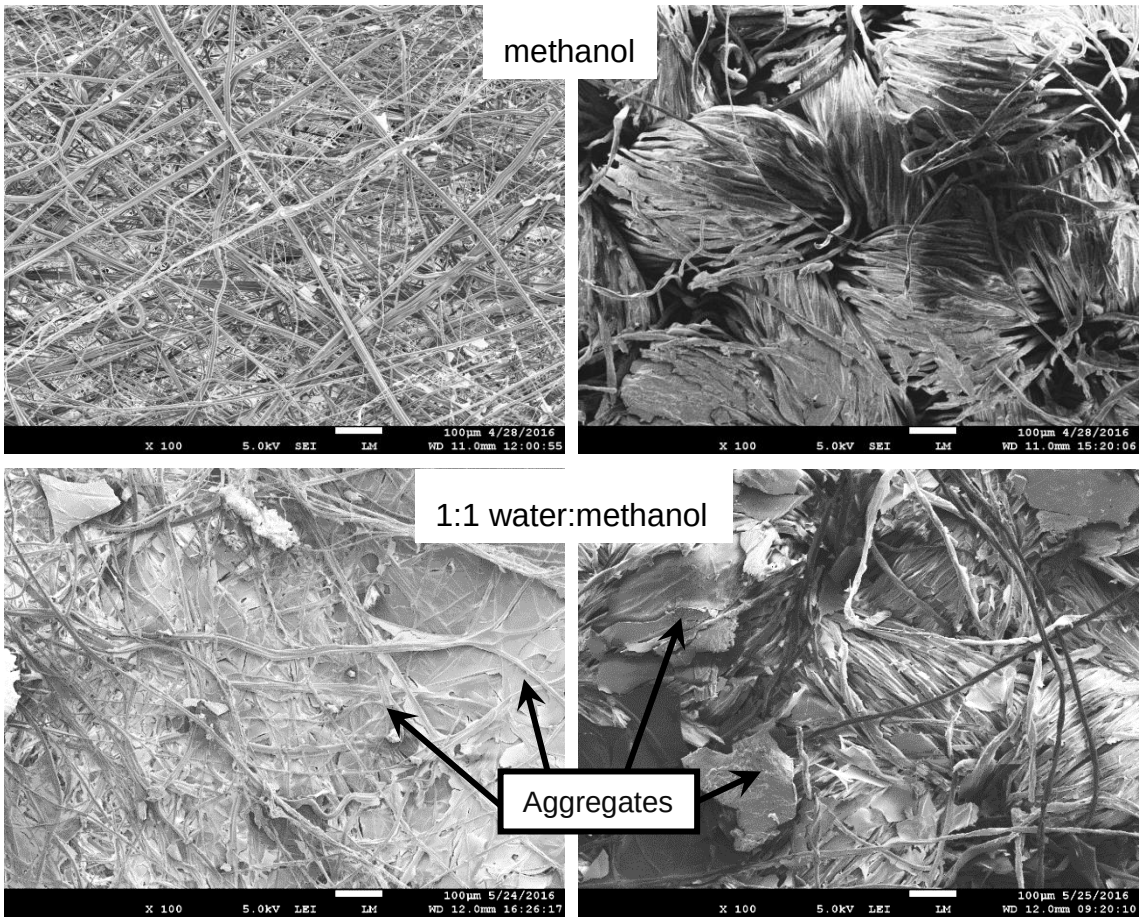

Figure 2-35. SEM images of non-woven fabric (left) and cotton fabric (right) treated with 1 wt/v% DBS in methanol and 1:1 water:methanol, scale bars of 100 µm.

The greater extent of nanofibre aggregation in 1:1 water:methanol is likely related to the lower MGC compared with methanol. There is no evidence that the hydrophilic cotton fabric changes the interaction of the nanofibres with the fabric surface. It could be that the change in solvent system has allowed greater penetration into the cotton fabric, allowing more DBS nanofibres to form within the fabric itself but from the images here, the cotton fabric does not have any significant differences to the non-woven. The cotton fabric has a regular woven structure which does not appear to encourage the generation of nanofibres across the junction points of the weft and warp as previously discussed with the nylon modified acrylic fabric used in the proof of concept experiment. This regular structure could be the downfall for this long-term application, as any CWA could diffuse through the holes at these junction points. So the cotton fabric was not progressed further.

2.17 Visual Observation of Commercial DBS and Solvent Combinations in Non-woven Fabric

After investigations with synthesised DBS and remembering the consideration of Hansen solubility parameters, SEM analysis was employed to visualise the coverage provided by each of the gelator/solvent combinations with commercial DBS.

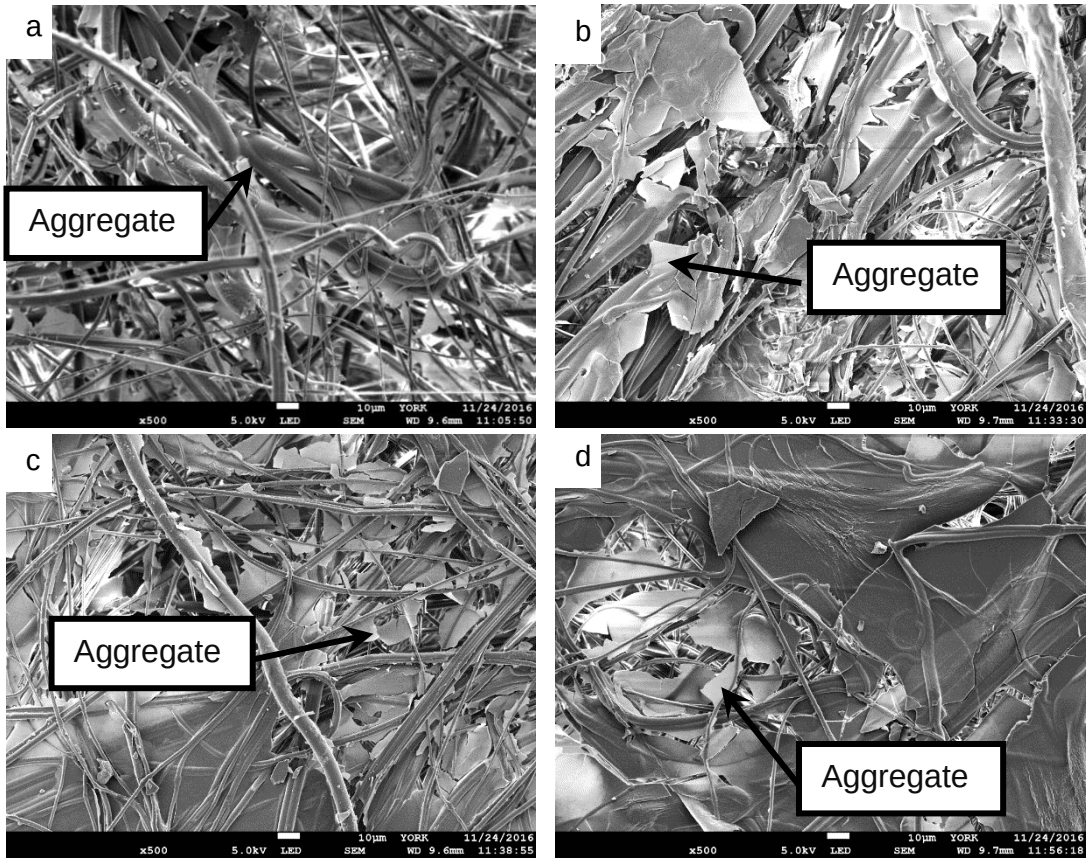

Figure 2-36. SEM images of DBS in 2-butanone on non-woven fabric at 0.4, 0.6, 0.8 and 1 wt/v%, scale bars of 10 µm.

Initially, 2-butanone was investigated as a solvent. As might be expected, as the concentration of DBS in solution increased, the deposition of nanofibres on the fabric also increased, here the surface coverage also increases. In Figure 2-36, the DBS nanofibres appear to be forming aggregates; preferring to self-aggregate rather than span out more widely. DBS forms nanofibres with a diameter of around 15 nm in 2-butanone, these small nanofibres can be seen in Figure 2-37.

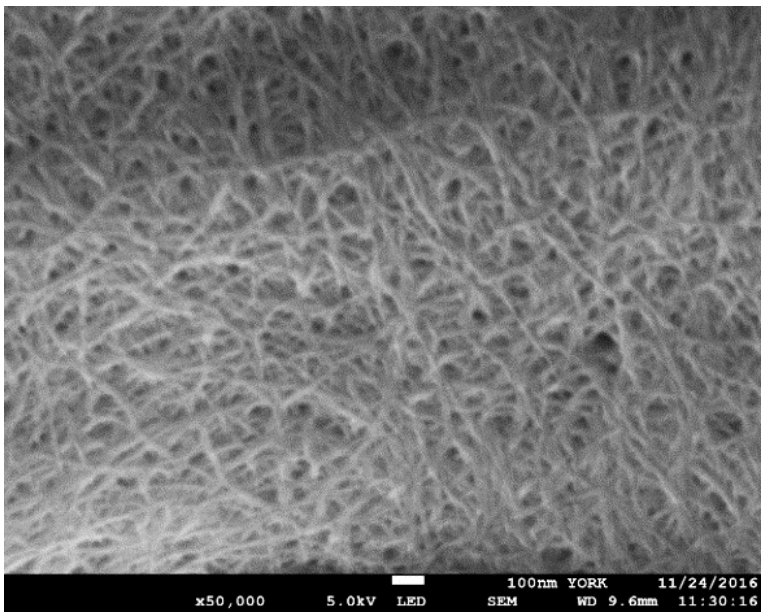

Figure 2-37. SEM image of 0.6 wt/v% gel of DBS in 2-butanone at higher magnification demonstrating DBS nanofibres, scale bars of 100 nm.

This small size could be having a large influence on the accessible morphologies. The small nanofibre size of DBS means that these systems have more relative surface area than larger nanofibres (such as those observed for BTA, see fabric modification section of introduction), and this may be a factor driving the aggregation. It may also be that the smaller nanofibres are more difficult to image in individual form and hence aggregates appear as a more dominant feature in SEM imaging.

Alternative solvents were tested, at their MGC values with commercial DBS to see what sort of coverage could be achieved and what nanoscale aggregates were present. The MGC of each solvent was chosen as this was the maximum loadings which allowed physical treatment of the fabric sample, with sufficient time to treat the fabric before gelation occurred.

Figure 2-38 shows a huge range of different morphologies. Dried from methanol, commercial DBS shows quite patchy coverage of the fabric, with some areas of almost complete coverage while other areas have very little coverage (e.g. top right to bottom right). The denser coverage shows sheets of nanofibres and the areas of less coverage show similar “clumpy” aggregates. Samples dried from chloroform show barely any coverage throughout the sample. The small amount of nanofibres which are present have aggregated into small clusters, similar to those observed in other solvents, whereas THF shows what looks like almost complete coverage. The ethyl acetate sample was very similar to methanol. Samples prepared with acetonitrile gives another

different morphology, with more angular aggregates observed, looking quite brittle and potentially less useful in terms of the filtration application. Fabrics dried from toluene, again, show patchy coverage, with one larger aggregate in the centre of the image and quite sparse coverage on the rest of the image. A few large aggregates, as demonstrated by the SEM image taken of DBS deposited from toluene in Figure 2-38, would not have the potential to filter. On first inspection, the sample dried from THF looks quite promising. The coverage appears dense, implying that aerosol should be caught on the mat of nanofibres. However, this sample had the highest MGC and was applied at the highest concentration. Deposition from acetone appears to yield a range of morphologies, from larger aggregates at the centre of the image to being more spread out between the fabric fibres. However, the coverage it provides is still patchy at best, as can be seen from Figure 2-39. The aggregates are very similar to previous aggregates.

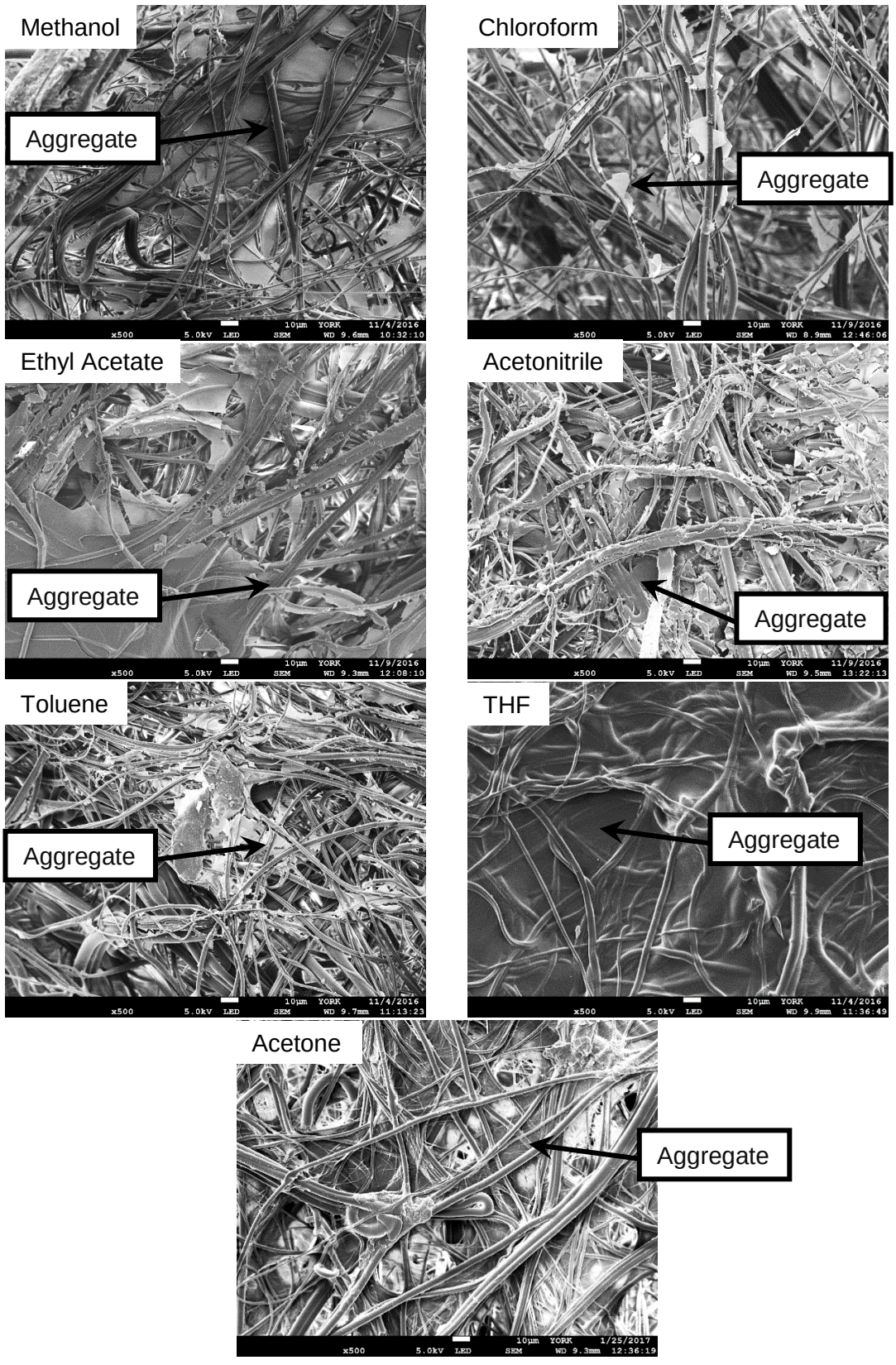

Figure 2-38. SEM images of DBS deposited from methanol, chloroform, ethyl acetate, acetonitrile, toluene, THF and acetone at the MGC on non-woven fabric, scale bars of 10 µm.

One could try and correlate the changes directly to the different loadings used. However, the coverage achieved using 0.7 wt/v% in acetone is far less than that with 0.4 wt/v% in ethyl acetate, and the coverage of 0.2 wt/v% in chloroform is less than 0.025 wt/v% in toluene. Therefore, although the concentrations used are a large factor for the morphology formed, they are not the only factor influencing the coverage. If the same loading had been used for all the samples, it would be very difficult to physically prepare the samples as some solvents, such as toluene, would form an instant gel and potentially precipitate at the highest loading, whereas if the samples had been prepared at the lowest loading (0.025 wt/v%) then most samples would have shown very little, if any visible aggregation.

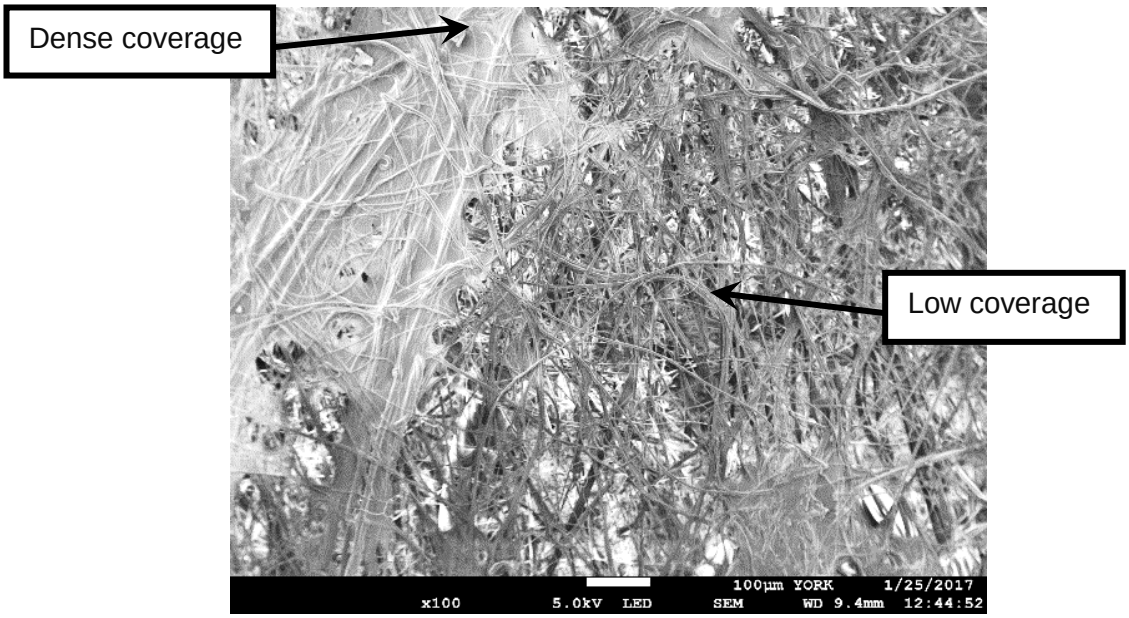

Figure 2-39. SEM image non-woven fabric treated with DBS in acetone at MGC, scale bars of 100 µm.

At this point, it is important to remember how artificial these images can be, and how important getting an overall look at each sample is, as each individual image only provides a small snapshot. Comparison of Figure 2-38 and Figure 2-40, shows the same DBS sample dried from THF. There is the same sort of coverage in the bottom right of Figure 2-40, but in the top section in particular, the coverage is a lot less dense.

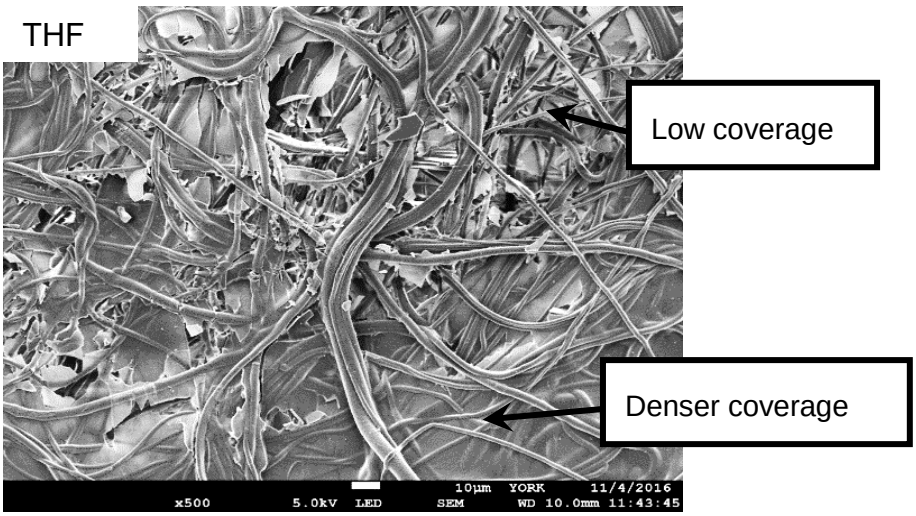

Figure 2-40. Second SEM image of DBS in THF, scale bars of 10 µm, same sample as Figure 2-38.

Finally, in this solvent investigation, DMF was investigated as a non-gelling solvent for DBS fabric modification, as all the other solvents investigated in this section form a gel. The SEM images for both 0.6 wt/v% and 1.0 wt/v% commercial DBS in DMF can be seen in Figure 2-41. Neither concentration shows much coverage. The aggregates seen in DMF are similar to those seen in other solvents. Interestingly, based only on these SEM images, it would be difficult to predict which nanofibres had come from gelling solvents and which had not. This suggests that assembly still takes place, even on drying from solvents which are not capable of supporting a full sample-spanning gel, suggesting that on drying solutions of DBS, nanofibre assembly is an effectively crystallisation.

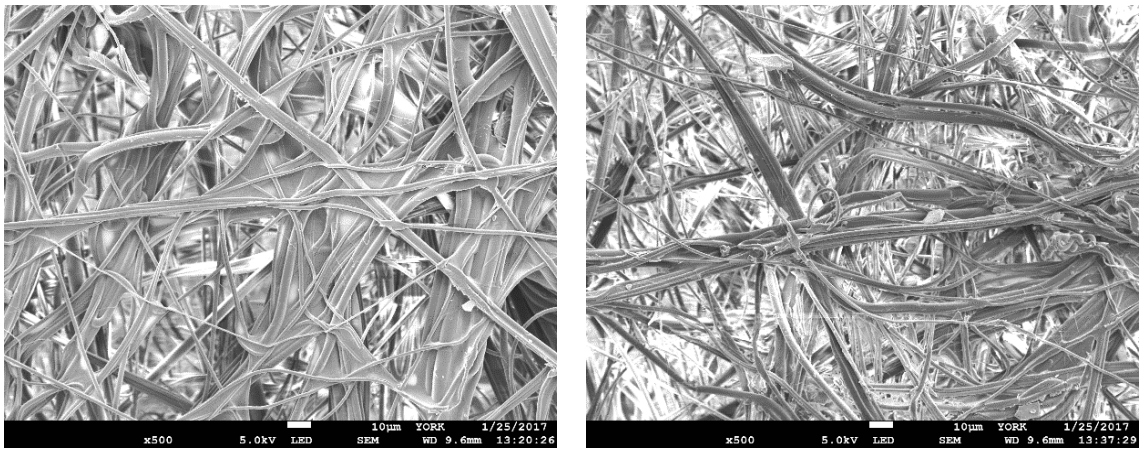

Figure 2-41. SEM images of non-woven fabric treated with 0.6 and 1.0 wt/v% DBS in DMF, scale bars of 10 µm.

In summary, DBS nanofibres always appear to have a tendency to assemble and then self-aggregate regardless of solvent. This could suggest that the very small diameter of DBS nanofibres means that they tend to aggregate in order to minimise surface energy.

In the interests of long-term application, DBS in 2-butanone and methanol were selected as typical apolar aprotic and polar protic solvents, respectively, and fabric modification was scaled up for testing.

2.18 Fabric Performance Testing of Non-woven Fabric Treated with Commercial DBS

Following the protocols outlined in the experimental section, fabrics were prepared with commercial DBS and tested in Leeds for two key properties; air permeability and water vapour permeability. Fabrics were also tested at Porton Down for filtration efficiency and Silsoe Spray Application Unit for real-world aerosol testing.

2.18.1 Air Permeability of Non-woven Fabric Treated with Commercial DBS

Air permeability (AP) is the flow of air passing through a given area of test fabric under a certain air pressure over a time period (volume of air per surface area per second ($cm^3/cm^2/s$)). The air permeability was tested to see how easily the air can pass through the fabric in order to give an indication of how easy it will be to control body temperature while wearing the clothing. Each sample was tested at least 5 times and the average was taken over a test area of 5 cm of fabric, with a test pressure of 100 Pa as per the British Standard.[421] The results presented in Figure 2-42 show the relationship between measured air permeability and the concentration of DBS used to prepare the non-woven fabric for testing.

It can be seen from Figure 2-42 that there is a very logical relationship between the concentration of the commercial DBS solution used to prepare the fabrics and the air permeability of the fabric. The addition of nanofibres led to a significant drop in air permeability. The more nanofibres deposited on the fabric, with increased concentration of commercial DBS solution treatment, leads to further decreases in air permeability, implying that the density of nanofibres has the largest effect.

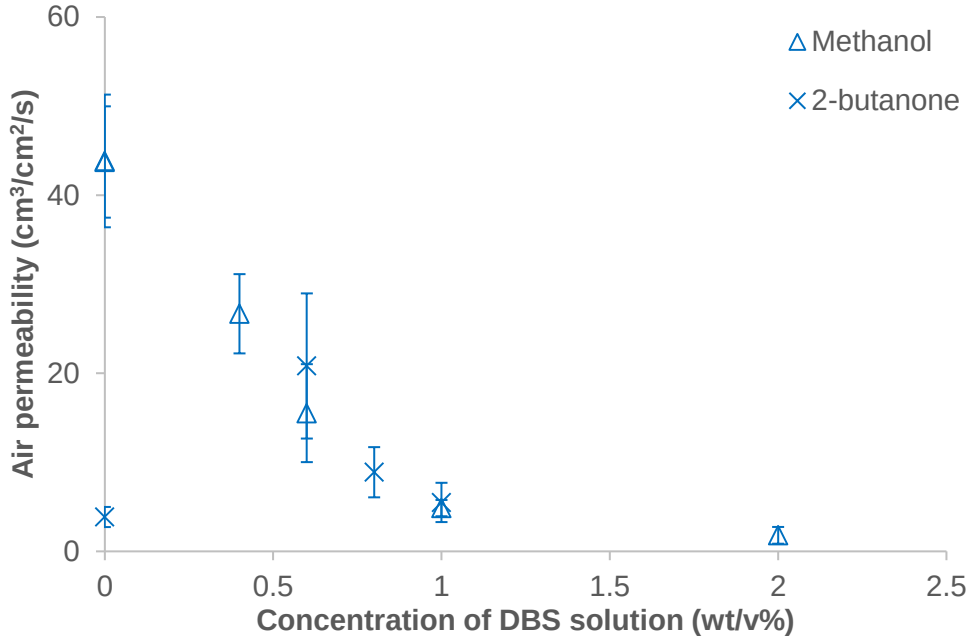

Figure 2-42. Graph of air permeability against concentration of DBS for methanol and 2-butanone.

It can also be seen that fabrics prepared with commercial DBS in either methanol and 2-butanone respond very similarly in this test, implying that the gelator, and not the solvent, affects the air permeability. Cleary above *ca.* 1 wt/v%, air permeability is almost completely inhibited under these testing conditions. These modified non-woven fabrics were further investigated by studying water vapour permeability.

2.18.2 Water Vapour Permeability of Non-woven Fabric Treated with Commercial DBS

Water vapour permeability (WVP) is a measure of how much water vapour can escape through a known area of fabric over a certain period of time. All WVP testing was performed relative to a standard fabric sample, defined in the British testing standards as “a precision, high tenacity polyester woven monofilament mesh with stated characteristics”.[422] This will be referred to as the standard reference fabric. Three specimens were tested for each sample. The “blank” fabrics underwent the same treatment as the treated fabrics but were soaked in just solvent rather than the solubilised gelator. The water vapour permeability gives an indication of how “wearable” the fabric is; i.e. it indicates how easy it would be for water vapour on the surface of the skin to evaporate.

All of the samples have been indexed against a standard reference sample as required by the British testing standard,[422] which had a WVP of around 1000 g/m^2/day (indexed

at 100%). The testing laboratory conditions were kept at *ca.* 293 K and *ca.* 65% relative humidity. The non-woven fabric used to prepare the samples is different to the material used for the standard reference sample, so small differences in the WVP are justifiable.

All the samples (Figure 2-43) gave very similar WVP values. The fabrics prepared with commercial DBS in 2-butanone gave the same indexed WVP as the blank fabric soaked in 2-butanone. This implies that the WVP is not significantly affected by the addition of nanofibres. It, therefore, appears that the increased nanofibre deposition from increased concentration of gelator solution on the fabric is not impeding the transport of water vapour.

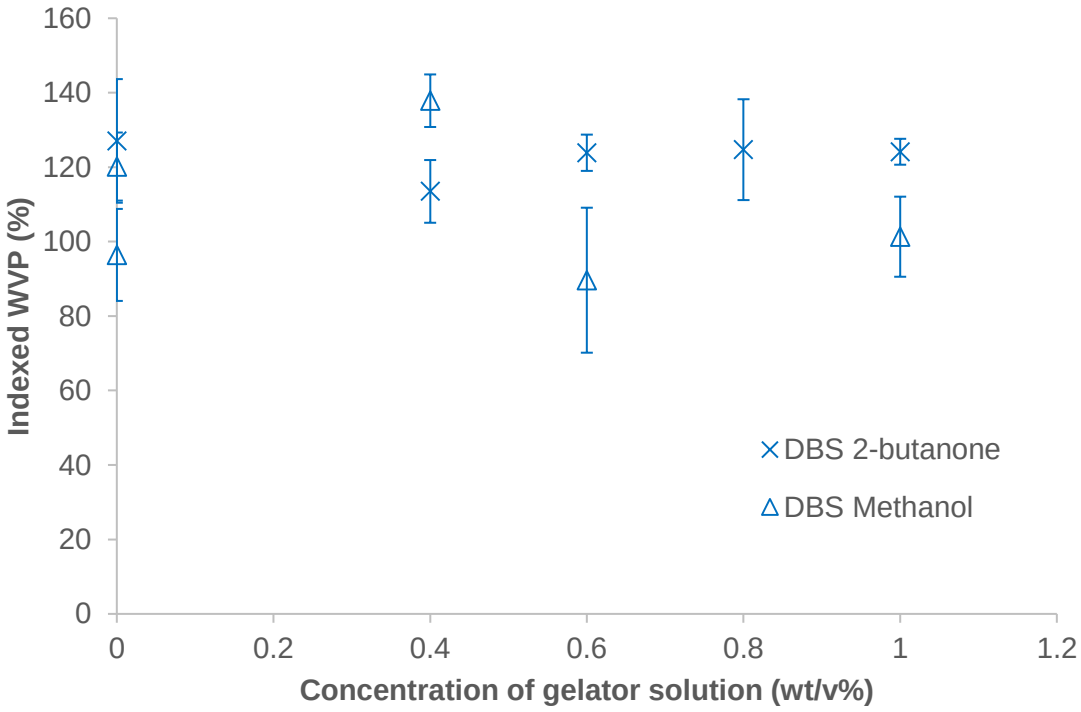

Figure 2-43. Graph of water vapour permeability against concentration of DBS for methanol and 2-butanone.

These results correlate with published results for electrospun nanofibres. Generally there is an increased resistance to airflow (decreased air permeability) correlating with add-on mass of nanofibres, with minimal impedance to water vapour permeability.[20, 372, 380, 389, 397, 400, 401] These literature results also tended to find a connection between air resistance and filtration performance, generally the increased air resistance (decreased air permeability), correlates with increase filtration efficiency.[372, 389, 397, 400, 401]

One could question why the nanofibres appear to be having so much impact on the permeability of air but not water vapour. Clearly, it can't be any size differences

between the molecules. It could be associated with molecular polarity and ability to penetrate through the DBS nanofibre filter mesh. However, there is also a fundamental physical difference between the experiments. Air permeability is tested at a pressure of 100 Pa over the time period of approximately 30 seconds, meaning air is forced through the fabric. If the air can't find a path, it is blocked, hence the reduction in air permeability. However, water vapour permeability is tested over a 24 hour time period under ambient conditions of temperature and pressure. This allows the water molecules time to diffuse through the fabric, finding a path. Hence it could be proposed that DBS nanofibres appear to affect air permeability under rapid flow pressure but not water vapour permeability under diffusion conditions and water vapour pressure.

2.18.3 Environmental WVP Testing of Non-woven Fabric Treated with Commercial DBS

To try and create a more realistic representation of these fabrics being worn, it was decided to test water vapour permeability in an environmental chamber. The water was raised to body temperature (308 K) to more accurately represent sweat evaporation from skin. The surrounding environment was kept as previously tested ambient conditions *ca.* 293 K and *ca.* 65% relative humidity.

As can be seen in Figure 2-44, the nanofibres still did not have a significant impact on water vapour permeability even at elevated water temperature. The indexed WVP is very similar to the blank fabric and most of the results at the same concentration at 293 K water. This was a positive result, as it provided the first indication that sweat could easily permeate through the nano-modified fabrics even at elevated temperatures, a key requirement for desired application.

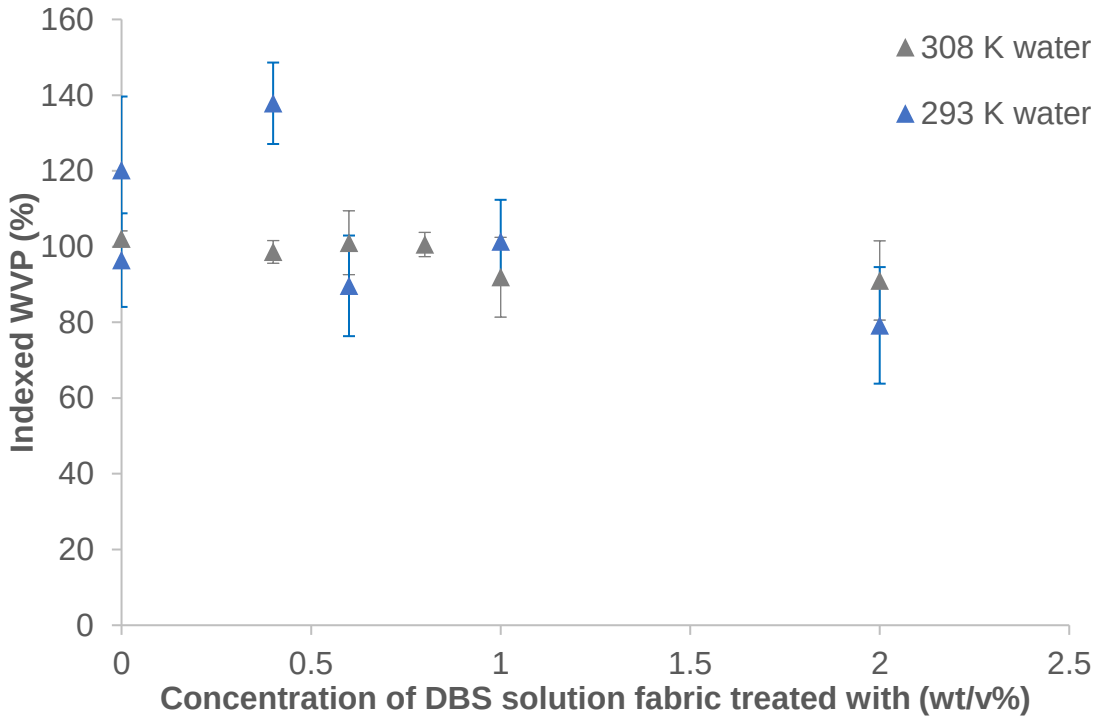

Figure 2-44. Environmental chamber WVP for commercial DBS solution soaked fabrics.

2.18.4 Effects of Testing of Non-woven Fabric Treated with Commercial DBS

The non-covalent interactions which underpin the self-assembly of DBS nanofibres are, by definition, weak interactions. To ensure the nanofibres were not damaged during the fabric testing, SEM images of before and after testing were taken. These could not be exactly the same section of fabric due to testing requirements, so the irregularity of the non-woven fabric obviously produces some changes in the images. As can be seen in Figure 2-45, the pressure used in the air permeability testing does not appear to significantly change the morphology of the nanofibres in the non-woven fabric. Both before and after the air permeability testing, the DBS nanofibres form assemblies with a nanofibre size of approximately 15 nm. Lower concentrations of commercial DBS in methanol, before and after SEM imaging, also showed no differences (data in the appendix).

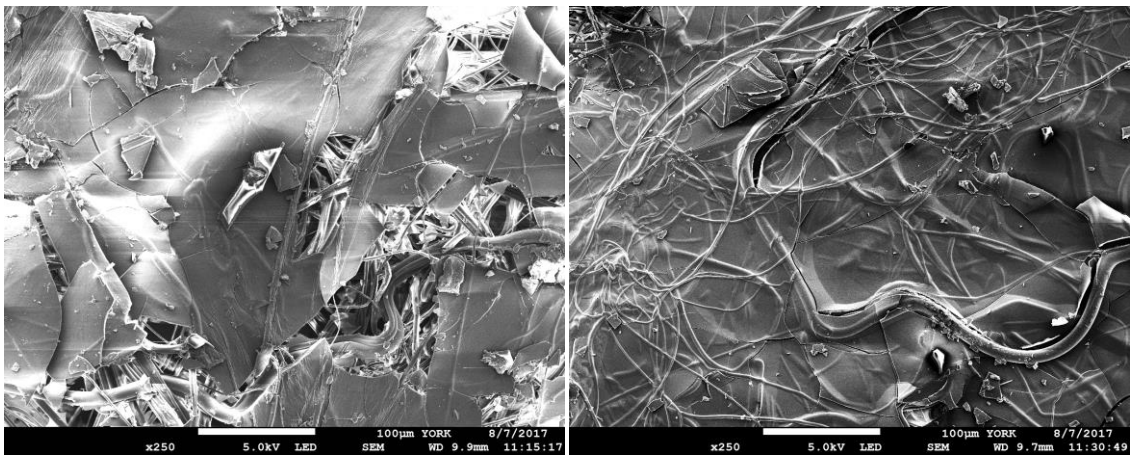

Figure 2-45. SEM images of non-woven fabric prepared with 1 wt/v% DBS in methanol before (left) and after (right) air permeability testing, scale bars of 100 µm.

Further, no negative effects from water vapour testing were observed, as demonstrated by Figure 2-46 for samples prepared from either solvent. These are positive results for the long-term application as they indicate the nano-modification can potentially survive wind and perspiration, which are both key environmental factors.

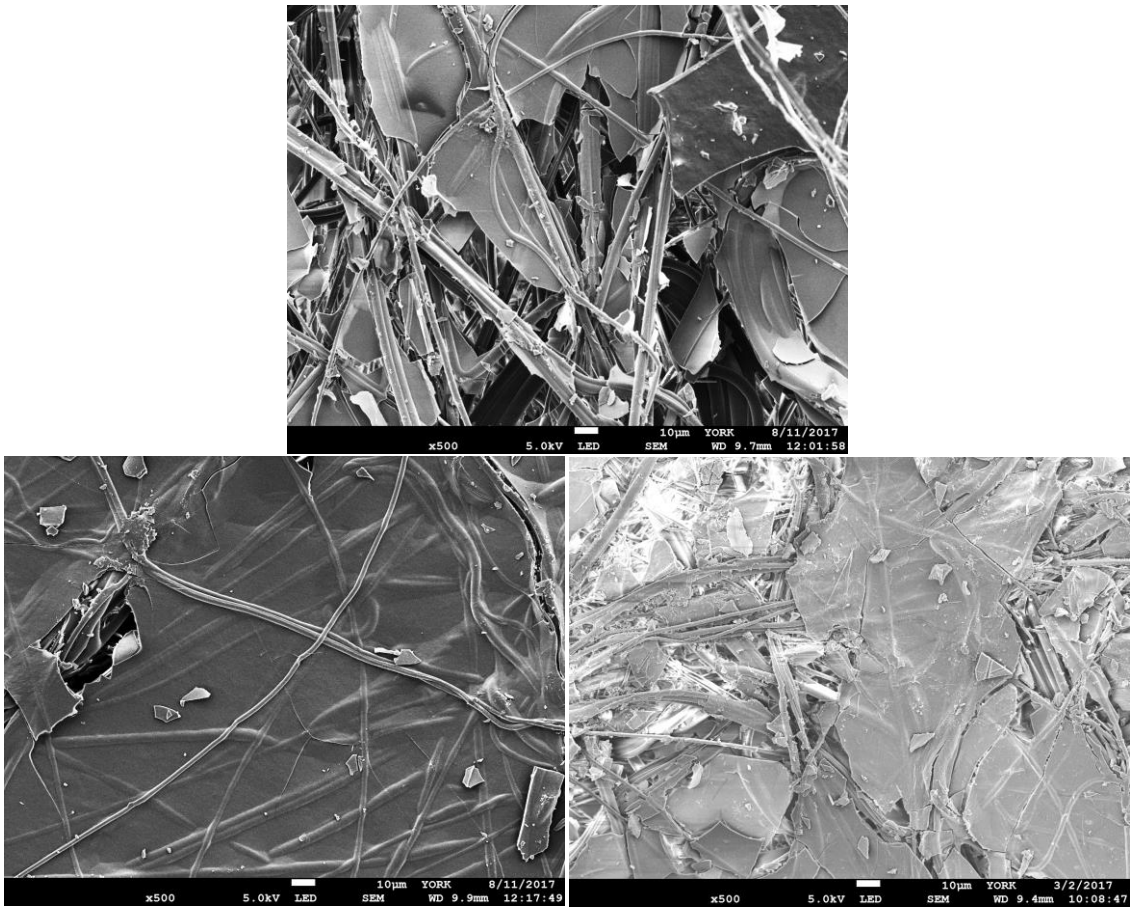

Figure 2-46. SEM images of non-woven fabrics prepared with 1 wt/v% DBS in 2-butanone, before (top) and after air permeability testing (bottom left) and water vapour permeability testing (bottom right), scale bars of 10 µm.

2.18.5 Robustness of Non-woven Fabric Treated with Commercial DBS

The robustness of these nano-modified fabrics to physical manipulation needed consideration. A sample was prepared for SEM, imaged, then removed and twisted between two sets of tweezers then returned to the SEM instrument for a second set of images to be taken. This was done to test the mechanical robustness of the nanofibres. The SEM image of the sample before and after physical manipulation can be seen in Figure 2-47.

It was difficult to image the fabric after the twisting, due to the disruption of the fabric structure. However, the aggregates that were easily seen before the twisting could not be seen as easily after. There would be an expectation to see at least some remnants of the aggregates seen on the fabric. However, there is a chance that the disruption seen is actually disruption of the metallic Pt/Pd coating on the sample which would be

expected to have high rigidity and could therefore break and rupture, minimising nanofibres seen due to charging of the sample.

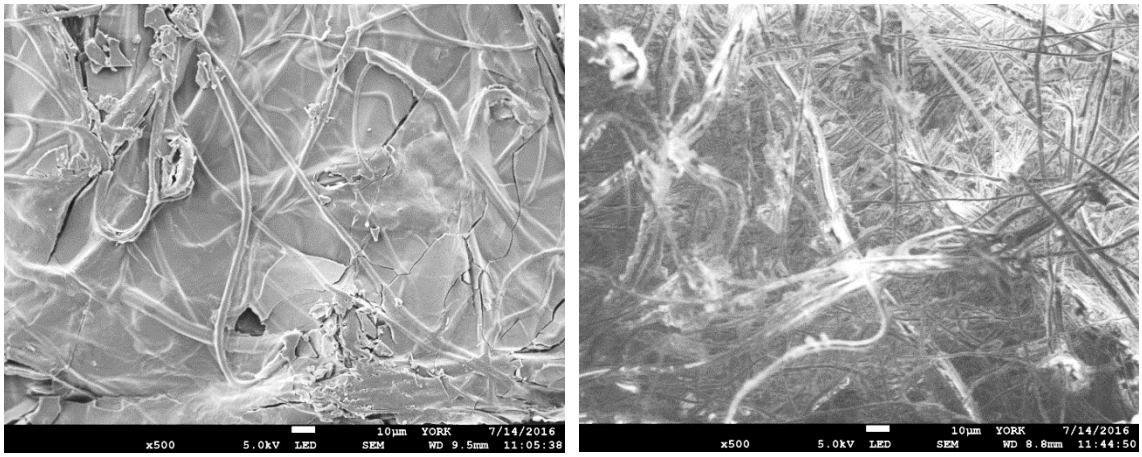

Figure 2-47. SEM images of non-woven fabric treated with 2 wt/v% DBS in methanol, before and after twisting, x500 magnification, scale bars of 10 µm.

2.18.6 Filtration Efficiency Testing of Non-woven Fabric Treated with Commercial DBS

A review of different protective textiles in use (including 14 non-woven fabrics) found that they generally have an air permeability of between 0 and 100 $cm^3\ cm^{-2}\ s^{-1}$ and a water vapour permeability of around 480 g $m^{-2}\ day^{-1}$.[372] The results seen so far with the non-woven fabric treated with DBS lie within this air permeability range and offer significantly higher WVP, as a result of the increased inherent WVP of the non-woven fabric used. The ability to withstand the testing conditions has also been demonstrated through visualisation of SEM images before and after testing. These preliminary results indicate that these prepared non-woven fabrics treated with DBS could be good potential candidates for protective barrier textiles.

Based on the positive results for AP and WVP, fabrics were then prepared and taken to DSTL for testing as an air filter against NaCl aerosol particles. Typically for nanofibre filters, electrospun polymer nanofibres are deposited on top of a support.[423] Our bottom-up approach forms the supramolecular nanofibres *in situ* by simple dipping of a non-woven fabric into a solution containing dissolved gelator molecules as previously discussed.

Filtration tests were performed on a small scale aerosol testing rig (SSATR) at Porton Down, with NaCl particles in the range 0.2 – 0.6 µm produced by an aerosol sprayer loaded with 1 wt/v% solution of NaCl (10 g l^{-1}) which produced a mist concertation of 13 mg m^3 at 12.71 l min^{-1}. A schematic of this testing rig can be seen in Figure 2-48.

Fabrics were prepared with solutions of 0, 0.4 and 0.8 wt/v% DBS in methanol and 0, 0.4, 0.6 and 0.8 wt/v% DBS in 2-butanone. The prepared fabrics were placed inside the rig with an exposed diameter of 16 cm, area 201 cm^2. The filtration experiments were conducted in a filter test rig with an air stream at a constant flow rate of 1.34 cm^3 cm^2 sec^{-1}, against an exposed fabric area of 201 cm^2 and a challenge presented by the aerosol particles of 100% from 1 wt/v% NaCl. Three samples of each fabric composite were prepared and tested. The air was sampled before and after the fabric, the pressure drop and downstream challenge were recorded every second for 6 minutes.

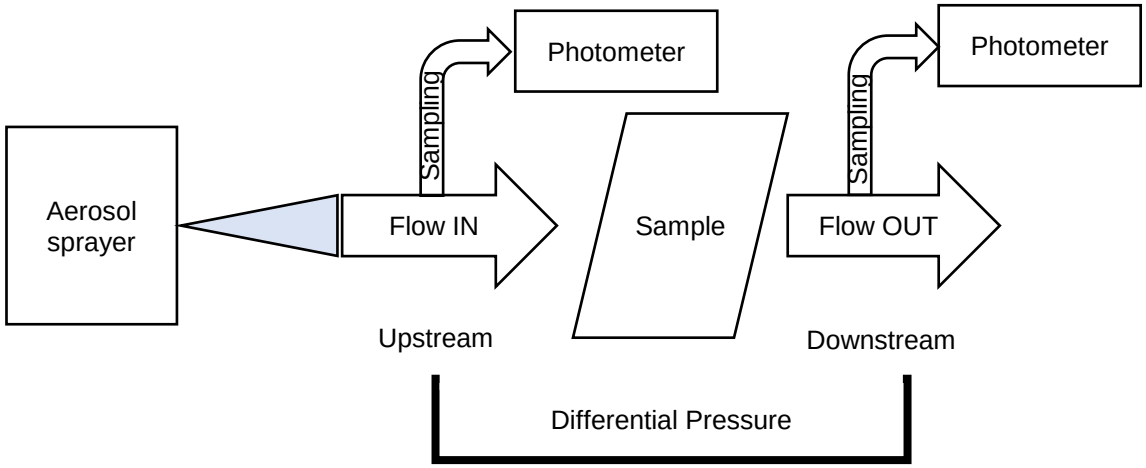

Figure 2-48. Schematic of Small Scale Aerosol Testing Rig (SSATR).

The differential pressure is defined as the pressure difference across the fabric (i.e. upstream pressure – downstream pressure). From Figure 2-49, the non-woven fabrics without nanofibres present, have a low differential pressure (<10 Pa). For the composites treated with DBS nanofibres, the differential pressure increased. This suggests that there are reduced pathways in the composite sample, making it more difficult for the air to get through. The increase in differential pressure supports the previously discussed relationship with air permeability, the higher the concentration of gelator used to prepare the fabric sample, the increased deposition of nanofibres within the sample, the lower the air permeability and higher the differential pressure. This result is also supported by the work of Schmidt *et al.* who demonstrated an order of magnitude difference in the differential pressure of nanofibre-microfibre non-woven composite samples when compared to those without nanofibres.[415] This pressure drop remained constant over the test period of six minutes, implying that the nanofibres remain intact for the duration of the testing. Schmidt *et al.* also found a constant differential pressure but tested over a longer time period of 24 hours. This suggests that our DBS nanofibres have good potential to remain intact over a longer time period.

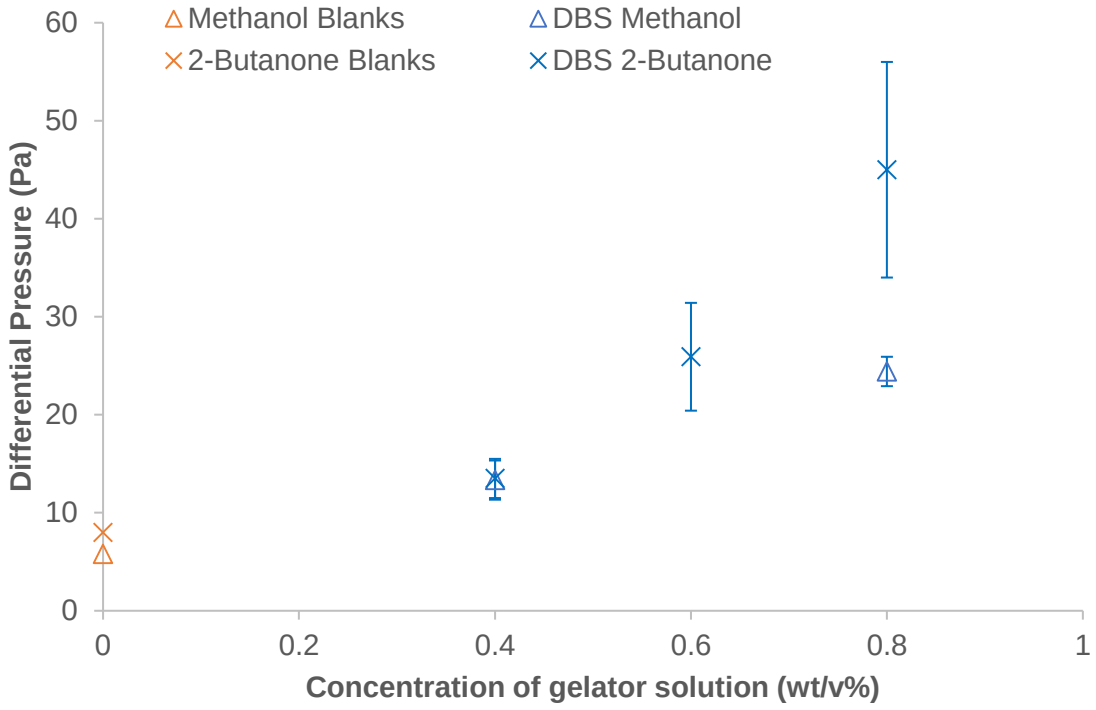

Figure 2-49. Graph of differential pressure against concentration of DBS solution.

The filtration efficiency is defined as the percentage of challenge (particles) removed by the filter medium. This is likely to depend on the size of the particulate matter although our detector could not detect the distribution of particulate matter. The deviations of the filtration efficiencies are shown as error bars on the results (see Figure 2-50).

As can be seen in Figure 2-50, the DBS treated fabrics performed similarly to the blank fabrics for 2-butanone, though the variation in filtration efficiency for the treated fabrics in this solvent gave rise to considerable errors (15% error on 78% filtration efficiency). The fabrics which were treated in methanol demonstrated a better filtration efficiency compared to the fabrics treated in 2-butanone, although the blank fabric soaked in methanol seemed to give the highest filtration efficiency result.

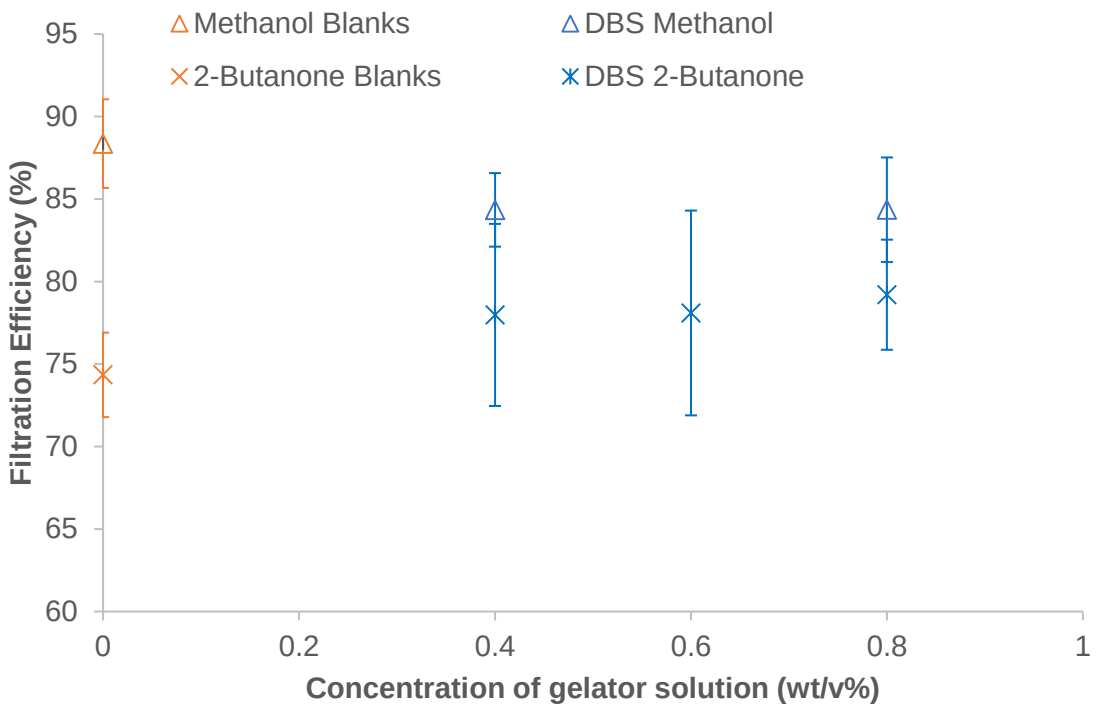

Figure 2-50. Graph of the filtration efficiency of NaCl aerosol particles against concentration of gelator solution used to treat fabrics for DBS.

Overall, it appears that the DBS nanofibres do not appear to have a significant impact on the filtration of NaCl particles. DBS treated fabric samples performed similarly to the blank fabric samples, both filtered out NaCl aerosol particles. The choice of solvent for soaking does appear to have a significant effect on the filtration efficiency, with methanol enhancing the filtration compared to 2-butanone. The inherent variability of the non-woven fabric is likely responsible for the large differences in the blank samples. As the concentration of gelator solution used to prepare the sample was increased, the differential pressure across the fabric sample increased. There does not appear to be a significant advantage in the higher concentrations of DBS in terms of filtration.

2.18.7 Aerosol Testing of Non-woven Fabric Treated with Commercial DBS

Fabrics were then prepared and taken to Silsoe Spray Application Unit (SSAU) for testing. This allowed determination of the ability of aerosols to penetrate these modified fabrics in a more relevant testing method for long-term application. This is a model for the way in which chemical weapons agents may be formulated on the battlefield.

Silsoe Spray Application Unit houses a wind tunnel which is 2 m high and 3 m wide. Liquid aerosol was sprayed into the tunnel, which dries to form aerosol particles. For this testing, fluorescein was used as the aerosol, because it is easy to measure and to

allow quantification of the results. The sprayer used in this testing created dried fluorescein with a diameter of 2-3 µm mass median diameter (MMD). This is larger than the diameter used for the NaCl particles.

A rig was constructed to allow testing of the prepared fabrics, as shown in Figure 2-51. The prepared fabrics were attached to a drainpipe of diameter 11 cm. Inside this drainpipe was a wire mesh, with three “collection tapes” distributed evenly vertically on the mesh. These collection tapes were to act as a ‘skin mimic’. The rear of the drainpipe was covered with a highly air permeable electrostatic fabric to stop any dried aerosol entering the pipe from the rear and affecting the deposition quantities while maximising airflow through the fabric sample. This rig was then placed inside the wind tunnel, under the ambient flow of dried fluorescein as shown in Figure 2-52. In one run, three blank fabrics and three treated fabrics (of the same concentration and gelator) were tested. This meant an average result could be gained and run-to-run variations plus any aerosol concentrations and wind variations across the tunnel should be accounted for. Each run alternated which side of the wind tunnel the blanks were arranged, i.e. for the first run they were positioned in the three positions nearest the door and then in the second run, they were in the three positions nearest the wall and the treated fabrics were nearest the door. A more detailed description of the testing can be found in the Experimental Section.

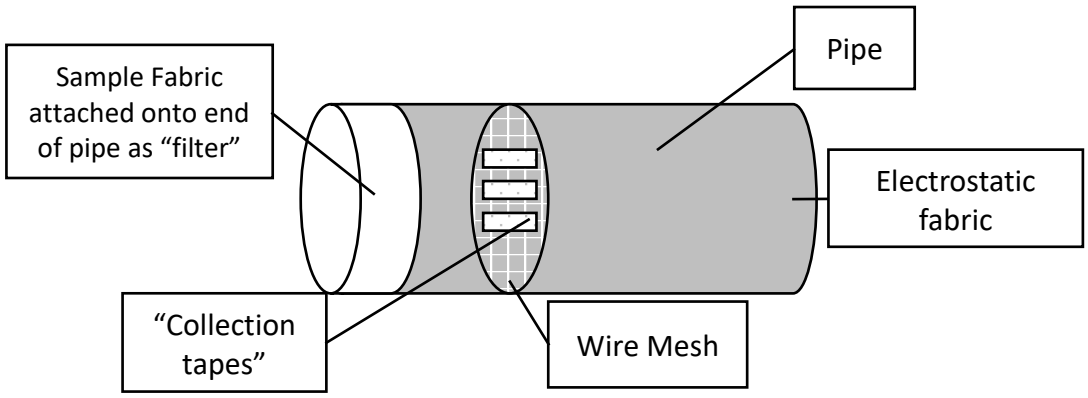

Figure 2-51. Rig set up for testing of treated fabrics at SSAU.

Figure 2-52. Demonstration of the 6 samples run each test within the wind tunnel; 3 blanks and 3 treated.

When the tubes were removed from the wind tunnel at the end of the test, there was a visible difference between the two fabrics. The “blank” fabrics that hadn’t been treated with gelator, were noticeably orange compared to the treated fabrics, implying that there is significantly more fluorescein in the untreated fabric causing the orange colour. To monitor how much aerosol was penetrating the fabric and reaching the skin mimic beneath, the tapes from the wire meshes were then carefully collected and analysed to determine how much fluorescein had passed through the fabric. The tapes were soluble so they were collected in individual plastic pots, to which a known aliquot of 0.01 M NaOH was added. NaOH was used to ensure that fluorescein was in the ionised state to ensure consistent response on the fluorimeter. The tapes were then dissolved and a smaller aliquot of the solution analysed in the fluorimeter. The more fluorescein deposited on the tapes, the higher the fluorescence of the solution and therefore the less aerosol the fabric had filtered out, assuming the same volume of air passed through. A higher response implies that more aerosol was able to penetrate through the fabric onto the skin of the wearer.

As can be seen in Figure 2-53, the DBS treated fabrics performed far better than the blank fabrics. There was a 33% decrease in fluorescein deposition from the blank sample to 0.2 wt/v% DBS. As the concentration of gelator increased, the deposition of fluorescein further decreased, implying an additional improvement in the filtration property.

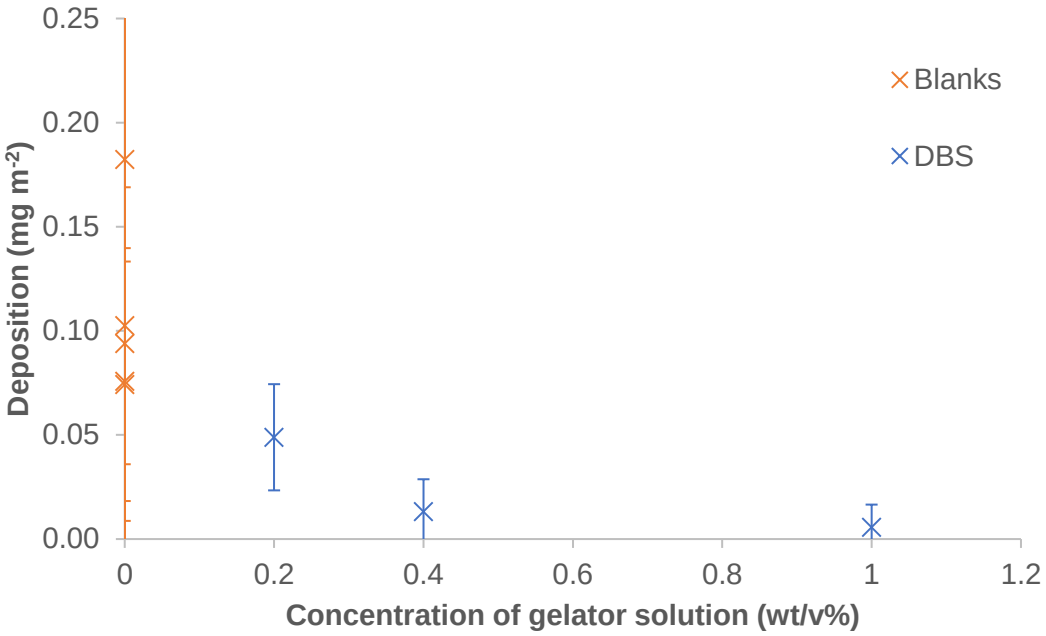

Figure 2-53. Graph of deposition of fluorescein on the collection tapes against concentration of gelator solution used to treat the fabrics with commercial DBS in 2-butanone.

As a result of the distinct colour differences in the fabrics seen, the amount of fluorescein deposited on the fabric was also analysed by the same method as the tapes; i.e. a circle was punched out of the fabric of a set size, washed with water, then an aliquot tested in the fluorimeter. However, unlike the tapes, the fabric was insoluble. Not all of the fluorescein was extracted during the washing process, so the results should be considered approximate, though they do follow the visual trend. The results are presented in Table 2-3.

Table 2-3. Deposition of fluorescein on the fabrics themselves for blanks and corresponding gelator concentration for DBS.

Concentration of gelator (wt/v%)	Deposition (mg m^{-2})
Blank	3.25
DBS 0.2%	4.14
DBS 0.4%	2.29
DBS 1%	0.77

The results from the washing of fabrics follow the visual trend; the untreated fabrics were more orange and therefore contained more fluorescein, except in the case of DBS 0.2 wt/v%. This particular sample (DBS 0.2 wt/v%) offered the best filtration result in this testing, with a lower tape deposition and higher deposition on the fabric itself.

This concentration also had the highest air permeability of the tested treated fabrics. On increasing gelator concentration, the fabrics contained less fluorescein (they also looked whiter).

This colour distinction between the blank and treated fabrics suggested something more than just filtration was at play. For pure filtration, one would expect the fabric which gave the lower tape deposition, i.e. filters out more fluorescein (the treated fabrics) to be more orange, i.e. containing more fluorescein than those that filtered less. The fluorescein should be deposited on the fabric during the filtering process. The fact the colours on these tested fabrics were the other way round was intriguing.

It was postulated that the filtration achieved by the treated fabrics could be related to the decreased air permeability seen in section 2.18.1. With increased concentration of gelator, a decrease in air permeability was seen. To investigate the relationship between air permeability and filtration (i.e. deposition on tapes), the two properties were plotted against one another in Figure 2-54. It is clear there is a relationship between air permeability of the treated fabric and the filtration property, with more air permeability giving rise to more nanoparticle deposition. This could, therefore, suggest that the modified fabrics are not simply acting as filters for aerosols, but have a mechanism preventing air passage under wind conditions and hence providing protection. The higher the concentration of gelator used, the more coverage is seen by SEM on the surface of the fabric, so a proportion of the fabric “pores” have been reduced in size by nanofibres, logically leading to a decrease in air permeability, simply because the air has to find a way through the composite. One can imagine that the more nanofibres on the surface of a fabric, the more probable filtration of dried aerosol particles by a simple catching mechanism based on the increased surface area of the nanofibre.

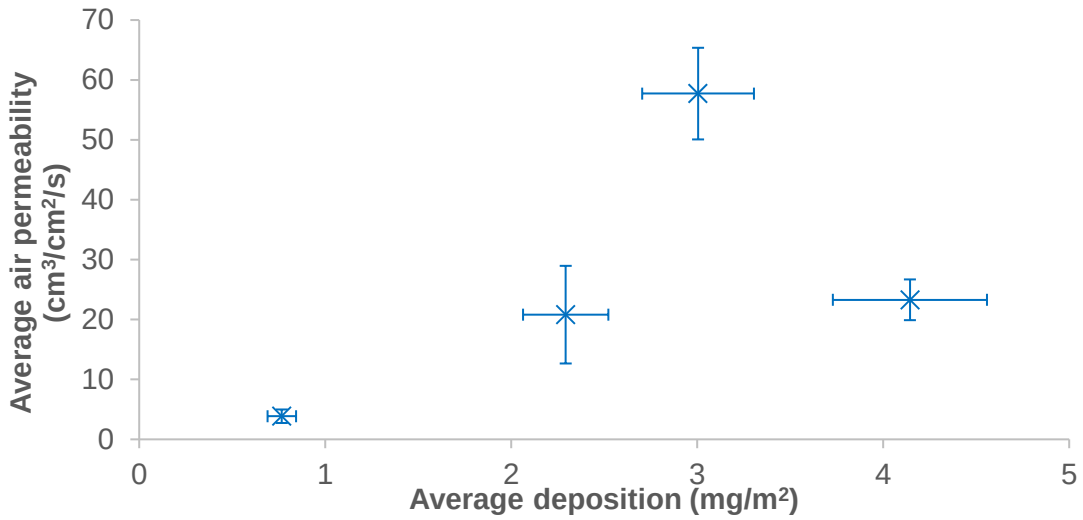

Figure 2-54. Graph of average fluorescein deposition on the fabric against average air permeability of each fabric at the same concentration of gelator solution for 0 wt/v%, 0.2 wt/v%, 0.4 wt/v% and 1.0 wt/v% in 2-butanone.

2.19 Conclusions

Various investigations to understand the variables which control self-assembled DBS nanofibres in fabrics have taken place. Through drying at room temperature under atmospheric conditions, it appears that solvent does not significantly impact on the morphology or diameter of the nanofibres. Drying conditions, particularly pressure, however, do have some role in the morphology formed.

Gel behaviour was investigated using solvent modification, rheology and T_{gel} measurement. In agreement with the literature, preferred gelation solvents could be correlated with Hansen solubility parameters. Furthermore, it was possible to correlate minimum gelation concentration with the precise location of the solvent in the three-dimensional 'Hansen space' – this is the first time this has been attempted. Solvent choice also influenced gel stiffness, 2-butanone also resulted in far stiffer gels than methanol, probably due to the aprotic nature of the solvent. The protic nature of methanol can interfere with the DBS intermolecular interactions, therefore disrupting gelation. It was found that increased DBS concentration produced stiffer, less elastic gels.

Rheology supported the simple visual observation of T_{gel} values, in that increased DBS concentration gave increased thermal stability. Gels in 2-butanone also had a slight increase in thermal stability than gels made in methanol.

A proof of concept experiment demonstrated the ability to self-assemble DBS nanofibres on the surface of a uniform textile. Differences between methods of application were investigated, with the use of a solution bath chosen for its relative ease of scale-up. Various fabrics have been investigated using SEM. Cross-sectional imaging of a fabric proved that the DBS nanofibres are indeed penetrating the fabric and are not just surface aggregates.

Large samples of non-woven fabric were selected for treatment with DBS, which assembled into nanofibres. It was found that increased deposition of nanofibres hindered air permeability, but the same level of deposition did not impede water vapour transport. It was reasoned that water vapour permeability testing is based on passive diffusion over a 24 hour time period, whereas air permeability testing is a more 'forced' experiment at high pressure (30 second time period). SEM imaging showed that neither form of testing significantly impacted on the nanofibres on the non-woven, indicating good physical stability of the nanosystems. Water vapour permeability was also tested in an environmental chamber to elevate the water temperature. Once again water vapour transport was not impeded, hopefully providing an indication that these fabrics would allow evaporation of water or sweat from the surface of the skin, allowing breathability.

At DSTL against the small scale aerosol testing rig, DBS-treated fabric samples performed similarly to blank fabric samples at filtering out NaCl aerosol particles. Testing the DBS treated fabrics in the wind tunnel at SSAU against an aerosol chemical warfare agent mimic (fluorescein) gave very positive results. Although minimal testing was completed due to cost and time constraints, the DBS-treated fabrics performed significantly better than the "blank" fabrics, minimising deposition of dried fluorescein onto the skin mimic tapes. Increased deposition of nanofibres led to a further reduction in the penetration of fluorescein. A composite made with around 0.2 wt/v% DBS would seem a favourable compromise between air permeability, fluorescein filtration and filtration efficiency of a range of particle sizes.

It was therefore felt to be important to compare DBS to the gelator in the literature originally identified as potential supramolecular nanofibres for air filtration. In the next chapter, this gelator molecule (BTA) is investigated and compared to our DBS system to gain a better understanding of self-assembly, and to benchmark our DBS materials against a key competitor.

Chapter 3 - *N,N',N"*-Tris(2-ethylhexyl)-1,3,5-benzenetricarboxamide (BTA) For Fabric Modification

For the purposes of the results in this chapter, 'BTA' will be used to represent the specific derivative *N,N',N"*-tris(2-ethylhexyl)-1,3,5-benzenetricarboxamide.

3.1 Synthesis of *N,N',N"*-Tris(2-ethylhexyl)-1,3,5-benzenetricarboxamide (BTA)

It was important to compare our studies on DBS to a known benchmark, so first, the literature system was repeated to ensure reproducibility and to investigate how the system worked in our fabric with our choice of solvents. These results would then allow comparison between the DBS results and BTA benchmark results. This would provide an understanding of how two structurally different gelators behave in the fabric.

BTA was synthesised using a synthetic route from the literature by Schmidt.[151] This involves a one step reaction between an amine and a triacyl chloride (Scheme 3-1).

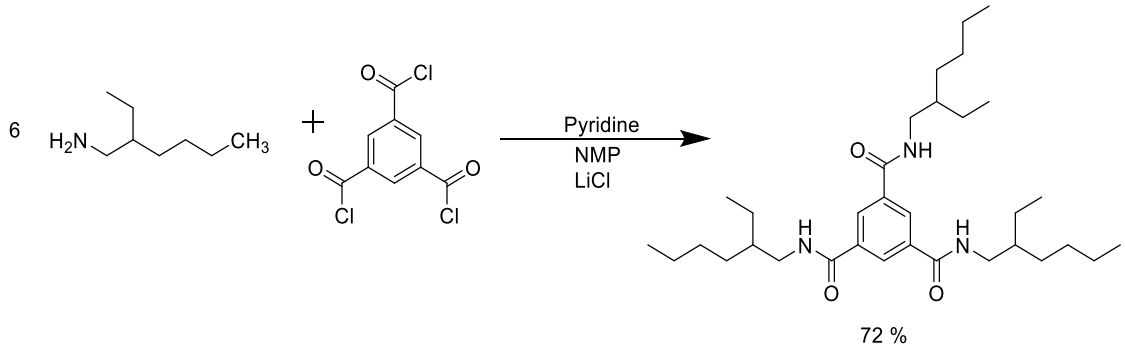

Scheme 3-1. Synthetic scheme of BTA.

1,3,5-Benzenetricarboxylic acid chloride was added under nitrogen at 0 °C to a mixture of anhydrous *N*-methylpyrrolidone, pyridine, lithium chloride and 2-ethylhexylamine. The reaction mixture was stirred overnight at 60 °C. After cooling to room temperature, the mixture was left for 48 hours. The reaction mixture was then poured into ice water to form a precipitate which was filtered off, and the product was isolated by recrystallization from methanol. The product appeared as white needle-like crystals and obtained in a yield of 72% which was better than the reported yield in the literature. The product was characterised by ^{1}H NMR, ^{13}C NMR, MS and IR spectroscopy. The 1H NMR spectrum showed a kay amide proton resonance at 8.6 ppm split into a triplet by the adjacent CH_2 group, with a resonance of 3 protons. Aromatic proton resonances were observed at 8.3 ppm with an integration of 3 protons. The CH_2 group adjacent to the amide is shown as a triplet at 3.2 ppm with a matching J coupling to the amide proton resonance with an integration of 6 protons. Mass spectrometry showed mass

ion values of 544.4455 $[M+H]^+$ (100%) correlating to the molecular ion with a proton, and 566.4270 $[M+Na]^+$ (6%).

Gels were observed with BTA with a MGC of 0.6 wt/v% in 2-butanone. A partial gel formed at 0.4 wt/v% BTA in 2-butanone.

3.1.1 Confirmation of the Literature Results in Our System

The original research paper that set the precedent for the present study, used *N,N',N"*-tris(2-ethylhexyl)-1,3,5-benzenetricarboxamide in 2-butanone,[415] hence initial investigations studied this gelator in both 2-butanone and methanol. This would provide understanding of the importance of solvent selection for this gelator and allow direct comparison to the DBS systems.

A range of concentrations from 0.4 wt/v% to 1.0 wt/v% of BTA in 2-butanone were prepared in a similar way to the method reported previously.[415] The main difference was that our methodology did not use a rig to hold the fabric, as generally, the samples used in this work were much smaller. A non-woven polypropylene fabric was treated by soaking small samples of the fabric in the BTA solutions for *ca.* 5 minutes, these were then removed and left to dry. The morphology of the composites was investigated by scanning electron microscopy (SEM). The SEM images of most concentrations are generally comparable with the images seen in the original literature. Each concentration was compared in turn, to allow easy comparison, starting with 0.4 wt/v% in Figure 3-1.

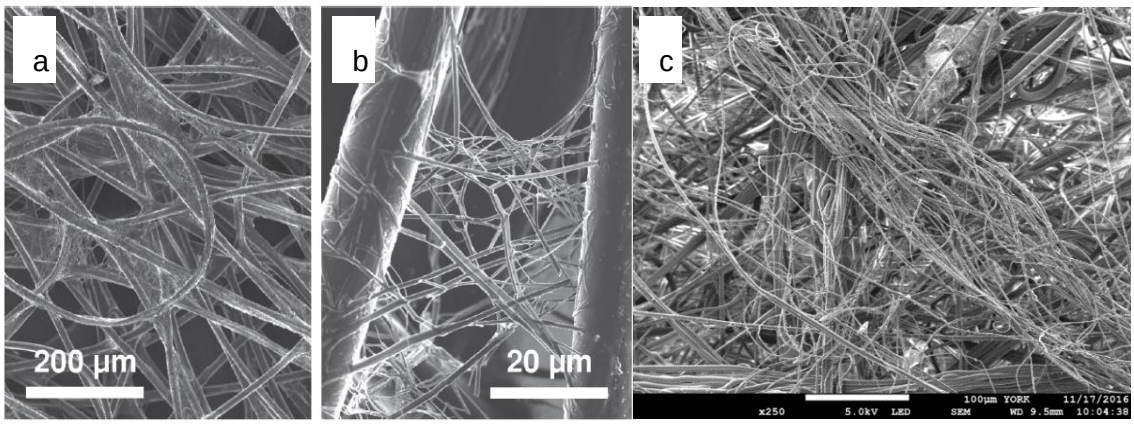

Figure 3-1. SEM images of non-woven fabrics prepared with 0.4 wt/v% BTA in 2-butanone; (a) and (b) are from the original work by Schmidt, reproduced from Ref 415 with permission from John Wiley & sons, (c) is this replicated work, scale bars of 200 µm, 20 µm and 100 µm.

The thick fibres belong to the non-woven fabric, whereas the thinner fibres are the BTA supramolecular nanofibres. At this low concentration, the biggest difference between the two studies is seen. The original work (in a and b) showed spanning of nanofibres across fabric fibres, whereas the replicated work shows limited spanning, instead showing aggregate bundles as illustrated in Figure 3-2.

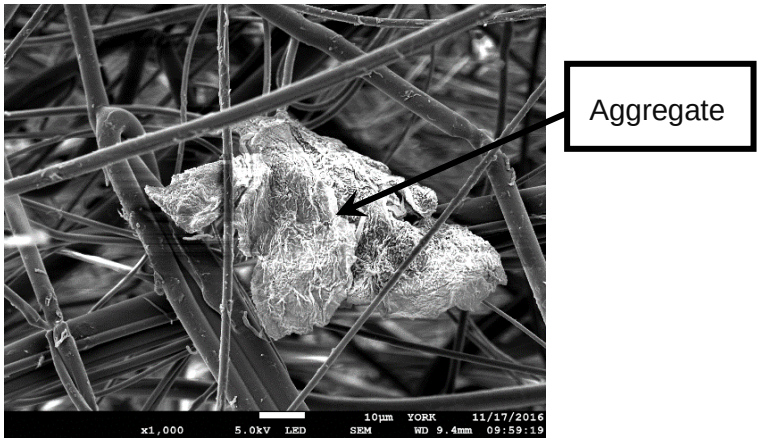

Figure 3-2. SEM image of 0.4 wt/v% BTA at higher magnification to show aggregation, scale bar of 10 µm.

The samples from both studies showed somewhat uneven filling of the openings in the fabric, with nanofibres, which tend to self-fixate, clumping together rather than spreading out.

It is important to note here, in contrast with the research using DBS in Chapter 2, that the self-assembled nanofibres of BTA have much larger diameters (*ca*. 450 nm). The large difference in structure leads to a dramatic difference in morphology. The DBS nanofibres formed are *ca.* 30x smaller than the BTA nanofibres in 2-butanone (15 nm *vs. ca.* 450 nm). This difference in diameter could very significantly influence the properties of the treated fabrics. It is unclear *a priori* whether it will be more beneficial to incorporate larger or smaller nanofibres into the fabrics. It is worth noting that the much smaller nanofibre diameters of DBS offer much larger relative surface area, which could have a range of advantages in terms of actual fabric modification, for example the potential to filter more particles. This size difference could also impact on how many fibres are formed for the same wt/v% concentration and has the potential to affect the interactions between nanofibres and consequently the amount of "spanning" generated.

Overall, 0.4 wt/v% is quite a low BTA concentration with respect to the minimum gelation concentration, as it formed a partial gel. It is interesting to note that the original study by Schmidt *et al.* reported 2-butanone as a non-gelling solvent for BTA,[415] however, during our replication, BTA did appear to form gels in 2-butanone. Concentrations of 0.6 wt/v% and above formed a white opaque gel overnight, whereas 0.4 wt/v% only formed a partial gel. This could help explain the differences visible at 0.4 wt/v%, between our work and the literature SEM images, if the solution gelled during the preparation, it may be harder for the fibres to spread over the surface of the fabric. There is evidence in the literature that gelation should be avoided to obtain supramolecular composites with morphologies suitable for air filtration.[417] Equally, there will be quite a complex drying process within the fabric, which could complicate matters further. At the slightly higher concentrations of 0.6 wt/v% and 0.8 wt/v%, which can be seen in Figure 3-3, a greater degree of similarity can be seen between the original work and our replicate study. The BTA nanofibres are spreading out over the surface of the fabric more completely than in the 0.4 wt/v% sample. BTA nanofibres do appear to "span" across various fabric fibres in both the original and replicated work. All the images show unfilled holes/gaps, but these are significantly smaller than the pores in the untreated non-woven and hence the modified fabric may be expected to provide better filtration properties.

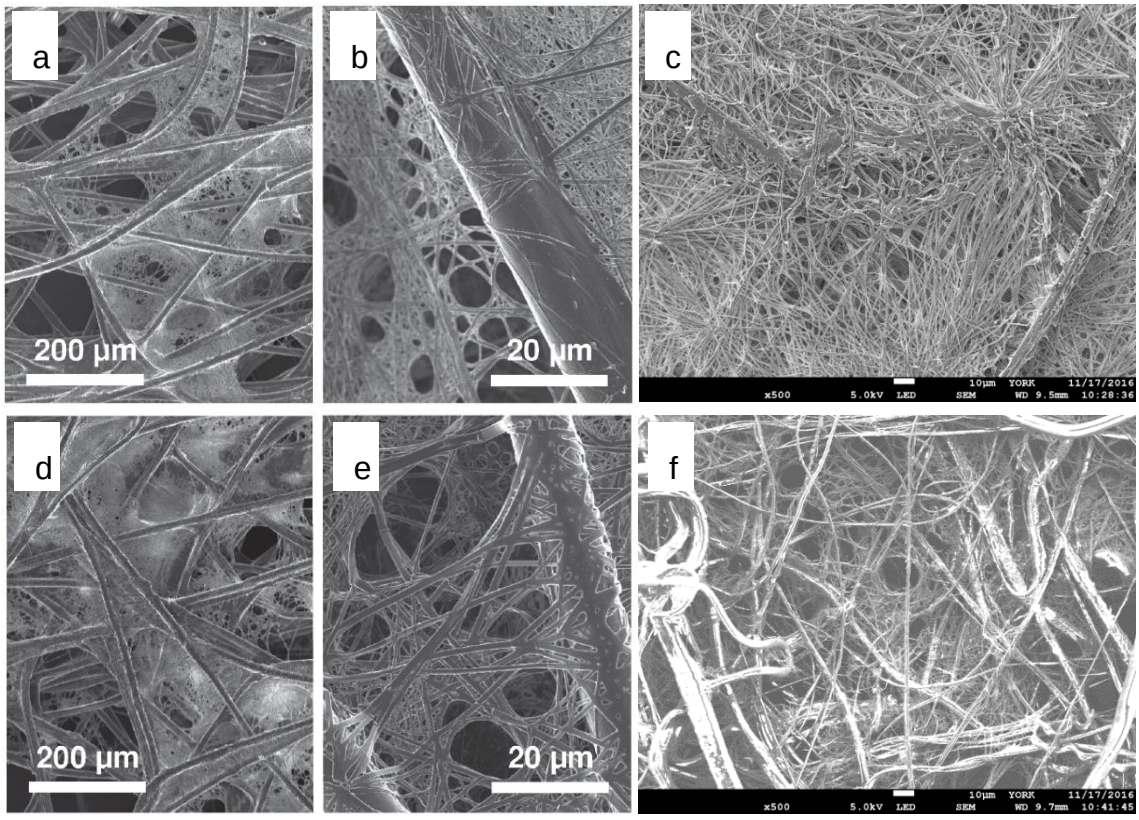

Figure 3-3. SEM images of non-woven fabric treated with 0.6 wt/v% BTA in 2-butanone; (a) and (b) are reproduced from Ref 415 with permission from John Wiley & sons, (c) is the replicated work; non-woven fabric treated with 0.8 wt/v% BTA in 2-butanone; (d) and (e) are reproduced from Ref 415 with permission from John Wiley & sons, (f) is the replicated work, scale bars of 200 µm, 20 µm and 10 µm.

At the highest concentration (1.0 wt/v%) shown in Figure 3-4, it is easy to see the similarities. The BTA nanofibres span across the larger fabric fibres, with a considerably “denser” coverage than at lower concentrations. This result agrees with the basic logic of higher concentration, giving more mass deposited on the fabric, and hence more nanofibres.

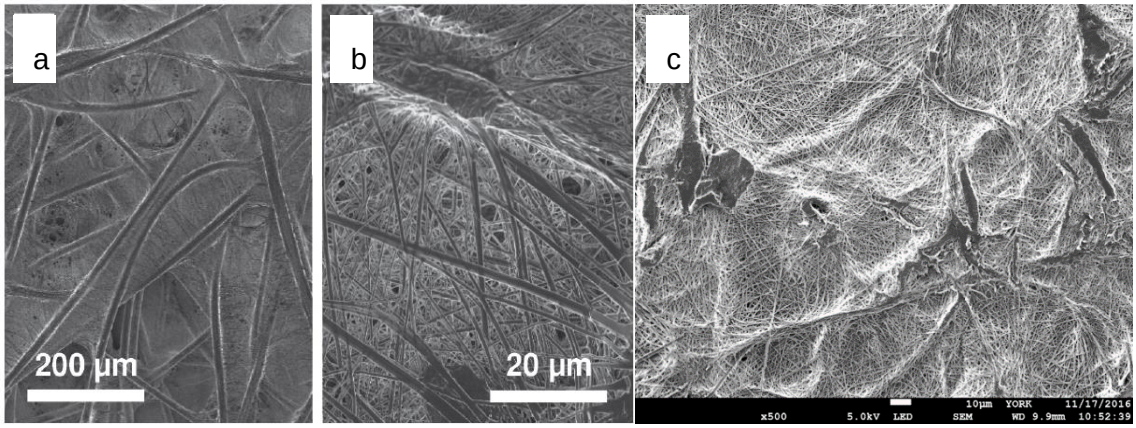

Figure 3-4. SEM images of 1.0 wt/v% BTA in 2-butanone; (a) and (b) are reproduced from Ref 415 with permission from John Wiley & sons, (c) is the replicated study, scale bars of 200 µm, 20 µm and 10 µm.

The mass gain of all these samples is much larger (15%, 14%, 15% and 23%, respectively) than quoted in the original work (2.8%, 4.4%, 6.4% and 7.0%). However, the published report used a much larger surface area (8.5 cm x 8.5 cm) compared to the SEM-sized samples that were prepared in the replicated work (0.5 cm x 0.5 cm).[415] Schmidt *et al.* also used a commercially available viscose/polyester non-woven fabric, whereas the replicated work uses a polypropylene non-woven fabric provided by DSTL. Therefore there are several variables that will impact on these mass differences. In summary, this study demonstrated that the approach reported by Schmidt *et al.* could be replicated under our conditions, employing fabrics from the studies using DBS in Chapter 2. The morphological differences between BTA and DBS are apparent with a very significant difference in diameter and morphology (Figure 3-5), and it was important to know if this would impact further on the fabric performance.

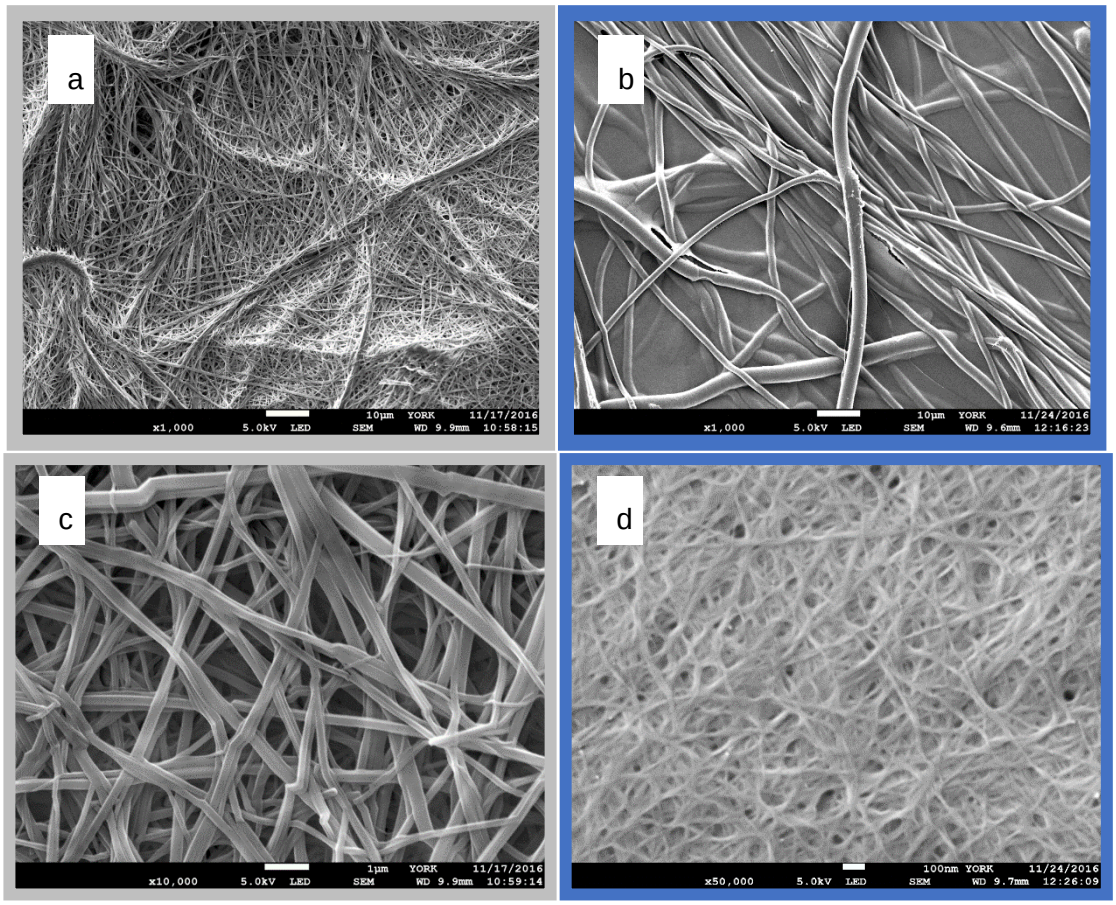

Figure 3-5. SEM images demonstrating coverage of 1 wt/v% BTA and DBS in 2-butanone on non-woven fabric at 3 different magnifications; (a) 1% BTA at x1000, (b) 1% DBS at x1000, (c) 1% BTA at x10 000 and (d) 1% DBS at x50 000 (scale bars at 10 µm in a and b, 1 µm in c and 100 nm in d).

3.1.2 Alternative Solvent Investigation

An alternative solvent was also used with BTA to see if any additional knowledge could be gained and transferred to our other gelator systems. To allow comparison with the work with DBS, BTA was studied in methanol. SEM images were visually significantly different when using methanol compared with 2-butanone as can be seen in Figure 3-6. Literature published in 2016, supported our results as Schmidt *et al.* demonstrated that solvent had a large effect on the morphology of BTA based nanofibres.[417] Instead of forming long, spanning nanofibres like in 2-butanone, in methanol BTA formed much shorter, more rigid looking nanofibres as seen in Figure 3-6. These nanofibres have larger fibre diameters than in 2-butanone, *ca*. 700 nm compared *ca*. 450 nm. Rather than spanning the fabric, these nanofibres appear much shorter and clump together in the fabric.

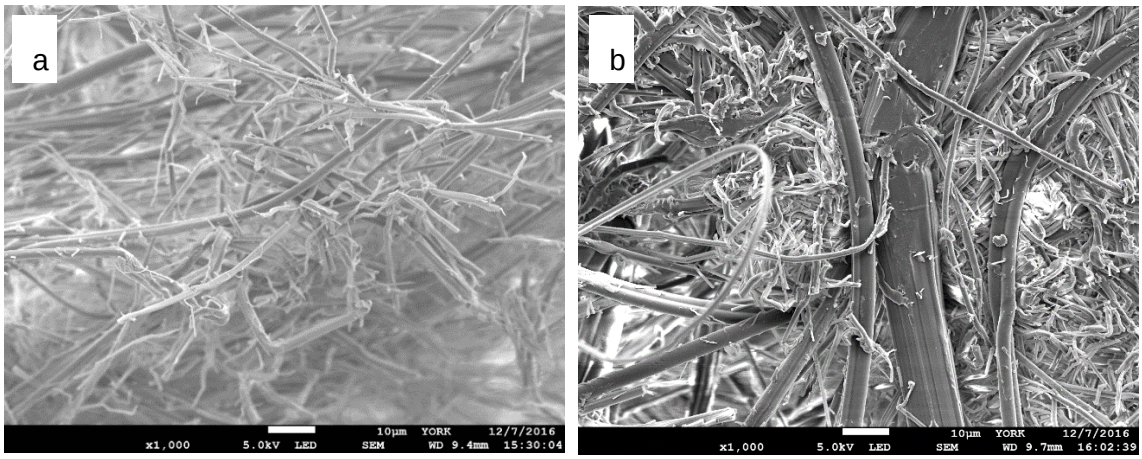

Figure 3-6. SEM images of BTA in methanol; (a) 0.6 wt/v% and (b) 1.0 wt/v%, scale bars of 10 µm.

Comparing Figure 3-7 with Figure 3-4 shows a marked difference in the structure of the composite. The coverage achieved in methanol is much more uneven, with some areas quite densely covered with nanofibres while other areas have less dense coverage (comparing the top right of Figure 3-7 to the bottom left for example). This implies that solvent can have a major impact on assembly mode and fabric compatibility, in agreement with the results published by Schmidt *et al.*[417] This also agrees to some extent with our own work reported using DBS as outlined in Chapter 2. It is difficult to determine how much of the changes are down to solvent polarity or other solvent properties such as volatility and as such, rate of evaporation.

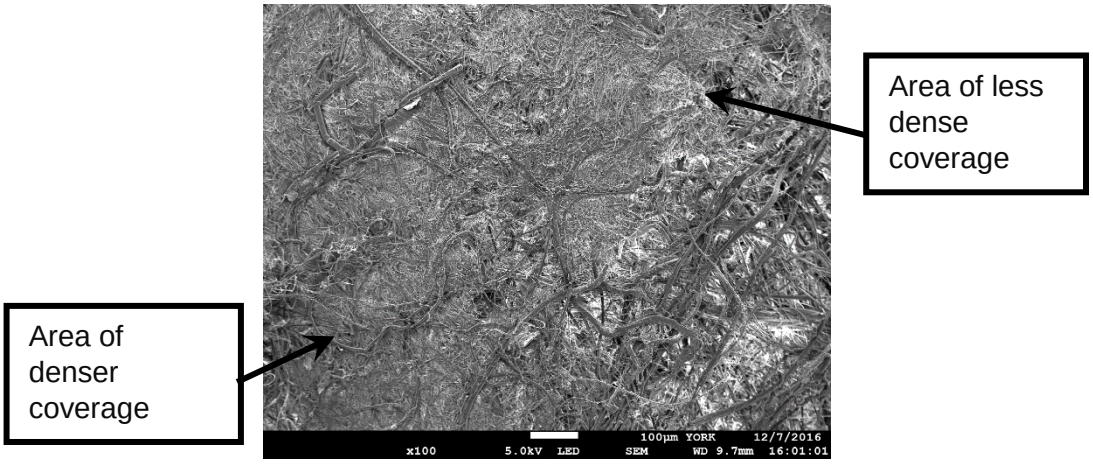

Figure 3-7. SEM image of 1.0 wt/v% BTA in methanol at low magnification, scale bar of 100 µm.

Further to these investigations, samples were scaled up and tested for fabric properties.

3.2 Fabric Performance Testing of BTA Prepared Fabrics

Following the protocols outlined in the experimental section, fabrics were prepared and tested at the University of Leeds with the for two key properties; air permeability and water vapour permeability. Other samples were tested at DSTL for filtration efficiency and Silsoe Application Spray Unit for real world testing. It was reasoned this would provide a "benchmark" from the literature to compare against our DBS results and allow us to determine just how effective DBS performance was against an established positive control.

3.2.1 Air Permeability of BTA Prepared Fabrics

Air permeability of the modified fabrics were tested as described in Chapter 2. The results presented in Figure 3-8 show the relationship between measured air permeability and the concentration of BTA used to prepare the fabrics.

It can be seen from Figure 3-8 that the results using BTA, closely match those previously seen with DBS. There is a logical relationship between the concentration of the gelator solution used to prepare the fabrics and the air permeability of the fabric. The addition of nanofibres, even at low concentrations, leads to a significant drop in air permeability. The more nanofibres deposited on the fabric, as concentration increases, the more significant the decrease in the air permeability, implying that the density of nanofibres has the largest effect on air permeability.

It can also be seen that fabrics prepared with either methanol or 2-butanone respond very similarly to this test, implying the solvent and precise details of nanofibre morphology do not appear to significantly affect air permeability.

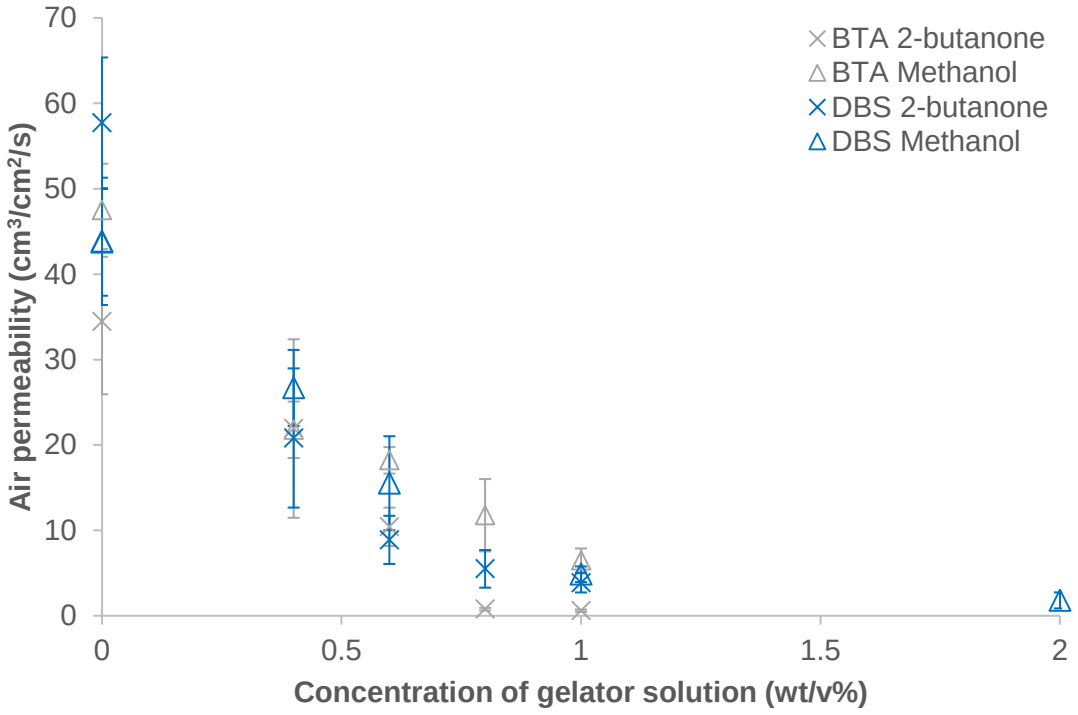

Figure 3-8. Graph of air permeability against concentration of gelator for methanol and 2-butanone.

These results show that DBS appears to contribute to fabric behaviour similarly to BTA. This is a positive initial result, indicating that DBS could make a suitable replacement for BTA as a gelator to form supramolecular nanofibres within a non-woven fabric, even though it has very different nanoscale morphology – forming much smaller nanofibres with much larger relative surface areas (see above).

3.2.2 Water Vapour Permeability of BTA Prepared Fabrics

The water vapour permeability of the modified fabrics were tested as described in Chapter 2. It appears that the WVP is not significantly affected by the addition of nanofibres. The results of BTA appear similar to those obtained using DBS (Figure 3-9) although it does appear that BTA nanofibre modified fabrics were less permeable to water vapour in each case. This could be due to the increased nanofibre size of BTA compared to DBS in 2-butanone (450 nm compared to 15 nm) or alternatively may reflect the more hydrophobic nature of BTA nanofibres compared with DBS. In this regard, it is notable that DBS is compatible with 1:1 methanol:water whereas BTA is not. This may suggest some advantage to using DBS rather than BTA which may reflect nanofibre size or hydrophobicity.

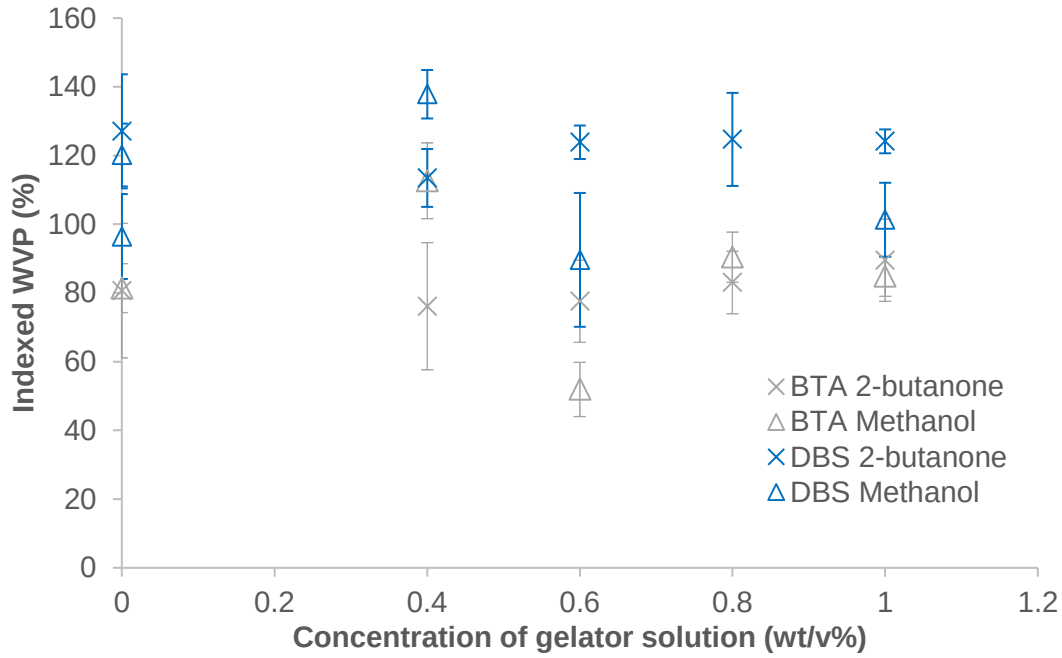

Figure 3-9. Graph of water vapour permeability against concentration of gelator for methanol and 2-butanone.

For both gelators, the results in 2-butanone appear more consistent, with less deviation than the larger fluctuations seen with methanol. This is supported by the SEM images of BTA in the two solvents. As can be seen from Figure 3-10 nanofibres from 2-butanone spread out and span across the fabric. This is completely different to the nanofibres dried from methanol, which as described above tended to be shorter and clump together more. It seems likely that the variability seen in the methanol results comes from these fluctuations in the samples themselves.

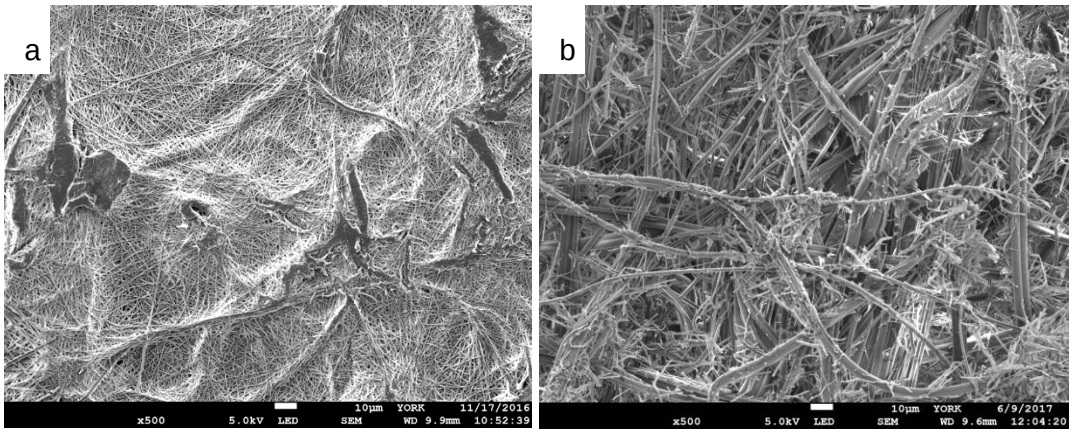

Figure 3-10. SEM images of BTA at 1 wt/v% in 2-butanone (a) and methanol (b), scale bars of 10 µm.

As described in Chapter 2, it can be proposed that nanofibres appear to affect air permeability under rapid flow pressure but have less impact on water vapour permeability under diffusion conditions and water vapour pressure.

3.2.3 Effects of Testing on BTA Nanofibres

The non-covalent interactions which underpin the self-assembly of the gelator nanofibres are, by definition, weak interactions. To ensure the nanofibres were not unduly damaged during the fabric testing, SEM images of 'before' and 'after' testing were recorded. These could not be performed on exactly the same section of fabric, so the irregularity of the non-woven fabric does produce some changes in the images as can be seen in Figure 3-11.

The coverage shown by BTA at 1 wt/v% in 2-butanone indicates spanning across the non-woven fabric fibres, but appeared patchy in places (Figure 3-7). After air permeability testing, the nanofibres seemed to have significantly reduced spanning. It looks like there is less coverage, and the nanofibres appear much shorter. After water vapour permeability testing, there is a mixture of coverage. There are really dense areas of coverage whereas some regions are less dense. Some shorter nanofibres were observed similarly to the post air permeability testing. This is significantly different to what was observed 'before' and 'after' testing of DBS modified fabrics in Chapter 2, and suggests that the larger BTA nanofibres may be less stable/robust. Instinctively, one would assume that the larger BTA nanofibres may be stronger and more robust but this is not the case. It can be reasoned that although BTA nanofibres are larger, this, in fact, makes them more brittle and susceptible to damage due to the air impacting on a greater cross-sectional area. It can also be reasoned that DBS nanofibres are smaller and therefore more flexible, so can 'give' on air impact without breaking. The result of BTA nanofibres after WVP testing suggests the self-assembled nanostructures may rearrange when exposed to water – perhaps as a result of its hydrophobicity.

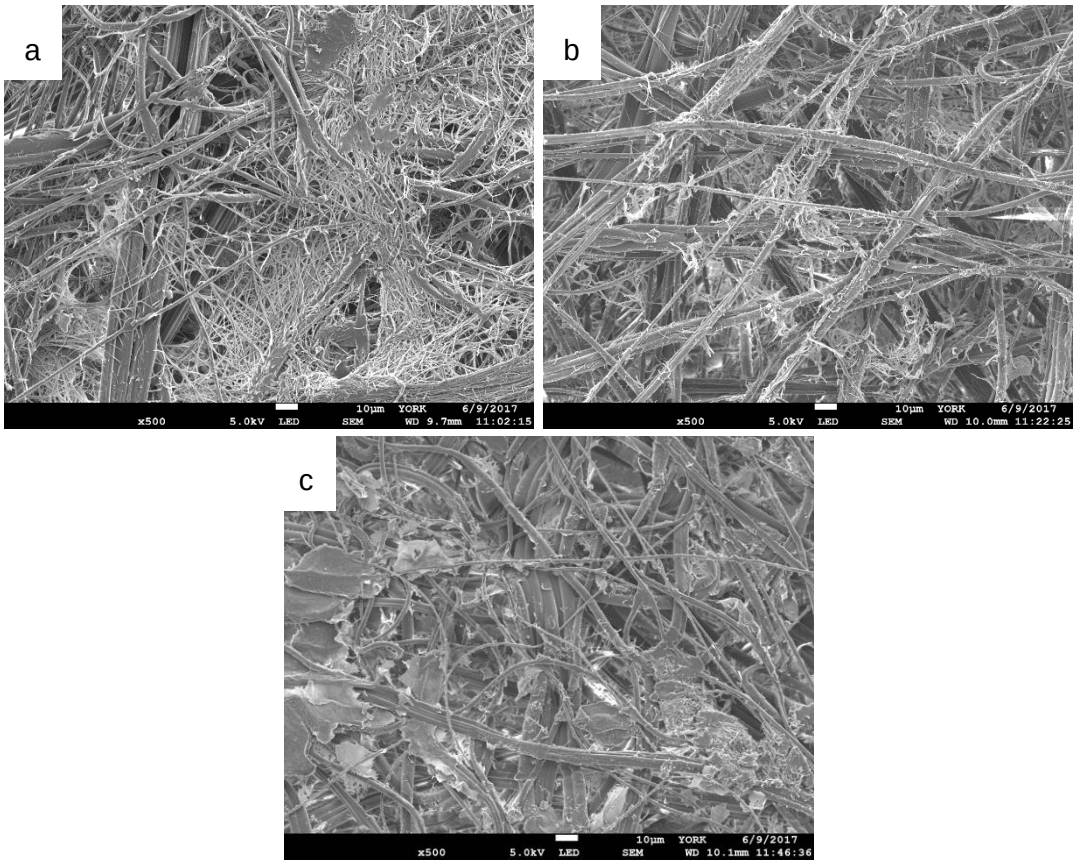

Figure 3-11. SEM images of BTA at 1 wt/v% in 2-butanone (a) prior to testing, (b) after air permeability testing, (c) after water vapour permeability testing, scale bars of 10 µm.

The sample, based on 0.4 wt/v% BTA 'before' and 'after' testing was investigated to confirm these observations. The coverage shown by BTA at 0.4 wt/v% in 2-butanone is much lower than that shown by 1 wt/v% as expected. The nanofibres are shorter and don't appear to span or spread out as much as at the other concentrations studied. After air permeability testing, the nanofibres seemed to show a bit less coverage, and were even shorter. After water vapour permeability testing, there was very little aggregation observed. This could be an artefact of sampling but may also reflect damage to the hydrophobic hydrogen bonding nanofibres induced by the pressure of the high level of water vapour.

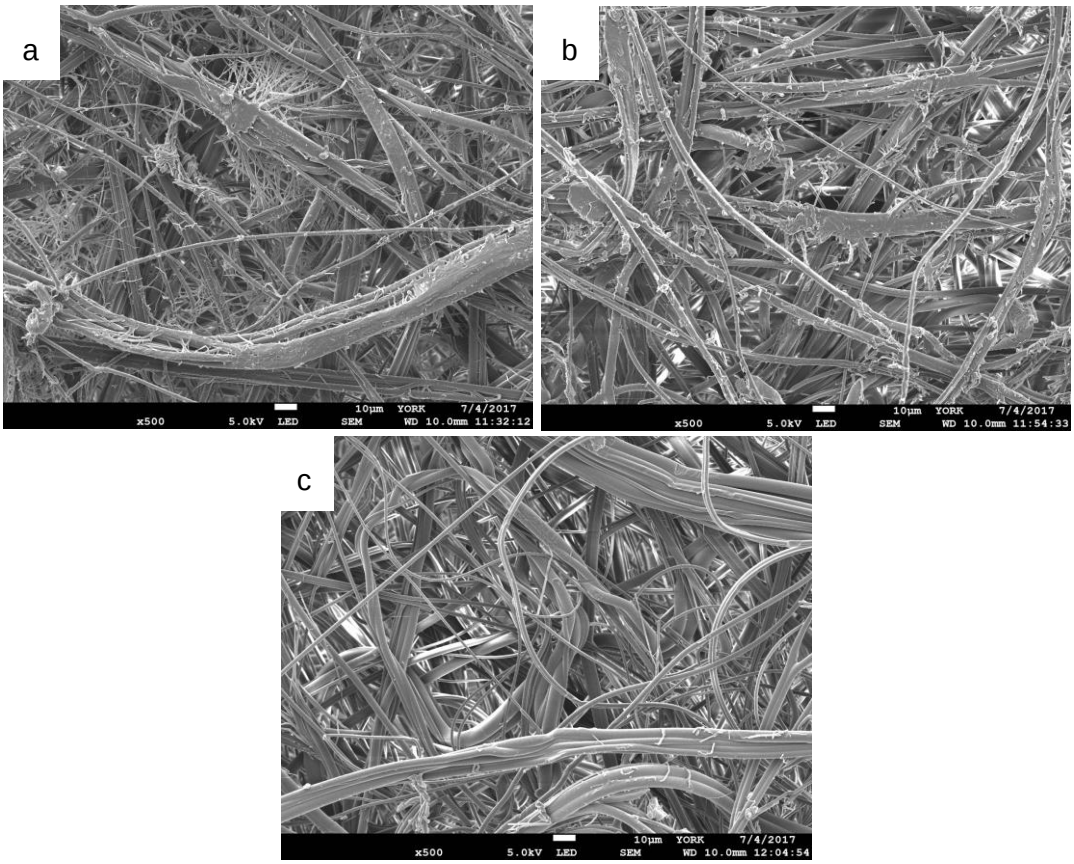

Figure 3-12 SEM images of BTA at 0.4 wt/v% in 2-butanone (a) prior to testing, (b) after air permeability testing, (c) after water vapour permeability testing, scale bars of 10 µm.

Generally, if there is an effect of testing, it appears to be more visible at higher concentrations of BTA. In summary, these results indicated that BTA achieved similar fabric performance results to DBS although also suggested that BTA nanofibres may be more damaged by testing and are less stable/robust. This could be a significant advantage for DBS in terms of garment lifetime and length of protection.

3.2.4 Filtration Efficiency Testing of BTA

It was important for the application to understand what effect the nanofibres have on the filtration properties of the fabric. Scaled up samples were taken to DSTL for filtration testing on a small scale aerosol testing rig. As described in Chapter 2, differential pressure increases with increased deposition of nanofibres. Schmidt *et al.* demonstrated an order of magnitude difference in the differential pressure of BTA nanofibre-microfibre non-woven composite samples compared to those without nanofibres.[415] Our results show an increase from 8 Pa on the blank fabric sample to 160 Pa on the 0.8 wt/v% BTA. This is a large increase which could imply that the

nanofibres are quite impermeable at this concentration. This pressure drop remained constant over the test period of six minutes, implying that the nanofibres remain intact for the duration of the testing. Schmidt *et al.* also found a constant differential pressure, but tested over a longer time period of 24 hours. This suggests that both our DBS and BTA nanofibres have good potential to remain intact over a longer time period. It is important to consider that this only measures airflow and not physical movement of the wearer.

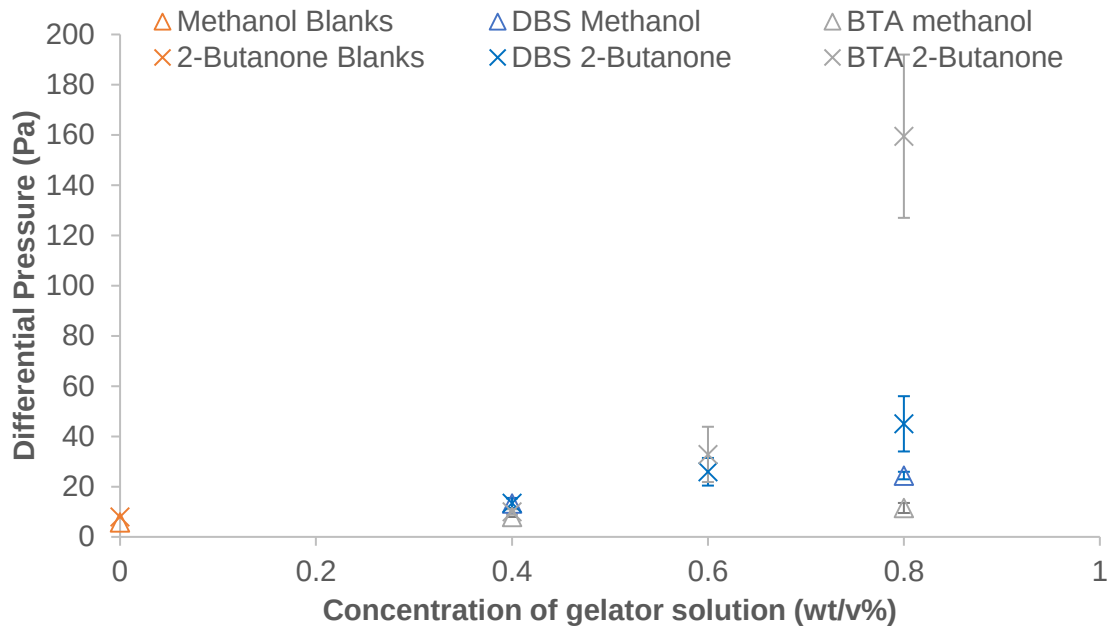

Figure 3-13. Graph of differential pressure against concentration of gelator solution.

The filtration efficiency results from Figure 3-14, suggest that as BTA is loaded into the fabrics, there is improved filtration efficiency as long as the system is loaded in 2-butanone and not methanol. This supports the observations with the two different morphologies seen with BTA when loaded from these two solvents. This also agrees with the results of Schmidt *et al.*[415] and might suggest that BTA nanofibres are more effective as filtration media than DBS. However, it should be noted that the error bars are still large and the overall filtration efficiency is not really any better than when using DBS. Nonetheless, this 2-butanone result hints that BTA can improve filtration efficiency under these conditions. However, the presence of BTA nanofibres in 2-butanone does not improve the system much beyond blank fabric in methanol. One of the issues is that, even as blanks, these fabrics are quite effective filtration media for aerosol, so the chance of seeing an improvement caused by the nanofibres is relatively small.

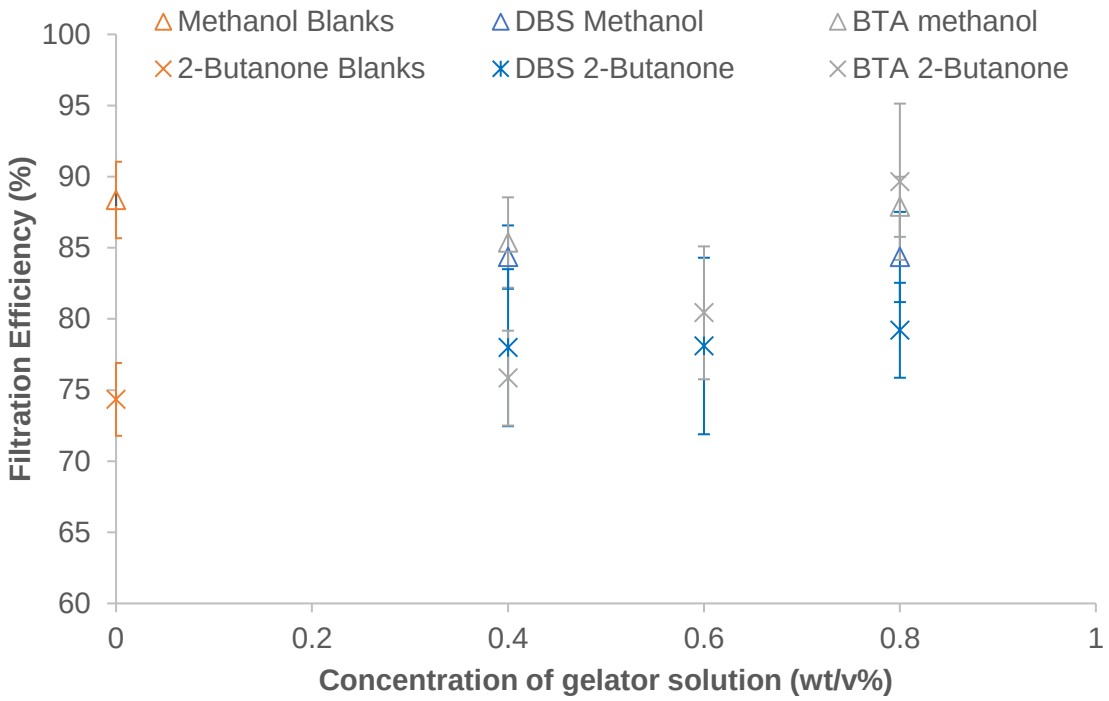

Figure 3-14. Graph of filtration efficiency of NaCl aerosol particles against concentration of gelator solution used to treat fabrics for DBS and BTA.

To get a more realistic picture of how these fabrics would perform in applications, where the air is not forced through the fabric but is worn by a soldier, samples were tested in a more realistic setting.

3.2.5 Aerosol Testing on BTA Prepared Fabrics

Fabrics were prepared and taken to Silsoe Spray Application Unit (SSAU) for testing. This allowed determination of the ability of aerosols to penetrate these modified fabrics. Testing was performed as described in Chapter 2.

When the tubes were removed from the wind tunnel at the end of the test, there was a distinct difference between the two fabrics as shown in Figure 3-15. The “blank” fabrics that hadn’t been treated with gelator, were noticeably orange compared to the treated fabrics, implying that there is significantly more trapped fluorescein in the untreated fabric. This particular example is 1 wt/v% BTA, which demonstrated one of the largest colour differences between the treated and untreated fabric. SEM images of 1 wt/v% BTA and DBS are shown in Figure 3-5. As a reminder, the DBS nanofibres formed are *ca.* 30x smaller in diameterthan the BTA nanofibres in 2-butanone (15 nm *vs. ca.* 450 nm).

Figure 3-15. Fabrics after the fluorescein aerosol testing; left = "blank", right = 1 wt/v% BTA.

After removal from the tunnel, the tapes behind the fabric were analysed to calculate the amount of fluorescein which had come through the fabric to be deposited on the tapes underneath. Figure 3-16 presents the amount of fluorescein deposited on the tapes against gelator loading. The treated fabrics gave much lower fluorescein deposition on the tapes than the blank fabrics. There is a 33% decrease in deposition of fluorescein from the blank sample to 0.2 wt/v% DBS. As the concentration of gelator was increased, the deposition of fluorescein further decreased, meaning an additional improvement in the filtration property. The DBS and BTA fabrics perform very similarly, suggesting that these gelators might be interchangeable (at least in terms of filtration of dried aerosol of *ca.* 2 nm).

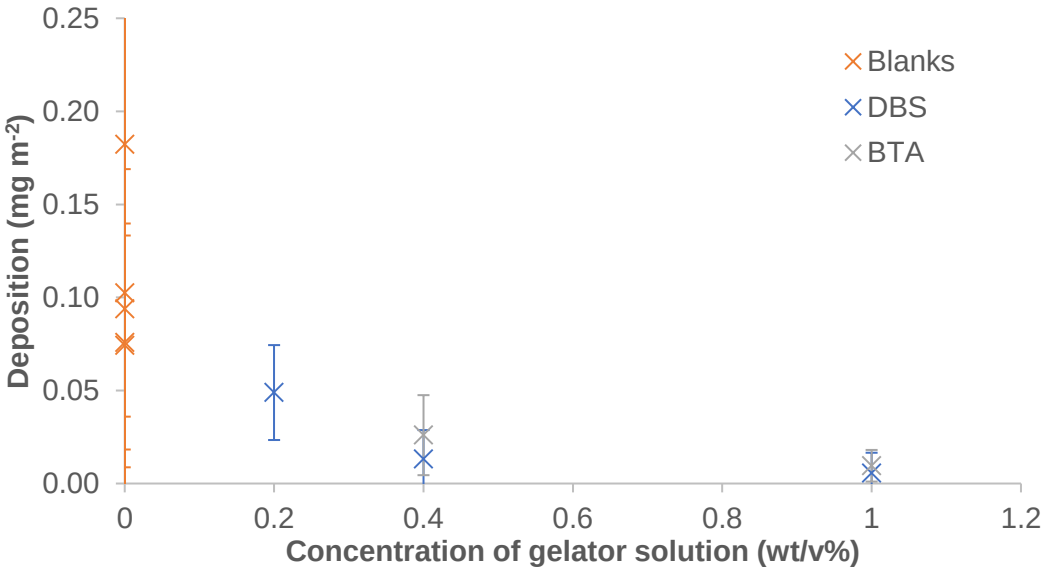

Figure 3-16. Graph of deposition of fluorescein against concentration of gelator solution used to treat the fabrics for DBS and BTA in 2-butanone.

Due to the distinct colour differences in the fabrics seen in Figure 3-15, the amount of fluorescein deposited on the fabric was also analysed by the same method as the tapes; i.e. a circle was punched out of the fabric of a set size, washed with 0.01 M NaOH, then an aliquot tested in the fluorimeter. However, unlike the tapes, the fabric was insoluble. Not all of the fluorescein was extracted during the washing process, so the results are approximate, though they do follow the visual trend (Table 3-1).

Table 3-1. Deposition of fluorescein on the fabrics themselves for blanks and corresponding gelator concentration for DBS and BTA.

Concentration of gelator (wt/v%) used in each run / Deposition (mg m^{-2})		**DBS 1%**	**DBS 0.4%**	**DBS 0.2%**	**BTA 1%**	**BTA 0.4%**
Fabrics	**Untreated**	2.73	4.01	3.01	4.83	4.78
	Treated	0.77	2.29	4.14	0.47	2.83

The results from the washing of fabrics follow the visual trend; the untreated fabrics were more orange and therefore contained more fluorescein, except in the case of DBS 0.2 wt/v%. With increased gelator concentration, the fabrics contained less fluorescein (they also looked whiter). Again, the results of DBS and BTA are very similar. As described in Chapter 2, there is a relationship between filtration and air permeability. It can be proposed that the mechanism of filtration is preventing air passage under wind conditions and hence providing protection.

3.3 Conclusions

BTA has been shown in the literature to act as a secondary network to enhance filtration across a range of particle sizes.[415, 417] During all fabric testing (air permeability testing, water vapour permeability testing, fluorescein filtration and filtration efficiency testing) BTA has shown comparable results to our other gelator, DBS. This implies that DBS should be able to be used as a commercial alternative to BTA to enhance filtration. However, notably DBS has much smaller nanofibre diameters (15 nm) than BTA (*ca.* 450 nm) and this will yield much larger relative surface areas. Furthermore, the DBS morphologies appeared to show less damage after sample testing, which suggests they may be more stable/robust. In particular, the DBS nanofibres appeared to have greater stability to water vapour which is of key importance in clothing applications. As such, it is suggested that DBS may offer advantages over BTA as a result of its broader solvent tolerance and its very different nanoscale dimensions.

Chapter 4 - Mixtures of 1,3:2,4-Dibenzylidene-D-sorbitol and *N,N',N"*-Tris(2-ethylhexyl)-1,3,5-benzenetricarboxamide (BTA) for Fabric Modification

4.1 Introduction to Two Component Gel Mixtures

There are precedents in the literature of creating hybrid gels, combining two systems in an attempt to harness the advantages of both materials.[281] In a number of cases, polymer gels have been combined with supramolecular gels to combine the tuneability of supramolecular gels with the robustness of the polymer gels.[57-59] Two supramolecular components have also been successfully combined.[287-294] As discussed in Chapter 1, there are multiple ways in which a two gelator component system can combine: co-assembly, self-sorting or disruption. Different combinations of gelators have demonstrated all of the scenarios.[286] The similarity of the structures is likely to influence the outcome, different structural motifs may encourage self-sorting, whereas similar structures may encourage co-assembly.[281] The properties of two component systems can often be tailored by tuning the ratio of components.[32, 294]

4.2 Combining DBS and BTA Initial Investigation

Following the precedent in the literature for combination of hybrid systems, it was of significant interest to investigate the combination of DBS and BTA, particularly as these two LMWGs operate on such significantly different length scales in terms of their nanofibre assemblies. The proposed benefit was to try to create a novel two component gelling network, with the potential to self-sort and generate two different size networks. This may then offer advantages when applied in fabric.

4.2.1 Rheology of Mixtures with One Gelator Varied

To gain initial insight into network formation in mixed DBS/BTA samples, it was decided to perform rheology in order to understand the macroscopic behaviour of materials comprised of mixtures compared with the two components individually.

All gels were formed in glass vials then moved onto the rheology plate. BTA presented as a very weak gel in 2-butanone and had a MGC in methanol of >3 wt/v%, so rheology could not be performed with 100% BTA. For example, even 1 wt/v% BTA in 2-butanone does not show the characteristic G'>>G", meaning that it is in fact not a true gel under oscillating stress. For this study, therefore, a constant concentration of DBS to maintain gel-phase behaviour was used and increasing amounts of BTA were added.

From Figure 4-1, the G' value appears to decrease from no BTA to the inclusion of 0.1 wt/v% BTA, which is just noise associated with the loading technique. The G' value of 0.6 wt/v% DBS gels appears reasonably constant at low loadings of BTA both in 2-butanone and methanol. Once 0.7 wt/v% BTA is present in methanol, however, the G' significantly increases. This is particularly interesting as this is below the minimum gelation concentration for BTA in methanol (3 wt/v%), so a sample-spanning BTA gel network would not necessarily be expected. It could be postulated therefore that some self-assembly of BTA is taking place which increases network stiffness. In 2-butanone, there is a significant increase in G' at 0.9 wt/v% BTA. Notably, in 2-butanone, the MGC is 0.7 wt/v%, therefore, this large increase in G' (gel natural stiffness) would suggest that a sample spanning BTA network is present. This would explain why at 0.9 wt/v% BTA, the G' in 2-butanone exceeds that in methanol. Interestingly, the increase of G' in 2-butanone induced by BTA is greater than expected based on the very weak gel, formed by this system. This may suggest some synergistic advantage of combining the two gelators. Two gel networks would be expected to be stiffer than a single gel network hence the significant increase in G'.

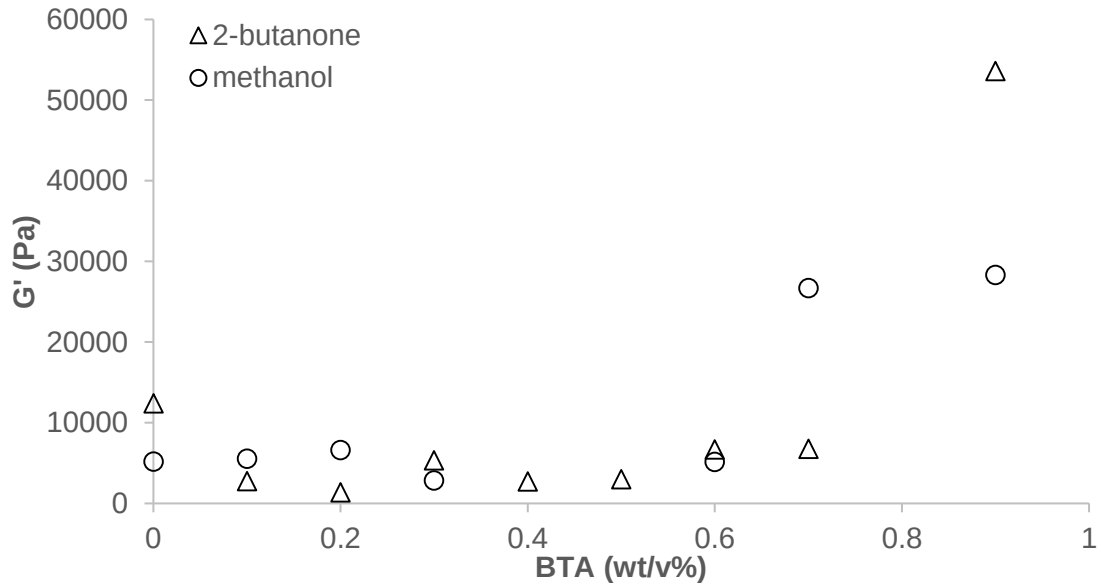

Figure 4-1. G' from frequency sweeps of mixtures with 0.6 wt/v% DBS and a varying concentration of BTA in both methanol and 2-butanone.

The T_{gel} values of varying BTA concentrations in the presence of 0.6 wt/v% DBS from Table 4-1 show very little deviation across the concentrations investigated. This trend supports the rheological results which demonstrated that across the same range of concentrations the samples had approximately the same G' up to 0.7 wt/v% BTA. It

also supports the negligible difference between the two different solvent systems. The significant increase in G' value by 0.9 wt/v% BTA might suggest a difference in T_{gel} value, but this is not seen. This suggests that the difference in network stiffness is not affecting the thermal stability of the gel formed. Overall this suggests that the 0.6 wt/v% DBS is controlling the thermal stability of the hybrid gel.

Table 4-1. T_{gel} values of 0.6 wt/v% DBS with a range of concentrations of BTA to support rheology in 2-butanone and methanol.

DBS concentration (wt/v%)	BTA concentration (wt/v%)	2-butanone T_{gel} (°C)	Methanol T_{gel} (°C)
0.6	0.1	40	40
0.6	0.2	40	40
0.6	0.3	41	42
0.6	0.4	39.5	40
0.6	0.5	39.5	40
0.6	0.6	41	41
0.6	0.7	39	42.5
0.6	0.9	41.5	42.5

The gelation of DBS is clearly dominating the behaviour of these mixtures, providing the gel stability. To investigate whether BTA does form nanofibres < 0.7 wt/v% in methanol, a sample was prepared using 0.6 wt/v% BTA in methanol on the surface of an SEM stub. The nanofibres produced can be seen in Figure 4-2. This demonstrates that nanofibres will form upon drying solutions of BTA at concentrations even below the MGC. Presumably assembly occurs as the solvent evaporates and the effective concentration increases.

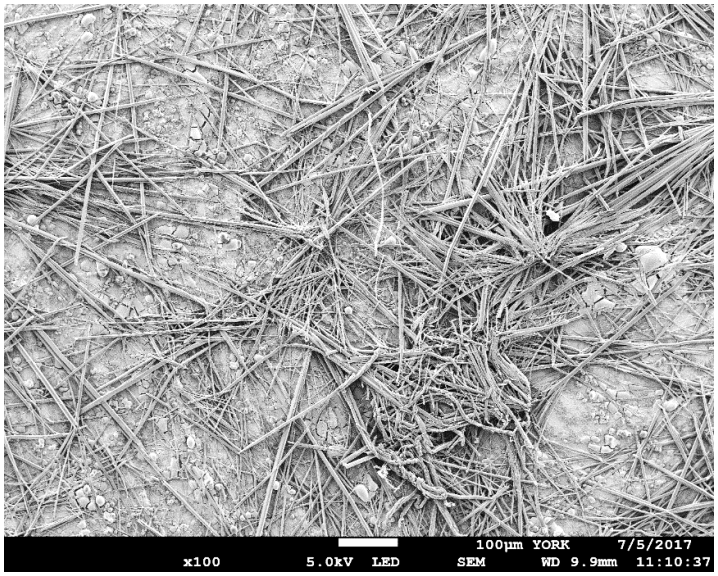

Figure 4-2. SEM image of 0.6 wt/v% BTA dried from methanol on an SEM stub.

It was also observed that maintaining the concentration of DBS and varying the concentration of BTA has little effect until significant loadings of BTA were reached. The concentration of both gelators were then varied simultaneously, giving an overall constant total loading. These results supported the previous conclusions, that 2-butanone produces stiffer gels than methanol and that the presence of BTA stiffens the DBS gel.

4.2.2 NMR Study of Two Component Network

In terms of understanding the role of these two gelators and to gain further insight into self-assembly, NMR spectra were recorded of both gelators individually at 0.6 wt/v% in deuterated methanol with DMSO as an internal standard at 24 and 72 hours. There was no change between the two time points, implying that all self-assembly occurred in the first 24 hours, with no significant changes in the following 48 hours. Resonances corresponding to the gelator were observed in both spectra, implying that not all of the gelator was in an immobile self-assembled structure but that some was also in the mobile liquid-like phase (Figure 4-3). By comparing the integrations of the DBS aromatic peaks to the known amount of DMSO, it was calculated that approximately 48% of the available DBS present is seen via NMR spectroscopy, hence 52% can be assumed to be assembled into ‘solid-like’ nanofibres under these conditions.

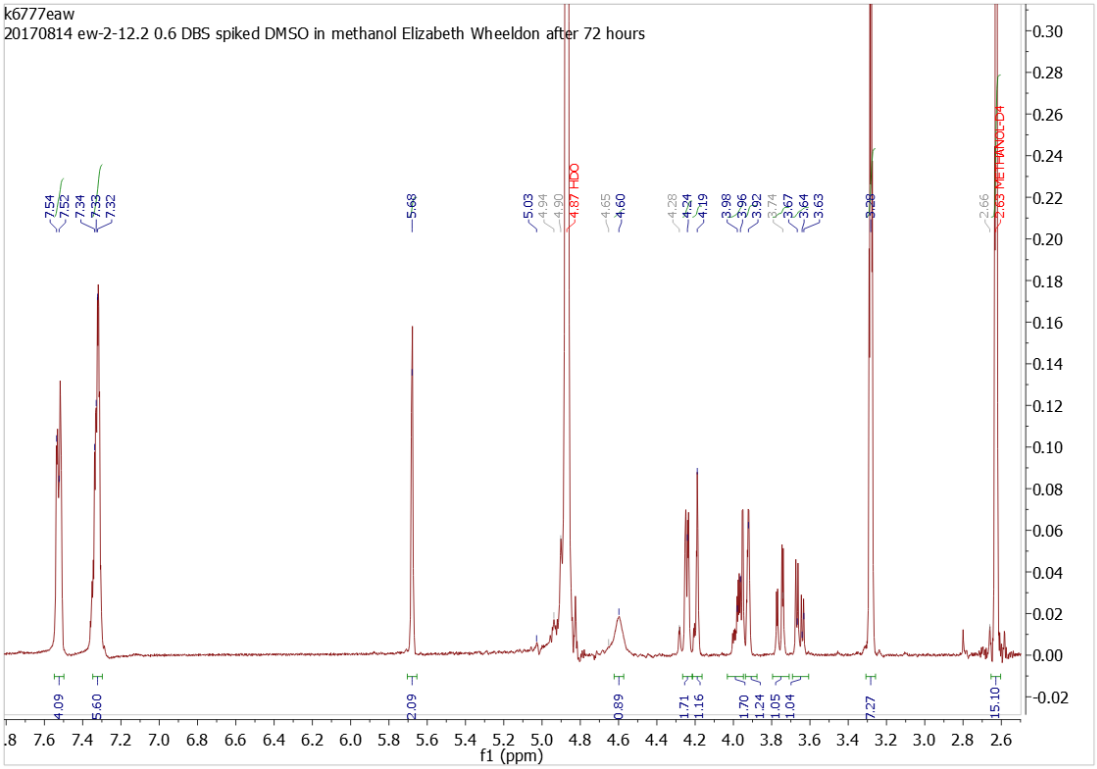

Figure 4-3. 0.6 wt/v% DBS in deuterated methanol spiked with DMSO.

For BTA, comparing the integrations of the BTA aromatic proton resonances to the known amount of DMSO used to spike the NMR, it was calculated that approximately 34% of the BTA present is visible in the NMR spectra, hence 66% can be considered NMR invisible while assembled into ‘solid-like’ structures.

A mixture of 0.6 wt/v% DBS and 0.6 wt/v% BTA in deuterated methanol spiked with DMSO was then investigated at the two time points. Again, little change was observed between the two time points, implying that whatever network had formed, had occurred fully during the first 24 hours (Figure 4-4).

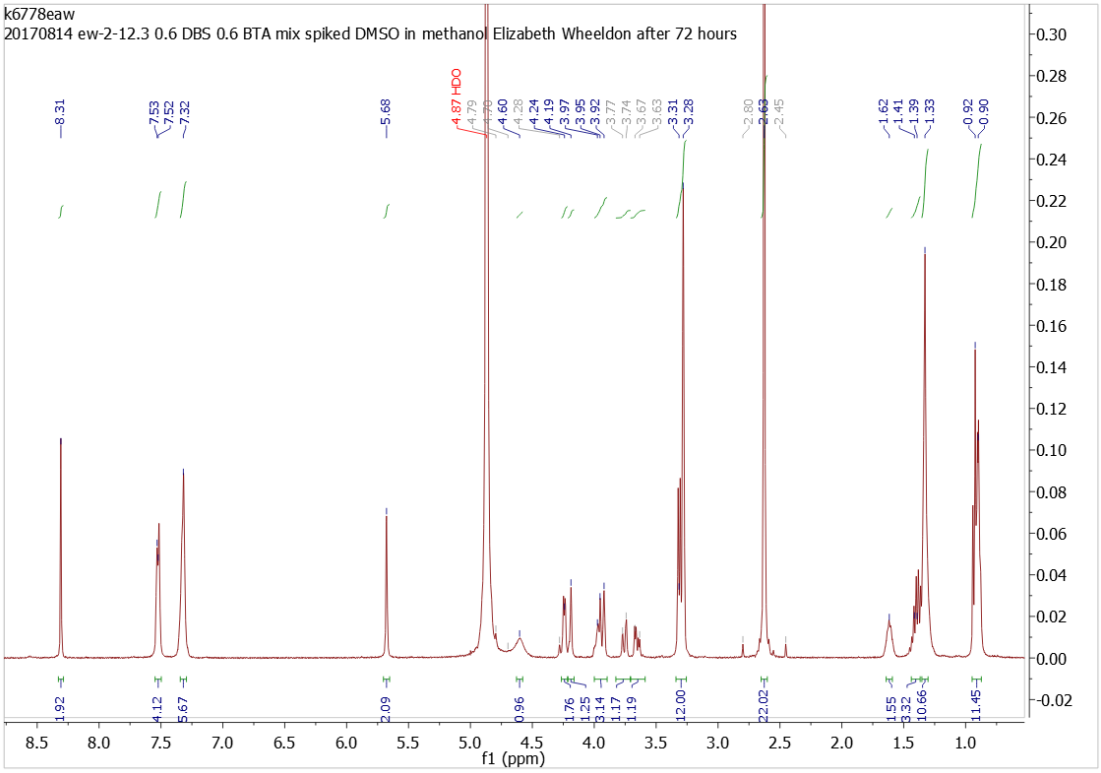

Figure 4-4. 0.6 wt/v% BTA 0.6 wt/v% DBS in deuterated methanol spiked with DMSO.

The mixed system gave an NMR spectrum which very closely matched the individual spectra for DBS and BTA. No proton resonances were shifted which suggests that the two gelators do not form specific interactions with one another. By comparing the integrations of the DBS and BTA aromatic proton resonances to the known amount of DMSO used to spike the NMR sample, it was possible to calculate that approximately 33% of the DBS and 34% of the BTA are visible in the NMR spectrum, meaning that 67% and 66%, respectively, are self-assembled into a ‘solid-like’ state. This is broadly similar to the individually investigated gelators. Overall this spectroscopic data strongly supports the view that these gelators can self-sort. Both DBS and BTA exhibit some

assembly under these conditions and their combination does not appear to significantly affect this under these conditions.

4.2.3 SEM Images of 0.6 wt/v% DBS and 0.6 wt/v% BTA

On the basis of the NMR spectroscopic investigation, a loading of 0.6 wt/v% DBS and 0.6 wt/v% BTA in methanol, dried on an SEM stub was examined. At this concentration in methanol, when investigated individually, BTA nanofibres had diameters of *ca.* 700 nm and DBS nanofibres were *ca.* 15 nm (see Section 3.1.2 and Section 2.8).

As can be seen from Figure 4-5, the two gelators self-sort beautifully into nanofibres on the two different length scales: the larger 700 nm nanofibres are comprised of BTA and the much smaller 15 nm nanofibre assembles from DBS. This would imply that the two systems are completely self-sorting, there is no evidence to imply that the two structures interact with one another. The lack of robustness, brought about by the non-covalent interactions, can be seen in both images as the smaller DBS nanofibres appear to rupture or tear alongside the larger BTA nanofibres, probably a drying effect.

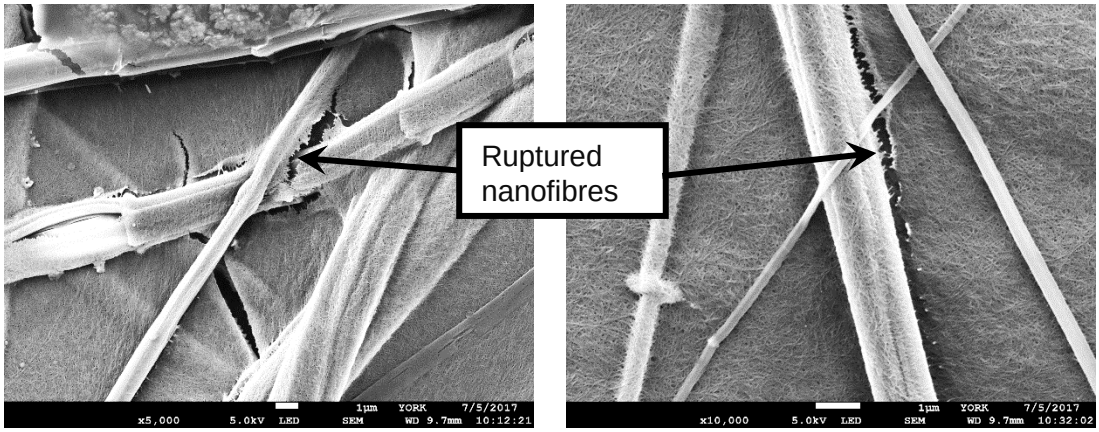

Figure 4-5. SEM images of 0.6 wt/v% DBS and 0.6 wt/v% BTA in methanol on an SEM stub at x5000 and x10000 magnification, scale bars of 1 µm.

Changing the solvent from methanol to 2-butanone resulted in quite a significant change in nanoscale morphology. SEM imaging of 0.6 wt/v% DBS and 0.6 wt/v% BTA in 2-butanone showed similar self-sorting but the BTA nanofibres appeared to have much smaller diameters. This is to be expected as it was demonstrated in Chapter 3 (Section 3.1.2) that the fibre diameter of BTA is largely solvent dependent. As demonstrated by Figure 4-6, BTA forms nanofibres with diameters of *ca.* 450 nm in 2-butanone, while DBS forms nanofibres *ca.* 15 nm in diameter. The two different size scales can clearly be distinguished. When methanol was used as a solvent, there didn't appear to be any interaction between the two different structures, making them truly

self-sorting. The SEM image of this dual gelator system in 2-butanone looks quite different to the same system in methanol. It could be suggested this may result from differences in the MGC. Both gelators are at or above their MGC concentrations in 2-butanone but only DBS is above its MGC in methanol.

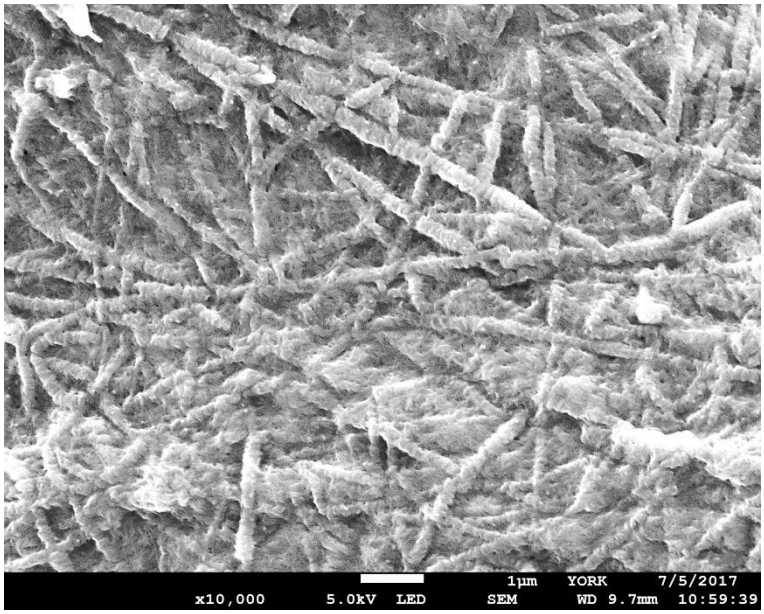

Figure 4-6. SEM image of 0.6 wt/v% DBS 0.6 wt/v% BTA in 2-butanone on an SEM stub at x10000 magnification with scale bar of 1 µm.

Overall, however, both solvents at this concentration showed clear self-sorting of the two gelators into nanofibres with two different length scales. This is consistent with the NMR which indicated molecular-scale self-sorting and the rheology which indicated a macroscopically reinforced and stiffer dual network was present. On a molecular scale, it is perhaps not surprising that DBS and BTA can self-sort. DBS assembles through hydrogen bonds and π-π stacking, as does BTA. However, both gelators have very different molecular shapes (Figure 4-7). DBS is butterfly shaped whereas BTA is flat and circular. For effective stacking, it therefore seems likely that self-complementary interactions will be thermodynamically preferred, which would lead to a self-sorted system.

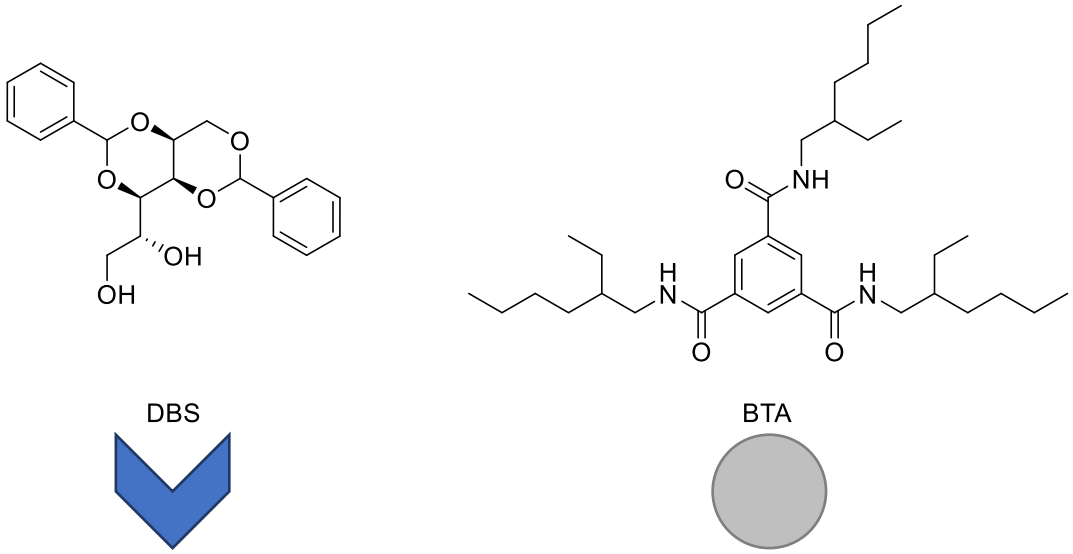

Figure 4-7. Chemical structure of both DBS and BTA gelators and their molecular shapes.

4.2.4 SEM Images of Non-Woven Fabric Prepared with 0.6 wt/v% DBS and 0.6 wt/v% BTA

This self-sorted dual-assembly system was used to treat fabric. For reference, the individual gelators in fabric are shown below at 0.6 wt/v% in both methanol and 2-butanone. It is clear from Figure 4-8 that both gelator and solvent have a significant impact on morphology. As discussed in previous chapters, BTA forms much larger nanofibres than DBS regardless of the solvent used. Using 0.6 wt/v% BTA in 2-butanone gave larger diameter, longer, more dispersed aggregates compared to DBS in 2-butanone. It was reasoned that these BTA aggregates could potentially give the DBS nanofibres more support and structure to form around.

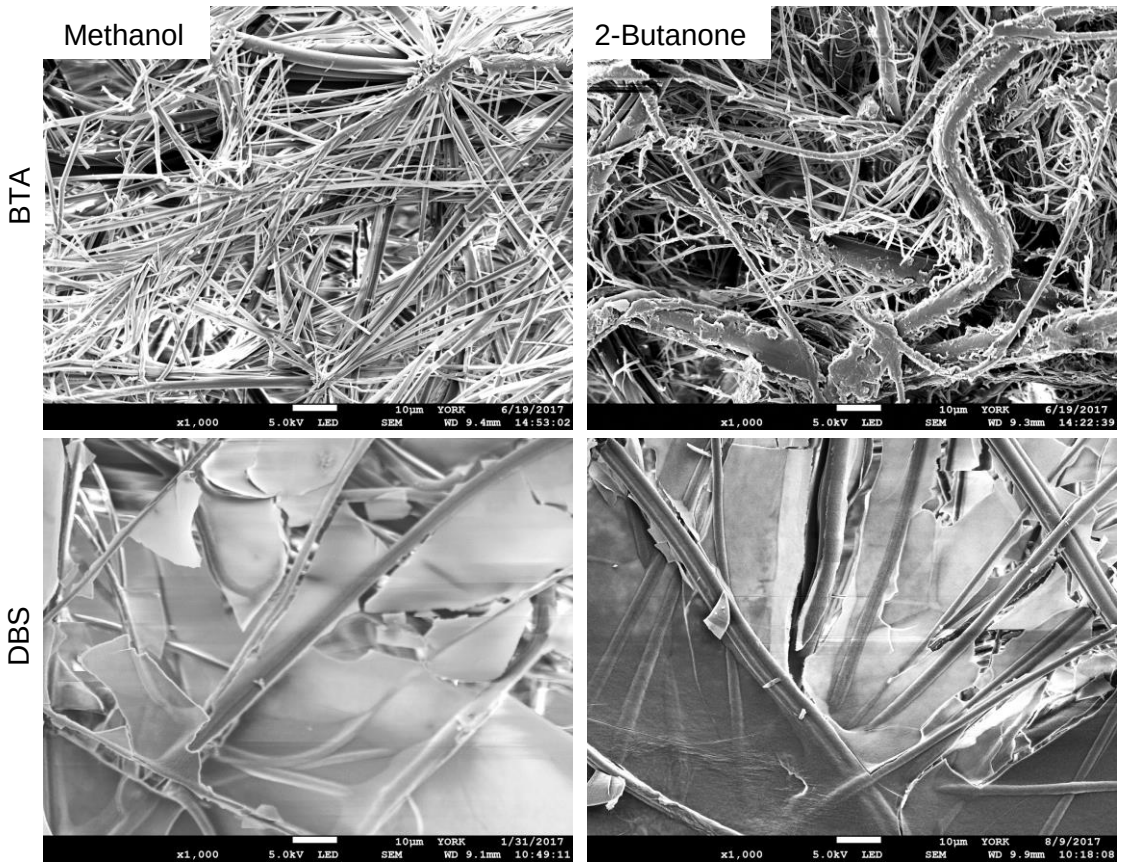

Figure 4-8. SEM images of 0.6 wt/v% of BTA and DBS individually in methanol and 2-butanone prepared on a non-woven fabric at x1000 magnification with scale bars of 10 µm.

The dual gelator methodology was then used in conjunction with the non-woven fabric to see if the fabric would disrupt the gelation of either system or significantly alter the observed nanoscale morphology.

The fabric prepared using methanol as solvent appeared as expected, just like the morphology seen on the SEM stub with the addition of fabric fibres. Three completely different length scales can be seen; fabric fibres (*ca.* 1 µm), BTA fibres (*ca.* 700 nm) and DBS nanofibres (*ca.* 15 nm). This is a rare example of a system in which 3 different fibrillar structures are independently present and demonstrates elegantly how self-assembly approaches can add to the complexity of fabrics.

From the low magnification image in Figure 4-9, the methanol mixture provides apparently uniform regular coverage with minimal gaps between different types of fibres. This could be very useful in terms of application due to the regularity of coverage and the multiple different scales of fibres present.

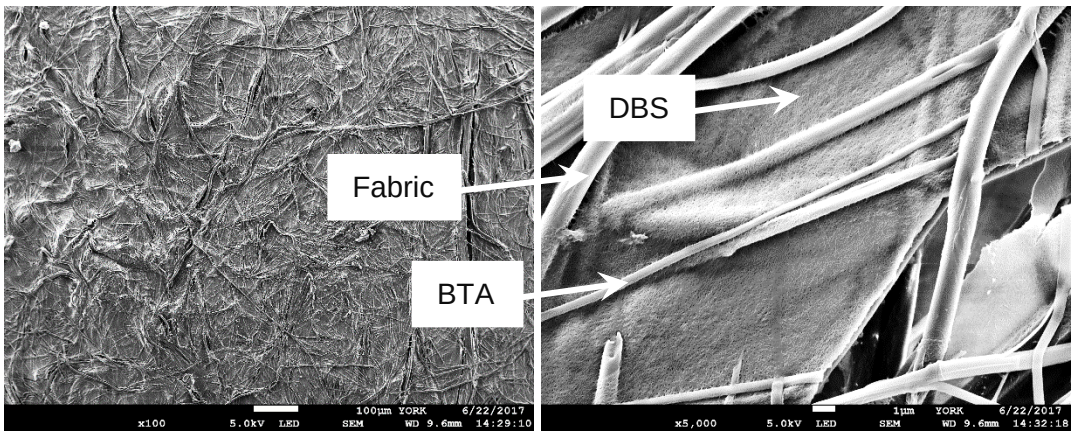

Figure 4-9. SEM images of non-woven fabric prepared with 0.6 wt/v% DBS and 0.6 wt/v% BTA in methanol at x100 and x5000 magnification, scale bars of 100 µm and 1 µm, respectively.

This dual component system was also tested using 2-butanone as a solvent. In the areas of the sample which showed even, uniform coverage (such as Figure 4-10 uniform coverage) it is easy to spot the three different scales; fabric fibres, BTA nanofibres and DBS nanofibres. The three sizes are easily distinguishable and the morphology of the self-sorting DBS and BTA system is very similar to that seen when the fabric was absent. The areas of more segmented coverage (as shown by Figure 4-10 segmented coverage) still demonstrated the three different morphologies but the aggregates look slightly different. In terms of application, it would be ideal if uniform coverage could be achieved across the whole sample. The inconsistencies demonstrated here using 2-butanone, raise questions about scale-up for application. The inconsistencies in the sample could allow penetration of CWAs through the fabric and thereby offering no protection. This system with a total loading of 1.2 wt/v% seemed to considerably affect the properties of the fabric, it became much stiffer to handle and lost some of its flexibility from the rigidity brought by the two gel networks formed within. For application, lower concentrations are therefore likely to be more interesting in terms of the end goal of maintaining the intrinsic fabric properties.

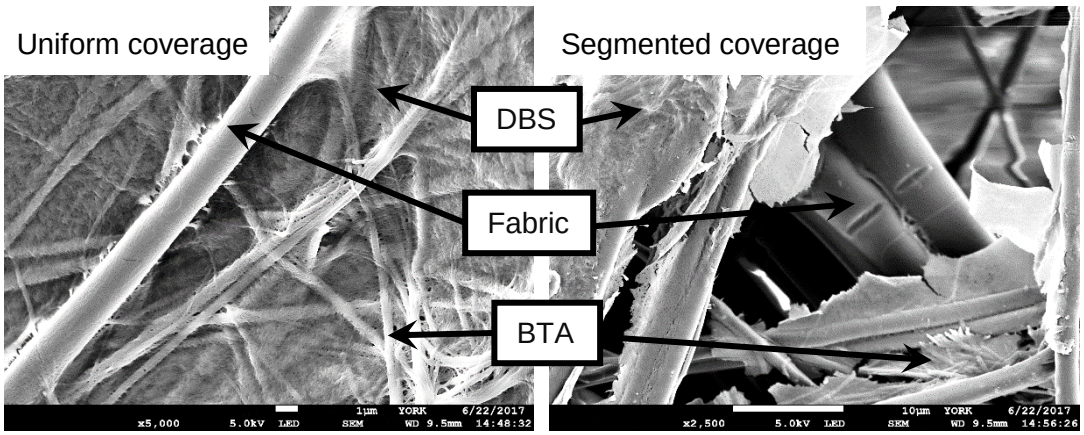

Figure 4-10. SEM images of non-woven fabric prepared with 0.6 wt/v% DBS and 0.6 wt/v% BTA in 2-butanone, at x5000 and x2500 magnification with scale bars of 1 µm and 10 µm, respectively.

Nonetheless, this is the first time that self-sorting of two gelators has been demonstrated within a fabric to give three different independent fibrillar objects, on three different length scales, simultaneously in the same material.

4.3 Total Loading of 0.6 wt/v% DBS and BTA Mixtures for Fabric Modification

With the long-term application in mind, it was important to minimise the concentration used. Mixtures with a total loading of 0.6 wt/v% were therefore investigated. The concentrations of the two components were also varied simultaneously to see if more uniform coverage across the whole scope of the sample could be achieved and to investigate how the morphology would change.

4.3.1 SEM Images of 0.6 wt/v% Mixtures of DBS and BTA

Using a mixture of 0.3 wt/v% BTA and 0.3 wt/v% DBS from both methanol and 2-butanone on a non-woven fabric achieves a good level of coverage as seen in Figure 4-11. Both samples also show the two distinctly sized nanofibres formed by DBS and BTA as previously discussed. As expected, BTA in methanol appears to have formed longer, more spread out nanofibres that support the aggregation of DBS nanofibres leading to a more uniform distribution across the fabric. This is therefore very promising in terms of application of self-assembling nanostructure to the fabric at practically useful loadings.

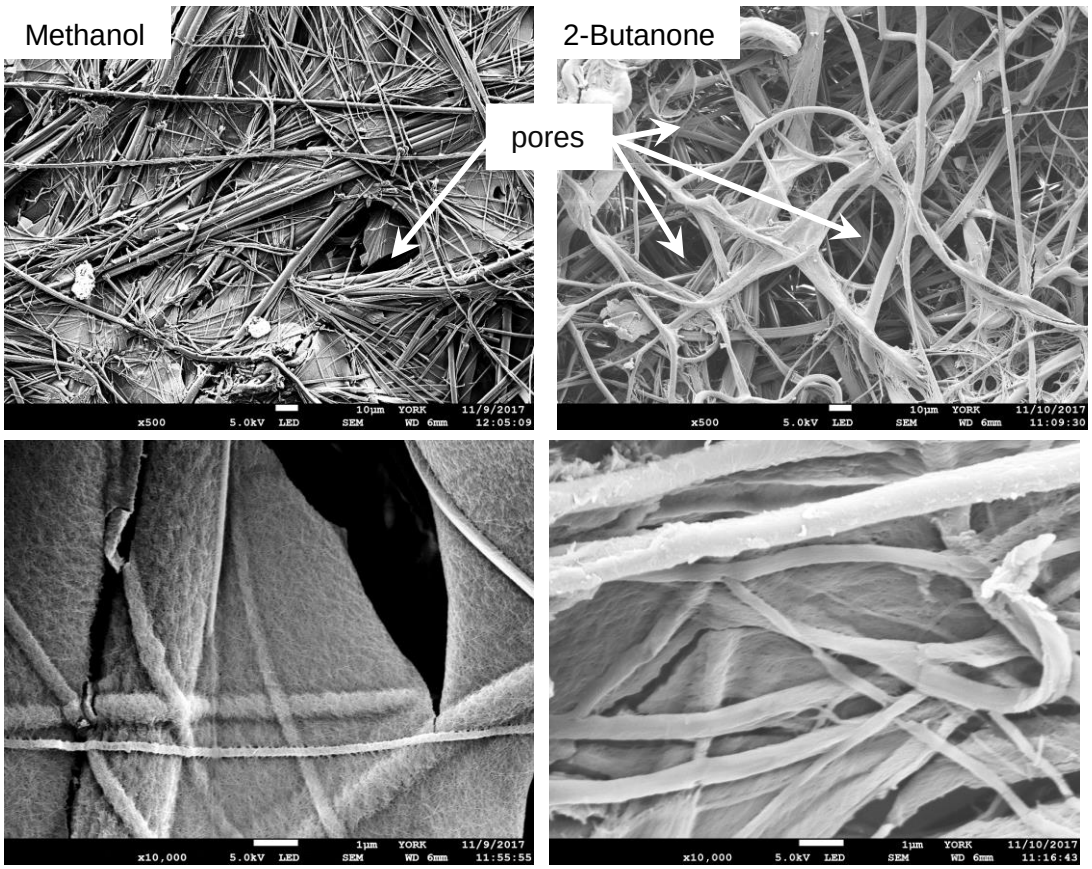

Figure 4-11. SEM images of 0.3 wt/v% BTA 0.3 wt/v% DBS in a non-woven fabric prepared from methanol and 2-butanone at x500 magnification with scale bars of 10 µm, followed by x10000 with scale bars of 1 µm.

In methanol, the loading of DBS was then increased and the loading of BTA decreased to compensate, to keep a constant total loading. Generally, the two morphologies formed appear very similar as can be seen in Figure 4-12. All systems contain two different sized nanofibres. As expected, the higher loading of DBS results in increased deposition of DBS nanofibres coating the BTA nanofibres, making the surface appear smoother. The decreased loading of BTA led to a reduction in the number of BTA nanofibres being observed. Samples prepared with 0.4 wt/v% DBS and 0.2 wt/v% BTA appeared very similar irrespective of solvent. Given the excellent fabric coverage observed with these mixed systems, they were scaled up and tested for air permeability.

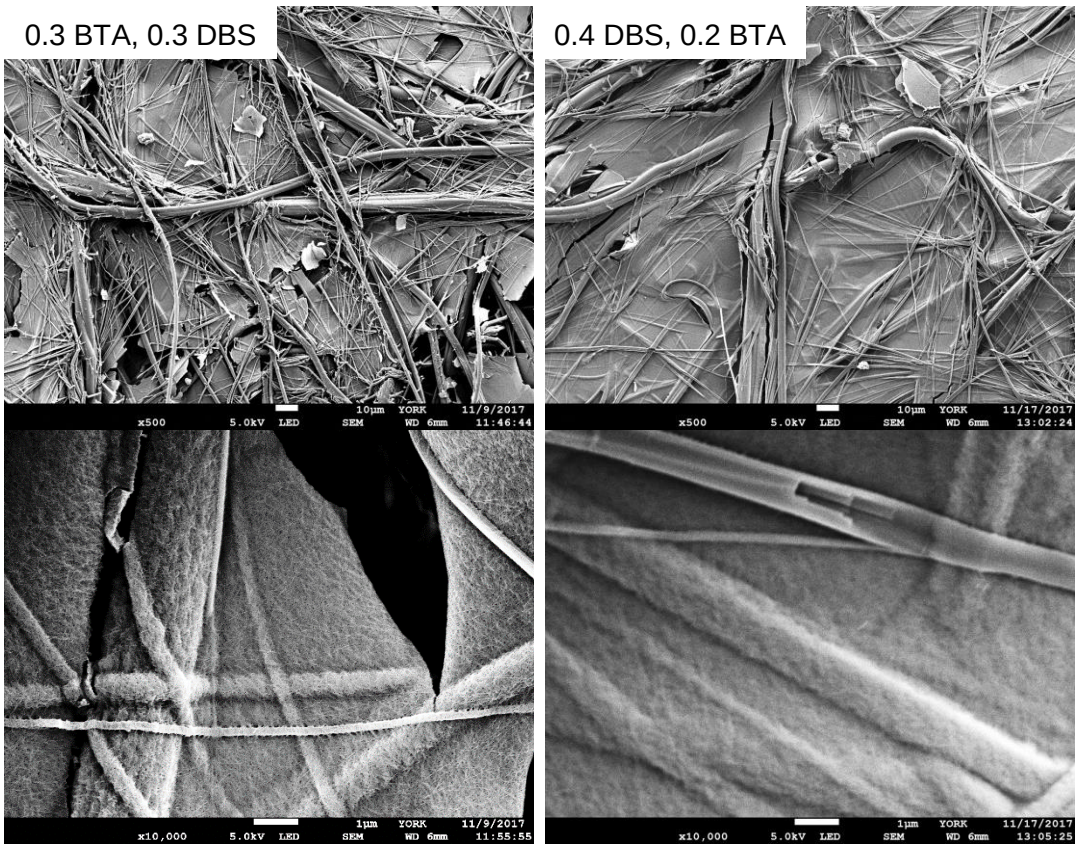

Figure 4-12. SEM images of 0.3 wt/v% BTA 0.3 wt/v% DBS and 0.4 wt/v% DBS and 0.2 wt/v% BTA in a non-woven fabric prepared from methanol at x500 magnification with scale bars of 10 µm, followed by x10000 with scale bars of 1 µm.

4.3.2 Air Permeability Testing of 0.6 wt/v% Total Loading

The air permeability for the system formed using a total combined loading of 0.6 wt/v% is shown in Figure 4-13. Fabrics prepared using 2-butanone gave higher air permeabilities than those with methanol. Using 2-butanone, the mixtures generally gave higher air permeabilities than the individual gelators, implying that this dual system minimises the effect on the intrinsic properties of the fabric.

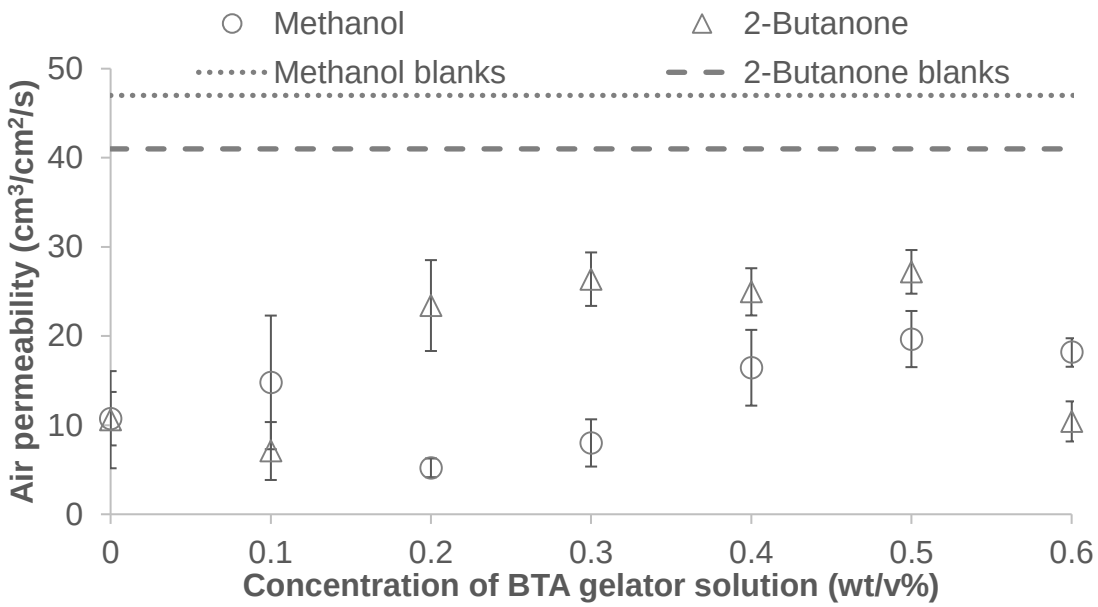

Figure 4-13. Air permeability of samples prepared with 0.6 wt/v% total concentration of gelators (with 0 wt/v% BTA = 0.6 wt/v% DBS and *vice versa*).

All the treated fabrics tested were at a lower air permeability than the blank fabrics. The difference in air permeability between the two solvent systems appears significant as it is outside the reported errors. It could be that the two different solvents "swell" the fabric different amounts but repeated testing of blank fabrics soaked in the corresponding solvents demonstrated this is not the case (Figure 4-14). Therefore the solvents cannot be swelling the non-woven itself. However, it can be clearly seen that the presence of self-assembled nanofibres significantly lowers the air permeability compared with blank solvents.

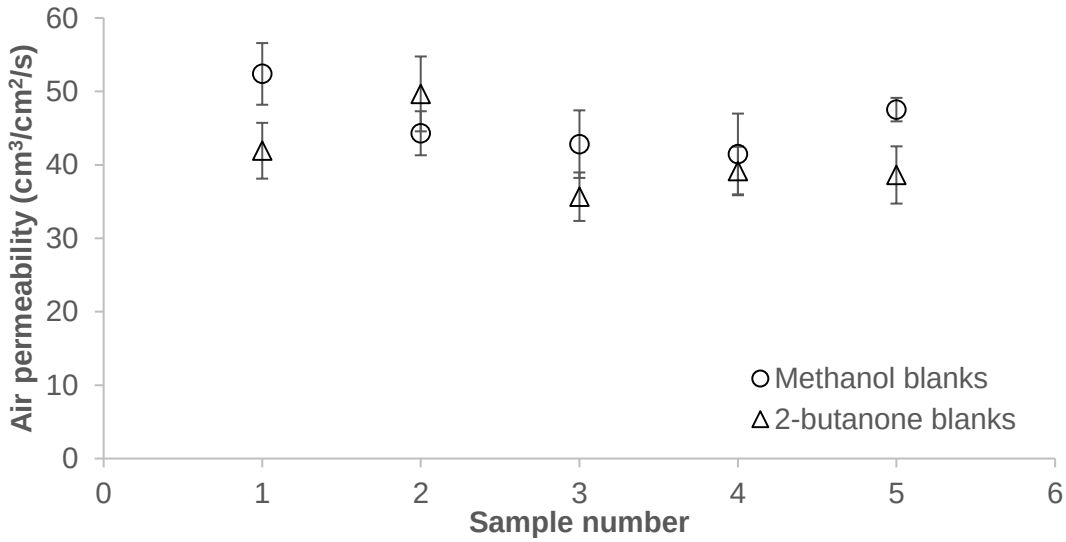

Figure 4-14. Multiple blank fabrics soaked in the corresponding solvent.

This implies that any changes seen in the differences in air permeability of the same mixtures in different solvents have to be as a result of the morphological change of the individual gelators as caused by the solvent. This is supported by the different morphologies formed from the two different solvents as supported by Figure 4-11, which shows that 2-butanone resulted in more pores or gaps, creating less resistance to air flow hence the higher air permeability.

4.3.3 Post Air Permeability SEM Imaging

It is important to be aware of the limitations of supramolecular nanofibres, particularly their limited robustness. As discussed previously in Chapters 2 and 3, DBS nanofibres were able to withstand air permeability and water vapour permeability testing, whereas the BTA nanofibres, appeared unable to withstand the testing, perhaps as a result of their different nanoscale morphology.

As can be seen from Figure 4-15, there were no significant differences between the prepared fabric before and after air permeability testing. This is reminiscent of the results after air permeability testing with DBS from Chapter 2, where the testing appeared to have very little effect on the nanofibre network formed. The BTA nanofibres seemed to deform after air permeability testing in Chapter 3, so this might suggest that DBS is providing some additional support to the BTA nanofibres in the mixture system, enhancing the overall robustness of the nanofibre network to the testing conditions. This would be a significant advantage of applying a hybrid approach. Changing the solvent system did not result in any differences in the fabric after testing.

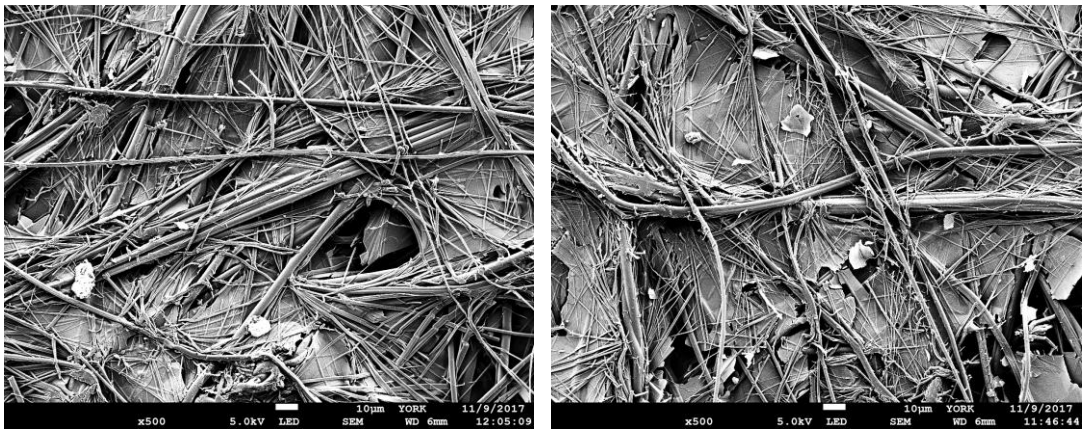

Figure 4-15. SEM images of 0.3 wt/v% DBS and 0.3 wt/v% BTA prepared in non-woven fabric using methanol before and after air permeability testing at x500 magnification with scale bars of 10 µm.

4.4 Total 0.4 wt/v% Loading of DBS and BTA Mixtures for Fabric Modification

In the interest of further efficiency for application, lower concentrations were also considered. Concentrations totalling 0.4 wt/v% were investigated across a range of stoichiometries.

4.4.1 SEM Images of 0.4 wt/v% Mixtures of DBS and BTA

A range of stoichiometries were imaged using SEM analysis. The amount of each individual gelator was varied from 100% of one gelator through to 100% of the other gelator. For reference, the 0.4 wt/v% DBS on a non-woven fabric had a morphology as shown in Figure 4-16.

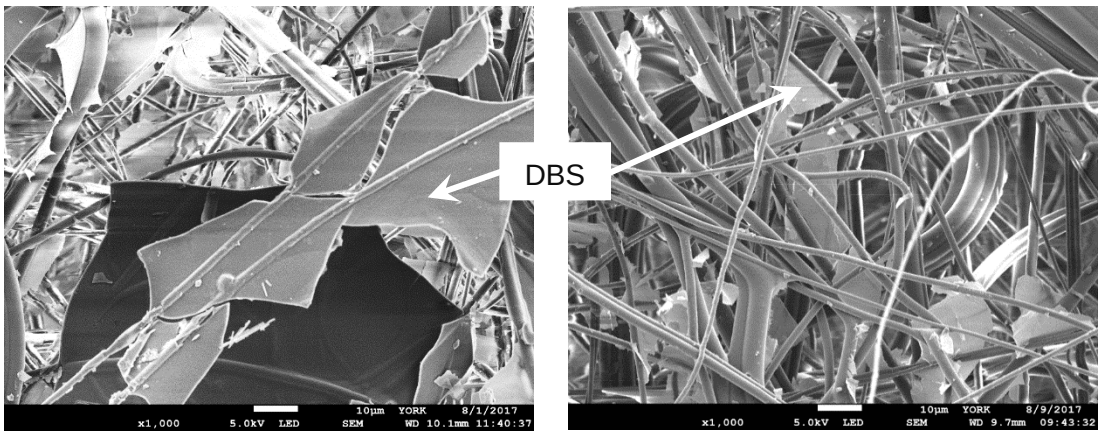

Figure 4-16. Reminder of SEM images of non-woven fabric prepared with 0.4 wt/v% DBS from methanol and 2-butanone at x1000 magnification with scale bars of 10 µm.

The large fibres from the non-woven fabric can be seen, as can large aggregated sheets of DBS (which contained lots of smaller DBS nanofibres of *ca.* 15 nm).

The concentration of DBS was reduced from 0.4 wt/v% to 0.3 wt/v% in the mixture, while the concentration of BTA was increased. Looking at the 0.3 wt/v% DBS and 0.1 wt/v% BTA mixture, there is a small, expected difference (Figure 4-17). The BTA nanofibres could be disrupting the DBS aggregates, potentially meaning that smaller “sheets” of DBS form (combined with the use of a lower concentration). However, both DBS aggregates and BTA nanofibres can be observed. The BTA nanofibres have the same size and shape, as those formed from the single gelator (Figure 4-18).

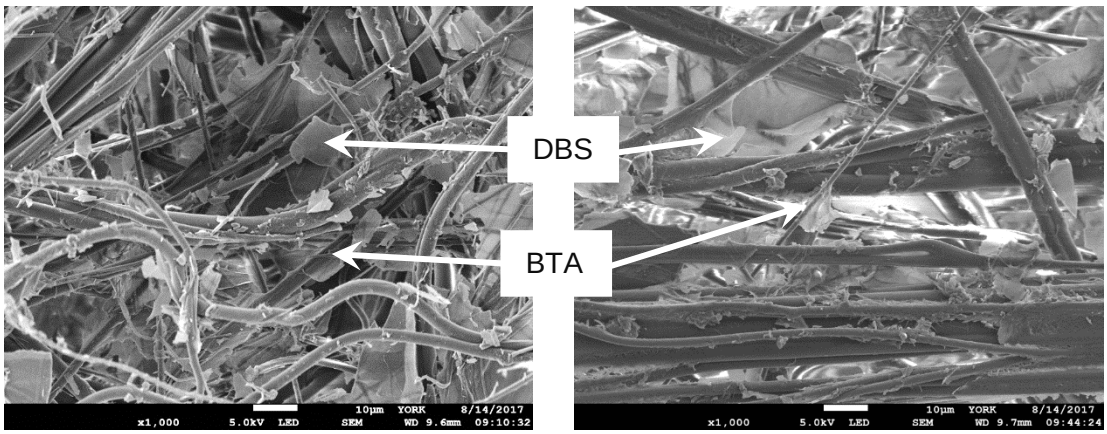

Figure 4-17. SEM images of non-woven fabric prepared with 0.3 wt/v% DBS 0.1 wt/v% BTA in methanol and 2-butanone at x1000 magnification with scale bars of 10 µm.

In Figure 4-18, with a single gelator, at 0.4 wt/v% BTA, it is quite difficult to distinguish BTA from the non-woven fabric in methanol. One can take an educated guess by selecting the slightly smaller fibres, but it is not definitive. It is far easier to see the BTA nanofibres in the fabric prepared from 2-butanone. Methanol appears to be the weaker system for long-term application, as the BTA doesn't span over the non-woven as it does in 2-butanone at these low concentrations.

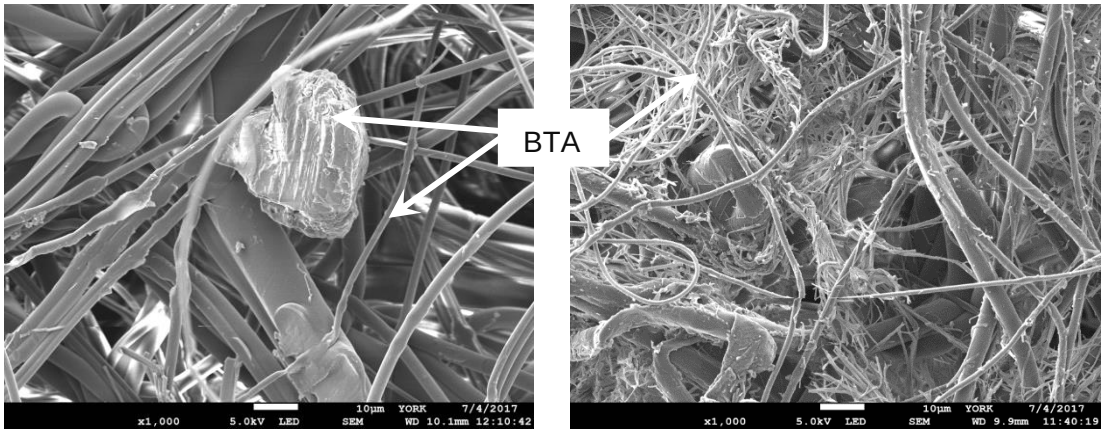

Figure 4-18. SEM images of non-woven fabric prepared with 0.4 wt/v% BTA in methanol and 2-butanone at x1000 magnification with scale bars of 10 µm.

As the concentration of DBS in the mixture of gelators is reduced and the concentration of BTA increased, the corresponding response in the sample supports the idea that the two gelators are genuinely self-sorting. As the loading of DBS is reduced, fewer DBS aggregates can be seen in the fabric, and more BTA nanofibres are observed with the increase of BTA loading (Figure 4-19).

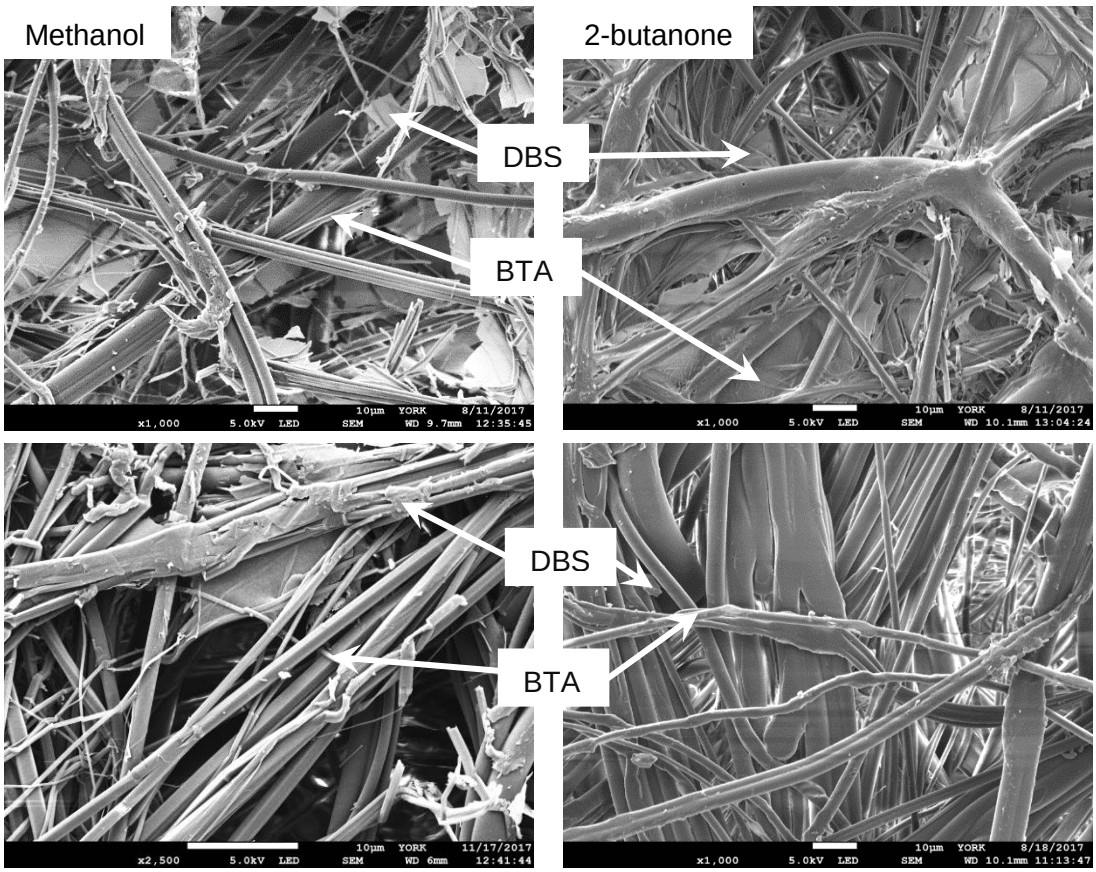

Figure 4-19. SEM images of non-woven fabrics prepared with 0.2 wt/v% DBS 0.2 wt/v% BTA in methanol and 2-butanone, and 0.1 wt/v% DBS 0.3 wt/v% BTA in methanol and 2-butanone at x1000 magnification with scale bars of 10 µm.

4.4.2 Air Permeability Testing of 0.4 wt/v% Total Loading

In terms of long-term application, all the different systems that have been viewed here were tested for air permeability.

Air permeability testing was conducted on fabric samples prepared using mixtures of gelators totalling 0.4 wt/v%. As discussed in Chapter 2, the testing was conducted at 100 Pa and repeated at least 5 times per sample. The air permeability testing results of 0.4 wt/v% total combined loading can be found in Figure 4-20.

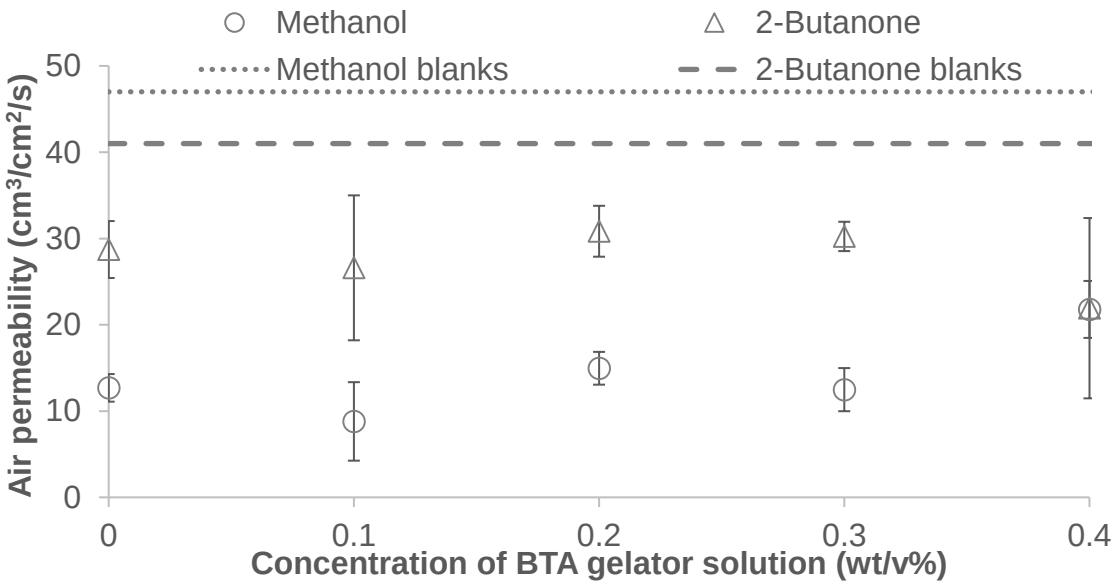

Figure 4-20. Air permeability of samples prepared with 0.4 wt/v% total concentration of gelators (with 0 wt/v% BTA = 0.4 wt/v% DBS and *vice versa*).

Supporting the results previously with 0.6 wt/v% total loading (Figure 4-13), fabrics prepared using 2-butanone gave higher air permeability than those with methanol. The systems investigated with a total loading of 0.4 wt/v% demonstrated less permeability than blank fabric which was soaked in solvent, showing the nanofibres are disrupting air flow through the sample. The lower weight loading gives a lower coverage, so demonstrates a higher air permeability than 0.6 wt/v% total loading.

The mixtures of gelators tended to have an air permeability approximately equal to 0.4 wt/v% DBS. The main exception to this was the samples that only contained BTA. This is likely due to the increased nanofibre size of BTA compared to DBS, hence one could expect fewer but larger nanofibres would have less of an influence of air permeability, as there is less likely to be a collision between a specific air molecule and nanofibres.

As seen by the SEM images, the two solvents present significantly different morphologies. BTA in 2-butanone spans the fabric, but in methanol aggregates together (Figure 4-18).

4.4.3 Post Air Permeability SEM Imaging

As previously mentioned, BTA nanofibres demonstrated significant modifications to their morphology after air permeability testing due to the forcing nature of this testing. It was important to investigate the impact of testing on these dual gelator systems. As at 0.6 wt/v% total loading, imaging after air permeability testing indicated little change – once again suggesting the presence of DBS may increase the robustness of BTA.

These positive results suggest that this dual system would be worth investigating further. Due to time and financial constraints, it was not possible to do any realistic filtration testing on this system.

4.5 Conclusions

In this Chapter, the combination of DBS and BTA at a range of loadings have been investigated and in two different solvents. Rheological investigations into the solid-like properties of the gel mixtures found that DBS was the dominant contributor when DBS loadings were kept constant and the loadings of BTA varied. In both solvents, G' remained constant until high loadings of BTA (150 wt/v% loadings of DBS) at which point the gel became significantly stiffer suggesting dual network formation. These results were supported by T_{gel} values. Gels using 2-butanone were generally stiffer than the same loadings in methanol, which supports the visual morphological differences, with BTA forming much larger diameter nanofibres in 2-butanone than in methanol. An NMR spectroscopic investigation implied that BTA and DBS self-assembled into solid like aggregates in a manner that was largely independent of one another, consistent with them self-sorting in mixtures.

In all cases, SEM images indicated DBS and BTA self-sort into two distinctly sized nanofibres. The exact morphology of the composite depended on the solvent used due to the behaviour of BTA nanofibres in the different solvents, respectively. These self-sorted systems could also be assembled *in situ* in a non-woven fabric, giving a material containing independent fibres on three different length scales (DBS, BTA and fabric). Mixtures with a constant total loading resulted in the expected trends; as the gelator loading decreased, less of that particular gelator was visible in the fabric. This supports the self-sorting mechanism. These systems were investigated for their potential impact on air permeability. Generally, mixtures with a total loading of 0.6 wt/v% resulted in higher air permeabilities than pure BTA or DBS at this weight loading. Mixtures with a total loading of 0.4 wt/v% performed similarly to the pure gelators. It is suggested that DBS may enhance the robustness of the overall network, as BTA nanofibres did not degrade on testing (unlike in Chapter 3 when BTA was used above).

Overall these mixtures of BTA and DBS constitute a novel and rare example of a self-sorting system with two very different length scales of nanofibres forming. With further optimisation, these could have potential to offer the same protection at lower loadings, minimising the impact on the intrinsic properties of the original non-woven fabric.

Chapter 5 - Derivatives of DBS for Fabric Modification

Although performing well in realistic functionality testing, instead of the fabric-spanning secondary network expected to be most suitable for filtration, DBS appeared by electron microscopy to form aggregates.

Derivatives of DBS have been reported in the literature.[50, 51, 57] A range of derivatives were therefore synthesised and investigated by SEM to see if a secondary "spanning" network could be achieved. It can be reasoned that the different solvent compatibilities of different derivatives may impact on the assembly kinetics and/or the ability to interact with the fabric microstructure. Three different derivatives of DBS were targeted in order to probe systems with a range of different polarities. As a general rule, peripheral substituents on gelators tend to play a dominant role in controlling the solubility profile and hence solvent compatibility of the gels formed. These groups also play a role in mediating fibril-fibril interactions and hence it can be reasoned that modifying gelator structures in this way may limit aggregation of the self-assembled nanofibres, enabling them to sample-span more effectively within a fabric.

5.1 1,3:2,4-Dibenzylidene-D-sorbitol-*p,p*'-dihydrazide (DBS-$CONHNH_2$) for Fabric Modification

5.1.1 Synthesis of DBS-$CONHNH_2$

The synthesis of DBS-$CONHNH_2$ is a two-step process.[50] The first step follows the general DBS synthesis; a condensation reaction between two equivalents of 4-methylcarboxyl benzaldehyde and D-sorbitol, carried out under nitrogen at 70 °C for four hours with *p*-toluene sulfonic acid monohydrate as a catalyst, in a mixture of cyclohexane and methanol to form DBS-CO_2Me. The product was then maintained under reflux in water followed by dichloromethane to remove the mono- and tri-substituted derivatives, respectively.[50] The methyl ester product was then maintained under reflux overnight in THF with hydrazine monohydrate to form DBS-$CONHNH_2$ (Scheme 5-1). The product was rinsed with deionised water to remove any impurities. A white powder was obtained in a 61% yield. Characterisation was performed using ^1H NMR, ^{13}C NMR and IR spectroscopies and mass spectrometry identified a mass ion of mass 497.1651 $[M+H]^+$ correlating to the molecular ion peak and a proton, confirmed [DBS-$CONHNH_2$] the product.[50]

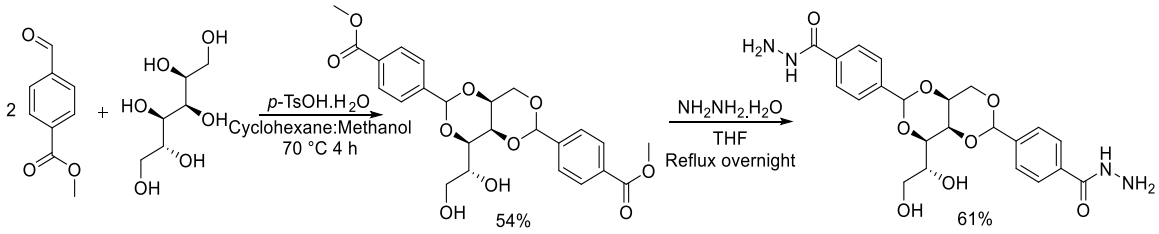

Scheme 5-1. Synthetic route of DBS-CONHNH$_2$.

5.1.2 SEM Images of DBS-CONHNH$_2$ Prepared From 1:1 Water:Methanol

DBS-CONHNH$_2$ is a hydrogelator with the peripheral groups significantly enhancing water solubility. Unlike DBS, DBS-CONHNH$_2$ was insoluble in methanol but had a MGC in 1:1 water:methanol of 0.6 wt/v%. Two concentrations of DBS-CONHNH$_2$ were prepared, one at the MGC and one at half the MGC value. These two concentrations were used to treat both non-woven (NW) and hydrophilic untreated woven cotton fabrics to investigate various combinations of hydrogelator, aqueous solvent system and hydrophilic fabric.

As can be seen from Figure 5-1, an increased concentration of DBS-CONHNH$_2$ resulted in increased nanofibre aggregation visible on the surface of the non-woven fabric. As a result of the significant clustering of nanofibre aggregates and a lack of flatter, sheet-like aggregates with a potential to span the fabric sample, neither of these systems were investigated further.

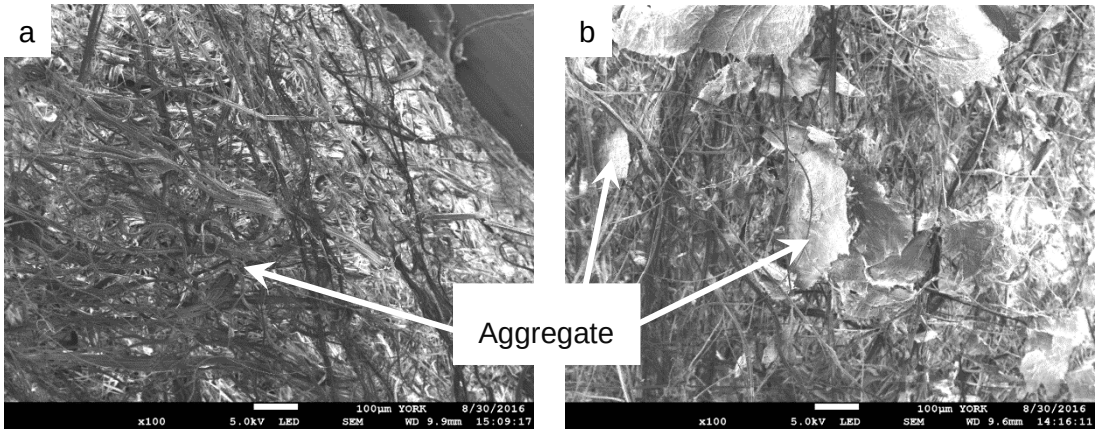

Figure 5-1. SEM images of NW fabric treated with (a) 0.3 wt/v% and (b) 0.6 wt/v% DBS-CONHNH$_2$ in 1:1 water:methanol x100 magnification, scale bars of 100 µm.

DBS-$CONHNH_2$ is a hydrogelator due to the peripheral groups. The hydrophilic cotton fabric was therefore reinvestigated at this point as a proof of concept, to gain further understanding of the balance between gelator, solvent and fabric.

Comparison images for cotton fabric prepared with 0.3 wt/v% and 0.6 wt/v% DBS-$CONHNH_2$ in 1:1 water:methanol are shown in Figure 5-2. When the cotton fabric was treated with the gelator, “leaf-like” aggregates appeared to form on the surface of the fabric. The cotton fabric seems to have more effective coverage than the non-woven fabric, but this could be due to it appearing to be a surface only aggregation event rather than spread through the full depth of the fabric. It was felt that these observations were not ideal for the desired application.

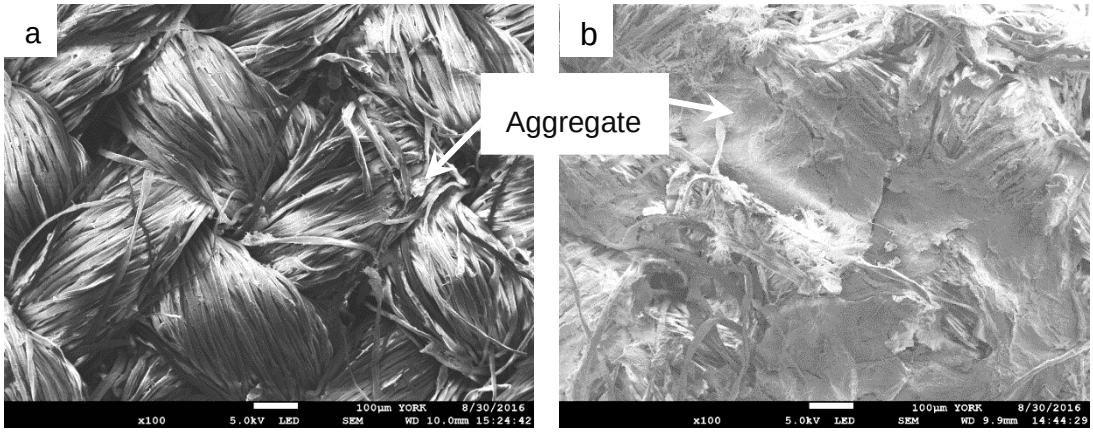

Figure 5-2. SEM images of cotton fabric treated with (a) 0.3 wt/v% and (b) 0.6 wt/v% DBS-$CONHNH_2$ in 1:1 water:methanol x100 magnification, scale bars of 100 µm.

5.1.3 SEM Images of DBS-$CONHNH_2$ Prepared From Water

As DBS-$CONHNH_2$ is a known hydrogelator, the deposition of nanofibres from water was studied. Water would be a green alternative to the previously discussed solvents for long-term application. DBS-$CONHNH_2$ has a MGC in water of 0.2 wt/v% and loadings of 0.1 and 0.2 wt/v% were tested. Above the MGC, application becomes challenging.

The non-woven fabrics showed minimal coverage at both concentrations (Figure 5-3). Significantly more aggregates could be seen on the fabrics treated with 0.1 wt/v% gelator than with 0.2 wt/v%. The gelation kinetics of DBS-$CONHNH_2$ are very different to those previously discussed for DBS. At 0.2 wt/v% DBS-$CONHNH_2$ in water, a gel forms very quickly. One reason for the increased aggregation of 0.1 wt/v% compared to 0.2 wt/v% of DBS-$CONHNH_2$ may be that 0.2 wt/v% forms a gel too rapidly, minimising

time for the solution to flow into the pores of the non-woven fabric before the gel network forms, stopping further movement. This suggests that self-assembly occurs too rapidly from the more concentrated 0.2 wt/v% solution to achieve effective coverage. This also indicates that the gelation kinetics of DBS-$CONHNH_2$ could minimise the practicalities of its use in this application. There would be the possibility of keeping the gelator solution at an elevated temperature, but in any case, the aggregates seen from this derivative did not appear to warrant further investigation.

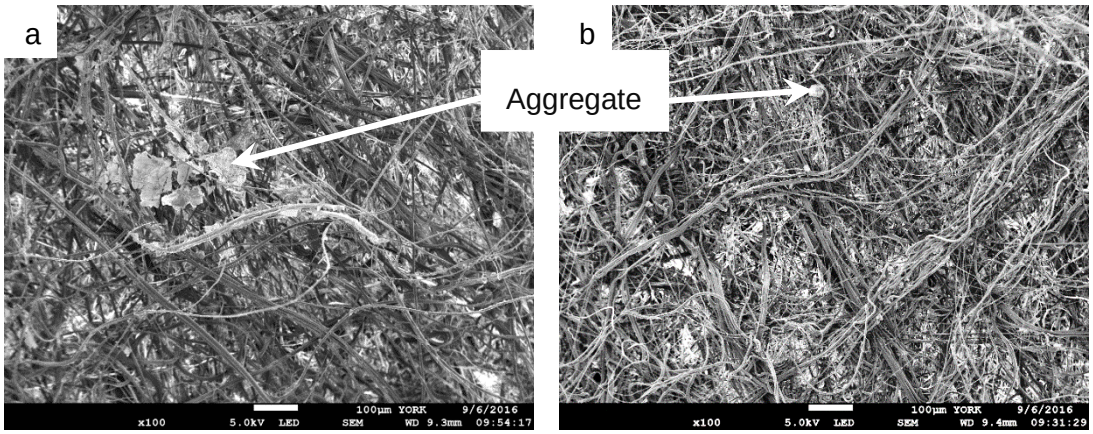

Figure 5-3. SEM images of NW fabric treated with (a) 0.1 wt/v% and (b) 0.2 wt/v% DBS-$CONHNH_2$ in water x100 magnification, scale bars of 100 µm.

At this point, the cotton fabric was reinvestigated. It was thought that the combination of pure water as a solvent and the hydrophilic surface of the fabric may lead to significant differences. Both images in Figure 5-4 show the formation of large aggregates on the surface of the fabric. The aggregates appear to clump together with no potential of sample spanning. Neither sample of the cotton fabric showed significant differences to the samples of cotton fabric previously investigated with 1:1 water:methanol.

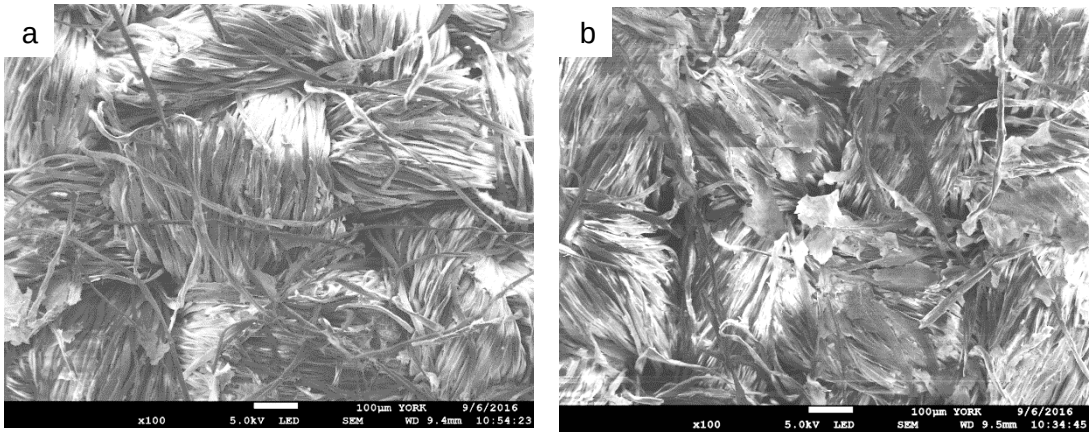

Figure 5-4. SEM images of cotton fabrics treated with (a) 0.1 wt/v% and (b) 0.2 wt/v% DBS-$CONHNH_2$ in water x100 magnification, scale bars of 100 µm.

In summary, DBS-$CONHNH_2$ did not appear to offer noteworthy advantages over the unsubstituted DBS under the conditions tested so this derivative was not investigated further.

5.2 1,3:2,4-Dibenzylidene-D-sorbitol-*p,p*'-dimethoxy (DBS-OCH_3) for Fabric Modification

5.2.1 Synthesis of DBS-OCH_3

The synthesis of DBS-OCH_3 is a simple one step reaction as reported by Whitelaw;[424] a condensation reaction between two equivalents of 4-methoxybenzaldehyde and D-sorbitol. This was carried out under nitrogen at 70 °C for four hours with *p*-toluene sulfonic acid monohydrate as a catalyst in a mixture of cyclohexane and methanol to form DBS-OCH_3 as shown in Scheme 5-2. The product was then washed with hot water and dichloromethane to remove the mono- and tri-substituted derivatives respectively. The product was obtained in 79% yield as a white powder. The chemical structure of the product was confirmed by ^{1}H NMR, ^{13}C NMR and IR spectroscopies and mass spectrometry which had a mass ion value at 441.1501 $[M+Na]^+$ (100%).

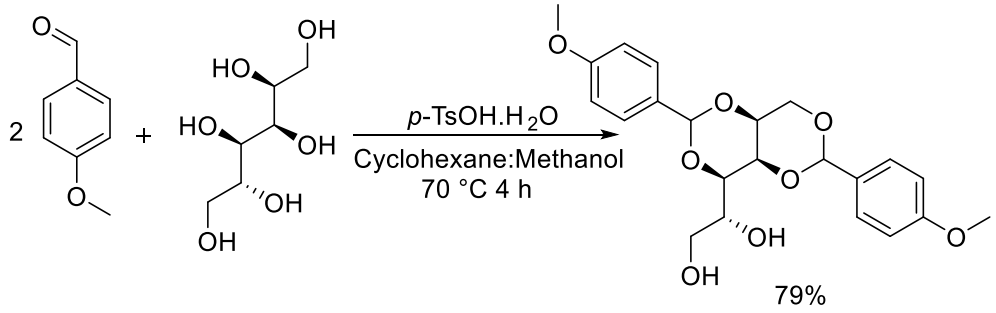

Scheme 5-2. Synthetic route of DBS-OCH_3.

5.2.2 SEM Images of DBS-OCH_3 Prepared From 1:1 water:methanol

The minimum gelation concentration of DBS-OCH_3 in 1:1 water:methanol is 0.1 wt/v% but a higher concentration (*ca.* 0.3 wt/v%) needs to be used to form stable gels. At 0.1 wt/v% the resulting network easily collapsed. The MGC in methanol was >3 wt/v%. Gels with DBS-OCH_3 in methanol were therefore not investigated but gels of DBS-OCH_3 in 1:1 water:methanol were investigated at 0.3 wt/v% and 0.15 wt/v%.

From Figure 5-5, DBS-OCH_3 aggregates were visible on the surface of the fabric treated with 0.3 wt/v% sample but not on that treated with 0.15 wt/v%. This is unusual, as this lower concentration is enough to form a weak gel network so some aggregation would have been expected. Aggregates could, however, be distributed throughout the

fabric. The top right hand corners of the electron microscopy images provide a useful comparison. At 0.3 wt/v% some aggregates are visible on the fabric fibres, whereas 0.15 wt/v% does not.

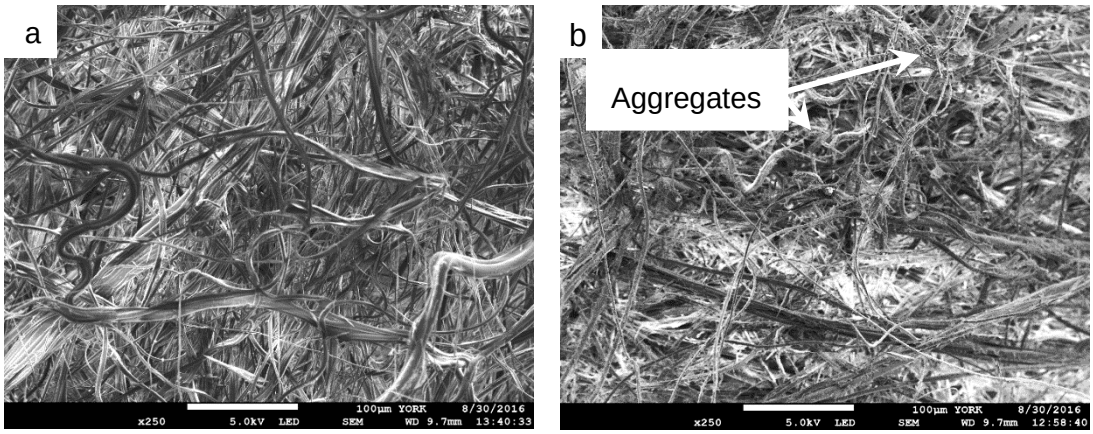

Figure 5-5. SEM images of NW fabrics treated with (a) 0.15 wt/v% and (b) 0.3 wt/v% DBS-OCH_3 in 1:1 water:methanol x250 magnification, scale bars of 100 µm.

At higher magnification, the fabric treated with 0.3 wt/v% DBS-OCH_3 shows small nanocrystal type aggregates (Figure 5-6). This derivative does not provide the desired fabric spanning, however, so was not optimised further.

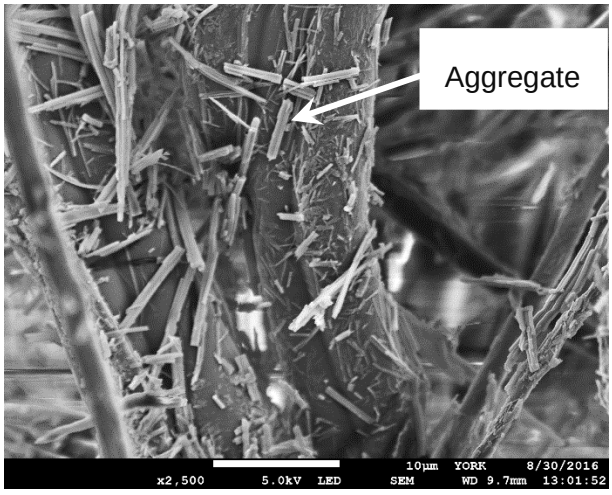

Figure 5-6. SEM images of NW fabric treated with 0.3 wt/v% DBS-OCH_3 in 1:1 water:methanol x 2500 magnification, scale bar of 10 µm.

DBS-OCH_3 was also prepared on a cotton fabric. As can be seen from Figure 5-7, similar coverage and aggregation is seen on the cotton fabric as for the non-woven fabric. The fabric treated with 0.3 wt/v% shows more aggregates than the fabric treated with 0.15 wt/v% as expected, but neither sample demonstrated spanning morphologies. The aggregates are more nanocrystal-like than those that have been

seen before. At higher magnification, it is easier to see these aggregates.

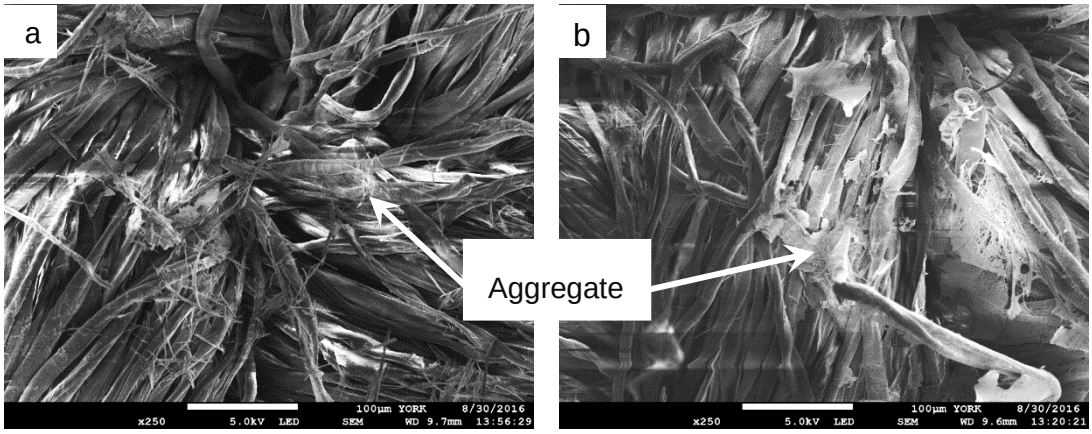

Figure 5-7. SEM images of cotton fabrics treated with (a) 0.15 wt/v% and (b) 0.3 wt/v% DBS-OCH_3 in 1:1 water:methanol x250 magnification, scale bars of 100 µm.

Figure 5-8 shows a particularly large “mat-like” structure formed by these thin, long and narrow aggregates. The entirety of the aggregates appeared to have deposited on the surface of the fabric, rather than penetrating and entwining with the fabric fibres themselves.

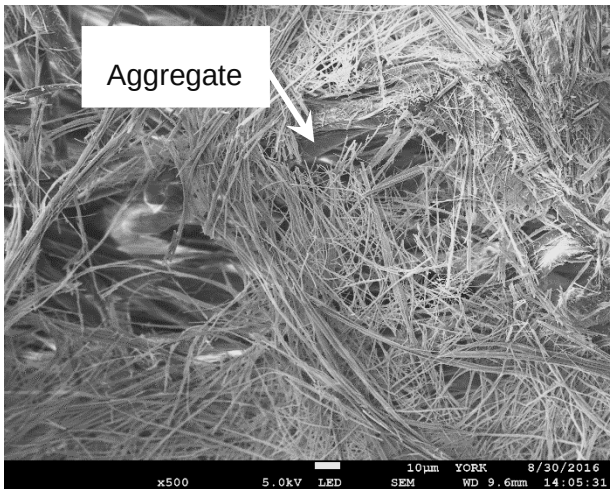

Figure 5-8. SEM images of cotton fabric treated with 0.15 wt/v% DBS-OCH_3 in 1:1 water:methanol x 500 magnification, scale bar of 10 µm.

Figure 5-9 demonstrated a small region of ‘spanning’ aggregates. However, as for Figure 5-8, the aggregates of nanofibres do not appear to be interacting particularly with the fabric fibres. In Figure 5-9 this region seems to be wrapping around a fabric fibre, more so than in Figure 5-8, but this sample does not appear to be spanning multiple fabric fibres. It does not look like the DBS-OCH_3 will be a suitable candidate for

fabric spanning. However, it was significantly better on the cotton fabric than DBS-$CONHNH_2$, which might suggest better compatibility with the hydrophilic fabric surface.

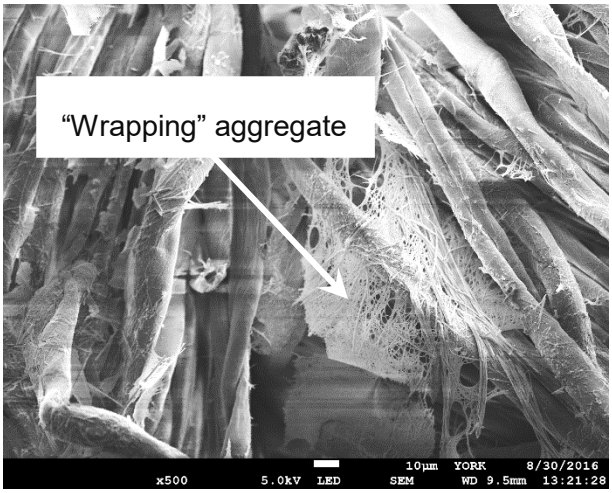

Figure 5-9. SEM image of cotton fabric treated with 0.3 wt/v% DBS-OCH_3 in 1:1 water:methanol x 500 magnification, scale bar of 10 µm.

5.3 1,3:2,4-Dibenzylidene-D-sorbitol-*p,p*'-dimethylthioether (DBS-SCH_3) for Fabric Modification

5.3.1 Synthesis of DBS-SCH_3

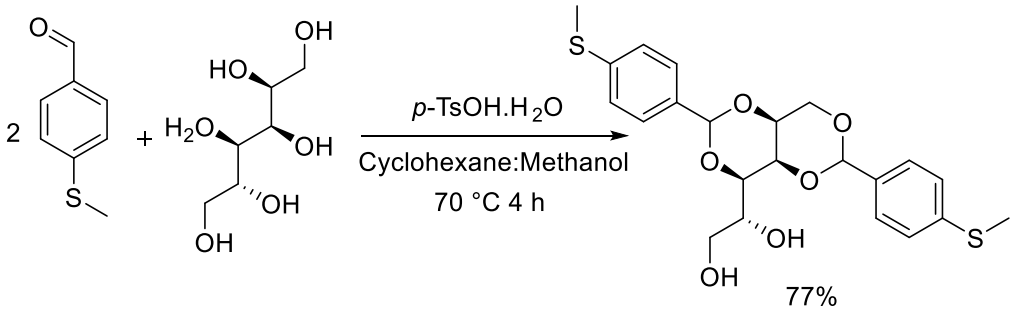

Scheme 5-3. Synthetic route of DBS-SCH_3.

The synthesis of DBS-SCH_3 is a simple one step reaction as reported by Whitelaw;[424] a condensation reaction between two equivalents of 4-methylthiobenzaldehyde and D-sorbitol. This was carried out under nitrogen at 70 °C for four hours with *p*-toluene sulfonic acid monohydrate as a catalyst in a mixture of cyclohexane and methanol to form DBS-SCH_3 as can be seen in Scheme 5-3. The product was then washed with hot water and dichloromethane to remove the mono- and tri-substituted derivatives, respectively. The product was obtained in a 70% yield as a white powder, which was confirmed by ^{1}H NMR, ^{13}C NMR and IR spectroscopies and mass spectrometry confirmed a mass ion value of 473.1078 $[M+Na]^+$ (100%).

5.3.2 SEM Images of DBS-SCH_3 Prepared From 1:1 Water:Methanol

As for the other DBS derivatives, DBS-SCH_3 was investigated in the co-solvent system of 1:1 water:methanol. The minimum gelation concentration of DBS-SCH_3 in 1:1 water:methanol was 0.05 wt/v%. This is much lower than the MGC of the other DBS derivatives and suggests that functionalisation with the SCH_3 group has a beneficial effect on the self-assembly and network formation. DBS-SCH_3 was investigated at 0.05 wt/v% and 0.1 wt/v%. It is worth noting that these are both low loadings compared to the previous investigations, and it might be expected that nanofibre loading onto the fabric would be ineffective. However, at higher concentration, full gel formation would prevent any good chance of fabric loading. However, the non-woven fabrics did show some presence of nanofibres. At increased concentrations there appeared to be more aggregates (Figure 5-10). The higher concentration shows thin spiky aggregates which seem to prefer to aggregate with themselves, or wrap around the fabric fibres, rather than spanning across the gaps in the fabric. The mass increases were measured and were small, in the region of 10%. Given the errors in this technique, it was difficult to quantify more precisely.

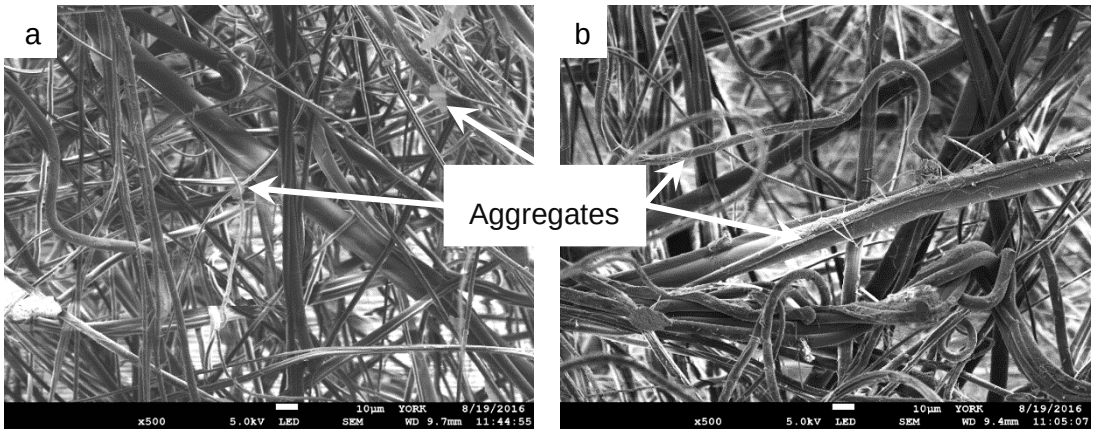

Figure 5-10. SEM images of NW fabrics treated with (a) 0.05 wt/v% and (b) 0.1 wt/v% of DBS-SCH_3 in 1:1 water:methanol x500 magnification, scale bars of 10 µm.

The cotton fabric (Figure 5-11) shows more aggregates than the non-woven fabric, giving reasonable coverage. These aggregates appear in the form of a matt of nanofibres on top of the fabric, which raises concerns that the aggregates are mostly on the surface of the fabric.

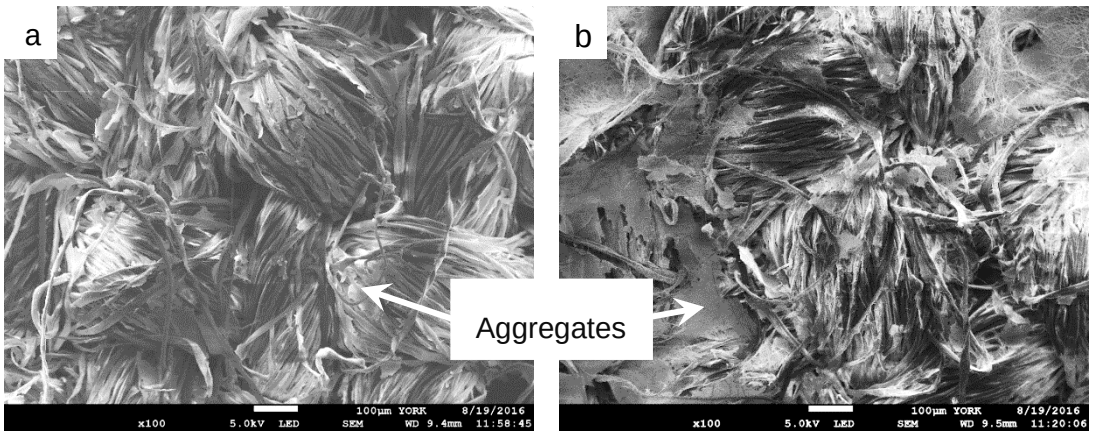

Figure 5-11. SEM images of cotton fabrics treated with (a) 0.05 wt/v% and (b) 0.1 wt/v% DBS-SCH_3 in 1:1 water:methanol x100 magnification, scale bars of 100 µm.

In the cotton fabric, the aggregates appear to only be present on the surface of the fabric (see Figure 5-12), so perhaps do not appear to provide fabric spanning throughout the depth of the fabric. Once again, greater compatibility between the gel network and the fabric would be desirable so DBS-SCH_3 was investigated with methanol as the solvent system.

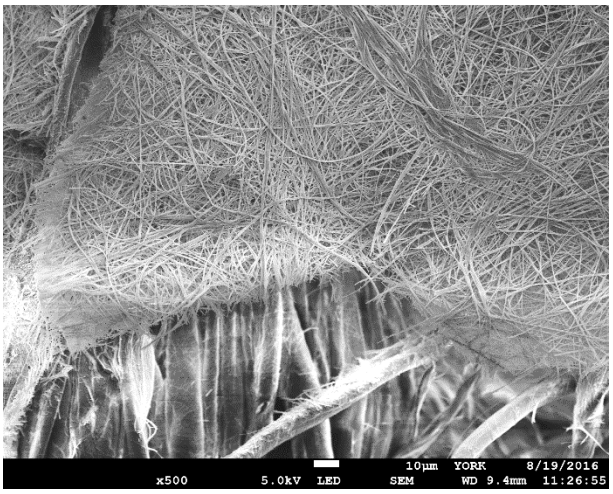

Figure 5-12. SEM image of cotton fabric treated with 0.1 wt/v% DBS-SCH_3 in 1:1 water:methanol x 500 magnification, scale bar of 10 µm.

5.3.3 SEM Images of DBS-SCH_3 Prepared From Methanol

The MGC of DBS-SCH_3 in methanol is 0.4 wt/v%. This higher MGC in methanol reflects the greater stability of DBS-SCH_3 in this solvent than in water:methanol. DBS-SCH_3 was therefore tested at loadings of 0.18 wt/v% and 0.4 wt/v% onto the fabric (Figure 5-13).

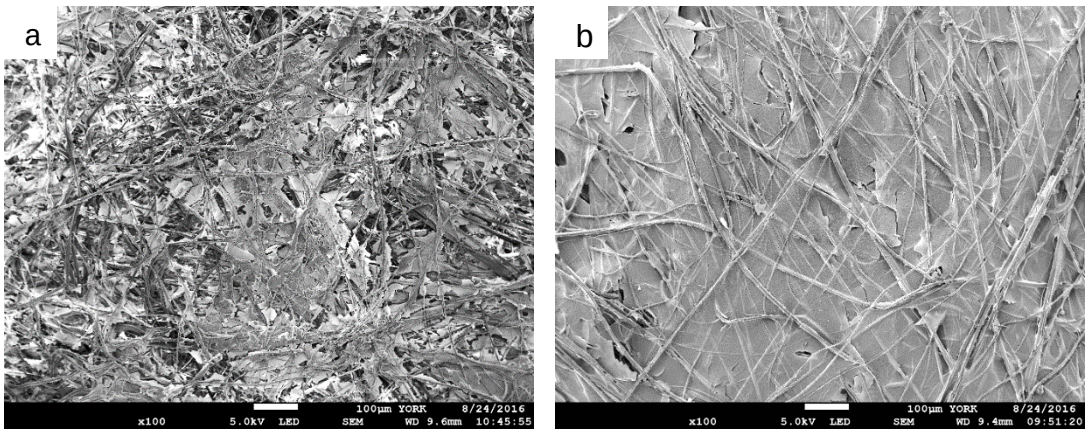

Figure 5-13. SEM images of NW fabrics treated with (a) 0.18 wt/v% and (b) 0.4 wt/v% DBS-SCH_3 in methanol x100 magnification, scale bars of 100 µm.

Particularly at the higher concentration, a dense matted coverage of DBS-SCH_3 nanofibres is visible. This is the best coverage and therefore has the most potential of any of the DBS derivatives investigated in this chapter. At higher magnification which can be seen in Figure 5-14, both samples have the same nanoscale morphologies, with the higher concentration providing greater coverage. Both concentrations demonstrate aggregates which seem to wrap around the fabric fibres, coating them with individual nanofibres as well forming aggregated self-supporting sheets of nanofibres.

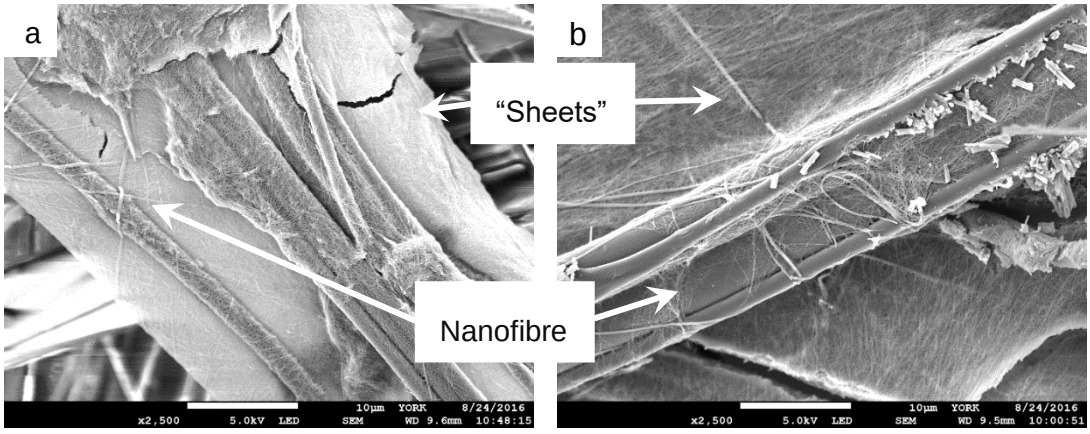

Figure 5-14. SEM images of NW fabrics treated with (a) 0.18 wt/v% and (b) 0.4 wt/v% DBS-SCH_3 in methanol x2500 magnification, scale bars of 10 µm.

The aggregates are still very 'sticky', generally preferring to interact with themselves or the fabric fibres, rather than to span the gaps between fabric fibres. However, much better coverage is seen on the non-woven fabric soaked in methanol than in the 1:1 water:methanol mix. This is probably likely as a result of the increased concentrations which were possible when using methanol as the solvent.

DBS-SCH_3 in methanol was therefore selected to prepare scaled-up samples for further fabric testing to compare to fabrics prepared using unsubstituted DBS (Chapter 2).

The cotton fabric shows less coverage in just methanol than the non-woven fabric (Figure 5-15 *vs.* Figure 5-13). The cotton fabric exhibits mostly self-aggregating "leaf-like" structures which appear completely self-supporting and appear to sit on the surface of the fabric.

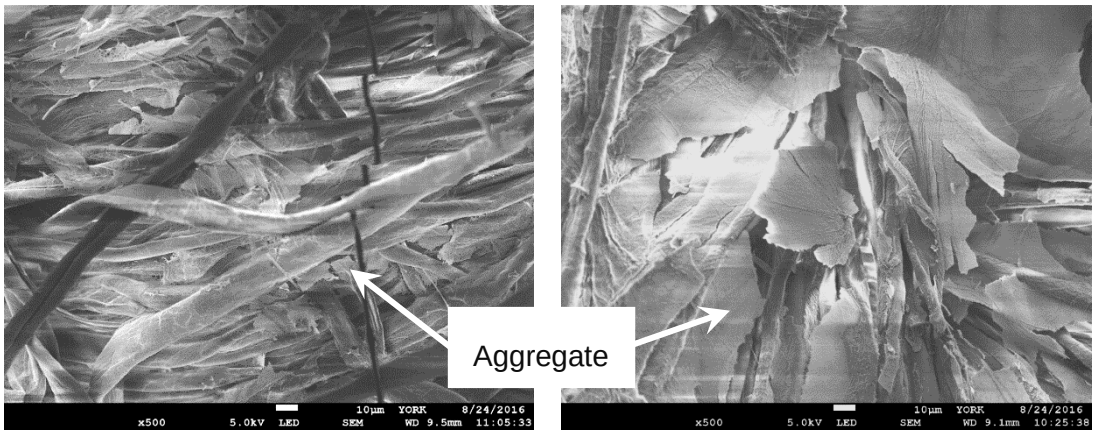

Figure 5-15. SEM images of cotton fabrics treated with 0.18 wt/v% and 0.4 wt/v% DBS-SCH_3 in methanol x500 magnification, scale bars of 10 µm.

Although the cotton fabric was useful to investigate the relationship between gelator, solvent and fabric, it was not used for further testing. DBS-SCH_3 in methanol on the non-woven fabric was selected for scale-up for further testing as it exhibited the most effective fabric coverage.

5.3.4 Air Permeability Testing of DBS-SCH_3

Given DBS-SCH_3 appeared to have the most effective coverage, samples of non-woven fabric soaked in DBS-SCH_3 in 1:1 water:methanol and methanol were prepared as previously discussed and tested for air permeability.

Within error, there was no significant change in the air permeability from the blank fabric to the treated fabric (Figure 5-16). The low loadings used with DBS-SCH_3 appear to have a negligible effect on the air permeability of the fabric. These differences are far smaller than those previously discussed when samples were prepared with unsubstituted DBS. This would support the original aim to increase the filtration properties of the fabric without impacting on the intrinsic properties of the fabric itself. Although, of course, there may simply be insufficient nanofibres present to achieve

actual filtration. It is worth noting that for unfunctionalized DBS loaded onto non-woven fabric, the air permeability had decreased by 39% at this loading. This, therefore, suggests significant differences in performance between DBS and DBS-SCH_3.

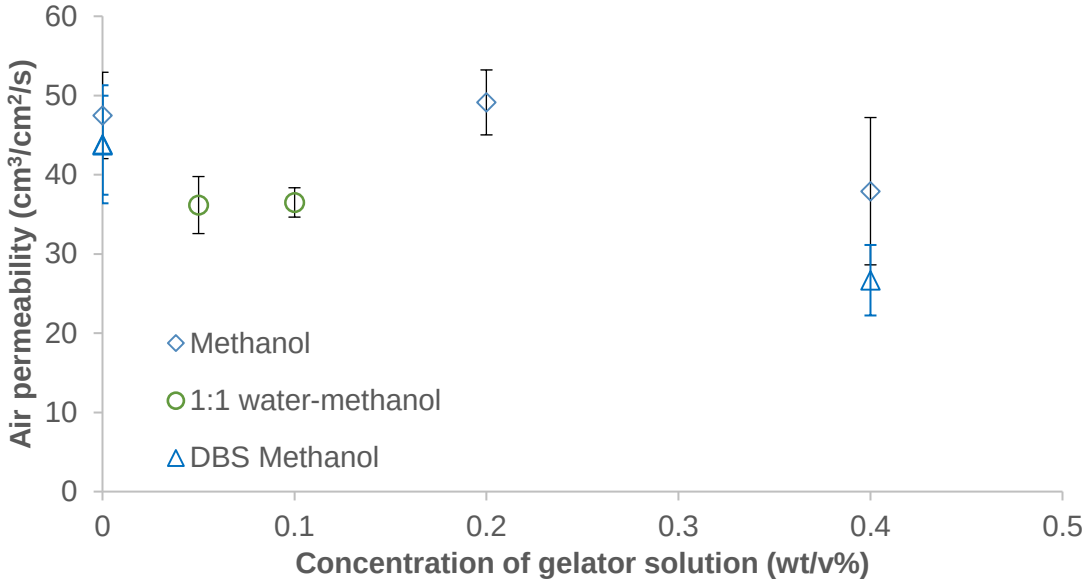

Figure 5-16. Graph of air permeability against concentration of DBS-SCH_3 for methanol and 1:1 water:methanol.

On the basis of this positive air permeability result, the water vapour permeability was also tested on freshly prepared samples.

5.3.5 Water Vapour Permeability Testing of DBS-SCH_3

The water vapour permeability gives an indication of how "wearable" the fabric is. Fresh samples were prepared as previously discussed at the same concentrations as for air permeability testing.

The trends in the water vapour permeability results from Figure 5-17 are not significantly different from the air permeability results. It appears that the presence of the DBS-SCH_3 nanofibres does not significantly influence the transportation of water vapour through the fabric. This supports the studies performed with DBS nanofibres, which also found that WVP was not significantly affected by the addition of nanofibres. If anything, there could be a slight increase in the indexed WVP with fabric treated with 0.2 wt/v% and 0.4 wt/v% of DBS-SCH_3 in methanol but this remains within error.

From the outcome of the SEM, AP and WVP testing, this DBS-SCH_3 system could present an additional option with respect to DBS. It is certainly interesting enough to

warrant additional future filtration testing. There was unfortunately insufficient time to perform this as part of the PhD project, and it would constitute part of future work.

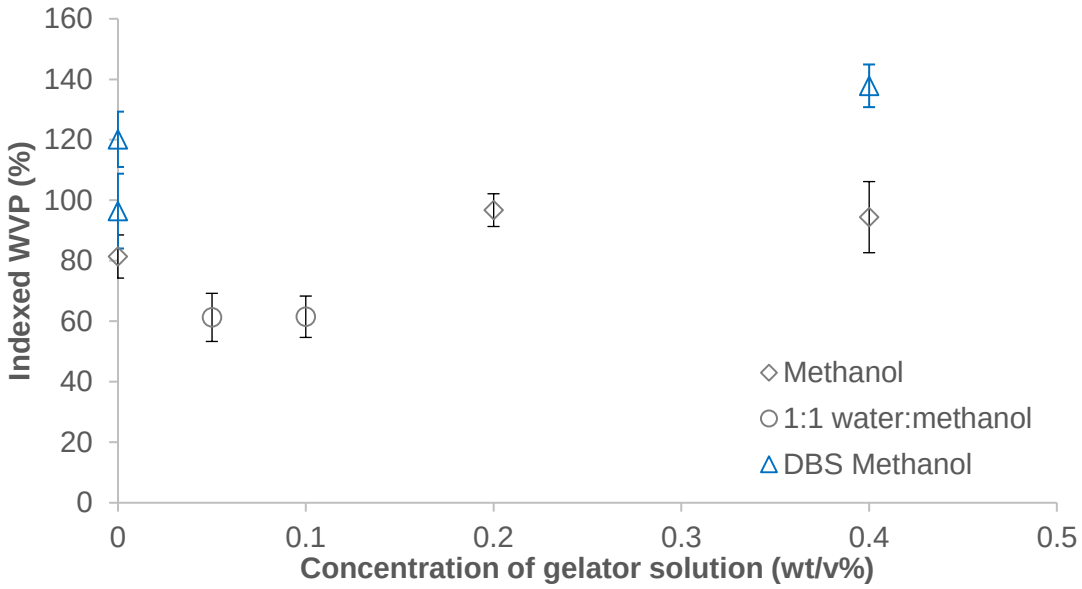

Figure 5-17. Graph of water vapour permeability against concentration of DBS-SCH_3 for methanol and 1:1 water:methanol.

5.4 Conclusions

Two of the derivatives investigated (DBS-$CONHNH_2$ and DBS-OCH_3) did not appear to offer any significant advantage over unsubstituted DBS. The morphologies and aggregates observed appeared to be clumped together. With similar aggregates discussed previously, these two DBS derivatives were not investigated further.

DBS-SCH_3 did show a morphology on the fabric which looked useful with good sample spanning, and further testing on fabric samples showed that at the loadings used (up to 0.4 wt/v%), there was no significant impact on the intrinsic AP or WVP of the fabric.

Of the derivatives investigated, DBS-SCH_3 in methanol and 1:1 water:methanol would warrant further testing.

Chapter 6 - Branching Nanofibre Networks

As discussed in Chapter 1, increased linkages and additional connections between nanofibres would have the potential to strengthen a gel network, so could be considered to provide additional robustness to DBS nanofibres. In fact, crosslinking has been used to design tough hydrogels, increasing the mechanical toughness of the gel network.[425] Furthermore, by investigating the branching of nanofibres it may be possible to increase the ability of the self-assembled system to form a more three-dimensional sample-spanning network. One method of increasing linkages between nanofibres is by creating branching junctions. Two different methods of branching are investigated; one physical method using polymer additives and one chemical method using a dimeric DBS structure.

6.1 Initial Polymer Additive Investigation – Poly(ethylene Glycol) to Aid Branching

The addition of a small amount of polymer has been reported to aid branching by a crystallographic mismatch mechanism.[59] Poly(ethylene glycol) (PEG) was selected as an initial polymer additive due to its excellent solubility. The structure of PEG can be seen in Figure 6-1.

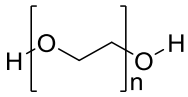

Figure 6-1. Structure of poly(ethylene glycol).

With the two end hydroxyl groups and the oxygen atoms distributed throughout the chain, PEG should have the ability to hydrogen bond with DBS and therefore get involved in the self-assembly, and is miscible with the solvent, methanol. It could be too soluble, but it was considered to be a good polymer for initial testing. Different molecular weight PEGs were investigated. PEG 4000, PEG 1500, PEG 600 and PEG 200 (based on the number average molecular weight) were tested at various loadings in a 0.6 wt/v% DBS in methanol. The appropriate amount of DBS was weighed into a vial, dissolved in the appropriate amount of solvent then transferred to another vial in which the correct amount of polymer had been weighed. The vial was then left under ambient conditions overnight for the gel to form.

6.1.1 Investigating Various Molecular Weights of PEG

In the literature, small amounts of polymer additives have been shown to act as branching promoters, changing the rheological properties of the gel.[284] Each gel sample prepared with varying molecular weights of PEG was investigated by rheology,

T_{gel}, and SEM measurements. Figure 6-2 shows the amplitude sweep of various weights of PEG at a loading of 0.1 wt/v% in 0.6 wt/v% DBS in methanol. PEG 4000 demonstrated a discontinuity at a shear strain of *ca.* 3%. This is likely to be the gel losing its elasticity through disruption of the gel network. The shear modulus (G') increases from the gel with no polymer, on the addition of polymer, and continues to increase as the molecular weight of the polymer increases. This increase in shear modulus (G'), indicates that the gels became stiffer. The linear viscoelastic region, defined as the flat region of the graph until 10% deviation, of the gels with PEG present extended to higher shear strain than the control DBS gel, implying that there is an enhancement of gel stability. The control gel G' value deviated by 10% at a shear strain of 0.5%, whereas the gels with PEG had shear strain values of 2.0, 8.1, 0.6 and 3.8% for PEG 200, 600, 1500 and 4000 respectively. The amplitude sweep is carried out to ensure that the frequency sweep is measured at a shear strain (%) within the linear viscoelastic region. It should be noted that rheological parameters have errors, primarily associated with sample preparation and loading.[420]

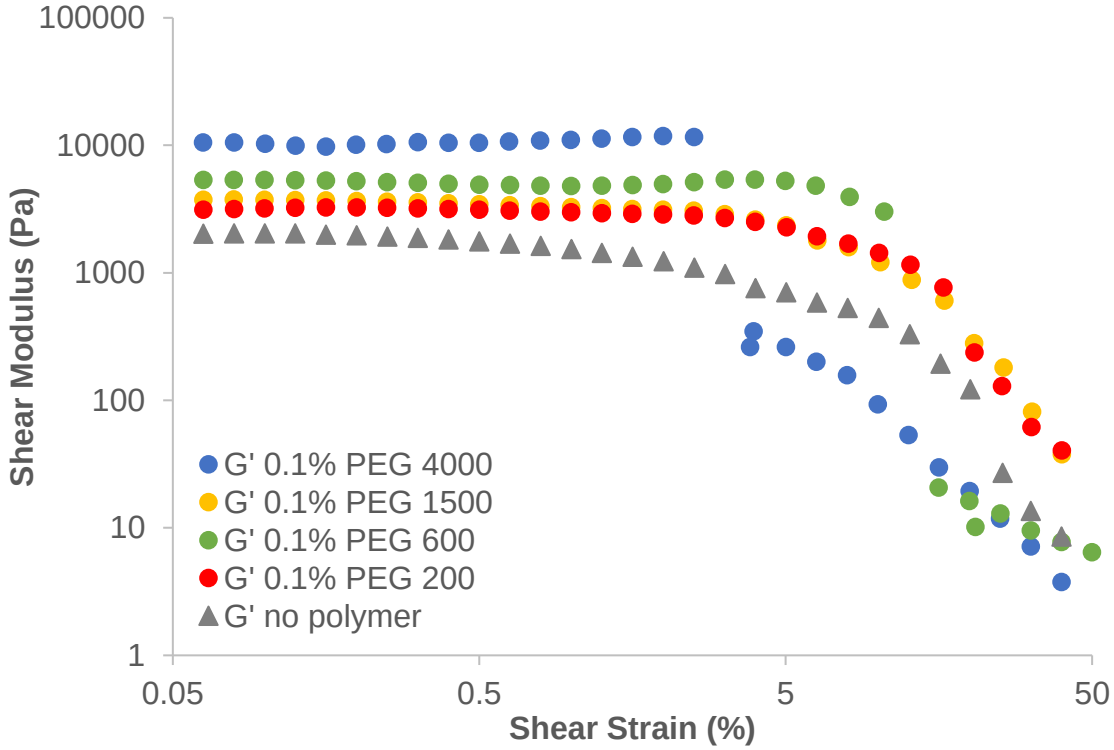

Figure 6-2. Amplitude sweeps of 0.6 wt/v% DBS in methanol loaded with 0.1 wt/v% PEG of various molecular weights.

The frequency sweep in Figure 6-3 showed that G'>>G", which is a characteristic feature of gels. For all the samples, the data is independent of frequency (i.e. mostly

straight lines). The same trend from the amplitude sweep can be seen, generally the higher the molecular weight of polymer the stiffer the sample. Differences in G' are outside what is reasonably expected as errors with the system modified with PEG 4000 being an order of magnitude stiffer. This would suggest that the presence of PEG has a significant impact on the rheological performance of the network which would suggest some intimate involvement with the self-assembly event.

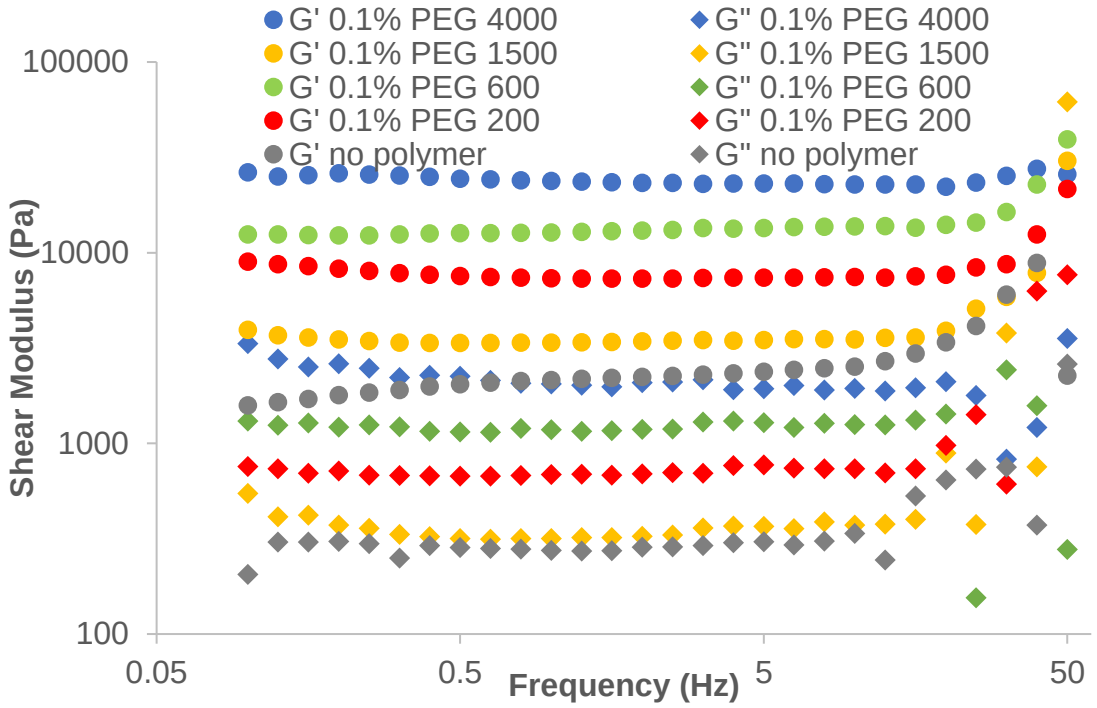

Figure 6-3. Frequency sweep of various weights of PEG in 0.6 wt/v% DBS in methanol at 0.1% shear strain.

The T_{gel} values for 0.6 wt/v% DBS in methanol, loaded with 0.1 wt/v% of the PEG were determined (Table 6-1). All appear to be within experimental error, suggesting that although the rheological properties of the network have changed, the thermal stability has essentially stayed the same.

Table 6-1. T_{gel} values of 0.1 wt/v% PEG in 0.6 wt/v% DBS in methanol.

PEG	T_{gel} / °C
None	41
4000	35
1500	41
600	41
200	40

Only two SEM images have been included as they were all very similar. Figure 6-4 presents the extremes of DBS with no polymer and PEG 4000. The observed morphologies are very similar. No obvious branching is seen at the fibre level. This doesn't mean it isn't occurring, there could be branching at the fibril level. The apparent directionality of the DBS in the absence of polymer is just an artifact of sample preparation. As such, SEM did not make readily apparent any nano/micro-scale reasons for differences in the rheological performance of DBS on the addition of PEG.

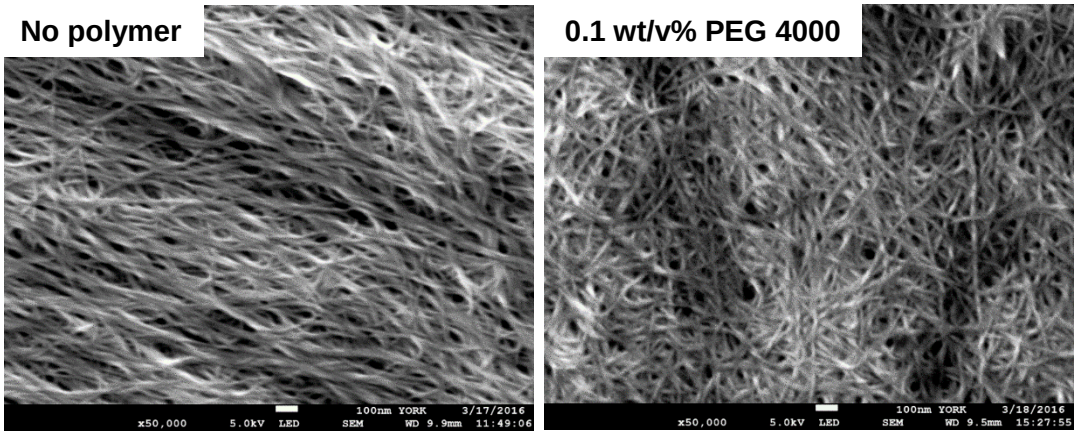

Figure 6-4. SEM images of 0.6 wt/v% DBS at x50 000 magnification on aluminium stub with no polymer and 0.1 wt/v% PEG 4000, scale bars of 100 nm.

6.1.2 Investigation of Varying Loading of PEG

The effect of polymer loading on macroscopic DBS gel performance was investigated using PEG 4000. It was reasoned that this system would show the most significant differences. Each gel sample was investigated using rheology and T_{gel} methods.

Considering the amplitude sweep of loadings of PEG 4000 from 0 to 0.2 wt/v%, there was no obvious trend in the G' (Figure 6-5). The 0.05 wt/v% PEG 4000 loading appears to closely match the rheology in the absence of polymer, which was expected as the lowest polymer loading should probably have the smallest effect. The G' of 0.1 wt/v% and 0.2 wt/v% PEG 4000, increased from the control, meaning that the gels are stiffer. However, 0.1 wt/v% PEG 4000 provided the stiffest gel. The LVRs of all the gels with polymer present were larger than the control DBS gel, implying that polymer enhances the stability of the gel towards shear. The control gel G' value deviated by 10% at a shear strain of 0.5%, whereas the gels with PEG had shear strain values of 5.0, 3.8 and 6.5% for 0.05 wt/v%, 0.1 wt/v% and 0.2 wt/v% PEG 4000, respectively – an order of magnitude difference.

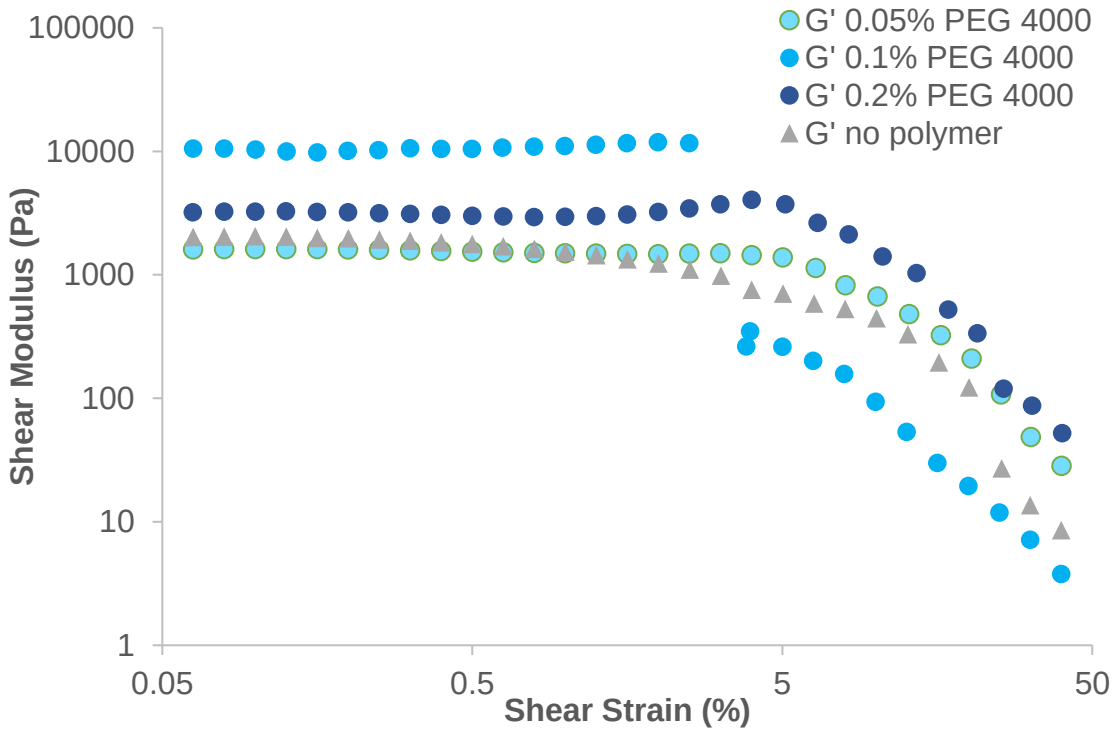

Figure 6-5. Amplitude sweep of various loadings of PEG 4000 in 0.6 wt/v% DBS in methanol.

PEG 600 was then investigated to determine if these trends were specific to the heaviest PEG or if it would generalise to the use of any PEG. PEG 600 was less soluble than PEG 4000, so could not be investigated at 0.2 wt/v%. Instead, 0.1 wt/v%, 0.05 wt/v% and 0.025 wt/v% were tested (Figure 6-6).

With PEG 600, all three loadings offered an enhancement of G' over the gel in the absence of polymer, meaning that DBS gels with PEG 600 form a stiffer network. As

more PEG 600 is included in the gel, the elastic modulus (G') increases with the maximum stiffness being observed for the highest loading. This would support a branching mechanism; if the network were branched there would be links between the fibres which could dissipate applied force, allowing the gel to respond more elastically. The LVRs of all the gels containing polymer are longer than the control, supporting the results from PEG 4000 that the polymer enhances the gel stability towards shear. The control gel G' value deviated by 10% at a shear strain of 0.5%, whereas the gels with PEG had shear strain values of 1.3, 5.1 and 8.1% for 0.025 wt/v%, 0.05 wt/v% and 0.1 wt/v% PEG 600 respectively – a significant increase. The difference between PEG 4000 and PEG 600 may reflect their different solubilities, which will change their ability to interact with the self-assembling DBS nanofibre network.

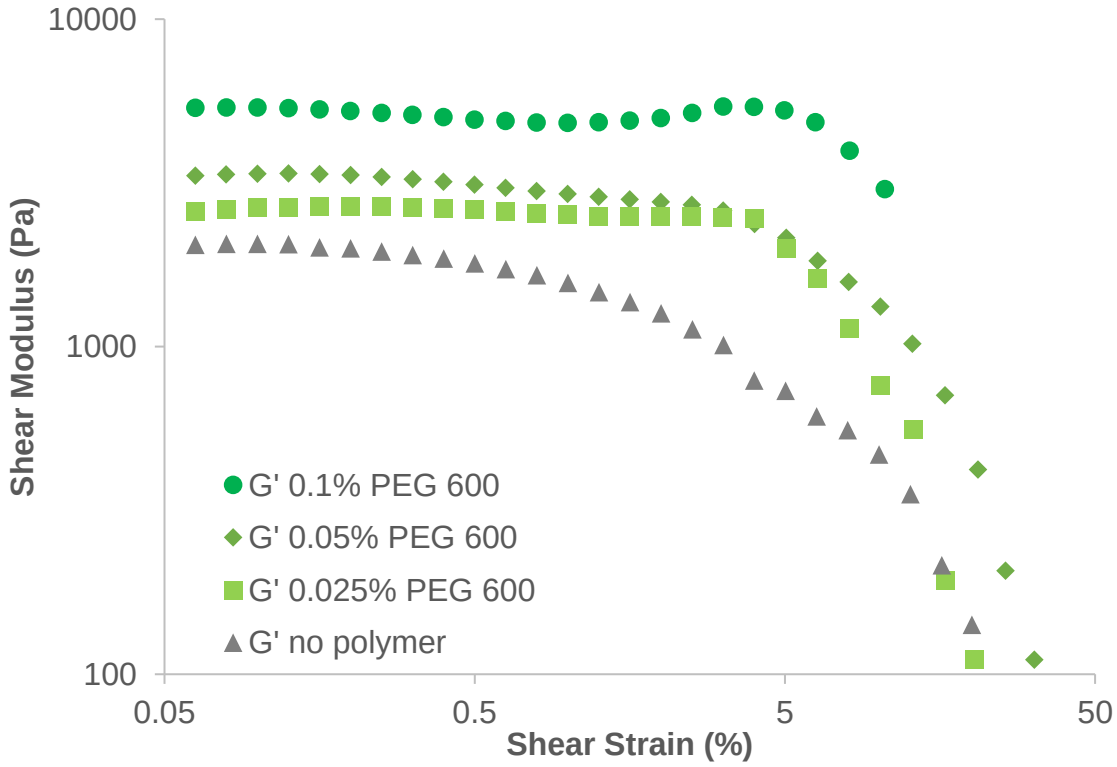

Figure 6-6. Amplitude sweep of various loadings of PEG 600 in 0.6 wt/v% DBS in methanol.

It should be noted that the differences in G' are relatively small, and errors may be significant.

To summarise, using different molecular weights of PEG at a loading of 0.1 wt/v% demonstrated increased the shear moduli (G') when compared to the gel with no polymer. The shear moduli continued to increase as the molecular weight of the

polymer was increased, implying that increased molecular weight of PEG produces stiffer gels in both the amplitude and frequency sweeps. The T_{gel} values suggested the thermal properties of the gel networks have essentially stayed the same, even though the rheological properties have changed. SEM did not provide evidence for any nano/micro-scale reasons for differences in the rheological performance of DBS. There were no obvious trends when the loading of polymer was varied. Generally, the gels with polymer present were stiffer than gels with polymer absent.

Appraisal of the literature surrounding polymer additives provides some criteria for selecting additives.[298,296]

1. The additives should have strong adsorption on the solid fibre surface (generally rigid structures). Polymers have more potential interacting points than monomers.
2. The additive should have strong physical interactions on the surface.
3. The additive should have limited solubility in the solvent, and therefore should adsorb onto the crystal surface more easily. If the solubility is too high, there can be a strong interaction with the solvent and the additive can be easily desorbed.

Based on these criteria, polyvinyl acetate (PVA) was chosen as the second polymer additive for investigation.

6.2 Poly(vinyl Acetate) to Aid Branching

With the mixed results seen with PEG, other polymers were also considered. Poly(vinyl acetate) (Figure 6-7) was selected as a comparative polymer, as it is soluble in methanol and it was thought that the moiety had potential to interact with DBS through hydrogen bond interactions.

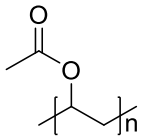

Figure 6-7. Structure of poly(vinyl acetate) (PVA).

High concentrations (>0.05 wt/v%) of PVA disrupted the gel network so much that gelation did not occur, supportive of the view that interaction with the self-assembling DBS unit was indeed possible. PVA was therefore investigated as an additive at much lower concentrations (0.01 wt/v%).

From Figure 6-8, all of the gels with PVA present had a higher G' implying that they were stiffer than the control gel without polymer although the differences are much smaller than those seen with PEG. The effect was largest for the PVA system with the highest molecular weight. Once again, increasing the molecular weight of the polymer appeared to enhance the stiffness. This would be supportive of a greater degree of network branching. The LVRs of the different gels appear very similar (1.3, 1.6, 0.8 and 1.3% shear strain for DBS, PVA 50 000, PVA 140 000 and PVA 170 000 respectively) which suggests that the PVA additive doesn't impact on the stability of the gel towards shear, unlike PEG which demonstrated a reduction in LVR as molecular weight increased.

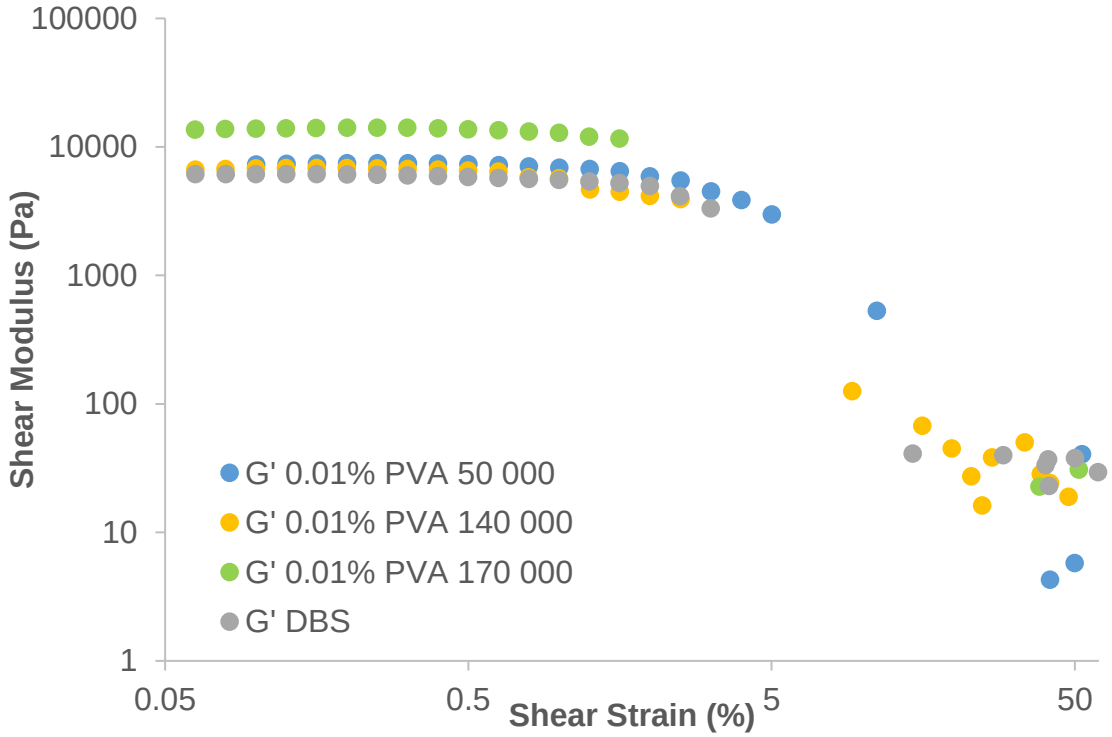

Figure 6-8. Amplitude sweep of various weights of PVA in 0.6 wt/v% DBS in methanol.

The T_{gel} values for 0.6 wt/v% DBS in methanol, loaded with 0.05 wt/v% of PVA, all appear to be within experimental error in Table 6-2. This suggests that although the rheological properties of the network have changed, the thermal stability has stayed roughly the same.

Table 6-2. T_{gel} values for 0.6 wt/v% DBS in methanol with 0.05 wt/v% PVA.

Molecular Weight of PVA used	T_{gel} (°C)
No PVA	41.5
50000	41.5
140000	39.0
170000	37.5

Only two SEM images have been included as they were all very similar. Figure 6-9 presents the mid-range molecular weight PVA 140 000 at both 0.01 wt/v% and 0.05 wt/v%. The observed morphologies are very similar and are identical to the images without polymer (as seen in Figure 6-4). No obvious branching is seen at the fibre level. SEM did not make readily apparent any morphological reasons for any differences in the rheological performance of DBS. PEG additives also showed no difference in the nano-/micro-scale network.

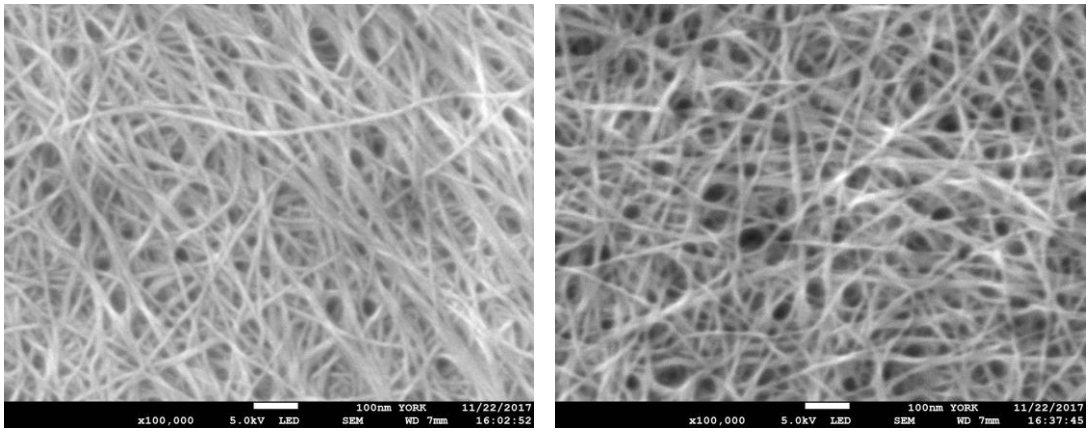

Figure 6-9. SEM images of 0.6 wt/v% DBS with 0.01 wt/v% and 0.05 wt/v% PVA 140 000 at x100000 magnification with scale bars of 100 nm.

In summary, it would appear that polymer additives do have a rheological impact on the properties of these gels but have limited effect on thermal stability or nano/microscale morphology. On this basis, another method of enhancing branching and modifying the network morphology was investigated, the use of a dimeric gelator.

6.3 Chemical Structure Method of Branching

The use of a dimeric gelator could potentially help link nanofibres together. Each end of the dimer could self-assemble into a different nanofibrill, effectively covalently linking two fibrills together. With multiple dimers present in each self-assembled nanofibrill, the robustness of the gel network could be significantly increased. Both ends of the dimer could self-assemble into the same nanofibre to minimise the free volume. Both these possibilities are shown in Figure 6-10. This approach has, perhaps surprisingly, not been previously explored in low, molecular weight gelator chemistry. Hayes and co-workers have successfully linked two gelators by an alkyl group, and demonstrated correlations of chain length with mechanical properties and minimum gelation concentration.[304] The gelation was only investigated with the pure synthesised dimer compounds, the authors did not report mix dimer and monomer to investigate gelation.

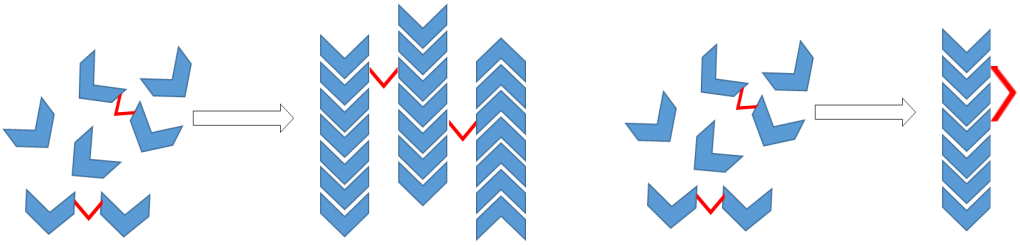

Figure 6-10. Schematic of dimeric potential self-assembly.

6.3.1 DBS Dimer Synthesis

A dimeric DBS structure was therefore proposed; a bola-amphiphile of DBS, with the goal of increasing the degree of branching. These covalent cross-linking units could also potentially strengthen the network, allowing it to survive in harsher environments and increasing its durability.

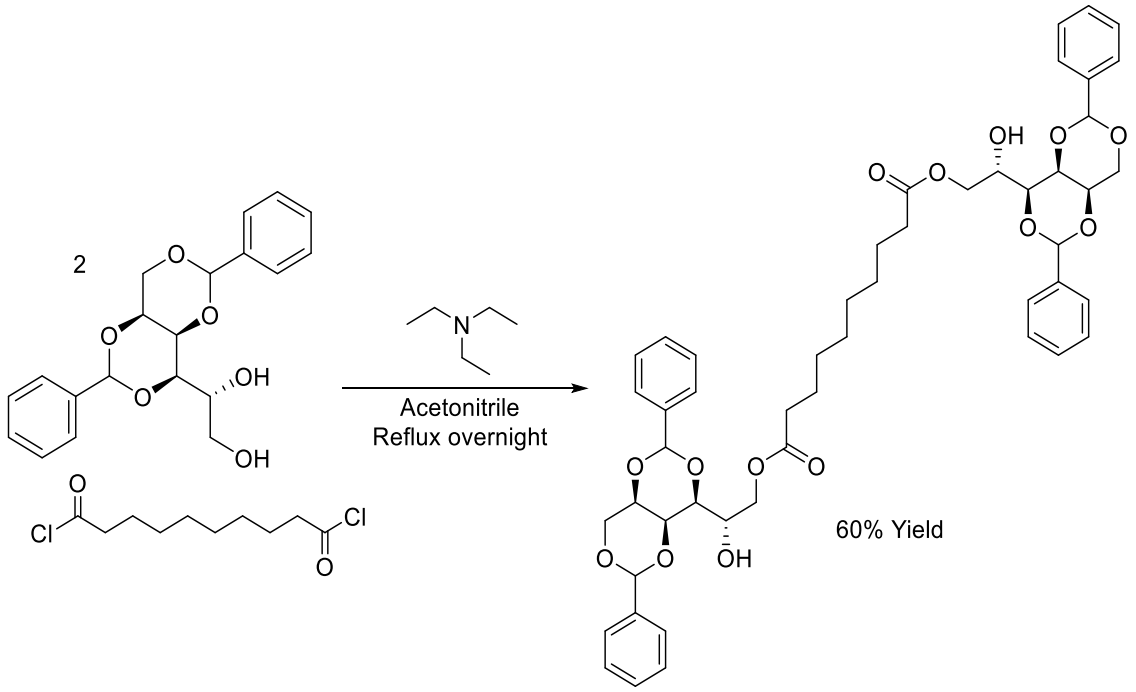

Scheme 6-1. Synthetic route of DBS dimer.

Based on the patent literature, a dimer of DBS was synthesised from two equivalents of DBS, sebacoyl chloride and an excess of triethylamine (Scheme 6-1).[149] After maintaining the reaction mixture under reflux in acetonitrile overnight, the solution was tipped into ice cold water and the dimer precipitated. Reaction of the primary alcohol of DBS rather than the secondary alcohols is favoured, as a result of its greater nucleophilicity.

After synthesis, the dimer was submitted for mass spectrometry and NMR spectroscopic analysis. The mass spectrum showed the correct mass to be present, and the integration of the proton resonances in the ^{1}H NMR spectrum imply a 2:1 ratio between DBS and alkyl linker unit.

Using infra-red spectroscopy (IR) as seen in Figure 6-11, there seemed to be a decrease in transmittance at 3207 cm^{-1} which could be indicative of a reaction of the OH group, and the carbonyl absorbance band at 1730 cm^{-1} is most likely to be the ester carbonyl, as the IR spectrum of sebacoyl chloride shows a absorbance band at <1700 cm^{-1}. This shift to higher wavenumbers would imply that the reaction was successful. There appeared to be only one carbonyl absorbance band which would imply full reaction conversion, rather than a carboxylic acid (or acyl chloride but this group is likely to have reacted) at one end of the molecule. In general, most other absorbance bands remained unchanged from DBS to the dimer structure.

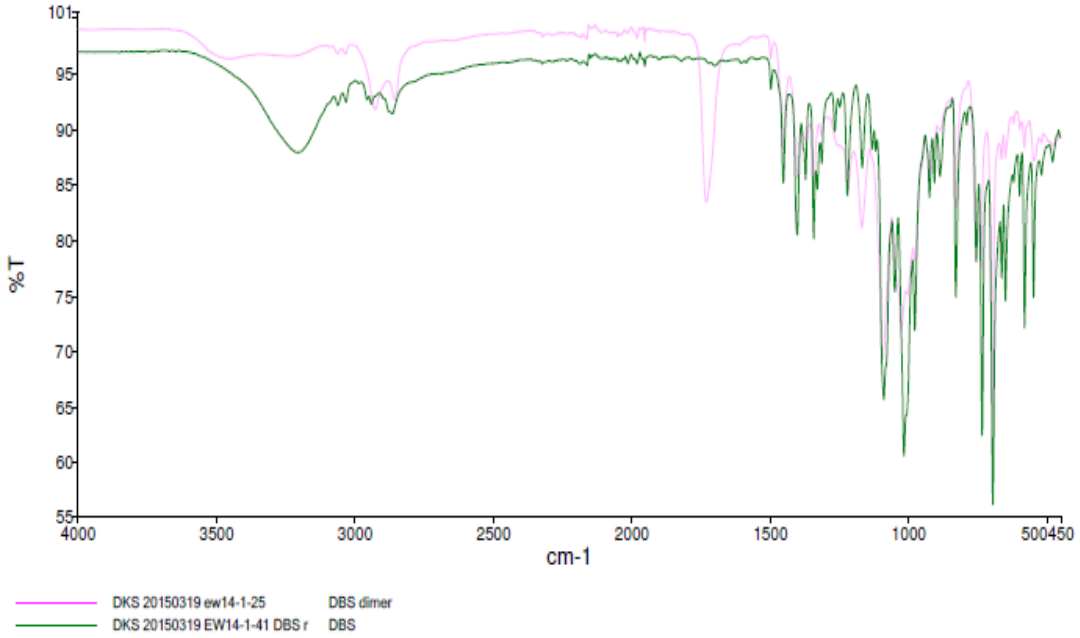

Figure 6-11. IR spectrum of DBS and DBS dimer.

6.3.2 DBS Dimer Interaction

In order to determine whether the dimer could assemble in the presence of DBS, an NMR spectroscopic experiment was performed to probe the immobilisation of the dimer. It is well-known that in NMR spectroscopy, solid-like gel nanofibres are invisible while gelator molecules dissolved in the solvent can be observed as sharp peaks and quantified with reference to an internal standard.[426, 427] A ^{1}H NMR spectrum was captured of the mixture containing the dimer and DBS, with DMSO as an internal standard. DBS was used at 3 w/v% to ensure a gel in methanol (MGC 0.6 w/v%), with 1 w/v% dimer and 2 µl of DMSO.

Using the ratio of integrated proton resonances of DMSO to the aromatic protons in the dimer, there appeared to be 29% of the dimer present in the very broad NMR spectrum, Figure 6-12 (broad even when run with more scans). This implies that 71% of the dimer is interacting with the solid-like network and thus cannot be seen in the NMR. This provided good initial evidence that the dimer became involved in the self-assembly process.

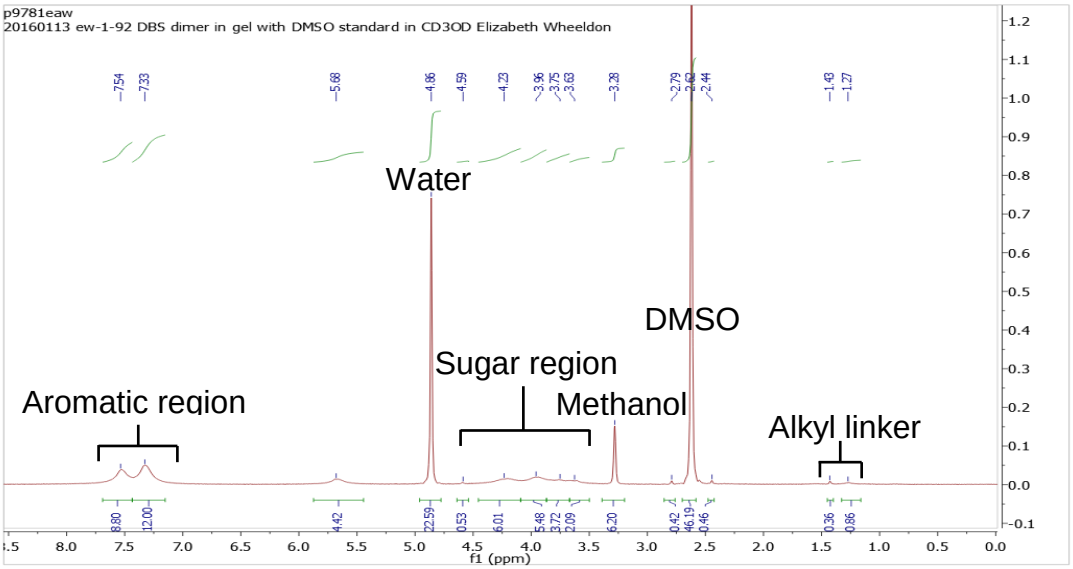

Figure 6-12. ^{1}H NMR Spectrum of DBS Dimer in DBS gel with DMSO as internal standard.

As can be seen from the SEM images in Figure 6-13, the typical DBS nanostructure was observed with nanofibres of *ca.* 15 nm. SEM did not make readily apparent any nano/micro-scale branching. However, the dimer could be causing branching at the fibril level rather than the fibre level.

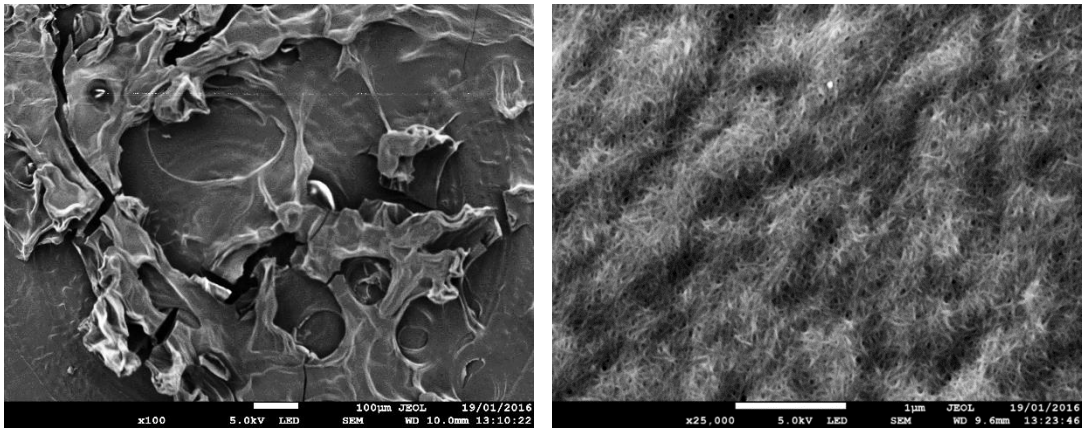

Figure 6-13. SEM images of 3 wt/v% DBS and 1 wt/v% dimer on aluminium stub, scale bars of 100 µm and 1 µm.

The sample was also tested in a non-woven to see if the fabric could help support the network and make any branching points more obvious (Figure 6-14). However, the nanoscale network had made negligible differences to any of the other nanoscale networks seen. There are no obvious branching points. The dimer could still be branching but at the fibril level rather than the fibre level.

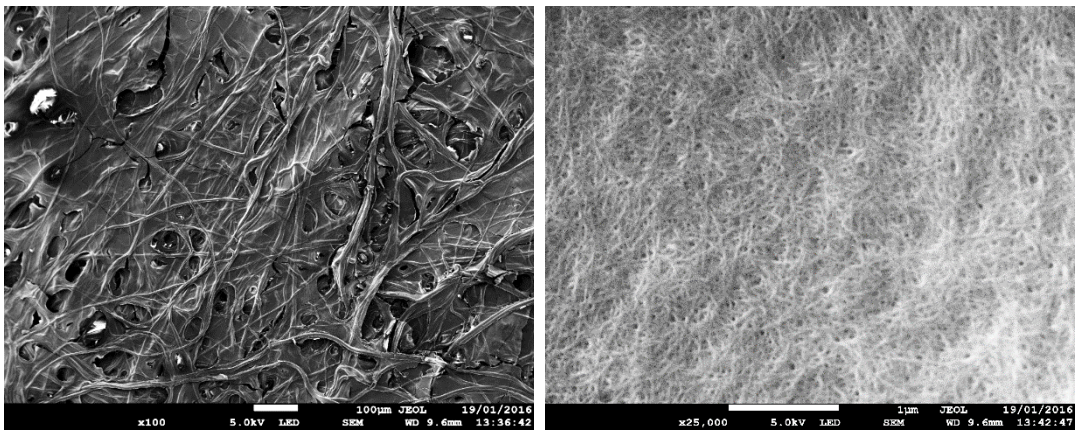

Figure 6-14. SEM images of non-woven fabric prepared with 3 wt/v% DBS and 1 wt/v% dimer, scale bars of 100 µm and 1 µm.

There was a lot more coverage on this non-woven sample than seen before, but this sample was prepared as a slow forming gel. As expected therefore 3 wt/v% DBS (five times the MGC of DBS in methanol) gave very dense coverage as seen in Figure 6-14.

6.4 Conclusions

Two different methods were used to try and initiate rheological and morphological changes by inducing nanofibre branching. Rheological results indicated that the addition of polymers (PEG and PVA) enhanced gel stability by increasing the gel LVR. Furthermore, in both cases, the stiffness of the gel could also be enhanced by polymer addition. All investigations with PEG showed that generally, the higher the molecular weight, the higher the G' value, and therefore the increased gel stiffness. There were no changes in thermal stability for PEG or PVA additives. All gels with the PVA present were stiffer than the control gel with no polymer. However, no morphological changes could be observed by SEM although this only observes microstructure and the underpinning nanostructure may have changed.

A dimer of DBS was successfully synthesised and NMR spectroscopic analysis studies showed it was, to some extent (71%), incorporated into self-assembled DBS nanofibres. SEM imaging on fabric suggested good coverage could be achieved, although this was performed at high DBS loading and further optimisation would be required. Further work could include additional investigation of this dimer, for example more detailed rheological study and an investigation of whether it has an effect on the network formed on a fabric.

Chapter 7 - Conclusions and Future Work

The aim of this project was to develop self-assembling nanostructures, which could be incorporated into a single layer fabric via self-assembly methods to achieve enhanced repellency of organic fluids and aerosols with minimal change to the intrinsic properties of the fabric. Ideally, these would be based on low-cost, industrially viable DBS gelators, although alternative gelators were considered.

Investigations with DBS have demonstrated that during drying at room temperature under atmospheric conditions, the solvent used does not significantly impact on the morphology or diameter of the nanofibres formed either on an SEM stub or within a fabric. However, drying samples under vacuum did appear to affect the morphology formed as “bushes” rather than ‘well dried’ objects were seen. The nanoscale network remained unaffected.

Minimum gelation concentrations of various solvents were correlated with the precise location of the solvent in three-dimensional ‘Hansen space’ – this is the first time this has been attempted. Solvent choice also influenced gel stiffness, 2-butanone resulted in far stiffer gels than methanol, probably due to the aprotic nature of the solvent. The protic nature of methanol can interfere with the DBS intermolecular interactions, therefore disrupting gelation. It was found that increased DBS concentration produced stiffer, less elastic gels. As expected, increased DBS concentration also gave increased thermal stability. Gels in 2-butanone also demonstrated higher thermal stability than gels made in methanol.

A proof of concept experiment demonstrated the ability to self-assemble DBS nanofibres on the surface of a previous uniform textile. Different methods of application were investigated, with the use of a solution bath chosen for its relative ease of scale-up. Various fabrics were investigated using SEM, including carbon cloth, cotton and non-woven fabrics. Cross-sectional imaging of a fabric verified that the DBS nanofibres were indeed penetrating the fabric and were not just surface aggregates.

Non-woven fabric treated with DBS was selected for large-scale testing. It was found that increased deposition of nanofibres (from increased gelator concentration) increased the air resistance in air permeability testing, but the same level of deposition, did not impede water vapour transport. This was supported by results using electrospun nanofibres from the literature. SEM imaging showed that these tests did not significantly impact on DBS nanofibres on the non-woven fabric, indicating good physical stability of the nanofibres. Water vapour permeability testing at an elevated temperature was not impeded, hopefully providing an indication that these fabrics

would allow evaporation of water or sweat from the surface of the skin, allowing breathability.

Against NaCl aerosol particles on small scale aerosol testing rig, DBS treated fabric samples performed similarly to untreated fabric samples. However, testing the DBS treated fabrics using a more realistic test method, where an incident air flow is able to move around the test samples, against a dry aerosol (fluorescein) gave very positive results. It is likely that this is as a result of decreased air permeability in the samples. One sample did appear to give genuine improvement, a composite made with around 0.2 wt/v% DBS. This system gave a lower tape deposition and higher deposition on the fabric itself during the testing with fluorescein. This concentration also had the highest air permeability of the tested treated fabrics so would seem a favourable compromise between all the factors but would warrant further testing; WVP and filtration testing. Although minimal testing was completed due to cost and time constraints, the DBS treated fabrics performed significantly better than the “blank” fabrics, minimising deposition of dried fluorescein onto the skin mimic tapes. Increased deposition of nanofibres in the fabric led to a further reduction in the penetration of fluorescein. Further testing could expand and confirm these results.

It was also important to compare DBS to the gelator in the literature originally identified as potential supramolecular nanofibres for air filtration. BTA had been shown to act as a secondary network to enhance filtration of a range of particle sizes. During all fabric testing (air permeability testing, water vapour permeability testing, fluorescein filtration and filtration efficiency testing) BTA demonstrated comparable results to our other gelator, DBS. This implies that DBS provides a commercial alternative to BTA to enhance filtration in a realistic setting. DBS has much smaller nanofibre diameters (15 nm) than BTA (*ca.* 450 nm), which has the potential to minimise effect on AP if the density of fibres could be reduced. Furthermore, DBS morphologies appeared to show less damage after sample testing, which suggests they may be more stable/robust. In particular, the DBS nanofibres appeared to have greater stability to water vapour which of a key importance in clothing applications. As such, it is suggested that DBS may offer advantages over BTA as a result of its tolerance to the testing methods and its very different nanoscale dimensions.

The combination of both gelators, DBS and BTA, at a range of loadings were investigated in two different solvents, 2-butanone and methanol. Rheological investigations of the gel mixtures found that DBS was the dominant contributor when DBS loadings were kept constant and the loadings of BTA varied. In both solvents, G’

remained constant until high loadings of BTA (150 wt/v% loadings of DBS). BTA gels using 2-butanone were generally stiffer than the same loadings in methanol, which supports the visual morphological differences seen via SEM that BTA forms much larger diameter nanofibres in 2-butanone then in methanol. An NMR investigation implied that BTA and DBS self-assembled into solid-like aggregates in a manner that was largely independent of one another, consistent with them self-sorting. Future work would also include comparison of a dual system against both gelators alone to determine if the dual system could enable better spanning in a woven fabric.

In all cases, SEM images indicated DBS and BTA self-sort into two distinctly sized nanofibres. The exact morphology of the composite was largely dependent on the morphology of the BTA nanofibres which varied in different solvents. These self-sorted systems could also be assembled *in situ* in a non-woven fabric, giving a material containing independent fibres on three different length scales (DBS, BTA and fabric). Mixtures with a constant total loading resulted in the expected trends; as one gelator loading decreased, less of that particular gelator was visible in the fabric. This also supports a self-sorting mechanism. These systems were investigated for their potential impact on air permeability. Generally, mixtures with a total loading of 0.6 wt/v% resulted in higher air permeabilities than pure BTA and DBS at this weight loading. Mixtures with a total loading of 0.4 wt/v% performed similarly to the pure gelators at the same weight loading. It is also suggested that the DBS enhances the robustness of the overall network, as BTA nanofibres did not degrade on testing as they did when used individually (as seen in Chapter 3).

Overall these mixtures of BTA and DBS show a novel self-sorting system with two very different length scales of nanofibres forming. With further optimisation, these could have potential to offer the same protection at lower loadings, minimising the impact on the intrinsic properties of the original non-woven fabric. These mixtures would be potential candidates for filtration testing, as it would be interesting to see how the presence of the three different sized networks could influence the filtration properties across a range of particle sizes.

A range of DBS derivatives were investigated. Both DBS-$CONHNH_2$ and DBS-OCH_3 did not appear to offer any significant advantage over unsubstituted DBS. The morphologies and aggregates observed appeared to be clumped together. With similar aggregates discussed previously, these two DBS derivatives were not investigated further. DBS-SCH_3 did show a morphology on the fabric which did look useful, with good sample spanning, and further testing on fabric samples showed that at the

loadings used (up to 0.4 wt/v%), there was no significant impact on the intrinsic AP or WVP of the fabric. This derivative shows good potential based on the testing to-date and would warrant further fabric testing, particularly with respect to filtration.

Nanofibre branching was attempted by two different methods: the inclusion of a small amount of polymer additive or addition of a dimer gelator. Rheological results indicated that the addition of polymers (PEG and PVA) enhanced gel stability by increasing the gel LVR and increased the stiffness of the gel. All investigations with PEG showed that generally, the higher the molecular weight, the higher the G' value, implying increased gel stiffness. There were no changes in thermal stability using PEG or PVA additives. All gels with the PVA present were stiffer than the control gel with no polymer. No morphological changes could be observed by SEM, although this only observes microstructure and the underpinning nanostructure may have changed. Future work could include investigating polymer additives for their impact on the fabric performance.

A dimer of DBS was successfully synthesised and NMR spectroscopic studies showed it was, to some extent (71%), incorporated into DBS nanofibres. Proof of concept SEM imaging of a fabric treated with a mixture of DBS and the dimer suggested good coverage could be achieved, although this was performed at high DBS loading and further optimisation would be required. Further work would include additional investigation of this dimer, including varying the loadings of both DBS and dimer to see if it influences the network formed with the fabric. Positive results via imaging would lead to scale-up and fabric testing to evaluate filtration performance against aerosols. Further work could also include rheology studies of DBS and dimer mixtures and mechanical testing both in and outside a fabric.

From an application perspective, two key issues remain: the nanofibre network is incomplete and the packing density of the DBS nanofibres is too high. The spanning needs to be improved so that filtration will be fully effective. Future work including using mixed gelators with potential to control the order in which the nanofibres form, could have the potential to improve the spanning. High nanofibre packing density seems to be making the materials act as membranes rather than filters, as evidenced by the large drops in air permeability seen with modified non-woven fabrics. Methods of reducing the packing density could significantly impact on the results. Other future work would include trialling different gelators with different sized nanofibres, their impact on the system and further studies on crosslinking to increase durability.

Chapter 8 - Experimental

8.1 Analysis techniques

All chemicals and solvents were purchased from commercial suppliers (Sigma Aldrich, Alfa Aesar or VWR) and used as provided. NMR spectra were recorded on a JEOL ECX400 (^{1}H 400 MHz, ^{13}C 100 MHz) spectrometer. Assignments were made via DEPT-135 and 2D, ^{1}H-^{1}H COSY and HMQC spectra. Samples were recorded as solutions using deuterated solvents as stated. Chemical shifts (δ) are quoted as parts per million and coupling constants are given in Hz. HRMS and ESI mass spectra were recorded on a Bruker Daltonics Microtof mass spectrometer. Infrared spectra were recorded on a Perkin Elmer Spectrum 2 fitted with an ATR sampling accessory. Absorbance bands are reported as wavenumber of maximum absorbance (cm^{-1}). Alpha D values were obtained using a Jasco DIP-370 digital polarimeter with 589 nm filter fitted. SEM images were obtained on a FEI Sirion XL30 or a JEOL 7800F Prime after splutter coating with 6 nm of Pt/Pd at a density of 19.52 g cm^{-3}. T_{gel} measurements were obtained using a high precision thermoregulated oil bath at 0.5 °C min^{-1} increments. Transparent screw-topped glass vials (2.5 or 8.5 mL) were used to prepare gels. Rheological measurements were obtained using a Malvern Instruments Kinexus Pro+ rheometer fitted with 20 mm parallel plate geometry using a 2.5 mm gap at 25 °C, using rSpace software.

8.1.1 Synthesis of 1,3:2,4-Dibenzylidene-D-sorbitol (DBS)[144]

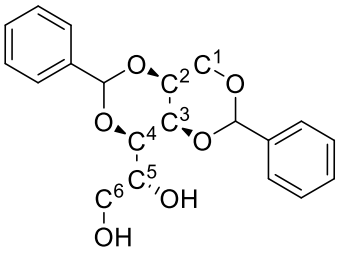

$C_{20}H_{22}O_6$

716.78 g mol^{-1}

D-Sorbitol (4.90 g, 26.9 mmol) was added to a mixture of cyclohexane (35 mL) and methanol (10 mL). A Dean-Stark apparatus was attached and the mixture was stirred at ~300 rpm at 50 °C for 20 minutes under a steady flow of nitrogen gas. *p*-Toluene sulfonic acid monohydrate (1.01 g, 5.31 mmol) and benzaldehyde (4.66 mL, 45.7 mmol) in methanol (20 mL) were stirred at room temperature for 20 minutes before being added dropwise to the D-sorbitol mixture. After the addition, the reaction temperature was increased to 70 °C and the reaction was stirred for 4 hours. The mixture was allowed to cool, before being washed with cold ethanol (300 mL) to

remove unreacted starting material. The crude product was dried under vacuum for 2 hours and left overnight to air dry. The mono-substituted derivative was removed by washing with hot water (400 mL) and the tri-substituted derivative was removed by washing with hot dichloromethane (400 mL). The desired disubstituted product was dried under vacuum for *ca.* 5 hours, then air dried overnight. The product was crushed to give a white powder (5.41 g, 15.1 mmol, 66% yield).

^{1}H NMR (400 MHz, CD_3OD): δ 7.44 (2xdd, J = 8.6, 1.7 Hz, 4H, Ar***H*** (meta)); 7.37-7.31 (m, 6H, Ar***H*** (ortho and para)); 5.63 (s, 2H, ArC***H***); 4.83 (d, J = 5.6 Hz, CHO***H***); 4.40 (dd, J = 5.8 Hz, 1H, CH_2O***H***); 4.16 (dd, J = 12.4, 1.6 Hz, 1H, OC^{1}***H₂***); 4.12 (dd, apparent t, J_{app} = 1.4, 1H, C^{3}***H***); 4.11 (dd, J = 12.4, 1.2 Hz, 1H, OC^{1}***H₂***); 3.91 (d, J = 1.2 Hz, 1H, C^{2}***H***); 3.82 (dd, J = 9.2, 1.6 Hz, 1H, C^{4}***H***); 3.74 (ddd, J = 11.2, 5.2, 2.4 Hz, 1H, C^{5}***H***); 3.57 (2xddd, J = 11.3, 5.2, 2.2 Hz, 1H, C^{6}***H₂***OH); 3.41 (ddd, apparent dt, J = 17.2, 5.5 Hz, 1H, C^{6}***H₂***OH).

^{13}C NMR (100 MHz, DMSO-d_6): δ 139.0 (2 x q ArC); 129.2 (2 x ArCH para); 129.1 (4 x ArCH meta); 128.5 (2 x ArCH ortho); 128.5 (2 x ArCH ortho); 99.8 (Ar-CH); 99.8 (Ar-CH); 78.1 (C^{5}H-OH); 70.6 (C^{3}H); 69.8 (C$^{1}H_2$); 68.9 (C^{2}H); 68.2 (C^{4}H); 63.1 (C$^{6}H_2$OH).

ESI-MS: 381.1308 $[M+Na]^+$ (100%), 359.1482 $[M+H]^+$ (25%)

HRMS: Calcd. $[M+Na]^+$ ($C_{20}H_{22}NaO_6$ in methanol) m/z = 381.1308; found $[M+Na]^+$ m/z = 381.1309 (error 0.1 ppm). Calcd. $[M+H]^+$ ($C_{20}H_{23}O_6$ in methanol) m/z = 359.1489; found $[M+H]^+$ m/z = 359.1482 (error 2.0 ppm)

IR v [cm^{-1}]: 3207*b* (O-H); 2866*w* (C-H); 1451m (C=C); 1402*m*; 1342*m*; 1089s; 1016*s*; 733*s*, 695*ssh*.

$[\alpha]_D^{RT}$: +33.2 (589 nm, 0.5 g/100 mL, MeOH)

Melting point: Onset 114 °C

8.1.2 Synthesis of 1,3:2,4-Dibenzylidene-D-sorbitol-*p,p*'-dimethyl ester (DBS-CO_2Me)[57]

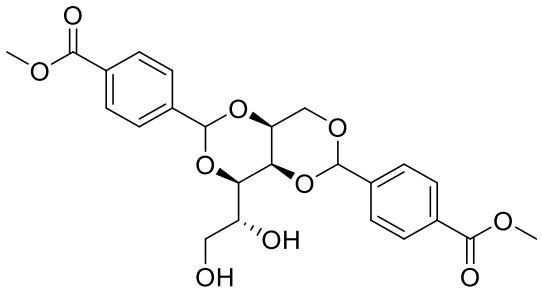

$C_{24}H_{26}O_{10}$

476.46 g mol^{-1}

D-Sorbitol (2.45 g, 13.4 mmol) was added to a mixture of cyclohexane (35 mL) and methanol (10 mL). Dean-Stark apparatus was attached and the mixture was stirred at ~300 rpm at 50 °C for 20 minutes under a steady flow of nitrogen. 4-Methylcarboxylbenzaldehyde (3.79 g, 23.1 mmol) and *p*-toluene sulfonic acid monohydrate (0.50 g, 2.63 mmol) in methanol (20 mL), were stirred at room temperature for 20 min before being added dropwise to the D-sorbitol mixture. After the addition, the reaction temperature was increased to 70 °C and the reaction was stirred for 4 hours. The mixture was allowed to cool, before being washed with cold ethanol (150 mL) to remove unreacted starting material. The crude product was dried on a high vacuum line for 2 hours and left overnight to air dry. The mono-substituted derivative was removed by refluxing for *ca.* 10 minutes with water (3 x 100 mL) and the tri-substituted derivative was removed under reflux for *ca.* 10 minutes with dichloromethane (3 x 100 mL). The product was dried on a high vacuum line for *ca.* 3 hours then air dried overnight. The product was a white powder (2.93 g, 6.18 mmol, 54% yield).

^{1}H NMR (400 MHz, DMSO-d_6): δ 7.95-7.93 (AA'XX' system, J_{app} = 8.4 Hz, 4H, Ar***H*** (meta)); 7.57-7.56 (AA'XX' system, J_{app} = 8.8, 8.4 Hz, 4H, Ar***H*** (ortho)); 5.72 (s, 2H, ArC***H***); 4.90 (d, J = 5.6 Hz, 1H, CHO***H***); 4.44 (dd, apparent t, J_{app} = 5.8 Hz, 1H, CH_2O***H***); 4.22-4.13 (m, 3H, OC^1***H_2***, C^3***H***); 3.97 (s, 1H, C^2***H***); 3.84-3.81 (m, 1H, C^4***H***); 3.81 (s, 6H, OC***H_3***); 3.81-3.74 (m, 1H, C^5***H***); 3.60-3.56 (m, 1H, C^6***H_2***OH); 3.44-3.42 (m, 1H, C^6***H_2***OH).

^{13}C NMR (100 MHz, DMSO-d_6): δ 166.5 (2 x C=O); 143.9, 143.6 (2 x q ArC); 129.6 (2 x ArCH ortho); 129.5 (2 x ArCH ortho); 127.0 (4 x ArCH meta); 130.2 (2 x q ArC para); 99.0 (Ar-C); 99.0 (Ar-C); 78.1 (C^5H); 70.7 (C^3H); 69.83 (C^1H_2); 69.0 (C^2H); 68.1 (C^4H); 63.1 (C^6H_2OH); 52.7 (OCH_3)

HRMS: Calcd. $[M+Na]^+$ ($C_{24}H_{26}NaO_6$ in THF) m/z = 497.1418; found $[M+Na]^+$ m/z = 497.1427 (error 1.8 ppm)

IR v [cm^{-1}]: 3246*b* (OH); 2956*w* (C-H); 1724*ssh* (C=O); 1399*m;* 1275*s*; 1093*s*; 1018*s;* 856*m;* 835*m*; 750*ssh*; 708*m*.

$[\alpha]_D^{RT}$: +44.6 (589 nm, 0.5 g/100 mL, DMF)

Melting point: Onset 181 °C

8.1.3 Synthesis of 1,3:2,4-Dibenzylidene-D-sorbitol-p,p'-dihydrazide (DBS-$CONHNH_2$)[50]

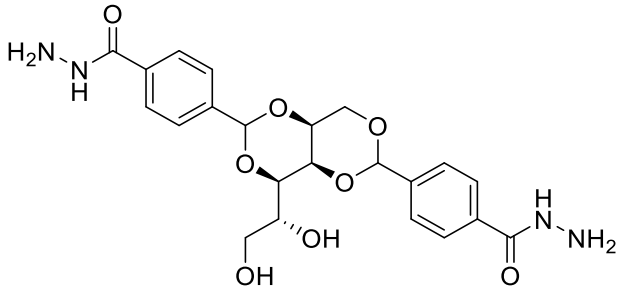

$C_{24}H_{26}N_4O_8$

474.47 g mol^{-1}

To DBS-CO_2Me (1.10 g, 2.32 mmol) in THF (40 mL), hydrazine monohydrate (6 mL, 120 mmol) was added. The reaction mixture was then heated under reflux overnight in an oil bath held at 85 °C. The white precipitate formed was filtered off and rinsed with deionised water (150 mL) and then washed with hot deionised water (150 mL). The product was dried under vacuum for 2.5 hours. The product was a white powder (0.67 g, 1.41 mmol, 61% yield).

^{1}H NMR (400 MHz, DMSO-d_6): δ 9.76 (s, 2H, N***H***NH_2); 7.80-7.78 (AA'XX' system, J_{app} = 8.4 Hz, 4H, Ar***H*** (meta)); 7.50-7.46 (AA'XX' system, J_{app} = 8.4 Hz, 4H, Ar***H*** (ortho)); 5.67 (s, 2H, ArC***H***); 4.89-4.88 (d, J = 6 Hz, 1H, CHO***H***); 4.47 (s, 4H, NHN***H₂***); 4.42 (2xd, apparent t, J = 5.8 Hz, 1H, CH_2O***H***); 4.21-4.11 (m, 3H, C^3***H***, OC^1***H₂***); 3.94 (s, 1H, C^2***H***); 3.85-3.81 (m, 1H, C^4***H***); 3.75-3.69 (m, 1H, C^5***H***); 3.59-3.53 (m, 1H, C^6***H₂***OH); 3.44-3.38 (m, 1H, C^6***H₂***OH).

^{13}C NMR (100 MHz, DMSO-d_6): δ 166.1 (2 x C=O); 141.8, 141.5 (2 x q ArC); 134.0, 134.0 (2 x q ArC para); 127.3 (4 x ArCH meta); 127.2 (2 x ArCH ortho); 126.6 (2 x ArCH ortho); 99.3 (Ar-C); 99.2 (Ar-C); 78.1 (C^5H); 70.6 (C^3H); 69.8 (C^1H_2); 69.0 (C^2H); 68.2 (C^4H); 63.1 (C^6H_2OH).

ESI-MS: 497.1651 $[M+Na]^+$ (100%)

HRMS: Calcd. $[M+Na]^+$ ($C_{22}H_{26}NaN_4O_8$ in DMF) m/z = 497.1643; found $[M+Na]^+$ m/z = 497.1651 (error 1.7 ppm)

IR v [cm^{-1}]: 3295*b* (N-H + O-H); 2956*w* (C-H); 1634*m* (C=O); 1340*m*; 1093*s*; 1021*m*; 1007*m*; 848*m*; 683*m*; 646*m*; 620*m*; 586*m*.

$[\alpha]_D^{RT}$: +42.6 (589 nm, 0.5 g/100 mL, DMF)

Melting point: Burns and decomposes >300 °C

8.1.4 Synthesis of 1,3:2,4-Dibenzylidene-D-sorbitol-*p,p*'-dimethoxy (DBS-OCH_3)[424]

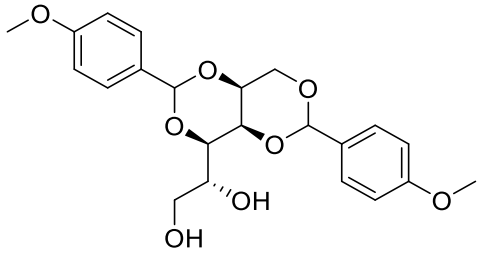

$C_{22}H_{26}O_8$

418.44 g mol^{-1}

D-Sorbitol (4.90 g, 26.9 mmol) was added to a mixture of cyclohexane (35 mL) and methanol (10 mL). A Dean-Stark apparatus was attached and the mixture was stirred at ~300 rpm at 50 °C for 20 minutes under a steady flow of nitrogen. 4-Methoxybenzaldehyde (6.546 mL, 53.8 mmol) and *p*-toluene sulfonic acid monohydrate (1.00 g, 5.26 mmol) in methanol (20 mL), were stirred at room temperature for 20 minutes before being added dropwise to the D-sorbitol mixture. After the addition, the reaction temperature was increased to 70 °C and the reaction was stirred for 4 hours. The mixture was allowed to cool, before being washed with cold ethanol (100 mL) to remove unreacted starting material. The crude product was left to air dry overnight.

The mono-substituted derivative was removed by washing with hot water (2 x 150 mL) and the tri-substituted derivative was removed by washing with hot dichloromethane (2 x 150 mL). The product was dried on a high vacuum line for *ca.* 3 hours then air dried overnight. The product was a white powder (8.89 g, 79% yield).

^{1}H NMR (400 MHz, DMSO-d_6): δ 7.36-7.30 (AA'XX' system, J_{app} = 8.4 Hz, 4H, Ar***H*** (meta)); 6.90-6.87 (AA'XX' system, J_{app} = 8.8, 0.8 Hz, 4H, Ar***H*** (ortho)); 5.57 (d, J = 1.2 Hz, 2H, ArC***H***); 4.09 (d, J = 6.4 Hz, 2H, OC^1***H$_2$***); 4.05 (s, 1H, CHO***H***); 3.84 (d, J = 1.2 Hz, 1H, C^3***H***); 3.82 (s, 1H, C^2***H***); 3.78-3.76 (m, 1H, C^4***H***); 3.71 (s, 6H, OC***H***$_3$); 3.54-3.52 (m, 1H, C^5***H***); 3.38-3.34 (m, 2H, C^6***H$_2$***OH)

^{13}C NMR (100 MHz, DMSO-d_6): δ 159.9, (2 x q ArC para); 132.4 (q ArC), 131.7, 131.4 (2 x ArCH ortho); 130.2 (q ArC), 128.0 (2 x ArCH ortho); 115.0 (2 x ArCH meta), 113.8, 113.7 (2 x ArCH meta); 99.8 (Ar-CH); 78.1 (C^5H); 70.5 (C^3H); 69.8 (C^1H_2); 68.8 (C^2H); 68.2 (C^4H); 63.1 (C^6H_2OH); 56.2, 55.6 (OCH_3).

ESI-MS: 441.1501 $[M+Na]^+$ (100%)

HRMS: Calcd. $[M+Na]^+$ ($C_{22}H_{26}NaO_8$ in methanol) m/z = 441.1520; found $[M+Na]^+$ m/z = 441.1501 (error 4.3 ppm)

IR ν [cm^{-1}]: 3207*b* (O-H); 2831*w* (C-H); 1614*m*; 1516*m* (C=C); 1401*m*; 1343*m*; 1248*s*; 1095*s*; 1006*s*; 832*m*; 780*m*; 616*m*.

$[\alpha]_D^{RT}$: +9.4 (589 nm, 0.5 g/100 mL, methanol)

Melting point: Onset 116 °C

8.1.5 Synthesis of 1,3:2,4-Dibenzylidene-D-sorbitol-*p,p*'-dimethylthioether (DBS-SCH_3)[424]

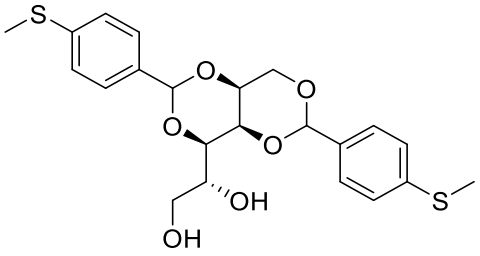

$C_{22}H_{26}O_6S_2$

450.56 g mol^{-1}

D-Sorbitol (2.45 g, 13.5 mmol) was added to a mixture of cyclohexane (35 mL) and methanol (10 mL). A Dean-Stark apparatus was attached and the mixture was stirred at ~300 rpm at 50 °C for 20 minutes under a steady flow of nitrogen. 4-Methylthiobenzaldehyde (3.20 mL, 26.9 mmol) and *p*-toluene sulfonic acid monohydrate (0.50 g, 2.6 mmol) in methanol (20 mL), were stirred at room temperature for 20 minutes before being added dropwise to the D-sorbitol mixture. After the addition, the reaction temperature was increased to 70 °C and the reaction was stirred for 4 hours. The mixture was allowed to cool, before being washed with cold ethanol (100 mL) to remove unreacted starting material. The crude product was left to air dry overnight.

The mono-substituted derivative was removed by washing with hot water (2 x 150 mL) and the tri-substituted derivative was removed by washing with hot dichloromethane (2

x 150 mL). The product was dried on a high vacuum line for *ca.* 3 hours then air dried overnight. The product was a white powder (3.78 g, 70% yield).

^{1}H NMR (400 MHz, DMSO-d_6): δ 7.37 -7.32 (AA'XX' system, J_{app} = 8.4, 7.2 Hz, 4H, Ar***H*** (meta)); 7.23-7.21 (AA'XX' system, J_{app} = 8.4, 1.2 Hz, 4H, Ar***H*** (ortho)); 5.58 (s, 2H, ArC***H***); 4.12-4.07 (m, 3H, OC^{1}***H$_2$***, C^{3}***H***); 3.87 (s, 1H, C^{2}***H***); 3.79-3.76 (m, 1H, C^{4}***H***); 3.71-3.67 (m, 1H, C^{5}***H***); 3.63-3.60 (m, 1H, C^{6}***H$_2$***OH); 3.55-3.52 (m, 1H, C^{6}***H$_2$***OH); 2.46 (s, 6H, SC***H$_3$***).

^{13}C NMR (100 MHz, DMSO-d_6): δ 139.2, 139.1 (2 x q ArC para); 135.9, 135.6 (2 x q ArC); 130.4 (2 x ArCH meta); 127.3 127.3 (2 x ArCH ortho); 125.9, 125.8 (2 x ArCH ortho); 125.7 (2 x ArCH meta); 99.5 (Ar-CH); 78.1 (C^{5}H); 70.5 (C^{3}H); 69.8 (C^{1}H$_2$); 68.8 (C^{2}H), 68.2 (C^{4}H), 63.1 (C^{6}H$_2$OH); 15.2, 14.4 (SCH$_3$).

ESI-MS: 473.1078 $[M+Na]^+$ (100%)

HRMS: Calcd. $[M+Na]^+$ ($C_{22}H_{26}NaO_6S_2$ in methanol) m/z = 473.1078; found $[M+Na]^+$ m/z = 473.1078 (error 3.1 ppm)

IR v [cm^{-1}]: 3209*b* (O-H); 2865*w* (C-H); 1603*m*; 1592*m*; 1497*m*; 1397*m*; 1343*m*; 1094*s*; 1015*s*; 832*m*; 818m; 774*m*; 589*m*; 550*m*.

$[\alpha]_D^{RT}$: +34.8 (589 nm, 0.5 g/100 mL, DMF)

Melting point: Onset 135 °C

8.1.6 Synthesis of Decanedioate bis-6-[1,3:2,4-Dibenzylidene-D-sorbityl] ester (DBS dimer)[149]

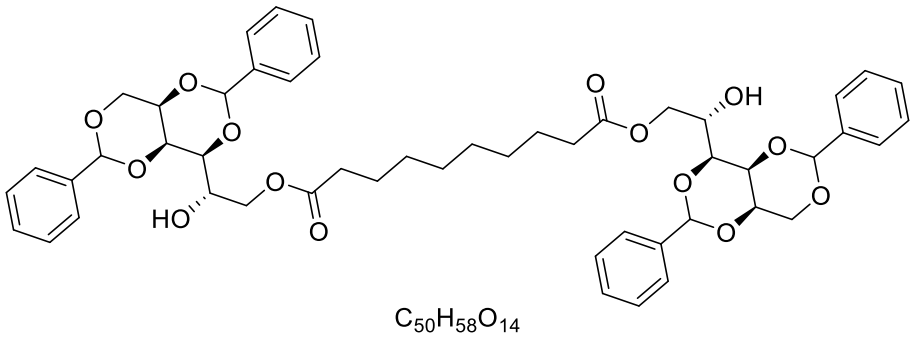

$C_{50}H_{58}O_{14}$

883.00 g mol^{-1}

1,3:2,4-Dibenzylidene-D-sorbitol (0.50 g, 1.4 mmol) was dissolved in acetonitrile (30 mL). Triethylamine (0.22 mL, 1.5 mmol) and sebacoyl chloride (0.15 mL, 0.7 mmol) were added and the mixture was heated under reflux overnight. The clear and colourless reaction solution was cooled, then tipped into cold deionised water (100

mL). The product was filtered off using a sintered glass funnel, and dried in the vacuum oven for 3 hours. The product was a beige powder (0.75 g, 0.85 mmol, 60% yield).

^{1}H NMR (400 MHz, DMSO-d_6): δ 7.60-7.33 (m, 20H, Ar***H***); 5.63 (s, 4H, ArC***H***); 5.42 (d, J = 5.6 Hz, 2H, CHO***H***); 4.27-4.13 (m, 8H, OC^{1}***H$_2$***, C^{3}***H***, C^{2}***H***); 3.98-3.84 (m, 6H, C^{4}***H***, C^{5}***H***); 3.84-3.72 (m, 2H, C***H***OH); 2.29-2.20 (m, 4H, C^{6}***H$_2$***O-DBS); 1.43 (s, 4H, DBS-COCH$_2$C***H$_2$***); 1.17-1.12 (m, 8H, DBS-COCH$_2$CH$_2$(C***H$_2$)$_4$***CH$_2$CH$_2$CO-DBS)

^{13}C NMR (100 MHz, $CDCl_3$): δ 137.7 (4 x q ArC); 129.2 (4 x ArCH para), 128.3 (8 ArCH meta), 126.5 (8 x ArCH ortho); 101.0 (2 x Ar-C); 100.8 (2 x Ar-C); 78.0 (2 x C^{5}H), 70.5 (2 x C^{3}H); 70.1 (2 x C^{1}H$_2$); 68.7 (2 x C^{2}H); 67.3 (2 x C^{4}H); 65.9 (2 x C^{6}H$_2$OH); 34.2, 29.0, 24.9 (8 x CH_2 alkyl).

ESI-MS: 905.3746 $[M+Na]^+$ (100%).

HRMS: Calcd. $[M+Na]^+$ ($C_{50}H_{58}O_{14}$ in chloroform) m/z = 905.3719; found $[M+Na]^+$ m/z = 905.3746 (error 3.1 ppm)

IR ν [cm^{-1}]: 3455*bw* (O-H); 2928*w* (C-H); 1730*m* (C=O); 1168*m*; 1093*sh*; 1027*m*; 827*m*; 754*m*; 738*m*; 696*sh*

$[\alpha]_D^{RT}$: +34.2 (589 nm, 0.5 g/100 mL, chloroform)

Melting point: Onset 163 °C

8.1.7 Synthesis of *N,N',N"*-tris(2-ethylhexyl)-1,3,5-benzenetricarboxamide (BTA)[151]

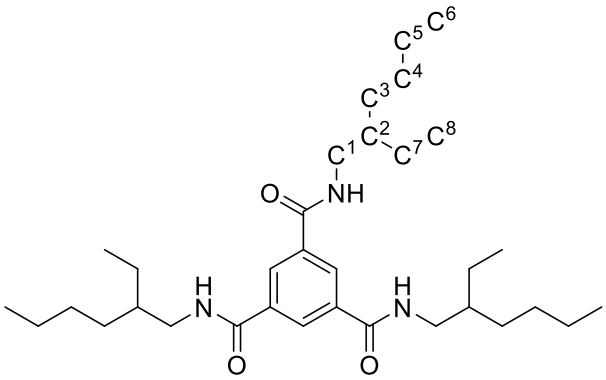

$C_{33}H_{57}N_3O_3$

543.84 g mol^{-1}

1,3,5-Benzenetricarboxylic acid chloride (2.65 g, 10 mmol) was added under nitrogen at 0 °C to a mixture of anhydrous *N*-methylpyrrolidone as a solvent (80 mL), pyridine as a base (20 mL), lithium chloride (0.1 g) and 2-ethylhexylamine (8.52 g, 66 mmol). The reaction mixture was stirred overnight at 60 °C. After cooling to room temperature, the

method deviated from the literature method. Leaving the mixture for 48 hours significantly enhanced the yield. The reaction mixture was then allowed to form a precipitate on pouring into ice water. The precipitate was filtered off, and the product was isolated by recrystallization from methanol. Yield (4.77 g, 87%). The product appeared as white needle-like crystals.

^{1}H NMR (400 MHz, DMSO-d_6): δ 8.57 (t, J = 5.6 Hz, 3H, N***H***); 8.30 (s, 3H, Ar-***H***); 3.16 (t, J = 6.0 Hz, 6H, C^1***H_2***); 1.52 (m, 3H, C^2***H***); 1.32-1.23 (m, 24H, (C^7***H_2***)C^3***H_2***C^4***H_2***C^5***H_2***); 0.84-0.81 (m, 18H, (C^8***H_3***)C^6***H_3***).

^{13}C NMR (100 MHz, DMSO-d_6): δ 166.2 (C=O); 135.7 (q ArC); 128.9 (other ArC); 43.1 (C^1H_2); 30.9 (C^2H); 28.9 (C^4H_2); 24.2 ((C^7H_2)C^3H_2); 23.0 (C^8H_3); 14.5 ($C^5H_2CH_3$); 11.2 (C^6H_3).

ESI-MS: 544.4455 $[M+H]^+$ (96%); 566.4270 $[M+Na]^+$ (4%)

HRMS: Calcd. $[M+Na]^+$ ($C_{33}H_{57}N_3NaO_3$ in methanol) m/z = 566.4292; found $[M+Na]^+$ m/z = 566.4270 (error 4.6 ppm) Calcd. $[M+H]^+$ ($C_{33}H_{58}N_3O_3$ in methanol) m/z = 544.4473; found $[M+H]^+$ m/z = 544.4455 (error 3.0 ppm)

IR v [cm^{-1}]: 3241*b* (O-H); 3076*m*; 2958m; 2925m (C-H); 2872m; 2858m; 1637*m* (C=O); 1558*m*; 1457*m*; 1441m; 1294*s*; 727*m*; 692*m*.

Melting point: Onset 285 °C

8.2 Preparation of Gels

A known amount of gelator was accurately weighed out into a 2 mL glass vial with an internal diameter of 9 mm. A Gilson pipette was used to add solvent to the vial. The sample was heated to just below the boiling point of the solvent with the cap on until the gelator dissolved and a homogeneous solution formed. The sample was then left overnight at room temperature to cool, forming a gel.

8.3 Minimum Gelation Concentration

Gels of decreasing concentration were formed. A sample of each concentration in a 2 mL glass vial with an internal diameter of 9 mm, was inverted to identify if the gel was self-supporting under gravity. The lowest concentration at which the gel could support its own weight when inverted was reported as the minimum gelation concentration (MGC).

8.4 T_{gel} testing

The temperature at which the gel sample broke down (T_{gel}) was determined using the vial 'inversion' method. Gels were made in 2 mL transparent screw-capped vials with an internal diameter of 9 mm using a solvent volume of 0.5 mL. The gel was immersed and heated in a thermostated oil bath with a 0.5 °C min^{-1} ramp. At each 0.5 °C temperature increment, the gel was removed from the oil bath and inverted. The temperature at which the gel could no longer hold its own weight upon inversion of the vial was recorded as the T_{gel} temperature.

8.5 NMR Mobility testing

A known amount of gelator was accurately weighed out into a 2 mL glass vial. Deuterated methanol was added (1 mL) and then the sample spiked with 2 µl of DMSO. Gilson pipettes were used to add solvent to the vial. The sample was heated to just below the boiling point of the solvent with the cap on until the gelator dissolved and a homogeneous solution formed. The sample was then transferred into an NMR tube and left overnight to form a gel. Where more than one gelator was present, each gelator was weighed separately then dissolved in 0.5 mL methanol spiked with 1 µl of DMSO before being mixed as two solutions in a glass vial before transferring to an NMR tube.

8.6 Rheological testing

Dynamic rheological measurements were performed using a Malvern Kinexus Pro+ rotational rheometer at 25 °C with parallel plate geometry (20 mm diameter) at a gap of 2.5 mm. All gels (1 mL volume) were prepared in a transparent 5 mL vial with an internal diameter of 13 mm, then de-moulded using a spatula and carefully transferred onto the bottom plate. Oscillatory amplitude sweeps were performed from 0.05% to 50% strain at 1 Hz, to determine the linear viscoelastic region (LVR) for each sample. Oscillatory frequency sweeps were performed from 50 Hz to 0.1 Hz under a shear strain of 0.1%, which was within the linear viscoelastic region for all samples. Data were processed using rSpace software.

8.7 Preparation of SEM samples

SEM samples were prepared by weighing a known mass of gelator into 2 mL vials, followed by the addition of 0.5 mL of solvent. The samples were then heated until all

the gelator had dissolved. A few drops of the solution were then pipetted directly onto the SEM stub and left to dry overnight at ambient conditions.

Generally, fabric samples were dip coated. A known amount of gelator was weighed into a 10 mL vial, followed by addition of 2 mL of solvent. The sample was then heated to dissolve the gelator, and then the whole solution was poured into a metal weighing boat containing the preweighed fabric. The fabric was left to soak in the solution for 5 min, before removing and placing on an aluminium block to dry. After drying overnight, the samples were reweighed and stuck onto the SEM stubs using double-sided tape.

8.7.1 Preparation of Fabrics - Dropping

A small square of fabric was cut and the gelator solution made up as in section 8.7. An aliquot of this solution was then pipetted onto the top of the fabric sample which in turn was on top of a flat aluminium surface. A Gilson pipette was used to accurately pipette aliquots onto the fabric. The fabric was then left to dry without moving it overnight and reweighed before attaching to an aluminium SEM stub with double sided sticky tape.

8.8 Fabric Testing

Samples of fabric were prepared for testing at the University of Leeds in the textile department, and left to dry overnight. They were then transferred to the fabric testing laboratory and conditioned for 24 hours at a set humidity and temperature (*ca.* 293 K and *ca.* 65% relative humidity) before being tested.

8.8.1 Determination of air permeability

Testing was completed to British Standard EN ISO 9073-15:2008 on a TexTest instrument, FX 3300 Lab Air. This specifies a method of measuring the velocity of an air flow passing perpendicularly through a given area of test specimen fabric under a prescribed air pressure differential over a given time period. Each test sample of at least 100 mm by 100 mm was clamped on the head of the test instrument and sealed. The suction was started and the air flow regulated until the desired pressure drop was attained. The air permeability was reported in units of $cm^3/cm^2/s$. Each fabric sample was tested at least 5 times over a test area of 5 cm^3 at a test pressure of 100 Pa as per the British Standard.

8.8.2 Water vapour permeable apparel testing

Testing was completed to British Standard 7209:1990 on a British Standard turntable breathability tester, which measures the water permeability, i.e. how much water is lost over a given time period.

A circular test specimen of 140 mm was sealed over the open mouth of a test dish, which contained water, and the assembly placed in a controlled atmosphere (65 ± 2% humidity, and temperature of 20 ± 2 °C) and rotated on a turntable for the duration of the test. Following an equilibrium period of 1 hour to establish the water vapour pressure gradient across the sample, successive weighings of the assembled dish were made and the rate of water vapour permeation through the specimen was determined relative to a reference fabric. The reference fabric was a precision, high tenacity polyester woven monofilament mesh with 18 µm mesh aperture, 32 µm yarn diameter, 196.1 threads per cm, 12.5% open area with a water vapour permeability (WVP) of around 1000 g/m^2/day. The WVP is given by the equation:

$$WVP = \frac{24M}{At}$$

where *M* is the loss in mass of the assembly over the time period t (in g); *t* is the time between successive weighings of the assembly (in h); *A* is the area of exposed test fabric (equal to the internal area of the test dish) (in m^2); where *A* is given by the equation:

$$A = \left(\frac{\pi d^2}{4}\right) \times 10^{-6}$$

where *d* is the internal diameter of the test dish (in mm).

The water vapour permeability index (*I*) is given by means of the following equation:

$$I = \left\{\frac{(WVP)_f}{(WVP)_r}\right\} \times 100$$

where $(WVP)_f$ is the mean water vapour permeability of the fabric under test; $(WVP)_r$ is the water vapour permeability of the reference fabric.

At least 3 samples of each fabric were tested over a range of time periods from 12 to 30 hours and the water vapour permeability and index calculated for each then averaged in units of g/m^2/day and no units respectively.

8.8.3 Filtration Testing

Samples were prepared in York then transported to Porton Down for testing. Filtration tests were performed on a small scale aerosol testing rig (SSATR) at Porton Down, with NaCl particles in the range 0.2 – 0.6 µm (averaged 0.3 µm) produced by an aerosol sprayer loaded with 1 wt/v% solution of NaCl (10 g l^{-1}). The prepared fabrics were placed inside the rig with an exposed diameter of 16 cm, area 201 cm^3. The filtration experiments were conducted in a filter test rig with an air stream at a constant flow rate of 16 l min^{-1}, against an exposed fabric area of 201 cm^3 and a challenge presented by the aerosol particles of 100% from 1 wt/v% NaCl. Three samples of each fabric composite were prepared and tested. The air was sampled before and after the fabric, the pressure drop and downstream challenge were recorded every second for 6 minutes. The small scale aerosol rig consisted of an upstream photometer 3000L, a downstream photometer 1250, a NaCl particle generator 2000 and a sample holder 1400S all from SFP Services Ltd. Also used to complete the testing were a DPM manometer 570S and Grant data loggers from 2010 series.

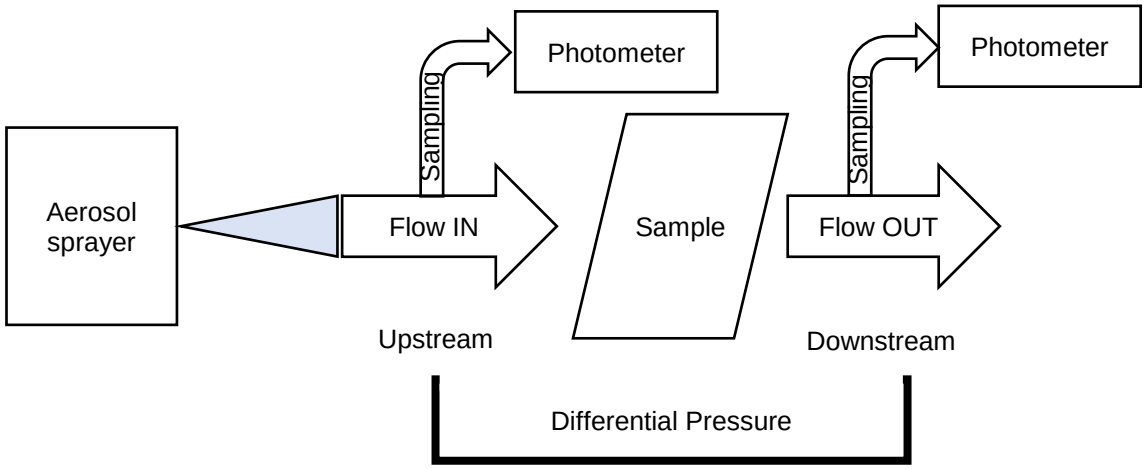

Figure 8-1. Schematic of Small Scale Aerosol Testing Rig (SSATR).

8.8.4 Wind Tunnel Testing

Fabric samples with a diameter of 14 cm were prepared in York then transported to Silsoe Application Spray Unit for testing in a wind tunnel.

Liquid aerosol can be sprayed into the tunnel, which dries to form aerosol particles. For this testing, fluorescein was used as the aerosol, simply as it is easy to measure and quantify the results via fluorimetry. In its liquid aerosol form, fluorescein has a diameter of about 20 µm, but in its dried form is only 2 µm. Fluorescein was sprayed into the tunnel at a known area density using a solution of known concentration.

A rig was constructed to allow testing of the prepared fabrics, as shown in Figure 8-2. The prepared fabrics were attached onto a drainpipe of diameter 11 cm. Inside this drainpipe was a wire mesh, with three “collection tapes” distributed evenly vertically on the mesh. The rear of the drainpipe was covered with an electrostatic fabric to stop any dried aerosol entering the pipe from the rear and affecting the deposition quantities. This rig was then placed inside the wind tunnel, under the ambient flow of dried fluorescein as in Figure 8-3. Each run alternated which side of the wind tunnel the blanks were arranged, i.e. for the first run they were positioned in the three positions nearest the door and then in the second run, they were in the three positions nearest the wall and the treated fabrics were nearest the door. In one run, 3 blank fabrics and 3 treated fabrics (of the same concentration and gelator) were tested. This meant an average result could be gained and run-to-run variations should be accounted for.

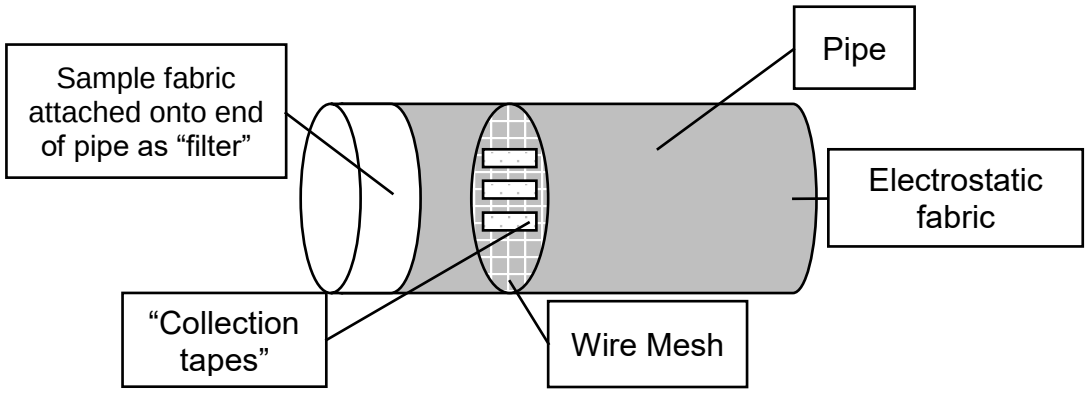

Figure 8-2. Rig set up for testing of treated fabrics at Silsoe.

Figure 8-3. Demonstration of the 6 samples run each test within the wind tunnel; 3 blanks and 3 treated.

The tapes from the wire meshes were carefully collected and analysed. The tapes are soluble so they were collected in individual plastic pots, to which a known aliquot of water was added. The tapes were then dissolved and a smaller aliquot of the solution analysed on the fluorimeter. The more fluorescein deposited on the tapes, the higher

the fluorescence of the solution aliquot and therefore the less aerosol the fabric had filtered out.

Appendix

Table A-1. Table of SEM images for 0.5 wt/v% DBS in methanol, chloroform and toluene at low and high magnification, scale bars of 1 µm and 200 nm, respectively.

	X 5000	X 75 000
Methanol	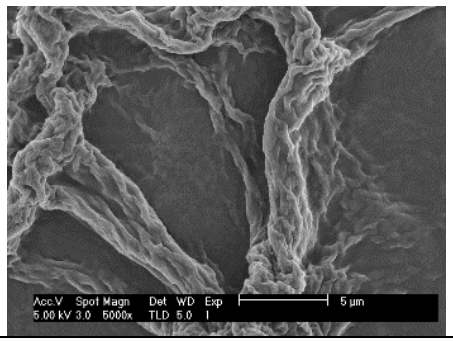	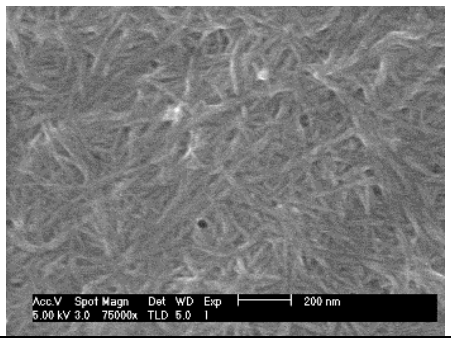
Chloroform	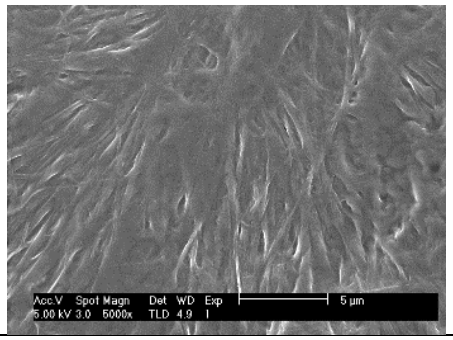	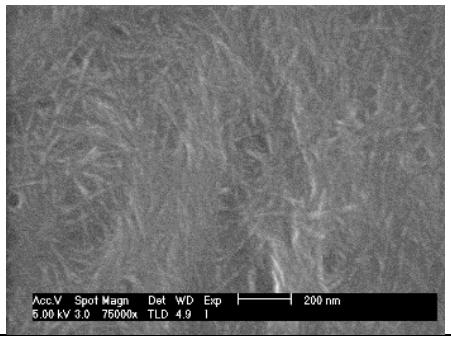
Toluene	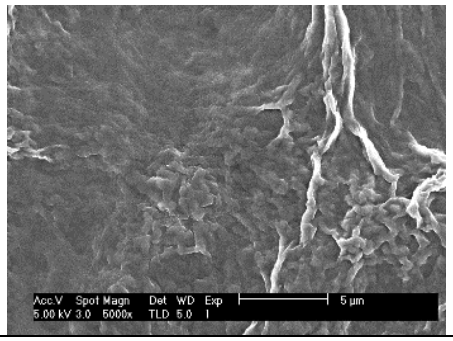	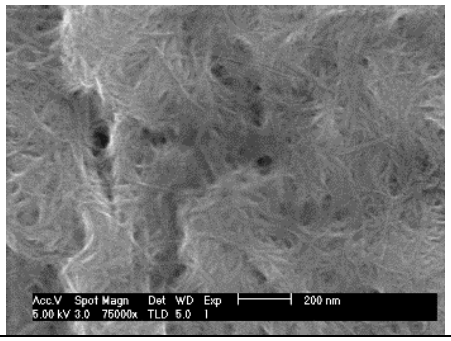

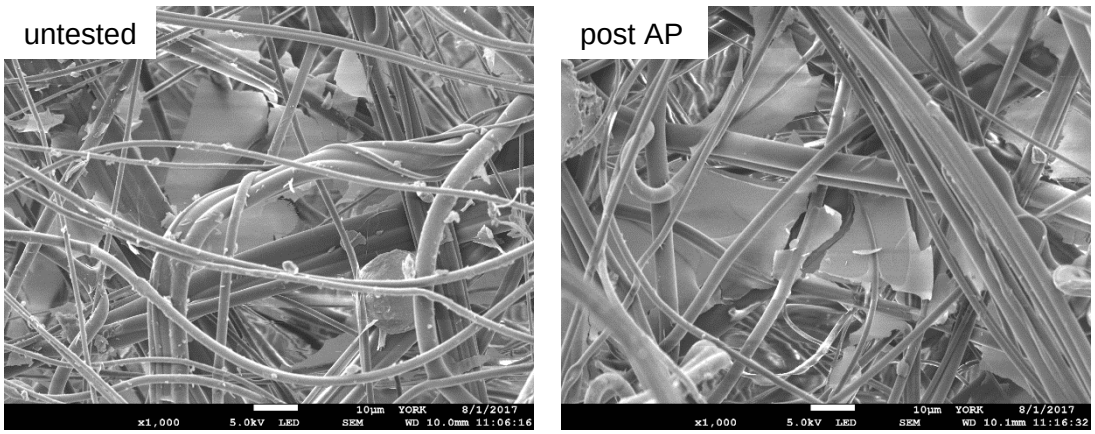

Figure A-0-1. SEM images of non-woven fabric prepared with 0.2 wt/v% DBS in methanol before and after air permeability testing with scale bars of 10 µm.

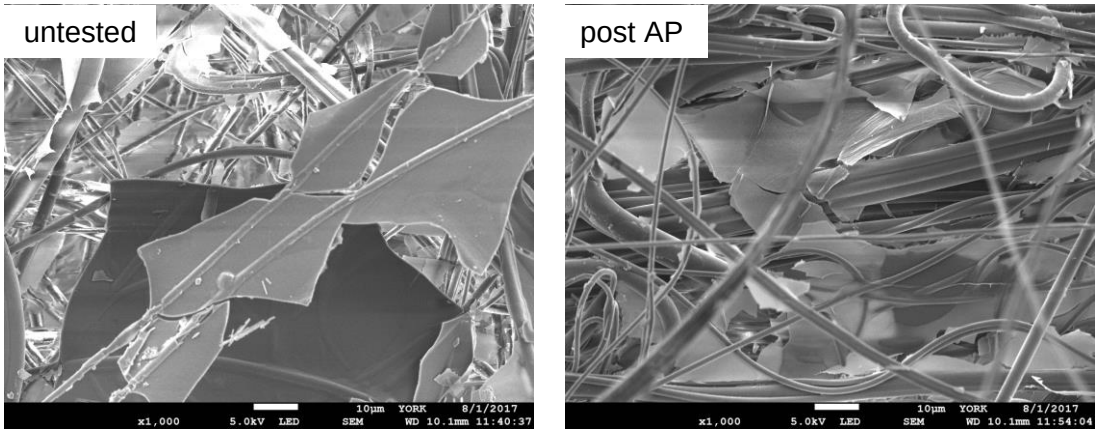

Figure A-0-2. SEM images of non-woven fabric prepared with 0.4 wt/v% DBS in methanol before and after air permeability testing with scale bars of 10 µm.

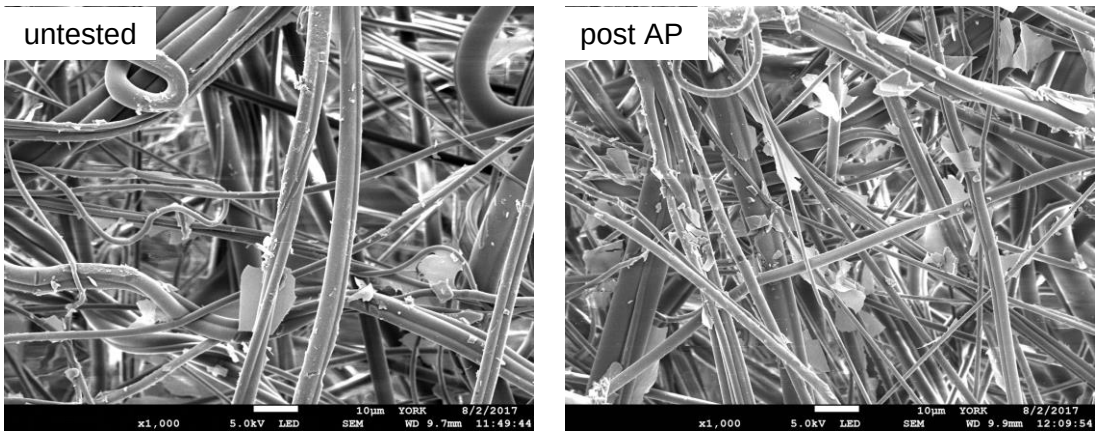

Figure A-0-3. SEM images of non-woven fabric prepared with 0.6 wt/v% DBS in methanol before and after air permeability testing with scale bars of 10 µm.

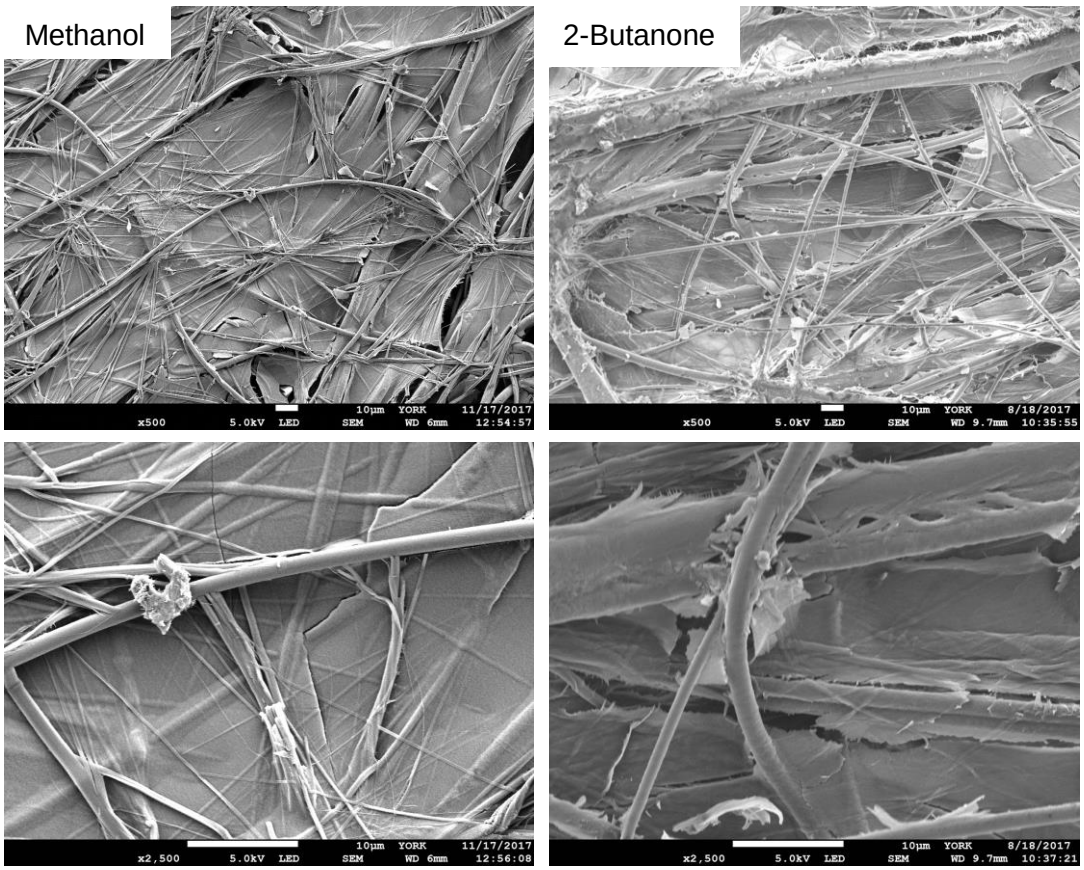

Figure A-0-4. SEM images of 0.4 wt/v% DBS 0.2 wt/v% BTA in a non-woven fabric prepared from methanol and 2-butanone at x500 magnification with scale bars of 10 µm, followed by x2500 magnification with scale bars of 10 µm.

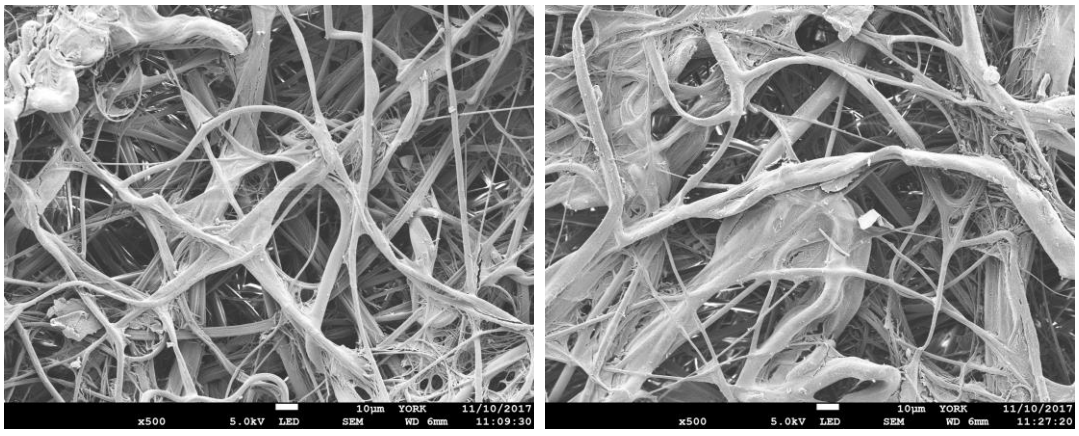

Figure A-0-5. SEM images of 0.3 wt/v% DBS and 0.3 wt/v% BTA prepared in non-woven fabric using 2-butanone before and after air permeability testing at x500 magnification with scale bars of 10 µm.

List of Abbreviations

AP	Air permeability
Ar	Aromatic
BC	Before Christ
BTA	*N,N',N"*-tris(2-ethylhexyl)-1,3,5-benzenetricarboxamide
ca.	Circa
$CDCl_3$	Deuterated chloroform
COSY	Correlation Spectroscopy
CWA	Chemical warfare agent
d	Doublet
dd	doublet of doublets
Da	Daltons
DBS	1,3:2,4-dibenzylidene-d-sorbitol
DBS-CO_2Me	1,3:2,4-Dibenzylidene-d-sorbitol-*p,p*'-dimethyl ester
DBS-$CONHNH_2$	1,3:2,4-Dibenzylidene-d-sorbitol-*p,p*'-dihydrazide
DBS-OCH_3	1,3:2,4-Dibenzylidene-d-sorbitol-*p,p*'-dimethylthioether
DBS-SCH_3	1,3:2,4-Dibenzylidene-d-sorbitol-*p,p*'-dimethoxy
DCM	Dichloromethane
DCP	Diethylchlorophosphate
DEPT	Distortionless enhancement by polarization transfer
DMF	Dimethylformamide
DMMP	Dimethyl methylphosphonate
DMSO	Dimethylsulfoxide
DSTL	Defence Science and Technology Laboratory
ESI-MS	Electrospray Ionisiation-Mass Spectroscopy
EVACP	Ethylene/vinyl acetate copolymer
FTIR	Fourier Transform Infrared
G'	Storage/elastic modulus
G"	Loss/viscous modulus
G*	Complex modulus
GD	Soman
HMQC	Heteronuclear Multiple-Quantum Correlation
HRMS	High resolution Mass spectrometry
HSA	R-12-hydroxystearic acid
HSP	Hansen Solubility Parameters
IR	Infrared
J	Coupling constant
K	Kelvin
kPa	Kilo Pascals
L-DHL	Lanosta-8,24-dien-3β-ol:24,25-dihydrolanosterol = 56:44
LED	Light emitting diode
LMWG(s)	Low molecular weight gelator(s)
LVR	Linear viscoelastic region
m	Multiplet
MBS	2,4-Monobenzylidene-d-sorbitol

mdeg	Millidegrees
MeOH	Methanol
MGC	Milligram
MGC	Minimum gelation concentration
MHz	Mega Hertz
min(s)	Minute(s)
mL	Millilitre
mm	Millimetre
mmol	Millimole
MMD	Mass median diameter
MS	Mass Spectroscopy
MSM	Meltblown-spunbond-meltblown
MW	Molecular weight
m/z	Mass to charge ratio
NASA	The National Aeronautics and Space Administration
NJC	New Japan Chemical Company
nm	Nanometres
NMR	Nuclear magnetic resonance
NW	Non-woven
Pa	Pascals
PCM	Phase change material
PDMS	Poly(dimethylsiloxane)
PEG	Poly(ethylene glycol)
PMMMS	Poly(methyl methacrylate comethacrylic acid
PNIPAM	Poly(N-isopropylacrylamide)
ppm	Parts per million
PPLG	N,N’-bisocta-decyl-2-(3-(pyridin-2-yl)-1H-pyrazol-1-yl)-l-glutamic amide
PTFE	Poly(tetrafluoroethane)
PVA	Poly(vinyl acetate)
q	Quartet
s	Singlet
SEM	Scanning electron microscopy
SSATR	Small scale aerosol testing rig
t	Triplet
TBS	1,3:2,4:5,6-Tribenzylidenne-d-sorbitol
TEM	Transmission electron microscopy
T_{gel}	Transition temperature from gel to solution
THF	Tetrahydrafuran
US	United States
UV	Ultra-violet
WVP	Water vapour permeability
WWI	World War I
% wt/v	Percent weight by volume
δ	Phase Angle / Chemical Shift
θ	Ellipticity
λ	Wavelength

References

1. J. Patocka and J. Fusek, *Cent. Eur. J. Public Health*, 2004, **12**, S75-77.
2. K. Ganesan, S. K. Raza and R. Vijayaraghavan, *J. Pharm. Bioallied Sci*, 2010, **2**, 166-178.
3. P. Aas, *Prehosp. Disaster Med.*, 2003, **18**, 306-312.
4. V. Gamba, A. Neritani and E. Schanze, *Third report of the Organization for the Prohibition of Chemical Weapons - United Nations Joint Investigative Mechanism*, Report S/2016/738, 2016.
5. T. Okumura, K. Suzuki, A. Fukuda, A. Kohama, N. Takasu, S. Ishimatsu and S. Hinohara, *Acad. Emerg. Med.*, 1998, **5**, 618-624.
6. M. Boopathi, B. Singh and R. Vijayaraghavan, *Open Text. J.*, 2008, **1**, 1-8.
7. W. B. Marzi, The Third International Symposium on protection against chemical warfare agents, Stockholm, Sweden, 1989, 21-24.
8. M. G. Katz, The Third International Symposium on protection against chemical warfare agents, Stockholm, Sweden, 1989, 25-31.
9. G. Huzhang, J. Qitai and Z. Lei, The Third International Symposium on protection against chemical warfare agents, Stockholm, Sweden, 1989, 33-38.
10. G. Fang, H. Dingmao, L. Guojin, Z. Weixin and L. Jiangge, The Third International Symposium on protection against chemical warfare agents, Stockholm, Sweden, 1989, 39-44.
11. G. Fang, The Second International Symposium on protection against chemical warfare agents, Stockholm, Sweden, 1986, 51-58.
12. E. E. Alexandroff, Second international symposium on protection against chemical warfare agents, Stockholm, Sweden, 1986, 67-76.
13. E. E. Alexandroff, Third international symposium on protection against chemical warfare agents, Stockholm, Sweden, 1989, 63-70.
14. V. Obsel and V. Stein, Fourth International Symposium on protection against chemical warfare agents, Stockholm, Sweden, 1992, 63.
15. S. Thandavamoorthy, N. Gopinath and S. S. Ramkumar, *J. Appl. Polym. Sci.*, 2006, **101**, 3121-3124.
16. S. Ramakrishna, K. Fujihara, W.-E. Teo, T. Yong, Z. Ma and R. Ramaseshan, *Mater. Today*, 2006, **9**, 40-50.
17. N. L. Lala, R. Ramaseshan, L. Bojun, S. Sundarrajan, R. S. Barhate, L. Ying-jun and S. Ramakrishna, *Biotechnol. Bioeng.*, 2007, **97**, 1357-1365.
18. L. Zhang, J. Luo, T. J. Menkhaus, H. Varadaraju, Y. Sun and H. Fong, *J. Membr. Sci.*, 2011, **369**, 499-505.
19. M. Montazer and S. B. Malekzadeh, *J. Polym. Res.*, 2012, **19**, 9980.
20. P. Gibson, H. Schreuder-Gibson and D. Rivin, *Colloids Surf., A*, 2001, **187**, 469-481.
21. R. Ramaseshan, S. Sundarrajan, Y. Liu, R. S. Barhate, N. Lala, L. and S. Ramakrishna, *Nanotechnol.*, 2006, **17**, 2947.
22. J. van Esch and B. Feringa, *Angew. Chem. Int. Ed.*, 2000, **39**, 2263-2266.

23. G. C. Maity, *J. Phys. Sci.*, 2007, **11**, 156-171.
24. D. Jordan Lloyd, *Colloid Chemistry*, The Chemical Catalog Co, New York, 1926.
25. P. Terech and R. G. Weiss, *Chem. Rev.*, 1997, **97**, 3133-3160.
26. J. W. Steed, *Chem. Commun.*, 2011, **47**, 1379-1383.
27. L. A. Estroff and A. D. Hamilton, *Chem. Rev.*, 2004, **104**, 1201-1218.
28. M. de Loos, B. L. Feringa and J. H. van Esch, *Eur. J. Org. Chem.*, 2005, **2005**, 3615-3631.
29. P. J. Flory, *Faraday Discuss. Chem. Soc.*, 1974, **57**, 7-18.
30. N. M. Sangeetha and U. Maitra, *Chem. Soc. Rev.*, 2005, **34**, 821-836.
31. P. Dastidar, *Chem. Soc. Rev.*, 2008, **37**, 2699-2715.
32. L. E. Buerkle and S. J. Rowan, *Chem. Soc. Rev.*, 2012, **41**, 6089-6102.
33. J. W. Steed, *Chem. Soc. Rev.*, 2010, **39**, 3686-3699.
34. S. S. Babu, V. K. Praveen and A. Ajayaghosh, *Chem. Rev.*, 2014, **114**, 1973-2129.
35. A. R. Hirst, D. K. Smith, B. Escuder and J. F. Miravet, *Angew. Chem. Int. Ed.*, 2008, **47**, 8002-8018.
36. G. Yu, X. Yan, C. Han and F. Huang, *Chem. Soc. Rev.*, 2013, **42**, 6697-6722.
37. D. K. Smith, *Chem. Soc. Rev.*, 2009, **38**, 684-694.
38. G. C. Maity, *J. Phys. Sci.*, 2013, **46**, 132-140.
39. J. Raeburn, A. Zamith Cardoso and D. J. Adams, *Chem. Soc. Rev.*, 2013, **42**, 5143-5156.
40. D. K. Kumar and J. W. Steed, *Chem. Soc. Rev.*, 2014, **43**, 2080-2088.
41. F. M. Menger and K. L. Caran, *J. Am. Chem. Soc.*, 2000, **122**, 11679-11691.
42. K. A. Houton, K. L. Morris, L. Chen, M. Schmidtmann, J. T. A. Jones, L. C. Serpell, G. O. Lloyd and D. J. Adams, *Langmuir*, 2012, **28**, 9797-9806.
43. J. R. Moffat and D. K. Smith, *Chem. Commun.*, 2008, 2248-2250.
44. M. de Loos, J. van Esch, I. Stokroos, R. M. Kellogg and B. L. Feringa, *J. Am. Chem. Soc.*, 1997, **119**, 12675-12676.
45. Y. Wang, L. Tang and J. Yu, *Cryst. Growth Des.*, 2008, **8**, 884-889.
46. J. Cui, Z. Shen and X. Wan, *Langmuir*, 2010, **26**, 97-103.
47. D. J. Adams, K. Morris, L. Chen, L. C. Serpell, J. Bacsa and G. M. Day, *Soft Matter*, 2010, **6**, 4144-4156.
48. J. H. van Esch, *Langmuir*, 2009, **25**, 8392-8394.
49. D. K. Smith, *Tetrahedron*, 2007, **63**, 7283-7284.
50. B. O. Okesola and D. K. Smith, *Chem. Commun.*, 2013, **49**, 11164-11166.
51. B. O. Okesola, V. M. P. Vieira, D. J. Cornwell, N. K. Whitelaw and D. K. Smith, *Soft Matter*, 2015, **11**, 4768-4787.
52. S. Banerjee, R. K. Das and U. Maitra, *J. Mater. Chem.*, 2009, **19**, 6649-6687.

53. L. Chen, J. Raeburn, S. Sutton, D. G. Spiller, J. Williams, J. S. Sharp, P. C. Griffiths, R. K. Heenan, S. M. King, A. Paul, S. Furzeland, D. Atkins and D. J. Adams, *Soft Matter*, 2011, **7**, 9721-9727.

54. M. J. Clemente, R. M. Tejedor, P. Romero, J. Fitremann and L. Oriol, *New J. Chem.*, 2015, **39**, 4009-4019.

55. K. Murata, M. Aoki, T. Suzuki, T. Harada, H. Kawabata, T. Komori, F. Ohseto, K. Ueda and S. Shinkai, *J. Am. Chem. Soc.*, 1994, **116**, 6664-6676.

56. D. Bardelang, F. Camerel, J. C. Margeson, D. M. Leek, M. Schmutz, M. B. Zaman, K. Yu, D. V. Soldatov, R. Ziessel, C. I. Ratcliffe and J. A. Ripmeester, *J. Am. Chem. Soc.*, 2008, **130**, 3313-3315.

57. D. J. Cornwell, B. O. Okesola and D. K. Smith, *Soft Matter*, 2013, **9**, 8730-8736.

58. D. J. Cornwell, B. O. Okesola and D. K. Smith, *Angew. Chem. Int. Ed.*, 2014, **53**, 12461-12465.

59. D. J. Cornwell and D. K. Smith, *Mater. Horiz.*, 2015, **2**, 279-293.

60. G. K. Veits, K. K. Carter, S. J. Cox and A. J. McNeil, *J. Am. Chem. Soc.*, 2016, **138**, 12228-12233.

61. R. Stan, N. Chira, C. Ott, C. Todasca and E. Perez, *Rev. Chim.*, 2008, **58**, 273-276.

62. K. J. C. van Bommel, M. C. A. Stuart, B. L. Feringa and J. van Esch, *Org. Biomol. Chem.*, 2005, **3**, 2917-2920.

63. X. Yang, G. Zhang and D. Zhang, *J. Mater. Chem.*, 2012, **22**, 38-50.

64. S. S. Rohner, J. Ruiz-Olles and D. K. Smith, *RSC Adv.*, 2015, **5**, 27190-27196.

65. S. Wu, J. Gao, T. J. Emge and M. A. Rogers, *Soft Matter*, 2013, **9**, 5942-5950.

66. J. Le Bideau, L. Viau and A. Vioux, *Chem. Soc. Rev.*, 2011, **40**, 907-925.

67. P. C. Marr and A. C. Marr, *Green Chem.*, 2016, **18**, 105-128.

68. T. Kato, Y. Hirai, S. Nakaso and M. Moriyama, *Chem. Soc. Rev.*, 2007, **36**, 1857-1867.

69. T. Kato, G. Kondo, K. Hanabusa, T. Kutsuna and M. Ukon, *US Patent 6074710*, 2000.

70. R. H. C. Janssen, V. Stümpflen, M. C. W. van Boxtel, C. W. M. Bastiaansen, D. J. Broer, T. A. Tervoort and P. Smith, *Macromol. Symp.*, 2000, **154**, 117-126.

71. N. Mohmeyer, P. Wang, H.-W. Schmidt, S. M. Zakeeruddin and M. Grätzel, *J. Mater. Chem.*, 2004, **14**, 1905-1909.

72. Z. Huo, S. Dai, C. Zhang, F. Kong, X. Fang, L. Guo, W. Liu, L. Hu, X. Pan and K. Wang, *J. Phys. Chem. B*, 2008, **112**, 12927-12933.

73. L. Li, Q. Zhang, H. Huo, J. Zhou and L. Li, *RSC Adv.*, 2016, **6**, 88820-88825.

74. S. Sun, J. Song, Z. Shan and R. Feng, *J. Electroanal. Chem.*, 2012, **676**, 1-5.

75. V. R. Basrur, J. Guo, C. Wang and S. R. Raghavan, *ACS Appl. Mater. Interfaces*, 2013, **5**, 262-267.

76. A. R. Hirst, I. A. Coates, T. R. Boucheteau, J. F. Miravet, B. Escuder, V. Castelletto, I. W. Hamley and D. K. Smith, *J. Am. Chem. Soc.*, 2008, **130**, 9113-9121.

77. S. Liu, W. Yu and C. Zhou, *Soft Matter*, 2013, **9**, 864-874.

78. Q. Jin, L. Zhang and M. Liu, *Chem. Eur. J.*, 2013, **19**, 9234-9241.

79. C. Liu, Q. Jin, K. Lv, L. Zhang and M. Liu, *Chem. Commun.*, 2014, **50**, 3702-3705.

80. C.-H. Gu, H. Li, R. B. Gandhi and K. Raghavan, *Int. J. Pharm.*, 2004, **283**, 117-125.

81. W. Edwards, C. A. Lagadec and D. K. Smith, *Soft Matter*, 2011, **7**, 110-117.

82. M. Raynal and L. Bouteiller, *Chem. Commun.*, 2011, **47**, 8271-8273.

83. A. R. Hirst and D. K. Smith, *Langmuir*, 2004, **20**, 10851-10857.

84. N. Yan, Z. Xu, K. K. Diehn, S. R. Raghavan, Y. Fang and R. G. Weiss, *Langmuir*, 2013, **29**, 793-805.

85. J. Gao, S. Wu and M. A. Rogers, *J. Mater. Chem.*, 2012, **22**, 12651-12658.

86. Y. Lan, M. G. Corradini, X. Liu, T. E. May, F. Borondics, R. G. Weiss and M. A. Rogers, *Langmuir*, 2014, **30**, 14128-14142.

87. K. K. Diehn, H. Oh, R. Hashemipour, R. G. Weiss and S. R. Raghavan, *Soft Matter*, 2014, **10**, 2632-2640.

88. Y. Lan, M. G. Corradini and M. A. Rogers, *Cryst. Growth Des.*, 2014, **14**, 4811-4818.

89. N. Yan, Z. Xu, K. K. Diehn, S. R. Raghavan, Y. Fang and R. G. Weiss, *J. Am. Chem. Soc.*, 2013, **135**, 8989-8999.

90. P. Lin, N.-X. Zhang, J.-J. Li, J. Zhang, J.-H. Liu, B. Zhang and J. Song, *Chin. Chem. Lett.*, 2017, **28**, 771-776.

91. C. Liu, M. Corradini and M. A. Rogers, *Colloid. Polym. Sci.*, 2015, **293**, 975-983.

92. Y. Lan, M. G. Corradini, R. G. Weiss, S. R. Raghavan and M. A. Rogers, *Chem. Soc. Rev.*, 2015, **44**, 6035-6058.

93. K. Hanabusa, M. Matsumoto, M. Kimura, A. Kakehi and H. Shirai, *J. Colloid Interface Sci.*, 2000, **224**, 231-244.

94. J. Makarević, M. Jokić, B. Perić, V. Tomišić, B. Kojić-Prodić and M. Žinić, *Chem. Eur. J.*, 2001, **7**, 3328-3341.

95. C. M. Hansen, *Hansen Solubility Parameters: A User's Handbook*, CRC Press, Boca Raton, Second edn., 2000.

96. S. Diaz-Oltra, C. Berdugo, J. F. Miravet and B. Escuder, *New J. Chem.*, 2015, **39**, 3785-3791.

97. I. A. W. Filot, A. R. A. Palmans, P. A. J. Hilbers, R. A. van Santen, E. A. Pidko and T. F. A. de Greef, *J. Phys. Chem. B*, 2010, **114**, 13667-13674.

98. M. M. J. Smulders, A. P. H. J. Schenning and E. W. Meijer, *J. Am. Chem. Soc.*, 2008, **130**, 606-611.

99. M. Gottlieb, C. W. Macosko, G. S. Benjamin, K. O. Meyers and E. W. Merrill, *Macromolecules*, 1981, **14**, 1039-1046.

100. D. R. Picout and S. B. Ross-Murphy, *Sci. World J.*, 2003, **3**, 105-121.

101. R. G. Weiss and P. Terech, *Molecular Gels*, Springer, The Netherlands, 2006.

102. V. J. Nebot and D. K. Smith, in *Functional Molecular Gels*, The Royal Society of Chemistry, 2014, pp. 30-66.

103. S. K. Patel, S. Malone, C. Cohen, J. R. Gillmor and R. H. Colby, *Macromolecules*, 1992, **25**, 5241-5251.

104. P. Terech, C. Rossat and F. Volino, *J. Colloid Interface Sci.*, 2000, **227**, 363-370.

105. P. Sollich, *Phys. Rev. E*, 1998, **58**, 738-759.

106. H. Huang, W. Li, H. Wang, X. Zeng, Q. Wang and Y. Yang, *ACS Appl. Mater. Interfaces*, 2014, **6**, 1595-1600.

107. S. Ikeda and K. Nishinari, *J. Agric. Food. Chem.*, 2001, **49**, 4436-4441.

108. R. G. Weiss, *J. Am. Chem. Soc.*, 2014, **136**, 7519-7530.

109. V. Breedveld, A. P. Nowak, J. Sato, T. J. Deming and D. J. Pine, *Macromolecules*, 2004, **37**, 3943-3953.

110. K. Almdal, J. Dyre, S. Hvidt and O. Kramer, *Polym. Gels Networks*, 1993, **1**, 5-17.

111. J. M. Gardlik and R. M. Burkes, *US Patent 5106999*, 1992.

112. H. Uchiyama, *US Patent 4131612*, 1978.

113. H. Uchiyama, *US Patent 4267110*, 1981.

114. H. Uchiyama, *US Patent 4483952*, 1984.

115. G. Machell, *US Patent 4562265*, 1985.

116. K. Murai, T. Kobayashi and K. Fujitani, *US Patent 4429140 A*, 1984.

117. T. Kobayashi, *US Patent 5120863*, 1992.

118. T. Kobayashi and K. Kujitani, *US Patent 4902807*, 1990.

119. J. P. Salome and G. Fleche, *US Patent 5023354*, 1991.

120. W. A. Scrivens and J. M. Salley, *US Patent 5731474*, 1998.

121. J. G. Lever, D. L. Dotson, J. D. Anderson, J. R. Jones and S. R. Sheppard, *US Patent 0281716*, 2013.

122. A. Pavankumar and P. V. Uppara, *US Patent 8871954*, 2014.

123. P. V. Uppara, P. Aduri, M. Sakhalkar and U. Ratnaparkhi, *US Patent 0281716*, 2013.

124. M. J. Meunier, *Ann. Chim. Phys.*, 1891, **22**, 21.

125. P. Thomas and M. Sibi, *Compt. Rend.*, 1926, **183**, 282-284.

126. P. Thomas and M. Sibi, *Compt. Rend.*, 1926, **182**, 314-316.

127. J. K. Wolfe, R. M. Hann and R. M. Hudson, *J. Am. Chem. Soc.*, 1942, **64**, 1493-1497.

128. S. J. Angyal and J. V. Lawler, *J. Am. Chem. Soc.*, 1944, **66**, 837-838.

129. T. G. Bonner, E. J. Bourne, P. J. V. Cleare and D. Lewis, *J. Chem. Soc. B*, 1968, 827-830.

130. D. J. Brecknell, R. M. Carman, J. J. Kibby and L. T. Nicholas, *Aust. J. Chem.*, 1976, **29**, 1859-1863.

131. J. Song, H. Sun, S. Sun and R. Feng, *Trans. Tianjin Univ.*, 2013, **19**, 319-325.

132. E. A. Wilder, R. J. Spontak and C. K. Hall, *Mol. Phys.*, 2003, **101**, 3017-3027.

133. D. Alperstein and D. Knani, *Polym. Adv. Technol.*, 2013, **24**, 391-397.

134. M. Watase, Y. Nakatani and H. Itagaki, *J. Phys. Chem. B*, 1999, **103**, 2366-2373.

135. S. Yamasaki and H. Tsutsumi, *Bull. Chem. Soc. Jpn.*, 1995, **68**, 123-127.

136. S. Yamasaki, Y. Ohashi, H. Tsutsumi and K. Tsujii, *Bull. Chem. Soc. Jpn.*, 1995, **68**, 146.

137. R. Stan, C. Ott, N. Sulca, A. Lungu and H. Iovu, *Materiale Plastice.*, 2009, **46**, 230.

138. L. Zhang, X. Wang, T. Wang and M. Liu, *Small*, 2015, **11**, 1025-1038.

139. H. Cao, P. Duan, X. Zhu, J. Jiang and M. Liu, *Chem. Eur. J.*, 2012, **18**, 5546-5550.

140. P. Duan, L. Qin, X. Zhu and M. Liu, *Chem. Eur. J.*, 2011, **17**, 6389-6395.

141. P. Duan, X. Zhu and M. Liu, *Chem. Commun.*, 2011, **47**, 5569-5571.

142. N. Yan, G. He, H. Zhang, L. Ding and Y. Fang, *Langmuir*, 2010, **26**, 5909-5917.

143. J. Cui, Y. Zheng, Z. Shen and X. Wan, *Langmuir*, 2010, **26**, 15508-15515.

144. R. Feng, L. Chen, Z. Hou and J. Song, *Trans. Tianjin Univ.*, 2007, **13**, 35-41.

145. W. Chen, Y. Yang, C. H. Lee and A. Q. Shen, *Langmuir*, 2008, **24**, 10432-10436.

146. J. Li, K. Fan, X. Guan, Y. Yu and J. Song, *Langmuir*, 2014, **30**, 13422-13429.

147. R. Stan, S. Rosca, C. Ott, S. Rosca, E. Perez, I. Rico-Lattes and L. Armand, *Rev. Roum. Chim.*, 2006, **51**, 609-613.

148. B. O. Okesola, S. K. Suravaram, A. Parkin and D. K. Smith, *Angew. Chem. Int. Ed.*, 2016, **55**, 183-187.

149. G. Malle and T. Luukas, *US Patent 0039862 A1*, 2013.

150. T. Curtius, *J. Prakt. Chem.*, 1915, **91**, 39-102.

151. A. Timme, R. Kress, R. Q. Albuquerque and H.-W. Schmidt, *Chem. Eur. J.*, 2012, **18**, 8329-8339.

152. P. J. M. Stals, M. M. J. Smulders, R. Martín-Rapún, A. R. A. Palmans and E. W. Meijer, *Chem. Eur. J.*, 2009, **15**, 2071-2080.

153. L. Brunsveld, B. J. B. Folmer, E. W. Meijer and R. P. Sijbesma, *Chem. Rev.*, 2001, **101**, 4071-4098.

154. P. J. M. Stals, J. C. Everts, R. de Bruijn, I. A. W. Filot, M. M. J. Smulders, R. Martín-Rapún, E. A. Pidko, T. F. A. de Greef, A. R. A. Palmans and E. W. Meijer, *Chem. Eur. J.*, 2010, **16**, 810-821.

155. M. P. Lightfoot, F. S. Mair, R. G. Pritchard and J. E. Warren, *Chem. Commun.*, 1999, 1945-1946.

156. D. Kluge, J. C. Singer, J. W. Neubauer, F. Abraham, H.-W. Schmidt and A. Fery, *Small*, 2012, **8**, 2563-2570.

157. S. Cantekin, D. W. R. Balkenende, M. M. J. Smulders, A. R. A. Palmans and E. W. Meijer, *Nat. Chem.*, 2011, **3**, 42-46.

158. M. Kristiansen, P. Smith, H. Chanzy, C. Baerlocher, V. Gramlich, L. McCusker, T. Weber, P. Pattison, M. Blomenhofer and H.-W. Schmidt, *Cryst. Growth Des.*, 2009, **9**, 2556-2558.

159. L. Brunsveld, A. P. H. J. Schenning, M. A. C. Broeren, H. M. Janssen, J. A. J. M. Vekemans and E. W. Meijer, *Chem. Lett.*, 2000, **29**, 292-293.

160. J. J. van Gorp, J. A. J. M. Vekemans and E. W. Meijer, *J. Am. Chem. Soc.*, 2002, **124**, 14759-14769.

161. T. Shikata, Y. Kuruma, A. Sakamoto and K. Hanabusa, *J. Phys. Chem. B*, 2008, **112**, 16393-16402.

162. C. F. C. Fitié, I. Tomatsu, D. Byelov, W. H. de Jeu and R. P. Sijbesma, *Chem. Mater.*, 2008, **20**, 2394-2404.

163. K. K. Bejagam, G. Fiorin, M. L. Klein and S. Balasubramanian, *J. Phys. Chem. B*, 2014, **118**, 5218-5228.

164. A. Sakamoto, D. Ogata, T. Shikata, O. Urakawa and K. Hanabusa, *Polym.*, 2006, **47**, 956-960.

165. E. Fan, J. Yang, S. J. Geib, T. C. Stoner, M. D. Hopkins and A. D. Hamilton, *J. Chem. Soc., Chem. Commun.*, 1995, 1251-1252.

166. A. Sakamoto, D. Ogata, T. Shikata and K. Hanabusa, *Macromolecules*, 2005, **38**, 8983-8986.

167. R. Q. Albuquerque, A. Timme, R. Kress, J. Senker and H.-W. Schmidt, *Chem. Eur. J.*, 2013, **19**, 1647-1657.

168. M. Wegner, D. Dudenko, D. Sebastiani, A. R. A. Palmans, T. F. A. de Greef, R. Graf and H. W. Spiess, *Chem. Sci.*, 2011, **2**, 2040-2049.

169. M. L. Bushey, T.-Q. Nguyen, W. Zhang, D. Horoszewski and C. Nuckolls, *Angew. Chem. Int. Ed.*, 2004, **43**, 5446-5453.

170. T. Metzroth, A. Hoffmann, R. Martin-Rapun, M. M. J. Smulders, K. Pieterse, A. R. A. Palmans, J. A. J. M. Vekemans, E. W. Meijer, H. W. Spiess and J. Gauss, *Chem. Sci.*, 2011, **2**, 69-76.

171. C.-L. Pai, M. C. Boyce and G. C. Rutledge, *Polym.*, 2011, **52**, 2295-2301.

172. Y. Zhou, M. Xu, T. Yi, S. Xiao, Z. Zhou, F. Li and C. Huang, *Langmuir*, 2007, **23**, 202-208.

173. H. Kinoshita, M. Sekiya and N. Makino, *US Patent 4115284*, 1978.

174. H. Yasui, T. Yoshida, H. Komiya, T. Oguchi and S. Okamura, *US Patent 4668411*, 1987.

175. H. Kinoshita, M. Mishima, M. Sekiya and K. Oyama, *US Patent 4780231*, 1988.

176. K. Hoffmann, G. Huber and D. Mäder, *Macromol. Symp.*, 2001, **176**, 83-92.

177. C. Fresenius, *German Patent 142397*, 1902.

178. B. Werke, *German Patent 171371*, 1903.

179. A. R. Patel, P. S. Rajarethinem, A. Gredowska, O. Turhan, A. Lesaffer, W. H. De Vos, D. Van de Walle and K. Dewettinck, *Food Funct.*, 2014, **5**, 645-652.

180. M. P. Breton, D. C. Boils-Boissier, D. R. Titterington, J. W. Thomas Jr., J. H. Banning, C. E. Bedford and J. D. Wuest, *US Patent 6872243*, 2005.

181. N. Chopra, M. N. Chretien, B. Keoshkerian, J. Eliyahu, D. W. Vanbesien and A. Godedama, *US Patent 9328248*, 2016.

182. J. Fernandez, *US Patent 4477282*, 1982.

183. J.-P. Boutique, L. J. Charles, T. R. Burckett, M. Bouilliche, D. A. Beckholt, S. R. Murthy and M. E. Tremblay, *US Patent 8293697*, 2012.

184. J. R. Ansari and B. Potts, *US Patent 5643866*, 1997.

185. K. Sumitomo, M. Takahashi and H. Fukuo, *US Patent 7943684*, 2011.

186. E. L. Roehl, *US Patent 4346079*, 1982.

187. E. L. Roehl and H. B. Tan, *US Patent 4154816*, 1979.

188. T. Saito, T. Teshigawara, M. Reger, H. Hoffmann, Y. Sugiyama and M. Kitajima, *US Patent 20140134255*, 2014.

189. B. Xing, M.-F. Choi and B. Xu, *Chem. Eur. J.*, 2002, **8**, 5028-5032.

190. J. F. Miravet and B. Escuder, *Chem. Commun.*, 2005, 5769-5798.

191. Y.-R. Liu, L. He, J. Zhang, X. Wang and C.-Y. Su, *Chem. Mater.*, 2009, **21**, 557-563.

192. N. Singh, K. Zhang, C. A. Angulo-Pachon, E. Mendes, J. H. van Esch and B. Escuder, *Chem. Sci.*, 2016, **7**, 5568-5572.

193. M. Maity and U. Maitra, *J. Mater. Chem. A*, 2014, **2**, 18952-18958.

194. T. C. Holmes, S. de Lacalle, X. Su, G. S. Liu, A. Rich and S. Zhang, *Proc. Natl. Acad. Sci. USA*, 2000, **97**, 6728.

195. J. Kisiday, M. Jin, B. Kurz, H. Hung, C. Semino, S. Zhang and A. J. Grodzinsky, *Proc. Natl. Acad. Sci. USA*, 2002, **99**, 9996.

196. R. G. Ellis-Behnke, Y.-X. Liang, S.-W. You, D. K. C. Tay, S. Zhang, K.-F. So and G. E. Schneider, *Proc. Natl. Acad. Sci. USA*, 2006, **103**, 5054-5059.

197. R. G. Ellis-Behnke, G. Schneider and S. Zhang, *US Patent 7846891*, 2010.

198. V. M. Tysseling-Mattiace, V. Sahni, K. L. Niece, D. Birch, C. Czeisler, M. G. Fehlings, S. I. Stupp and J. A. Kessler, *J. Neurosci.*, 2008, **28**, 3814.

199. S. Zhang, M. A. Greenfield, A. Mata, L. C. Palmer, R. Bitton, J. R. Mantei, C. Aparicio, M. O. de la Cruz and S. I. Stupp, *Nat. Mater.*, 2010, **9**, 594.

200. J. D. Hartgerink, E. Beniash and S. I. Stupp, *Science*, 2001, **294**, 1684.

201. T. Liebmann, S. Rydholm, V. Akpe and H. Brismar, *BMC Biotechnology*, 2007, **7**, 88.

202. E. V. Alakpa, V. Jayawarna, A. Lampel, K. V. Burgess, C. C. West, S. C. J. Bakker, S. Roy, N. Javid, S. Fleming, D. A. Lamprou, J. Yang, A. Miller, A. J. Urquhart, P. W. J. M. Frederix, N. T. Hunt, B. Péault, R. V. Ulijn and M. J. Dalby, *Chem*, 2016, **1**, 298-319.

203. M. Zhou, A. M. Smith, A. K. Das, N. W. Hodson, R. F. Collins, R. V. Ulijn and J. E. Gough, *Biomaterials*, 2009, **30**, 2523-2530.

204. H. Komatsu, S. Tsukiji, M. Ikeda and I. Hamachi, *Chem. Asian J.*, 2011, **6**, 2368-2375.

205. Y. Hu, W. Gao, F. Wu, H. Wu, B. He and J. He, *J. Mater. Chem. B*, 2016, **4**, 3504-3508.

206. L. Applegarth, N. Clark, A. C. Richardson, A. D. M. Parker, I. Radosavljevic-Evans, A. E. Goeta, J. A. K. Howard and J. W. Steed, *Chem. Commun.*, 2005, 5423-5425.

207. E. Carretti, L. Dei, P. Baglioni and R. G. Weiss, *J. Am. Chem. Soc.*, 2003, **125**, 5121-5129.

208. E. Carretti, L. Dei and R. G. Weiss, *Soft Matter*, 2005, **1**, 17-22.

209. C. E. Earle, *US Patent 2274676*, 1942.

210. C. E. Earle, *US Patent 2274675*, 1942.

211. R. M. Neer, *Napalm: An American Biography*, Harvard University Press, Cambridge, 2015.

212. L. F. Fieser, G. C. Harris, E. B. Hershberg, M. Morgana, F. C. Novello and S. T. Putnam, *Ind. Eng. Chem.*, 1946, **38**, 768-773.

213. K. J. Mysels, *Ind. Eng. Chem.*, 1949, **41**, 1435-1438.

214. P. Reich and V. W. Sidel, *N. Engl. J. Med.*, 1967, **277**, 86-88.

215. M. Kristiansen, M. Werner, T. Trervoort, P. Smith, M. Blomenhofer and H.-W. Schmidt, *Macromolecules*, 2003, **36**, 5150-5156.

216. B. Fillon, A. Thierry, B. Lotz and J. Wittmann, *J. Therm. Anal. Calorim.*, 1994, **42**, 721-731.

217. M. Blomenhofer, S. Ganzleben, D. Hanft, H.-W. Schmidt, M. Kristiansen, P. Smith, K. Stoll, D. Mäder and K. Hoffmann, *Macromolecules*, 2005, **38**, 3688-3695.

218. T. D. Danielson, J. Rockwood and N.A. Mehl, *US Patent 8653165*, 2014.

219. M. Gahleitner, C. Grein, S. Kheirandish and J. Wolfschwenger, *Int. Polym. Proc.*, 2011, **26**, 2-20.

220. K. Hamada and H. Uchiyama, *US Patent 4016118*, 1977.

221. R. L. Mahaffey, *US Patent 4371645*, 1983.

222. G. R. Titus and J. L. Williams, *US Patent 4808650*, 1989.

223. J. W. Rekers, *US Patent 5049605*, 1991.

224. Z. Horvath, B. Gyarmati, A. Menyhard, P. Doshev, M. Gahleitner, J. Varga and B. Pukanszky, *RSC Adv.*, 2014, **4**, 19737-19745.

225. J. You, W. Yu and C. Zhou, *Ind. Eng. Chem. Res.*, 2014, **53**, 1097-1107.

226. S. Liu, W. Yu and C. Zhou, *Macromolecules*, 2013, **46**, 6309-6318.

227. H. Gankema, M. A. Hempenius, M. Möller, G. Johansson and V. Percec, *Macromol. Symp.*, 1996, **102**, 381-390.

228. U. Beginn, S. Keinath and M. Möller, *Macromol. Chem. Phys.*, 1998, **199**, 2379-2384.

229. W. Lai, S. J. Tseng and Y. Chao, *Langmuir*, 2011, **27**, 12630-12635.

230. W.-C. Lai, *Soft Matter*, 2011, **7**, 3844-3851.

231. J. R. Moffat, G. J. Seeley, J. T. Carter, A. Burgess and D. K. Smith, *Chem. Commun.*, 2008, 4601-4603.

232. G. J. Seeley, D. K. Smith, J. R. Moffat and A. Burgess, *Patent WO2009127845*, 2009.

233. L. Wei-Chi and T. Shen-Chen, *Nanotechnol.*, 2009, **20**, 475606.

234. W.-C. Lai, S.-C. Tseng, S.-H. Tung, Y.-E. Huang and S. R. Raghavan, *J. Phys. Chem. B*, 2009, **113**, 8026-8030.

235. S. Wangsoub, F. J. Davis, G. R. Mitchell and R. H. Olley, *Macromol. Rapid. Commun.*, 2008, **29**, 1861-1865.

236. J. Lipp, M. Shuster, G. Feldman and Y. Cohen, *Macromolecules*, 2007, **41**, 136-140.

237. J. Siripitayananon, S. Wangsoub, R. H. Olley and G. R. Mithcell, *Macromol. Rapid Commun.*, 2004, **29**, 1861-1865.

238. M. Y. Kariduraganavar, F. J. Davis, G. R. Mitchell and R. H. Olley, *Polym. Int.*, 2010, **59**, 827-835.

239. Y. Ono, K. Nakashima, M. Sano, Y. Kanekiyo, K. Inoue, S. Shinkai, M. Sano and J. Hojo, *Chem. Commun.*, 1998, 1477-1478.

240. S.-i. Kawano, S.-i. Tamaru, N. Fujita and S. Shinkai, *Chem. Eur. J.*, 2004, **10**, 343-351.

241. Y. Ono, K. Nakashima, M. Sano, J. Hojo and S. Shinkai, *Chem. Lett.*, 1999, **28**, 1119-1120.

242. M. Yamanaka, K. Sada, M. Miyata, K. Hanabusa and K. Nakano, *Chem. Commun.*, 2006, 2248-2250.

243. T. Schamper, M. Jablon, M. H. Randhawa, A. Senatore and J. D. Warren, *J. Cosmet. Sci.*, 1986, **37**, 225-231.

244. B. D. Hofrichter, J. M. Gardlik, P. A. Sawin, J. P. Luebbe and B. J. Bradbury, *US Patent 5429816*, 1995.

245. J. A. Muszik and W. Diehrichs, *US Patent 3576776*, 1971.

246. G. Gierenz, W. Klauck, R. Hoefer and R. Gruetzmacher, *US Patent 5371131*, 1994.

247. T. Ando and Y. Yamazaki, *US Patent 3846363*, 1974.

248. H. Fukuo and S. Tsujio, *US Patent 6203910*, 2001.

249. E. A. Wilder, K. S. Wilson, J. B. Quinn, D. Skrtic and J. M. Antonucci, *Chem. Mater.*, 2005, **17**, 2946-2952.

250. R. E. Johnsons, N. Karim and R. K. Dawson, *Patent WO2011056450*, 2011.

251. N. Karim, T. D. Jones, K. M. Lewandowski, B. D. Craig, S. B. Mitra and J. Yang, *US Patent 8445558*, 2013.

252. Y. K. Ghosh and S. Bhattacharya, *Chem. Commun.*, 2001, 185.

253. T. Saito, Y. Matsuzawa, S. Ninagawa, M. Honna, M. Takesada and M. Takehara, *US Patent 3969087*, 1976.

254. T. Kobayashi, Y. Kawashima, M. Yoshimura, M. Sugiura, T. Nobe and S. Fujimoto, *US Patent 4502975*, 1985.

255. S. Bhattacharya and Y. Krishnan-Ghosh, *Chem. Commun.*, 2001, 185-186.

256. S. R. Jadhav, P. K. Vemula, R. Kumar, S. R. Raghavan and G. John, *Angew. Chem. Int. Ed.*, 2010, **49**, 7695-7698.

257. H. Oh, N. Yaraghi and S. R. Raghavan, *Langmuir*, 2015, **31**, 5259-5264.

258. B. O. Okesola and D. K. Smith, *Chem. Soc. Rev.*, 2016, **45**, 4226-4251.

259. S. Ray, A. K. Das and A. Banerjee, *Chem. Mater.*, 2007, **19**, 1633-1639.

260. F. Rodriguez-Llansola, B. Escuder, J. F. Miravet, D. Hermida-Merino, I. W. Hamley, C. J. Cardin and W. Hayes, *Chem. Commun.*, 2010, **46**, 7960-7962.

261. D. M. Wood, B. W. Greenland, A. L. Acton, F. Rodríguez-Llansola, C. A. Murray, C. J. Cardin, J. F. Miravet, B. Escuder, I. W. Hamley and W. Hayes, *Chem. Eur. J.*, 2012, **18**, 2692-2699.

262. S. Basak, N. Nandi, S. Paul, I. W. Hamley and A. Banerjee, *Chem. Commun.*, 2017, **53**, 5910-5913.

263. A.-C. Couffin-Hoarau, A. Motulsky, P. Delmas and J.-C. Leroux, *Pharm. Res.*, 2004, **21**, 454-457.

264. J.-C. Leroux and G. Bastiat, *US Patent 8815944*, 2014.

265. J.-C. Leroux and A.-C. Couffin-Hoarau, *US Patent 7691408*, 2010.

266. F. Plourde, A. Motulsky, A.-C. Couffin-Hoarau, D. Hoarau, H. Ong and J.-C. Leroux, *J. Controlled Release*, 2005, **108**, 433-441.

267. B. Xing, C.-W. Yu, K.-H. Chow, P.-L. Ho, D. Fu and B. Xu, *J. Am. Chem. Soc.*, 2002, **124**, 14846-14847.

268. Y. Gao, Y. Kuang, Z.-F. Guo, Z. Guo, I. J. Krauss and B. Xu, *J. Am. Chem. Soc.*, 2009, **131**, 13576-13577.

269. T. Furuishi, K. Tomono, T. Suzuki, T. Fukami and K. Kunimasu, *US Patent 20120264742*, 2012.

270. K. Iwanaga, T. Sumizawa, M. Miyazaki and M. Kakemi, *Int. J. Pharm.*, 2010, **388**, 123-128.

271. B. Martin, F. Brouillet, S. Franchesci and E. Perez, *AAPS PharmSciTEch*, 2017, **18**, 1261-1269.

272. E. J. Howe, B. O. Okesola and D. K. Smith, *Chem. Commun.*, 2015, **51**, 7451-7454.

273. P. R. A. Chivers and D. K. Smith, *Chem. Sci.*, 2017, **8**, 7218-7227.

274. M. A. Ramin, K. R. Sindhu, A. Appavoo, K. Oumzil, M. W. Grinstaff, O. Chassande and P. Barthélémy, *Adv. Mater.*, 2017, **29**, 1605227-n/a.

275. C. R. King, D. W. Bristol and M. L. English, *US Patent 20140178480*, 2014.

276. K. E. Broaders, S. J. Pastine, S. Grandhe and J. M. J. Fréchet, *Chem. Commun.*, 2011, **47**, 665-667.

277. T. H. Kim, D. G. Kim, M. Lee and T. S. Lee, *Tetrahedron*, 2010, **66**, 1667-1672.

278. J. R. Hiscock, I. L. Kirby, J. Herniman, G. John Langley, A. J. Clark and P. A. Gale, *RSC Adv.*, 2014, **4**, 45517-45521.

279. J. R. Hiscock, M. R. Sambrook, N. J. Wells and P. A. Gale, *Chem. Sci.*, 2015, **6**, 5680-5684.

280. J. R. Hiscock, M. R. Sambrook, J. A. Ede, N. J. Wells and P. A. Gale, *J. Mater. Chem. A*, 2015, **3**, 1230-1234.

281. J. Raeburn and D. J. Adams, *Chem. Commun.*, 2015, **51**, 5170-5180.

282. A. R. Hirst and D. K. Smith, *Chem. Eur. J.*, 2005, **11**, 5496-5508.

283. P. Chakraborty, B. Roy, P. Bairi and A. K. Nandi, *J. Mater. Chem.*, 2012, **22**, 20291-20298.

284. J.-L. Li and X.-Y. Liu, *Adv. Funct. Mater.*, 2010, **20**, 3196-3216.

285. J. L. Li, X. Y. Liu, C. S. Strom and J. Y. Xiong, *Adv. Mater.*, 2006, **18**, 2574-2578.

286. C. Colquhoun, E. R. Draper, E. G. B. Eden, B. N. Cattoz, K. L. Morris, L. Chen, T. O. McDonald, A. E. Terry, P. C. Griffiths, L. C. Serpell and D. J. Adams, *Nanoscale*, 2014, **6**, 13719-13725.

287. K. Sugiyasu, S.-I. Kawano, N. Fujita and S. Shinkai, *Chem. Mater.*, 2008, **20**, 2863-2865.

288. M. M. Smith and D. K. Smith, *Soft Matter*, 2011, **7**, 4856-4860.

289. J. R. Moffat and D. K. Smith, *Chem. Commun.*, 2009, 316-318.

290. E. R. Draper, J. R. Lee, M. Wallace, F. Jackel, A. J. Cowan and D. J. Adams, *Chem. Sci.*, 2016, **7**, 6499-6505.

291. S. Onogi, H. Shigemitsu, T. Yoshii, T. Tanida, M. Ikeda, R. Kubota and I. Hamachi, *Nat. Chem.*, 2016, **8**, 743-752.

292. E. R. Draper, E. G. B. Eden, T. O. McDonald and D. J. Adams, *Nat. Chem.*, 2015, **7**, 848.

293. D. J. Cornwell, O. J. Daubney and D. K. Smith, *J. Am. Chem. Soc.*, 2015, **137**, 15486-15492.

294. E. R. Draper, M. Wallace, R. Schweins, R. J. Poole and D. J. Adams, *Langmuir*, 2017, **33**, 2387-2395.

295. X. Y. Liu and P. D. Sawant, *Angew. Chem. Int. Ed.*, 2002, **41**, 3641-3645.

296. X. Y. Liu, P. D. Sawant, W. B. Tan, I. B. M. Noor, C. Pramesti and B. H. Chen, *J. Am. Chem. Soc.*, 2002, **124**, 15055-15063.

297. X. Y. Liu and P. D. Sawant, *Adv. Mater.*, 2002, **14**, 421-426.

298. J.-L. Li and X.-Y. Liu, *J. Phys. Chem. B*, 2009, **113**, 15467-15472.

299. J.-L. Li, B. Yuan, X.-Y. Liu, X.-G. Wang and R.-Y. Wang, *Cryst. Growth Des.*, 2011, **11**, 3227-3234.

300. R. Lam, L. Quaroni, T. Pedersen and M. A. Rogers, *Soft Matter*, 2010, **6**, 404-408.

301. K. Hanabusa, A. Itoh, M. Kimura and H. Shirai, *Chem. Lett.*, 1999, **28**, 767-768.

302. L. Chen, S. Revel, K. Morris, D. G. Spiller, L. C. Serpell and D. J. Adams, *Chem. Commun.*, 2010, **46**, 6738-6740.

303. G. Pont, L. Chen, D. G. Spiller and D. J. Adams, *Soft Matter*, 2012, **8**, 7797-7802.

304. B. C. Baker, A. L. Acton, G. C. Stevens and W. Hayes, *Tetrahedron*, 2014, **70**, 8303-8311.

305. M. C. Lina and B. F. Alison, *Smart Mater. Struct.*, 2014, **23**, 053001.

306. H. M. Ibrahim and M. M. Reda, *Int. J. Innov. Sci. Eng. Technol.*, 2015, **2**, 512-519.

307. M. Hashem, M. El-Bisi, S. Sharaf and R. Refaie, *Carbohydr. Polym.*, 2010, **79**, 533-540.

308. H.-S. Seong, J.-P. Kim and S.-W. Ko, *Text. Res. J.*, 1999, **69**, 483-488.

309. S. Zhang, W. S. Shim and J. Kim, *Mater. Des.*, 2009, **30**, 3659-3666.

310. J. Hu, H. Meng, G. Li and S. I. Ibekwe, *Smart Mater. Struct.*, 2012, **21**, 053001.

311. S. Mondal, *Appl. Therm. Eng.*, 2008, **28**, 1536-1550.

312. X. Deng, L. Mammen, H.-J. Butt and D. Vollmer, *Science*, 2012, **335**, 67-70.

313. A. N. Netravali and T. Bahners, *J. Adhes. Sci. Technol.*, 2010, **24**, 45-75.

314. B. Martel, M. Weltrowski, D. Ruffin and M. Morcellet, *J. Appl. Polym. Sci.*, 2002, **83**, 1449-1456.

315. D. Wei, Y. Chen and Y. Zhang, *Carbohydr. Polym.*, 2016, **136**, 543-550.

316. X. Zhu, Z. Zhang, B. Ge, X. Men, X. Zhou and Q. Xue, *J. Colloid Interface Sci.*, 2014, **432**, 105-108.

317. L. Fang, X. Zhang and D. Sun, *Carbohydr. Polym.*, 2013, **91**, 363-369.

318. W. Zhang, X. Lu, Z. Xin and C. Zhou, *Nanoscale*, 2015, **7**, 19476-19483.

319. W. Ye, J. H. Xin, P. Li, K.-L. D. Lee and T.-L. Kwong, *J. Appl. Polym. Sci.*, 2006, **102**, 1787-1793.

320. Q. Li, S.-L. Chen and W.-C. Jiang, *J. Appl. Polym. Sci.*, 2007, **103**, 412-416.

321. Y. Shin, D. I. Yoo and K. Min, *J. Appl. Polym. Sci.*, 1999, **74**, 2911-2916.

322. S. Lee, J.-S. Cho and G. Cho, *Text. Res. J.*, 1999, **69**, 104-112.

323. S. Jiang, E. Newton, M. Y. Chun-Wah and C.-W. Kan, *Text. Res. J.*, 2007, **77**, 85-91.

324. A. Kulkarni, A. Tourrette, M. M. C. G. Warmoeskerken and D. Jocic, *Carbohydr. Polym.*, 2010, **82**, 1306-1314.

325. M. W. Huh, I.-K. Kang, D. H. Lee, W. S. Kim, D. H. Lee, L. S. Park, K. E. Min and K. H. Seo, *J. Appl. Polym. Sci.*, 2001, **81**, 2769-2778.

326. A. Bozzi, T. Yuranova and J. Kiwi, *J. Photochem. Photobiol., A Chem*, 2005, **172**, 27-34.

327. A. Tourrette, N. De Geyter, D. Jocic, R. Morent, M. M. C. G. Warmoeskerken and C. Leys, *Colloids Surf., A*, 2009, **352**, 126-135.

328. G. Decher, *Science*, 1997, **277**, 1232.

329. B. Ding, J. Kim, E. Kimura and S. Shiratori, *Nanotechnol.*, 2004, **15**, 913.

330. I. Chopra, *J. Antimicrob. Chemother.*, 2007, **59**, 587-590.

331. The Project on Emerging Nanotechnologies, http://www.nanotechproject.org/cpi/, (accessed 07/04/2016, 2016).

332. N. Duran, P. D. Marcato, G. I. H. De Souza, O. L. Alves and E. Esposito, *J. Biomed. Nanotechnol.*, 2007, **3**, 203-208.

333. S. T. Dubas, P. Kumlangdudsana and P. Potiyaraj, *Colloids Surf., A*, 2006, **289**, 105-109.

334. I. Sondi and B. Salopek-Sondi, *J. Colloid Interface Sci.*, 2004, **275**, 177-182.

335. H. J. Lee, S. Y. Yeo and S. H. Jeong, *J. Mater. Sci.*, 2003, **38**, 2199-2204.

336. H. Y. Lee, H. K. Park, Y. M. Lee, K. Kim and S. B. Park, *Chem. Commun.*, 2007, 2959-2961.

337. P. Ilana, A. Guy, P. Nina, G. Geoffrey, M. Serguei and G. Aharon, *Nanotechnol.*, 2008, **19**, 245705.

338. S. Tarimala, N. Kothari, N. Abidi, E. Hequet, J. Fralick and L. L. Dai, *J. Appl. Polym. Sci.*, 2006, **101**, 2938-2943.

339. F. Zhang, X. Wu, Y. Chen and H. Lin, *Fibers Polym.*, 2009, **10**, 496-501.

340. M. H. El-Rafie, A. A. Mohamed, T. I. Shaheen and A. Hebeish, *Carbohydr. Polym.*, 2010, **80**, 779-782.

341. T. M. Benn and P. Westerhoff, *Environ. Sci. Technol.*, 2008, **42**, 4133-4139.

342. L. Geranio, M. Heuberger and B. Nowack, *Environ. Sci. Technol.*, 2009, **43**, 8113-8118.

343. M. Gorenšek and P. Recelj, *Text. Res. J.*, 2007, **77**, 138-141.

344. J. C. McGeer, R. C. Playle, C. M. Wood and F. Galvez, *Environ. Sci. Technol.*, 2000, **34**, 4199-4207.

345. H. T. Ratte, *Environ. Toxicol. Chem.*, 1999, **18**, 89-108.

346. A. W. Andren and D. E. Armstrong, *Environ. Toxicol. Chem.*, 1999, **18**, 1-2.

347. P. J. Hauser and A. H. Tabba, *Color. Technol.*, 2001, **117**, 282-288.

348. J. D. Guthrie, *US Patent 2459222*, 1949.

349. J. D. Guthrie, *Text. Res. J.*, 1947, **17**, 625-629.

350. M. Hartmann, *US Patent 1777970*, 1930.

351. M. N. Micheal, F. M. Tera and S. F. Ibrahim, *J. Appl. Polym. Sci.*, 2002, **85**, 1897-1903.

352. Q. Zhu, Q. Gao, Y. Guo, C. Q. Yang and L. Shen, *Ind. Eng. Chem. Res.*, 2011, **50**, 5881-5888.

353. Z.-Y. Deng, W. Wang, L.-H. Mao, C.-F. Wang and S. Chen, *J. Mater. Chem. A*, 2014, **2**, 4178-4184.

354. R. J. Plunkett, *US Patent 2230654*, 1941.

355. R. W. Gore, *US Patent 3953566*, 1976.

356. R. W. Gore, *US Patent 4187390*, 1980.

357. H. Qi, K. Sui, Z. Ma, W. Dong, X. Sun and J. Lu, *Text. Res. J.*, 2002, **72**, 93-97.

358. W. A. Daoud, J. H. Xin and X. Tao, *J. Am. Ceram. Soc.*, 2004, **87**, 1782-1784.

359. D. F. Cheng, C. Urata, M. Yagihashi and A. Hozumi, *Angew. Chem. Int. Ed.*, 2012, **51**, 2956-2959.

360. L. Wang and T. J. McCarthy, *Angew. Chem. Int. Ed.*, 2016, **55**, 244-248.

361. X. X. Zhang and X. M. Tao, *Textile Asia*, 2001, **32**, 45-49.

362. B. Yang, W. M. Huang, C. Li and L. Li, *Polym.*, 2006, **47**, 1348-1356.

363. H. Y. Jiang, S. Kelch and A. Lendlein, *Adv. Mater.*, 2006, **18**, 1471-1475.

364. R. A. Siegel and B. A. Firestone, *Macromolecules*, 1988, **21**, 3254-3259.

365. H. Feil, Y. H. Bae, J. Feijen and S. W. Kim, *Macromolecules*, 1992, **25**, 5528-5530.

366. K. Asaka and K. Oguro, *J. Electroanal. Chem.*, 2000, **480**, 186-198.

367. P. M. Xulu, G. Filipcsei and M. Zrínyi, *Macromolecules*, 2000, **33**, 1716-1719.

368. A. Bashari, N. Hemmatinejad and A. Pourjavadi, *Polym. Adv. Technol.*, 2013, **24**, 797-806.

369. J.-L. Hu, B.-H. Liu and W.-G. Liu, *Text. Res. J.*, 2006, **76**, 853-860.

370. K. T. Meilert, D. Laub and J. Kiwi, *J. Mol. Catal. A: Chem.*, 2005, **237**, 101-108.

371. T. Yuranova, R. Mosteo, J. Bandara, D. Laub and J. Kiwi, *J. Mol. Catal. A: Chem.*, 2006, **244**, 160-167.

372. S. Lee and S. K. Obendorf, *J. Text. Inst.*, 2007, **98**, 87-98.

373. K. Kosmider and J. Scott, *Filtr. Sep.*, 2002, **39**, 20-22.

374. W. L. Simm, *US Patent 3994258*, 1976.

375. D. Groitzsch and E. Fahrback, *US Patent 4618524*, 1986.

376. E. Tyrolczyk, K. Wielgus, M. Szalata, J. Makowiecka, D. Wesołek, D. Lipiński, J. Zeyland, M. Szalata and R. Słomski, *Chemik*, 2012, **66**, 1219-1228.

377. A. Lushnikov, *J. Aerosol Sci.*, 1997, **28**, 545-546.

378. R. S. Barhate and S. Ramakrishna, *J. Membr. Sci.*, 2007, **296**, 1-8.

379. N. Bhardwaj and S. C. Kundu, *Biotechnol. Adv.*, 2010, **28**, 325-347.

380. P. W. Gibson, H. L. Schreuder-Gibson and D. Rivin, *AIChE J.*, 1999, **45**, 190-195.

381. N. Mao and S. J. Russell, *J. Text. Inst.*, 2000, **91**, 244-258.

382. Y. C. Ahn, S. K. Park, G. T. Kim, Y. J. Hwang, C. G. Lee, H. S. Shin and J. K. Lee, *Curr. Appl. Phys.*, 2006, **6**, 1030-1035.

383. J. M. Deitzel, J. Kleinmeyer, D. Harris and N. C. Beck Tan, *Polym.*, 2001, **42**, 261-272.

384. A. Buer, S. C. Ugbolue and S. B. Warner, *Text. Res. J.*, 2001, **71**, 323-328.

385. H. Schreuder-Gibson, P. Gibson, K. Senecal, M. Sennett, J. Walker, W. Yeomans, D. Ziegler and P. P. Tsai, *J. Adv. Mater.*, 2002, **34**, 44-55.

386. B. Liu, S. Zhang, X. Wang, J. Yu and B. Ding, *J. Colloid Interface Sci.*, 2015, **457**, 203-211.

387. L. Juan, S. XiaoFei, G. Feng, l. LiQu, C. Rui, C. ChunYing and Z. Zhong, *Sci. China Technol. Sci.*, 2014, **57**, 239-243.

388. X.-H. Qin and S.-Y. Wang, *J. Appl. Polym. Sci.*, 2008, **109**, 951-956.

389. W. W.-F. Leung, C.-H. Hung and P.-T. Yuen, *Sep. Purif. Technol.*, 2010, **71**, 30-37.

390. R. S. Barhate, C. K. Loong and S. Ramakrishna, *J. Membr. Sci.*, 2006, **283**, 209-218.

391. R. Gopal, S. Kaur, Z. Ma, C. Chan, S. Ramakrishna and T. Matsuura, *J. Membr. Sci.*, 2006, **281**, 581-586.

392. X. Qin and S. Wang, *J. Appl. Polym. Sci.*, 2006, **102**, 1285-1290.

393. D. Shou, L. Ye and J. Fan, *Polym.*, 2014, **55**, 3149-3155.

394. P. Li, C. Wang, Y. Zhang and F. Wei, *Small*, 2014, **10**, 4543-4561.

395. C. Yang, *Chin. J. Chem. Eng.*, 2012, **20**, 1-9.

396. A. Podgórski, A. Bałazy and L. Gradoń, *Chem. Eng. Sci.*, 2006, **61**, 6804-6815.

397. H.-S. Park and Y. Park, *Korean J. Chem. Eng.*, 2005, **22**, 165-172.

398. N. Wang, X. Wang, B. Ding, J. Yu and G. Sun, *J. Mater. Chem.*, 2012, **22**, 1445-1452.

399. Z.-M. Huang, Y. Z. Zhang, M. Kotaki and S. Ramakrishna, *Compos. Sci. Technol.*, 2003, **63**, 2223-2253.

400. S. Lee and S. K. Obendorf, *Text. Res. J.*, 2007, **77**, 696-702.

401. M. Faccini, C. Vaquero and D. Amantia, *J. Nanomater.*, 2012, **2012**, 9.

402. J. Matulevicius, L. Kliucininkas, T. Prasauskas, D. Buivydiene and D. Martuzevicius, *J. Aerosol Sci.*, 2016, **92**, 27-37.

403. S. Sundarrajan, K. L. Tan, S. H. Lim and S. Ramakrishna, *Procedia Eng.*, 2014, **75**, 159-163.

404. G. Fu, Z. Su, X. Jiang and J. Yin, *Polym. Chem.*, 2014, **5**, 2027-2034.

405. X. Li, H. Kong and J. He, *Indian J. Phys.*, 2015, **89**, 175-179.

406. N. Vitchuli, Q. Shi, J. Nowak, M. McCord, M. Bourham and X. Zhang, *J. Appl. Polym. Sci.*, 2010, **116**, 2181-2187.

407. A. Y. Mikheev, Y. M. Shlyapnikov, I. L. Kanev, A. V. A*v*seenko and V. N. Morozov, *Eur. Polym. J.*, 2016, **75**, 317-328.

408. L. Bromberg, W. R. Creasy, D. J. McGarvey, E. Wilusz and T. A. Hatton, *ACS Appl. Mater. Interfaces*, 2015, **7**, 22001-22011.

409. Y. Chuanfang, *Chin. J. Chem. Eng.*, 2012, **20**, 1-9.

410. E. Krieg, H. Weissman, E. Shirman, E. Shimoni and B. Rybtchinski, *Nat. Nano.*, 2011, **6**, 141-146.

411. F. Piana, M. Facciotti, G. Pileio, J. R. Hiscock, W. Van Rossom, R. C. D. Brown and P. A. Gale, *RSC Adv.*, 2015, **5**, 12287-12292.

412. C. Wilson, M. J. Main, N. J. Cooper, M. E. Briggs, A. I. Cooper and D. J. Adams, *Polym. Chem.*, 2017, **8**, 1914-1922.

413. A. Raghavanpillai, S. Reinartz and K. W. Hutchenson, *J. Fluorine Chem.*, 2009, **130**, 410-417.

414. B. P. Krishnan, S. Mukherjee, P. M. Aneesh, M. A. G. Namboothiry and K. M. Sureshan, *Angew. Chem.*, 2016, **128**, 2391-2395.

415. H. Misslitz, K. Kreger and H.-W. Schmidt, *Small*, 2013, **9**, 2053-2058.

416. V. A. Mallia, D. L. Blair and R. G. Weiss, *Ind. Eng. Chem. Res.*, 2016, **55**, 954-960.

417. D. Weiss, D. Skrybeck, H. Misslitz, D. Nardini, A. Kern, K. Kreger and H.-W. Schmidt, *ACS Appl. Mater. Interfaces*, 2016, **8**, 14885-14892.

418. P. F. Deng, Y. G. Feng, F. H. Xu and J. Song, *Fine. Chem.*, 2007, **24**, 1056-1060.

419. J. W. Goodwin and R. W. Hughes, *Rheology for Chemists An Introduction*, Royal Society of Chemistry, Cambridge, 2008.

420. P. S. Santos, M. G. Abiad, M. A. Carignano and O. H. Campanella, *Rheol. Acta*, 2012, **51**, 3-11.

421. B. S. Institution, *Textiles. Test methods for nonwovens. Determination of air permeability*, 2008, **BS EN ISO 9073-15:2008**.

422. B. S. Institution, *Specification for water vapour permeable apparel fabrics*, 1990, **BS 7209:1990**.

423. S. Agarwal, A. Greiner and J. H. Wendorff, *Adv. Funct. Mater.*, 2009, **19**, 2863-2879.

424. N. K. Whitelaw, PhD Thesis, University of York, 2016.

425. X. Zhao, *Soft Matter*, 2014, **10**, 672-687.

426. M. Wallace, J. A. Iggo and D. J. Adams, *Soft Matter*, 2015, **11**, 7739-7747.

427. B. Escuder, M. Llusar and J. F. Miravet, *J. Org. Chem.*, 2006, **71**, 7747-7752.